FACULDADE DE ENGENHARIA DA UNIVERSIDADE DO PORTO

Integrating SMED and Mechanical Design for Changeover Reduction in Beverage Packaging Lines

António Rocha Esteves



Mestrado em Engenharia Mecânica

Supervisor: Prof. José Joaquim da Mota Machado

July 17, 2026

© António Rocha Esteves

Integrating SMED and Mechanical Design for Changeover Reduction in Beverage Packaging Lines

António Rocha Esteves

Mestrado em Engenharia Mecânica

July 17, 2026

Resumo

As perdas associadas à mudança de formato de novas referências constituem uma das principais limitações à flexibilidade das linhas de produção, incluindo as linhas de enchimento de bebidas. Esta dissertação, desenvolvida em parceria com o Super Bock Group, na fábrica de Leça do Balio, estuda estas perdas na encartonadora Kisters e na máquina de packs Mead, combinando a metodologia Single Minute Exchange of Die (SMED) com o projeto mecânico, dois domínios que a literatura trata habitualmente de forma isolada. O contributo central da dissertação é um método estruturado para a transição entre ambos: o SMED é aplicado até atingir um limite demonstrável, a partir do qual novos ganhos exigem redesenho mecânico e não apenas melhoria nos processos.

Um diagnóstico histórico identifica a Kisters como o estrangulamento crítico e localiza o mecanismo responsável pela desconfiança dos operadores no sistema de ajuste digital, atribuindo-o a um terceiro grau de liberdade não contabilizado. Foram implementadas e validadas em contexto real intervenções processuais, entre elas a externalização de tarefas, um esquema de ajuste otimizado e normalizado, e uma ferramenta digital de apoio com fases sequenciais, recuperando um valor operacional estimado de €22,000 por ano. Este valor é um limite deliberadamente conservador, uma vez que a capacidade recuperada em períodos de elevada procura apresenta um valor realizável substancialmente superior. O redesenho de um suporte de dobragem sem ferramentas reduziu o tempo dessa tarefa em 78,5% e a sua variância em 99,3%, com significância estatística conclusiva.

Onde estas medidas convergiram numa tarefa manual residual e fisicamente limitada, o resultado da otimização derivada do SMED foi transposto diretamente como dados de projeto para um retrofit, seguindo a norma VDI 2221, do Módulo de Alimentação de Cartão da Kisters da Linha 1. Este sistema de ajuste automático foi totalmente especificado e validado analiticamente (Método dos Elementos Finitos, KISSsoft, análise de fiabilidade), embora não implementado. O trabalho demonstra que a otimização de gestão de operações e o projeto mecânico clássico constituem uma sequência complementar para a redução do tempo de mudança de formato, e não alternativas concorrentes.

Palavras-chave: SMED • Redução de Tempo de Setup • Projeto Mecânico • Design para Mudanças de Referência

Abstract

Changeover losses are a primary constraint on the flexibility of high-speed beverage packaging lines. This dissertation, developed at the Super Bock Group's plant in Leça do Balio, addresses these losses on the Kisters and Mead secondary-packaging machines by combining the Single-Minute Exchange of Die (SMED) methodology with formal machine design, two domains the literature typically treats separately. The central contribution is a structured method for transitioning between them: SMED is applied until it reaches a demonstrable design ceiling, beyond which further gains require mechanical redesign rather than procedural refinement.

A historical diagnosis identified the Kisters as the critical bottleneck and located the mechanism behind operators' distrust of the digital adjustment system in an unaccounted-for third degree of freedom. Procedural interventions (task externalisation, a mathematically optimised and standardised adjustment scheme, and a phase-gated digital support tool) were deployed and field-validated, recovering an estimated €22,000 per year valued at operating cost alone. This is a deliberately conservative floor, since recovered capacity during high-demand periods carries a substantially higher realisable value. A redesigned tool-less folding bracket reduced its adjustment task time by 78.5% and its variance by 99.3% under statistically conclusive testing.

Where these measures converged on a residual, physically limited manual task, the SMED-derived optimisation output was carried directly as design input into a VDI 2221 retrofit of the Cardboard Cutout Feeding Module. This automatic adjustment system was fully specified and analytically validated through FEA, KISSsoft cross-validation, and a duty-cycle-appropriate reliability analysis, though not physically built. The work demonstrates that operations-management optimisation and classical machine design form a complementary, data-driven sequence for changeover reduction rather than competing alternatives.

Keywords: SMED • Changeover Reduction • Machine Design • Design for Changeover (DFC)

The United Nations Sustainable Development Goals

The United Nations Sustainable Development Goals (SDGs) establish a global framework for systemic sustainability. This dissertation directly aligns with this framework by operating at the intersection of mechanical design optimization and operational resource efficiency. Rather than advocating for capital-intensive equipment replacement, this research focuses on retrofitting legacy beverage packaging machinery, thereby mitigating embedded carbon expenditures and advancing circular economy principles.

The primary SDGs targeted by this investigation are defined as follows:

SDG 9: Build resilient infrastructure, promote inclusive and sustainable industrialisation, and foster innovation.

SDG 12: Ensure sustainable consumption and production patterns.

SDG	Target	Contribution	Performance Indicators and Metrics
9	9.4	Mechanical retrofits and automated adjustments to extend the operational lifecycle of legacy assets and reduce technical variability without new-build capital investment.	• Reduction in carriage travel span variability (mm). • Minimisation of changeover downtime per SKU transition (min).
	9.5	Development and implementation of digital changeover support tools applying systematic engineering innovation to legacy plant infrastructure.	• Adoption rate of digital support tools across shift teams (%).
12	12.2	Eliminating manual trial-and-error configurations through mathematically optimised, exact-constraint designs to maximize resource efficiency.	• Reduction in start-up material scrap and downstream product waste.
	12.5	Re-engineering the Folding Bracket as a low-cost sacrificial component that fails safely under collision loads to completely prevent catastrophic frame damage and scrap.	• Material cost per replaceable unit ($< €0.15$). • Component procurement lead time vs. outsourced fabrication.

Agradecimentos

Primeiramente, tenho que agradecer encarecidamente ao Professor José Machado, pela sua orientação e disponibilidade incansável ao longo deste projeto, por me ter ajudado a navegar pelas diferentes partes deste desafio e por me aconselhar sempre o melhor percurso para mim. A realização desta dissertação não teria sido possível sem ele. Extendo o agradecimento também a todos os restantes Professores que ao longo destes 5 anos me fizeram crescer não só como Engenheiro mas especialmente como pessoa.

Ao Super Bock Group, agradeço pela oportunidade de ser integrado num problema real do contexto de Engennharia Mecânica, algo que vou levar certamente como uma experiência positiva. Um obrigado especial ao Serviço de Enchimento. Luís, Pedro, Fábio, Nuno, Rodrigo e Fati pela orientação tanto no projeto como no dia-a-dia e aos Estagiários SB 2025/2026 especialmente ao Kiko, à Diana, ao Miguel, ao Bruno, ao Nuno e ao Miguel pelo companheirismo ao longo desta jornada.

Aos meus pais, pelo apoio e amor incondicional ao longo dos últimos 23 anos, por acreditarem em mim em todas as situações, por quererem sempre o meu melhor e por me darem todas as condições necessárias e mais algumas para que eu sucedesse em todos os meus projetos, o maior dos obrigados. Teria sido impossível sem eles atingir tudo que atingi até agora. Ao Lipe, à Mafalda, à Bozinha e à minha restante família agradeço também por me acompanharem ao longo deste percurso de perto.

Por fim um agradecimento especial aos que realmente tornaram este processo possível durante os últimos 5 anos. A todos os meus amigos, colegas e ao NEEM; em especial à Direção, à Grupeta e aos Patos; obrigado por me acompanharem todos os dias, pela partilha de todos os momentos e por moldarem profundamente a pessoa que sou hoje. Não podia ter arranjado um melhor grupo de pessoas para me acompanhar durante os últimos 5 anos. Não poderia estar mais grato.

António Esteves

Declaração de Honra

Declaro que a presente dissertação é de minha autoria e não foi previamente apresentada e avaliada nesta ou em outra instituição. As referências a outros autores (afirmações, ideias, pensamentos), assim como a utilização de trabalhos publicados respeitam escrupulosamente as regras da atribuição, e encontram-se devidamente indicadas no texto e nas referências bibliográficas, de acordo com as normas de referenciação. Tenho consciência de que a prática de plágio ou de autoplágio constituem ilícitos académicos, conforme estabelecido no Código de Ética da U.Porto.

Declaro, ainda, que utilizei ferramentas de Inteligência Artificial para a realização de parte da presente dissertação, e essa utilização e os seus resultados foram objeto de cuidada verificação para deteção de erros, imprecisões, atribuições infundadas ou outras formas de enviesamento de conteúdos e argumentos, bem como de determinação de autoria.

António Rocha Esteves



Contents

1 Introduction **1**
- 1.1 Context . . . 1
- 1.2 Motivation and Problem Statement . . . 3
- 1.3 Objectives . . . 3
- 1.4 Dissertation Structure . . . 4

2 Literature Review **6**
- 2.1 Beer Brewing Process . . . 6
- 2.2 Packaging Lines . . . 7
  - 2.2.1 Packaging Lines Design . . . 7
- 2.3 Lean Manufacturing . . . 9
- 2.4 5S Methodology . . . 10
- 2.5 Single Minute Exchange of Die . . . 10
- 2.6 Mathematical Optimisation in Setup Operations . . . 13
  - 2.6.1 Operations Research in Setup Reduction . . . 13
  - 2.6.2 Bridging SMED with Mathematical Programming . . . 14
- 2.7 Industry 5.0 and the Digitalisation of Tacit Knowledge . . . 15
- 2.8 Engineering Design in Retrofitting . . . 16
  - 2.8.1 Design for Changeover . . . 16
  - 2.8.2 Automated and Self-Positioning Adjustment Systems . . . 18
  - 2.8.3 Systematic Design in Constrained Environments (VDI 2221) . . . 18
  - 2.8.4 Environmental Constraints in Beverage Packaging . . . 20
  - 2.8.5 Research Methodology: Design Science Research and Action Research . . . 20
- 2.9 Research Gaps and Methodological Synthesis . . . 21

3 Initial Considerations and Methodology **24**
- 3.1 Production Floor Organisation . . . 24
- 3.2 Technical Description of the Equipment . . . 26
  - 3.2.1 Kisters . . . 26
  - 3.2.2 Mead . . . 31
- 3.3 Format Setup Changeover . . . 33
  - 3.3.1 Kisters . . . 33
  - 3.3.2 Mead . . . 35
- 3.4 Changeover Analysis Methodology . . . 36
  - 3.4.1 SKU Portfolio and Setup Typology . . . 36
  - 3.4.2 SMED . . . 38
  - 3.4.3 Adjustment Values Case Study . . . 38

4 Analysis of the Current-State Production System **40**
4.1 Classification of Critical and Non-Critical Changeovers . . . 40
4.2 SMED Analysis . . . 41
4.3 Lack of Standardisation . . . 42
4.3.1 Format Part Identification . . . 43
4.3.2 Changeover Procedures . . . 43
4.4 Adjustment Values Case Study Observations . . . 44

5 Proposed Solutions **48**
5.1 Separation of Tasks . . . 48
5.2 Externalisation of Internal Tasks . . . 48
5.2.1 Mead . . . 49
5.2.2 Kisters . . . 49
5.3 Streamlining Internal and External Tasks . . . 50
5.3.1 Redesign of the Folding Bracket Mechanical System . . . 50
5.4 Adjustment Values Update and Box Configuration Optimisation . . . 59
5.4.1 Box Configuration Optimisation . . . 59
5.4.2 Adjustment Values Update and Sustainability . . . 63
5.5 Development of the Digital Changeover Support Tool . . . 64
5.5.1 User Access and Context Initialisation . . . 64
5.5.2 SKU Validation and Algorithmic Classification . . . 65
5.5.3 Guided Execution Workflow . . . 68
5.5.4 Administrative Utilities and Data Governance . . . 69
5.5.5 End-to-End System Data Flow . . . 70

6 Results and Discussion **72**
6.1 Structure and Key Performance Indicators . . . 72
6.2 Task Externalisation . . . 73
6.2.1 Pre-adjustment of the Product Feeding Module's Trolley . . . 73
6.2.2 Proactive Retrieval of Format Parts . . . 74
6.3 Redesign of the Folding Bracket . . . 76
6.3.1 Quantitative Time and Motion Analysis . . . 76
6.3.2 Empirical Structural and Mechanical Evaluation . . . 78
6.3.3 Economic Viability and the Mechanical Fuse Paradigm . . . 79
6.3.4 Operator Ergonomics and Qualitative Feedback . . . 79
6.4 Adjustment Values Optimisation and Update . . . 80
6.4.1 Shop-Floor Deployment and the Empirical Adaptation Window . . . 80
6.4.2 Quantitative Changeover Performance Evaluation . . . 80
6.4.3 Shop-Floor Governance and Human Factors . . . 82
6.5 Digital Changeover Support Tool . . . 82
6.5.1 Iterative Feedback Loop and Initial Perceptions . . . 82
6.5.2 Proof-of-Concept . . . 83
6.6 Overall Discussion . . . 84
6.7 Economic Analysis . . . 88

7 Case Study: Design of an Automatic Adjustment System **90**
7.1 Design Methodology Execution . . . 90
7.2 Clarifying the Task . . . 91
7.3 Conceptual Design . . . 99
7.3.1 Actuation . . . 100
7.3.2 Transmission System and Coupling . . . 102
7.4 Embodiment Design . . . 102
7.4.1 Cardboard Feeding Roller Conveyor . . . 103
7.4.2 Cardboard Storage Unit . . . 113
7.4.3 Transportation System . . . 119
7.5 Detail Design . . . 133
7.5.1 Roller Conveyor . . . 134
7.5.2 Cardboard Storage Unit . . . 140
7.5.3 Transportation System . . . 145
7.5.4 Global Safety Factor Synthesis . . . 153
7.6 Automation and Control Logic . . . 156
7.6.1 Hardware and Network Architecture . . . 156
7.6.2 Motion Control Technology Object Architecture . . . 157
7.6.3 Sequential State Machine . . . 157
7.6.4 Verification . . . 158
7.7 Failure Mode and Effects Analysis (FMEA) . . . 160
7.8 Economic Feasibility Assessment . . . 164
7.9 Closing Synthesis . . . 166

8 Conclusions and Future Work **167**
8.1 Fulfilment of Objectives . . . 167
8.2 Scientific and Industrial Contributions . . . 169
8.3 Limitations . . . 170
8.4 Future Work . . . 171

References **172**

A Changeovers Observations **178**

B Adjustment Values Spreadsheet **184**

C Standard Operating Procedures **186**

D Mathematical Optimisation Models **188**
D.1 Model 1: Mixed-Integer Linear Programming (MILP) . . . 188
D.2 Model 2: Name-Based Linear Program (LP) . . . 190

E Digital Tool Specifications **192**
E.1 Context Initialisation and SKU Validation . . . 192
E.2 Guided Execution Workflow . . . 193
E.3 Administrative Menu . . . 194

F Conceptual Design Trade Studies **196**
F.1 Actuation Candidates . . . 196
F.2 Transmission and Coupling Candidates . . . 197
F.3 Cardboard Storage Unit Torque Derivations . . . 198

G Transportation System Detailed Calculations **199**
G.1 Rejected Baseline Pulley Configuration . . . 199
G.2 Belt Length and Idler Tensioning Travel . . . 200
G.3 Jackshaft Force Resolution, Bearing Reactions, and Fatigue Derivation . . . 203

H Housing FEA Result Fields **206**
H.1 Cardboard Storage Unit Housings . . . 206
H.2 Transportation System Housing . . . 209

I Standard Mechanical Components Used **211**
I.1 Linear Units' Reference Sheet . . . 211
I.2 Transportation System's Linear Units . . . 212
I.3 Roller Conveyor's linear Units . . . 214
I.4 Roller Conveyor's Stepper Motor's Reference Sheet . . . 217
I.5 Stepper Motor's Technical Drawing . . . 221
I.6 Indexing Plungers Technical Sheet . . . 222
I.7 M20 Blanking Plug Technical Sheet . . . 224
I.8 O-Rings Technical Sheets . . . 226
I.9 Elastomer Jaw Coupling Technical Sheet . . . 230
I.10 Wiska M12 Blanking Plug and O-Ring Technical Sheets . . . 232

J Technical Drawings **234**

K Automatic Adjustment System's SCL Code **243**

List of Figures

1.1 OEE evolution in Lines 1, 2, 5 and 6 at Super Bock Group (SBG) from January 2024 to December 2025 . . . 2
1.2 Decomposition of the main time losses contributing to OEE reduction . . . 2

2.1 Beer Brewing Process . . . 7
2.2 Optimal Operating Condition of the Critical Machine [8] . . . 8
2.3 V-Graph of Machine Capacities Anchored to the Filler . . . 9
2.4 Changeover Duration Before and After SMED Implementation . . . 11
2.5 VDI 2221 Design Methodology Flowchart [50] . . . 19

3.1 Organisational Team Structure for SBG's Packaging Lines . . . 25
3.2 Innopack Kisters WSP Advanced Wrap-Around Shrink Packer [58]. . . . 26
3.3 M01 - Product Feeding Module (Line 2) . . . 27
3.4 M02 - Formatting Module (Line 2) . . . 27
3.5 M09 - Cardboard Cutouts Feeding Module (Line 2) . . . 28
3.6 M03 - Folding Module (Line 2) . . . 29
3.7 M05 - Rotation Module (Line 2) . . . 29
3.8 M04 - Film Module (Line 2) . . . 30
3.9 M07 - Retraction Module (Line 2) . . . 30
3.10 WestRock Cluster-Pak EVOTECH [59] . . . 31
3.11 Digital Position Indicator and Name Tag . . . 35

4.1 Examples of Inconsistent or Absent Identification Systems . . . 43
4.2 Spatial Coordinate System of the Cutout Transportation Mechanism . . . 45
4.3 Bottle Configurations by Box Type . . . 46
4.4 Absence of Defined Slider Configurations . . . 46

5.1 Folding Bracket Baseline Design . . . 51
5.2 Folding Bracket Legacy Disassembly Sequence . . . 51
5.3 Rest-Position Interference Testing on the Active Production Line . . . 54
5.4 New Bracket Design . . . 56
5.5 Bracket's Side Profile Comparison . . . 58
5.6 Slicer Results for the 3D-Printed Bracket . . . 58
5.7 Structural Obstruction of the Slider . . . 59
5.8 Initial Menu . . . 65
5.9 Consolidated SKU Comparison and Decision Panel . . . 68
5.10 System Initialisation, Input Validation, and Algorithmic Classification Sequence . . . 71
5.11 Guided SMED Execution Loop: Operator Workflow per Changeover . . . 71

7.1 Example of Cardboard Cutout Overlapping Error Due to Poor Adjustments . . . 92
7.2 Defective Cardboard Cutout . . . 93
7.3 Distribution of Occurrences Across the Universe of Observed Changeovers . . . 93
7.4 Time Distributions of Observed Changeovers Based on Their Frequency of Occurrence . . . 94
7.5 M09-060 Adjustment Point and Related Linear Guides . . . 95
7.6 Cardboard Roller Conveyor and Transverse Guide Adjustment Mechanism . . . 96
7.7 Cardboard Storage Unit and Respective Adjustment Points . . . 96
7.8 Cardboard Debris Present Throughout the M09 Module . . . 100
7.9 Roller Conveyor Transmission: Parallel Power Distribution to the Two Linear Guides 104
7.10 Roller Conveyor Direct-Drive Architecture: Stepper Motor, Coupling, and Housing Assembly . . . 110
7.11 M09-025 Transmission: Direct Spur-Gear Drive to a Single Linear Guide . . . 114
7.12 M09-021 Transmission: Sequential Drivetrain with Dual-Bearing-Isolated Universal Joint . . . 114
7.13 M09-010/012 Transmission: Parallel Chain-and-Sprocket Drive to Two Linear Guides . . . 114
7.14 Transportation System Transmission: Three-Point Asymmetric Parallel Layout . 119
7.15 Rust buildup and Cardboard Dust . . . 120
7.16 Linear Unit 1 Spatial Envelope and Surrounding Clearances . . . 122
7.17 Linear Unit 2 Spatial Envelope and Surrounding Clearances . . . 123
7.18 Linear Unit 3 Spatial Envelope, Side View . . . 123
7.19 Boundary Conditions Established for the Roller Conveyor Housing FEA Validation 135
7.20 Von Mises Stress Results from the Roller Conveyor Housing FEA Simulation . . 136
7.21 Displacement Results from the Roller Conveyor Housing FEA Simulation . . . 136
7.22 Final 3D CAD Assembly for the Roller Conveyor Solution . . . 140
7.23 Cardboard Storage Unit CAD Assembly . . . 145
7.24 Boundary Conditions of the Housing Assembly in the Transportation System . . 147
7.25 Transportation System Solution CAD Assembly . . . 152
7.26 Completed PROFINET Network: CPU, HMI, and 12 Drives, All Assigned as IO Devices . . . 159
7.27 PROFIdrive Standard Telegram 3 Configuration, M09-001 LU1 Drive . . . 159
7.28 Positioning Axis Technology Object Hardware Interface Configuration, M09-001 LU1 . . . 159
7.29 FB_Motion_Sequence, Compiled with Zero Errors and Zero Warnings . . . 160

A.1 Illustrative Gantt Chart of observed Changeover . . . 183

E.1 Dropdown menus in the initial interface . . . 192
E.2 SKU validation states . . . 192
E.3 Complete and correct input data on the first interface . . . 193
E.4 Task rendering typologies . . . 193
E.5 Line-specific media support . . . 193
E.6 Administrative section access . . . 194
E.7 Add and Edit SKU features in the Admin Menu . . . 194
E.8 Historical Data feature inside the Admin Menu . . . 195

H.1 Boundary Conditions on the M09-025 Housing FEA Simulation . . . 207
H.2 FEA Simulation Results on the M09-025 Housing . . . 207

H.3 Boundary Conditions Established for Each Cardboard Storage Unit Housing Design 208
H.4 Stress and Displacement Results from the FEA Simulation on the M09-010/012 Housing 208
H.5 Stress and Displacement Results from the FEA Simulation on the M09-021 Housing 209
H.6 Stress Results from the FEA Simulation on the Transportation System Housing–Lid Assembly (Horizontal Orientation) 209
H.7 Displacement Results from the FEA Simulation on the Transportation System Housing–Lid Assembly (Horizontal Orientation) 210
H.8 Stress Results from the FEA Simulation on the Vertical-Orientation Transportation System Housing–Lid Assembly 210
H.9 Displacement Results from the FEA Simulation on the Vertical-Orientation Transportation System Housing–Lid Assembly 210

List of Tables

2.1 Evolution and Critical Considerations of Setup Reduction Methodologies 12
2.2 Comparative Analysis of Engineering Design Paradigms for Retrofitting 21

3.1 Technical Specification of Bottle and Can Packaging Lines at SBG 24
3.2 Technical Specification of Keg Packaging Lines at SBG 25
3.3 Kisters Changeover Classification 37

4.1 Range of Adjustment Values at M09-060 by Box Program 44

5.1 Comparison of Mechanical Properties for Candidate Bracket Materials [60–62]. . 53
5.2 Engineered FDM Process Parameter Matrix for the Functional PETG Folding Bracket. 57
5.3 Optimisation Problem Constraints 60
5.4 Comparison of Model 1 (Unconstrained Theoretical Optimum) and Model 2 (Deployed, Name-Based Configuration) 62
5.5 SKU Database Schema and Attribute Specifications 66
5.6 Kisters Machine Changeover Classification Rules 67
5.7 Historical Data Table Schema and Captured Metrics 70

6.1 Performance Comparison - Trolley Guide-Rail Pre-Adjustment 74
6.2 Performance Comparison – Proactive Retrieval of Format Parts 75
6.3 Statistical Comparison of Total Task Execution Times for Folding Bracket Adjustment. 77
6.4 Line 1 Changeover Duration Performance Metrics Before and After Software Optimisation 81
6.5 Master Synthesis of Operational States and Key Outcomes Across Chapters 5 and 6 84
6.6 Illustrative Ceiling Estimate for Combined Stage 1/2 Interventions, Lines 2 and 6. 86
6.7 Consolidated Annual Economic Impact of Deployed Interventions 89

7.1 Spindle Adjustment Points Distributed Across the Machine's Modules 92
7.2 Global Functional and Project Specifications 98
7.3 Pairwise Comparison Matrix for Actuation Selection Criteria 101
7.4 Weighted Decision Matrix for Actuation Selection (AHP-Derived Weights) . . . 101
7.5 Robustness Check: Equal-Weight Re-Evaluation 101
7.6 RK Rose+Krieger EP-II 40 Linear Unit Specifications 103
7.7 Architecture Evaluation Matrix for the Roller Conveyor Actuation Solution . . . 107
7.8 Comparative Specifications of Standard NEMA Stepper Motor Frames 108
7.9 Roller Conveyor NEMA 34 Stepper Motor Specifications 108
7.10 GWE 5104 Coupling Specifications 109

7.11 Torque Measured at the Cardboard Storage Unit Adjustment Points 113
7.12 Cardboard Storage Unit Torque Sizing Results 115
7.13 Cardboard Storage Unit NEMA 34 Stepper Motor Specifications 116
7.14 Comparative Analysis of Synchronous Belt Tooth Profiles for High-Stiction Applications 125
7.15 Technical Specifications of the Finalised, Load-Optimised Two-Stage HTD 5M System 126
7.16 Jackshaft Axial Geometry and Coordinate Map 132
7.17 Hand Calculation vs. KISSsoft Cross-Validation 133
7.18 Roller Conveyor Fastening and Joint Specification Matrix 140
7.19 Cardboard Storage Unit Housing FEA Results 142
7.20 Cardboard Storage Unit Joint Fastening Specification Matrix 144
7.21 Transportation System Fastening Specification Matrix 152
7.22 Safety Factor Synthesis Matrix - Complete System Overview 153
7.23 PLC Network Devices and IP Addressing 156
7.24 Motion Control Technology Object Architecture 157
7.25 Sequence State Machine 158
7.26 Failure Mode and Effects Analysis - Governing Items by Subsystem 161
7.27 Estimated Bill of Materials - Automatic Adjustment System 165

A.1 Changeover Observations Log (February – May 2026) 178
A.2 Clusters of Kisters' Tasks by Module 179
A.3 Clusters of Mead's Tasks by Module 181

G.1 Technical Specifications of the Initial Baseline Proposal for the Two-Stage HTD 5M System 199

List of Acronyms

FEUP Faculty of Engineering of the University of Porto
SDG Sustainable Development Goal
SBG Super Bock Group
OEE Overall Equipment Effectiveness
SMED Single Minute Exchange of Die
SKU Stock Keeping Unit
SOP Standard Operating Procedure
DSR Design Science Research
TPM Total Productive Maintenance
TPS Toyota Production System
CIP Clean In Place
AR Action Research
PETG Polyethylene Terephthalate Glycol
FDM Fused Deposition Modelling
MILP Mixed-Integer Linear Programming
HMI Human-Machine Interface
BMT Breakdowns and Malfunctions Time
COT Changeover Time
RUT Ramp-Up Time
DFMA Design for Manufacture and Assembly
FMEA Failure Mode and Effects Analysis
OR Operations Research
DFC Design for Changeover
KPI Key Performance Indicators

Chapter 1

Introduction

This dissertation in Mechanical Engineering is developed within the business context of Super Bock Group (SBG), as the culminating project for the Master's Degree in Mechanical Engineering at the Faculty of Engineering of the University of Porto (FEUP). The focus of this study is the integration of Single Minute Exchange of Die (SMED) methodology with Machine Design optimisation, to reduce changeover and ramp-up times in beverage packaging lines. This work was conducted in the second semester of the academic year 2025/2026.

1.1 Context

In recent decades, various production industries have undergone profound transformations in their product portfolios and production environments. To achieve visibility, market coverage, and a competitive edge, businesses were required to adapt and produce different variations of their products, in size, packaging, labelling, or type. This transformation resulted in higher operating costs and complexity. Additionally, the different industries had to adapt their production lines to produce multiple products using the same machines. This resulted in time losses due to changeover and ramp-up procedures.

A changeover is the process of stopping production to reconfigure equipment on the production lines for the next Stock Keeping Unit (SKU). Ramp-up denotes the time required for the line to resume nominal-speed operation. According to the Overall Equipment Effectiveness (OEE) framework, the non-productive time associated with this process (changeover and ramp-up) is categorised as Setup and Adjustment loss, which constitutes a primary element of Availability loss.

Similar to other businesses in the food and beverage industry, SBG must adapt its production processes to address changing consumer trends and requirements. From January 2024 to December 2025, OEE performance across Lines 1, 2, 5 and 6 remained relatively stable, fluctuating within a range of approximately 54% to 66%, with an overall average of 58.8% (Figure 1.1). No sustained upward or downward trend is observed; instead, the indicator demonstrates a recurring seasonal pattern, with relative peaks in July and August in both years and troughs concentrated

around January, April, and December. This consistency suggests that the efficiency losses examined in this dissertation are structural rather than isolated or transient, underscoring the importance of a systematic analysis of their underlying causes.

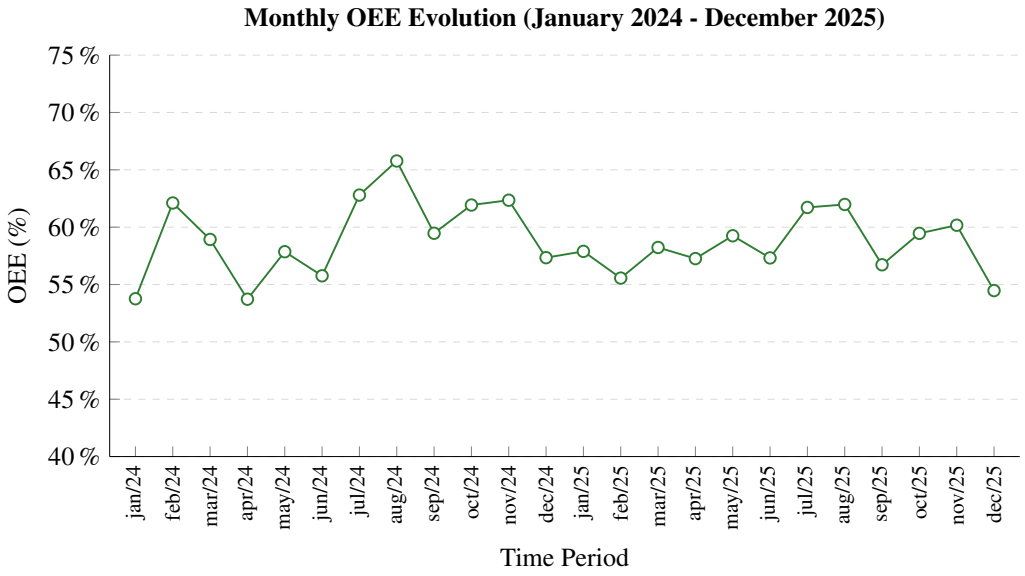


Figure 1.1: OEE evolution in Lines 1, 2, 5 and 6 at SBG from January 2024 to December 2025

Figure 1.2 presents the distribution of the most relevant time losses contributing to OEE reduction, in Lines 1, 2, 5 and 6 during 2025 production (annual OEE averaged 61.63%). The time losses are mainly influenced by the Breakdowns and Malfunctions Time (BMT), and, most relevant to this dissertation, both the Changeover Time (COT) and Ramp-Up Time (RUT).

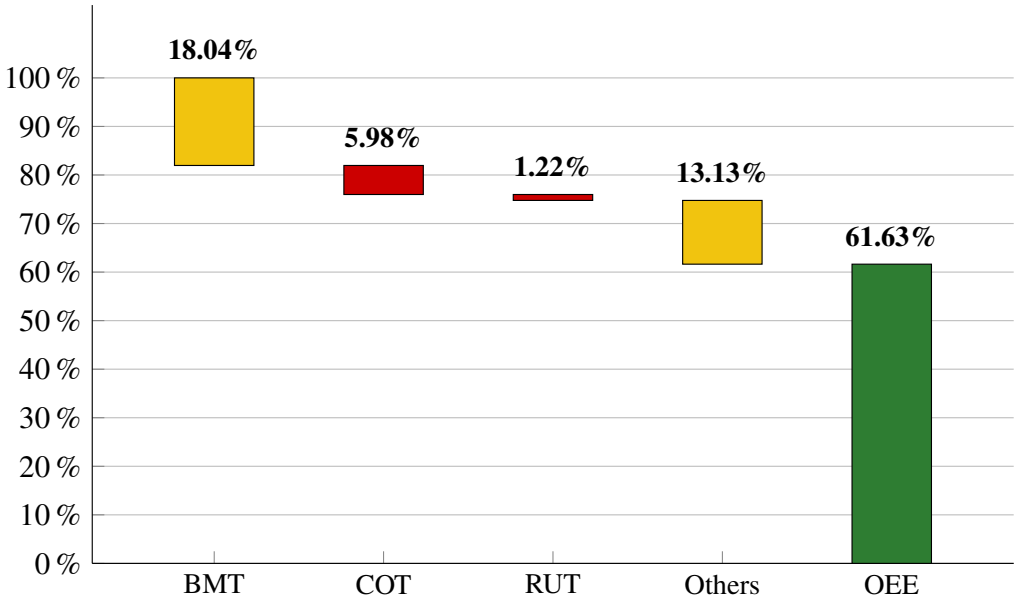


Figure 1.2: Decomposition of the main time losses contributing to OEE reduction

1.2 Motivation and Problem Statement

Although breakdown and malfunction losses (18.04%) are greater in aggregate than changeover and ramp-up losses ($\approx 7.2\%$), they are not the focus of this study. Breakdown reduction is addressed within maintenance engineering and Total Productive Maintenance (TPM), which manage stochastic failures through reliability and condition-monitoring strategies. In contrast, changeover is a planned, recurring, and deterministic event whose duration is determined by procedure and machine design, which are the variables examined in this dissertation. Changeover represents the most controllable loss and is concentrated on a single identifiable bottleneck, the Kisters. Furthermore, its significance is understated when considering downtime share alone: shorter, repeatable setups reduce the batch-size constraint that increases inventory and limits responsiveness to demand. Therefore, the recovered capacity provides strategic value beyond the minutes regained.

This project studies four bottling and canning lines (Lines 1, 2, 5, and 6) and focuses on the packing machines (Kisters and Mead). An analysis of 24 months of production-order data demonstrates that the Kisters machine served as the line-critical bottleneck during a significant proportion of changeovers across all four lines, reaching up to 47.8% on Line 5. In contrast, the Mead packer was identified as line-critical only five times during the same period. Preliminary shopfloor observations reveal two primary root causes for this loss: a procedural factor, involving task allocation and the absence of standardisation across shift teams, and a physical factor, concerning the reliability of the machine's adjustment indicators. These causes require distinct intervention strategies, which form the central premise of this dissertation: SMED and machine design represent two essential, sequential stages within a unified improvement process for SBG's packaging lines.

1.3 Objectives

The primary objective of this dissertation is to reduce the changeover and ramp-up times on SBG's beverage packaging lines through the application of SMED-based process improvements and the mechanical redesign of adjustment mechanisms. This objective is addressed through five specific objectives, each corresponding to a distinct stage of the research.

1. The current-state changeover process is diagnosed and classified by distinguishing critical from non-critical changeovers and quantifying the contribution of each task to overall downtime.

2. The SMED methodology is applied to the Kisters and Mead machines by separating internal from external setup tasks, converting internal tasks to external where feasible, and streamlining the remaining internal operations.

3. A mathematical optimisation model for the machine's adjustment values is formulated and validated, thereby replacing operator trial-and-error with a standardised, repeatable configuration.

4. A digital changeover support tool is designed and deployed to sustain standardisation across shifts and to reduce classification and data-entry errors.

5. An automatic adjustment system is developed to eliminate the manual tasks that procedural improvements cannot address, expanding beyond the threshold of procedural SMED.

The objectives constitute a unified, cumulative sequence rather than discrete workstreams. Objective 1 establishes the empirical baseline. Objective 2 applies classical SMED methodology to this baseline. Objectives 3 and 4 extend SMED beyond its conventional procedural scope by incorporating mathematical optimisation and digital standardisation. Objective 5 represents the transition from procedural to mechanical intervention, which is pursued only after the diminishing returns of the preceding stages have been demonstrated.

The primary distinction between the two phases of this research is not the presence of mechanical design, but its intended function. In Objective 2, design facilitates streamlining; for example, the folding bracket increases the speed and repeatability of a manual task, although the task remains manual. In contrast, Objective 5 fundamentally differs: once process improvements have reduced a task to its irreducible manual minimum, the automatic adjustment system eliminates the manual component entirely rather than merely accelerating it. Identifying the point at which component-level streamlining is exhausted and only system-level automation provides further improvement defines the design ceiling that this dissertation aims to locate and surpass.

1.4 Dissertation Structure

This dissertation comprises eight chapters.

Chapter 2 reviews the base literature, including Lean Manufacturing, 5S, SMED, mathematical optimisation of setup operations, Industry 5.0, and the digitalisation of tacit knowledge, as well as engineering design frameworks for retrofitting, such as VDI 2221. The chapter concludes by identifying the research gap this work addresses.

Chapter 3 outlines the production floor, describes the Mead and Kisters equipment under investigation, and details the methodology for observing and classifying changeovers.

Chapter 4 provides a diagnostic analysis of the current-state production system, establishing the baseline for evaluating proposed solutions.

Chapter 5 presents the proposed solutions, consisting of task separation, externalisation, and streamlining; the redesign of the folding bracket; the adjustment-value optimisation model; and the digital changeover support tool.

Chapter 6 reports the results of these interventions, evaluated against the Key Performance Indicators defined for the project.

Chapter 7 presents the case study central to Objective 5, focusing on the systematic engineering design of an automatic adjustment system for the Kisters machine.

Chapter 8 concludes the dissertation by evaluating the achievement of each objective, articulating the scientific and industrial contributions, discussing limitations, and proposing directions for future research.

Chapter 2

Literature Review

This chapter synthesises existing literature to establish the theoretical foundation for an integrated framework that combines SMED methodology with mechanical retrofit design to reduce changeover time. The chapter first outlines the brewing and packaging-line context that motivates the production environment under study, followed by a review of the operational concepts of Lean Manufacturing, 5S, and SMED. Subsequently, mathematical optimisation techniques for setup operations and the Industry 5.0 perspective on digitalising tacit knowledge are presented. The argument then shifts to mechanical engineering frameworks, including Design for Changeover, automated positioning systems, and VDI 2221, which lay the basis for the proposed retrofit. The chapter concludes by identifying the research gap at the intersection of operational and mechanical engineering domains that this dissertation aims to address.

2.1 Beer Brewing Process

Although beer consumption has a history spanning millennia [1], the pertinent context for this analysis is the shift from artisanal to industrial production. The introduction of the thermometer, saccharometer, and microbiological control during the eighteenth and nineteenth centuries established the standardisation necessary for modern high-speed beverage filling lines [2] .

This standardisation is directly relevant to the packaging line, as filling performance relies on the consistency of upstream brewing processes. Variability in the beer's physicochemical properties, such as CO_2 saturation, temperature, and colloidal stability, affects the filling valve and can lead to excessive foaming or incorrect fill levels [3]. These deviations increase rejection rates and require more unplanned stops or manual intervention, consequently undermining the standardised conditions required for effective SMED implementation and demonstrating that physical process stability is a prerequisite for operational optimisation. This upstream process consists of several stages presented in Figure 2.1.

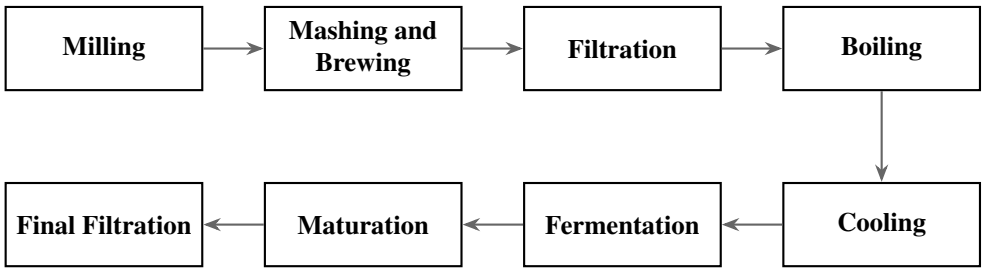


Figure 2.1: Beer Brewing Process

2.2 Packaging Lines

This section presents an overview of packaging-line machinery and associated design principles. A packaging line is a system of individual machines connected by conveyors and buffers, which are functionally integrated to perform a packaging task [4]. In the beer industry, three primary line types are used: bottles, cans, and kegs.

Although core filling machinery is largely standardised, line design is determined by its intended application. Flexible lines accommodate short production runs and varied formats, while dedicated lines maximise throughput for a single product. The choice between extensive parallel units with large buffers and a lean serial layout depends on available floor space and capital investment [5]. Since constructing a new line requires significant capital, engineering efforts typically focus on upgrading existing lines rather than building new ones [6]. This constraint, combined with ongoing pressures related to cost and product consistency, underpins this thesis's focus on changeover time [7].

A beer packaging line proceeds through a sequence of inspection, filling, sealing, pasteurisation, and labelling stages, with variations primarily determined by the container type. One-way bottles and cans follow a similar process, differing only in capping versus double-seam sealing, whereas returnable bottles first undergo a dedicated washing stage. The final stage before palletising is packing, which constitutes the primary focus of this project. Given that the SKU portfolio includes loose-bottle boxes, multipacks, and trays, packing requires dedicated machines arranged in series. For example, a tray containing four six-packs requires one machine to form the six-packs and another to group and shrink-wrap them. This diversity of configurations and the consequent need to reconfigure several machines during each changeover represent the central operational challenge addressed in this thesis.

2.2.1 Packaging Lines Design

The design of a packaging line begins with establishing project requirements: package types and configurations, production volume and speed, space limitations, and industry standards. Even minor differences carry through the whole line. The choice between one-way glass, returnable glass, or both, and between formats such as 10-packs, 6-pack trays, or 30-loose boxes, affects every machine, buffer, and spatial allocation. Because these variables are interdependent, requirements

gathering is iterative and continues throughout the design process, alongside decisions on operator count, equipment placement, and Clean In Place (CIP) requirements [6]. Most breweries outsource this design and construction to specialised packaging-system suppliers rather than maintaining an in-house team.

Modern packaging lines are universally designed using a two-component buffer strategy. The first is buffering through accumulation, which may be static (physical accumulation tables) or dynamic (varying the length and speed of conveyors between machines).

The second component is set by each machine's speed. The critical, or core, machine establishes the line's nominal speed, based on factors such as process and quality requirements, mechanical complexity, productivity and availability, capable speed, and machine cost [8]. In most beverage lines, the filler is the critical machine, setting the pace for all others, and its continuous operation is essential to productivity. To guarantee uninterrupted flow, machines upstream and downstream of it are provided with surplus capacity, ensuring a consistent infeed supply and adequate discharge space (Figure 2.2) [5]. This surplus allows them to recover after a stoppage: once the buffer has been partially depleted, the extra speed returns the system to its pre-failure condition. Structurally, each upstream machine is designed with higher capacity than the one after it, and each downstream machine with higher capacity than the one before, typically in 10% increments [8].

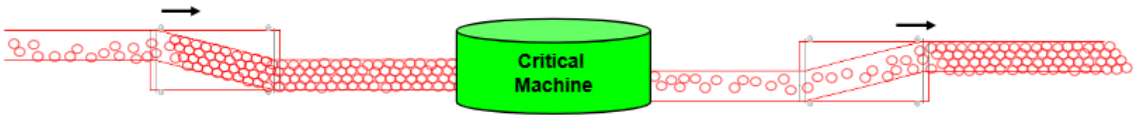


Figure 2.2: Optimal Operating Condition of the Critical Machine [8]

This configuration results in a "V-graph" of production capacities across the stages of the line, with the filling unit representing the lowest capacity point. The V-graph serves as a key visual tool in buffer strategy, illustrating the maximum output of machine groups in operational sequence (Figure 2.3). Machines adjacent to the core unit are intentionally provided with additional capacity, producing a V-shaped profile anchored by the core stage. In certain cases, the filler does not serve as the critical machine. For example, when producing smaller-sized boxes (such as 12-loose or 15-loose boxes), the packer becomes the line's bottleneck, demanding adjustments to the V-graph. With the evolution of packaging lines and their machines' reliability, the V-graph curve might flatten as buffers become obsolete [5].

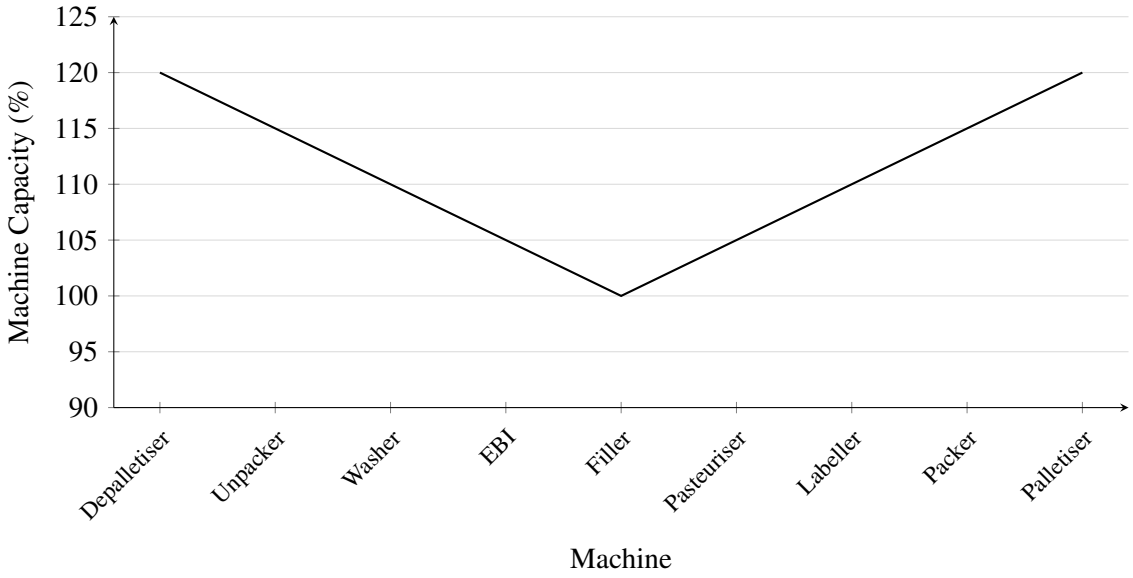


Figure 2.3: V-Graph of Machine Capacities Anchored to the Filler

2.3 Lean Manufacturing

Lean Manufacturing originates in the Toyota Production System (TPS). Ohno [9] reframed production around a timeline perspective rather than batch quantity, arguing that the push logic of the Fordist mass-production model generates overproduction, which he identified as the most fundamental of seven wastes (muda), since it masks and accumulates the others: waiting, transportation, over-processing, excess inventory, unnecessary motion, and defects. Womack and Jones [10] later formalised this as Lean Thinking, a shift from individual machines to continuous product flow, and added an eighth waste: underutilised human potential.

In the beverage industry, these wastes take specific forms, and Lean flow meets process-industry constraints. Production is governed by the physical properties of the liquids handled and by mandatory, time-intensive CIP sanitation cycles [11]. Over-processing appears as container overfilling, causing substantial material loss at high volume, while waiting is driven by CIP cycles and upstream starvation [12]. For food and beverage processors, continuous flow is not only an efficiency measure but a determinant of quality and safety, since shorter lead times mitigate shelf-life degradation [12].

Sustainable waste elimination depends on stabilising process variability. Liker [13] holds that standardised work is the basis for all improvement, a principle that Costa et al. [14] apply to food and beverage packaging, where lean practice must be combined with statistical process control to prevent line stoppages and cascading defects. This requirement for standardisation provides the basis for the transition to the 5S and SMED methodologies discussed next.

2.4 5S Methodology

While Lean provides a framework for eliminating waste, the 5S methodology establishes the physical and operational baseline necessary for process stability. Within the context of SMED, 5S is frequently misunderstood as mere housekeeping. However, the literature defines it as a management system that creates a visual workplace in which abnormalities are immediately apparent [15]. Osada [15], the foundational theorist of 5S, asserts that without the discipline of Sort (Seiri), Set in Order (Seiton), Shine (Seiso), Standardise (Seiketsu), and Sustain (Shitsuke), advanced optimisation efforts are built on an unstable foundation. Gapp, Fisher, and Kobayashi [16] further argue that 5S achieves its intended outcomes only when implemented as an integrated management system rather than as a series of isolated tasks.

Three of the 5S pillars directly influence changeover performance in beer packaging. Seiso integrates cleaning with inspection, enabling early detection of mechanical wear or fluid leaks common in bottling before they cause unplanned downtime during changeovers. Seiton addresses the searching waste identified by Shingo [17] as a primary contributor to internal setup time. Systematically arranging tools and change parts by frequency of use [18] allows external components such as star wheels, guides, and labelling plates to be staged while the machine remains operational. Without this arrangement, the internal-to-external transition central to SMED remains inconsistent. Seiketsu sustains these improvements: standardised toolkits and staged setups, maintained consistently across shifts, prevent sorting and ordering from reverting to disorder [18], thereby establishing the reliable baseline required for effective SMED interventions. Consequently, 5S serves as a continuous stabilising force, enabling SMED to achieve and sustain rapid changeovers.

2.5 Single Minute Exchange of Die

Within manufacturing performance management, OEE serves as the standard metric for evaluating equipment performance under the TPM framework, integrating Availability, Performance, and Quality into a single composite index [19]. According to Nakajima's [19] taxonomy of the "Six Big Losses", planned downtime for format changeovers, referred to as Setup and Adjustment loss, is classified as a primary Availability loss, distinct from unplanned equipment failures or in-process quality defects. In high-variety beverage packaging lines, this loss category is particularly significant. Rossi-Huamán et al. [20] identify changeovers as the principal driver of OEE loss in high-variety beverage bottling operations. In OEE terms, SMED is the tool specifically designed to reduce the Setup and Adjustment component of Availability loss. The OEE baseline values reported in Chapter 1 quantify the magnitude of this loss at SBG's lines prior to intervention.

The SMED conceptual framework originated to address the economic demands of high-variety, low-volume manufacturing. Primarily developed by Shigeo Shingo, SMED was formalised to mitigate the bottleneck of setup times, which historically required large order sizes and elevated inventory levels. According to Shingo [17], setup operations are not immutable constraints but variables that can be optimised through systematic analysis. The primary objective of SMED is

to minimise the time required to transition a machine from producing the last acceptable product of one batch to the first acceptable product of the next, ideally achieving a single-digit number of minutes. For more complex changeovers, this target may be adjusted.

Shingo's methodology is based on a fundamental distinction between two categories of activities: Internal Setup Activities, which are operations that can only be performed when the machine is stopped , and External Setup Activities, which are operations that can be performed while the machine remains in production. Shingo [17] outlines four conceptual stages for SMED implementation, described in the following topics and depicted in Figure 2.4.

- **Preliminary Stage: As-Is -** At this stage, no distinction exists between internal and external setup activities. Operators perform tasks without a defined sequence, resulting in considerable machine downtime.
- **Stage 1: Separation of Internal and External Setup Activities -** This stage is considered the most critical. By identifying tasks that can be performed while the machine is operating, Shingo contends that setup times can be reduced by 30% to 50% without significant equipment modifications.
- **Stage 2: Conversion of Internal Setup to External Setup -** This stage requires re-evaluating internal tasks to determine whether they can be shifted to external time. Examples include pre-setting measurements and utilising standardised fixtures.
- **Stage 3: Streamlining All Aspects of the Setup Operation -** After tasks have been separated and converted, the remaining internal and external activities are optimised through parallel operations, the use of functional clamps, and the elimination of unnecessary adjustments.

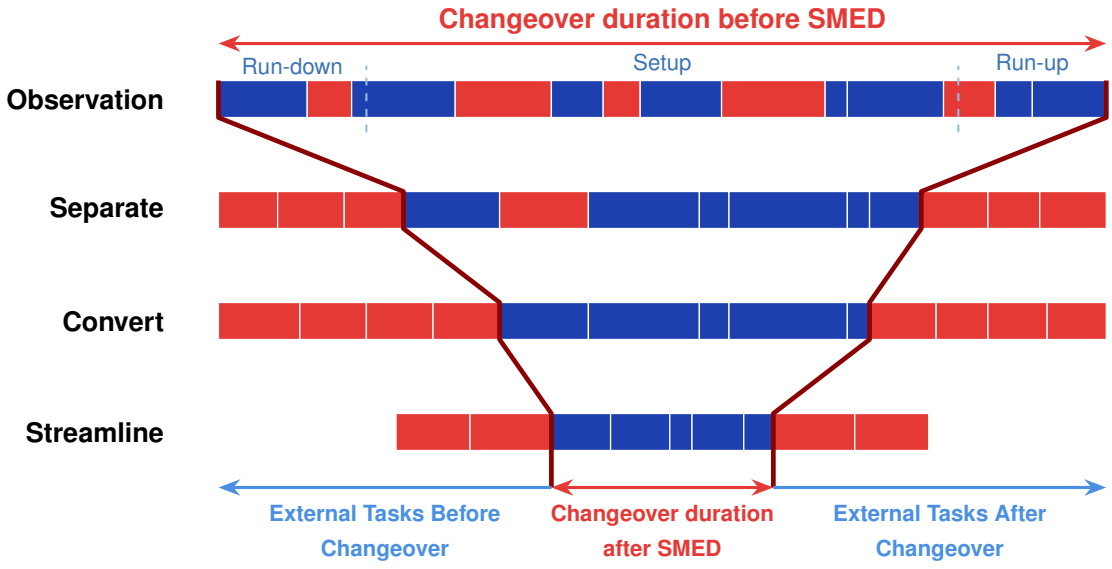


Figure 2.4: Changeover Duration Before and After SMED Implementation

Although Shingo's methodology has been transformative, academic discourse has identified notable limitations in its original application. McIntosh et al. [21] argue that Shingo's approach emphasises procedural and organisational changes, often overlooking constraints imposed by mechanical design. They assert that Shingo's stages presuppose equipment flexibility sufficient for rapid changeovers. In the context of complex machinery, such as high-speed beer packaging lines, procedural improvements eventually encounter a design ceiling, particularly since production companies typically do not design the equipment they use. This critique emphasises the need to move beyond organisational adjustments and pursue technical redesigns, such as implementing adjustable guide rails or automated changeover systems, to overcome inherent physical limitations.

Recent literature has pursued enhancing Shingo's classical model by integrating it with other Lean tools to establish foundational stability. Rossi-Huamán et al. [20] demonstrate the operational synergy between 5S and SMED specifically within beverage bottling environments. Their research indicates that without a disciplined 5S environment, the External Setup phase of SMED remains inefficient due to time lost searching for tools or managing disorganised workspaces. Their case study confirms that an integrated 5S approach significantly reduces setup variations and establishes the baseline stability necessary for SMED to achieve sustainable changeover reductions in complex packaging settings.

As packaging machines increase in sophistication, reliance on trial-and-error adjustments, often the most time-consuming aspect of internal setup, becomes a significant liability. Almomani et al. [22] propose integrating conventional SMED with Multiple Criteria Decision-Making techniques. Their research suggests that, in high-complexity environments, the selection of technical solutions such as universal guide rails or standardised modular components should be guided by rigorous evaluation of technical feasibility, cost, and impact on cycle time. This transition from intuition-based to engineered setups aligns with the evolving requirements of the beverage industry, where format changes demand high precision and repeatability.

Table 2.1 synthesises the literature discussed in the SMED section, summarising the focus and boundaries of procedural tools' capacity.

Table 2.1: Evolution and Critical Considerations of Setup Reduction Methodologies

Methodology & Authors	**Core Paradigm**	**Focus**	**Limitations**
Classical SMED Shingo [17]	Procedural separation and conversion of Internal and External setup activities.	Standardising and optimising human workflows to minimise machine idle time.	Can face diminishing returns when setup variance stems from inherent analog or manual machine calibrations.

Continued on next page...

Table 2.1 – Continued from previous page

Methodology & Authors	Core Paradigm	Focus	Limitations
Integrated 5S & SMED Rossi-Huamán et al. [20]	Synergising workplace organisation with setup sequence optimisation.	Establishing environmental stability, workspace visibility, and predictable tool staging.	Leaves the underlying kinematic constraints of the machinery unaddressed.
Multi-Criteria SMED Almomani et al. [22]	Algorithmic frameworks for evaluating and prioritising setup improvement vectors.	Quantifying operational, economic, and complexity metrics to justify tactical interventions.	Typically requires secondary engineering design frameworks to map to physical hardware constraints.
Classical SMED Critique McIntosh et al. [21]	Critical evaluation of the practical limits and structural assumptions of Shingo's approach.	Highlighting operational contexts where procedural optimisations yield plateauing performance gains.	Does not prescribe a standardised mechanical design methodology to alter equipment architecture.

2.6 Mathematical Optimisation in Setup Operations

Although the SMED methodology defines a core approach for eliminating waste during machine changeovers, its traditional application remains heuristic. Shingo's [17] procedural rules specify task organisation but lack mathematical mechanisms for determining optimal machine parameters. In highly constrained, multi-format packaging environments, reliance on operator intuition to configure machines introduces variability and subpar performance. To address this issue, contemporary manufacturing increasingly employs Operations Research (OR) and mathematical optimisation.

2.6.1 Operations Research in Setup Reduction

In OR, the reduction of changeover inefficiencies is typically addressed through production planning and scheduling optimisation. Allahverdi [23], in a comprehensive review of setup considerations in manufacturing, observes that most mathematical literature focuses on Sequence-Dependent Setup Times. In this framework, the time required to adjust a machine depends on the immediate predecessor product. Traditional OR methodologies minimise total setup time by algorithmically routing and scheduling production orders to group similar formats. Although this

approach effectively reduces the frequency of major changeovers, it treats the physical changeover process as a fixed, immutable time penalty. It optimises the sequence of changeovers but does not address the machine's mechanical execution or spatial configuration limits.

Addressing this gap requires selecting among several optimisation paradigms capable of handling spatial configuration problems: metaheuristics such as Genetic Algorithms (GA) and Simulated Annealing (SA), Non-Linear Programming (NLP), unsupervised clustering methods such as K-means, and Mixed-Integer Linear Programming (MILP). The optimal choice depends on the specific structure and scale of the problem, rather than any inherent superiority of a particular method.

Metaheuristics are typically preferred for large-scale, NLP-hard combinatorial problems where exact methods become computationally intractable. For small-to-moderate-scale problems, exact methods remain tractable and are preferable because they guarantee a global optimum and, unlike stochastic metaheuristics, consistently return the same solution on every run [24]. Reproducibility is particularly important in mechanical positioning contexts, as a non-deterministic optimiser would undermine the standardisation that SMED aims to achieve. Non-Linear Programming is unnecessary in this context because the governing geometric relationships in machine changeover (clearances, reach limits, indexer travel) are additive functions of linear position variables. Therefore, no nonlinear formulation is required, and introducing one would increase the risk of local-optimum entrapment without providing structural benefits. Unsupervised clustering methods such as K-means can group values by dimensional similarity [25], but operate solely on distance minimisation in feature space. They lack mechanisms for encoding hard physical constraints, such as maximum indexer travel or mutual exclusivity between configurations, and therefore cannot guarantee a feasible mechanical solution.

MILP combines strengths that the other methods individually lack for the specific types of problems that can be encountered in beverage filling lines: it guarantees a global, reproducible optimum at this problem scale, and it natively expresses the changeover problem's actual structure (continuous spatial positions alongside discrete configuration or group assignment), which none of GA, SA, NLP, or K-means does simultaneously. As established in the production planning literature, MILP can encode physical boundaries, mechanical interferences, and spatial limits directly as linear inequality constraints. MILP provides an effective framework for modelling complex industrial systems including both continuous and discrete variables [26]. Within physical machine changeovers, continuous variables typically govern spatial parameters, such as the exact positioning or linear displacement of adjustable mechanisms. In contrast, discrete variables (binary or integer-valued) denote logical states and operational decisions, such as assigning a specific product format to a standardised machine configuration.

2.6.2 Bridging SMED with Mathematical Programming

Despite the established maturity of both SMED and MILP, a significant gap exists in the literature regarding their direct integration on the shop floor. In the beverage and packaging industry, MILP has been validated as an effective tool for optimising sequence-dependent setup times. However,

a critical review indicates that its application is predominantly limited to macro-level production scheduling and lot-sizing [27, 28]. Its application at the micro-level, specifically for discretising and optimising continuous physical spatial constraints, such as guide rail positioning, remains underexplored.

Manual adjustment of continuous mechanisms, such as a threaded rod on a packaging machine, effectively constitutes an attempt to solve a spatial optimisation problem through trial and error. Applying MILP to cluster various SKU dimensions into discrete, mathematically optimised physical configurations constrains the machine's infinite adjustability into a finite set of optimal, zero-variance setpoints. This transition from heuristic manual adjustment to mathematically validated configurations represents an essential evolution of SMED, guaranteeing that machine parameters meet both rigorous kinematic safety requirements and the requirements for standardised human operation. This thesis addresses this gap by applying MILP not to scheduling changeovers but to mathematically optimising the physical kinematics of the SMED intervention.

2.7 Industry 5.0 and the Digitalisation of Tacit Knowledge

Although mechanical retrofitting and mathematical optimisation establish the physical constraints required for rapid changeovers, the sustainability of these improvements relies on strict adherence to standardised procedures. Rather than viewing digitalisation solely as an extension of Industry 4.0's efficiency-focused agenda, Breque et al. [29] define Industry 5.0 in terms of three complementary pillars: human-centricity, resilience, and sustainability. This framework explicitly positions technology as a means of empowering rather than replacing the worker. In traditional Lean Manufacturing, the maintenance of SMED and 5S practices is highly dependent on operator discipline and paper-based Standard Operating Procedures (SOPs). In complex environments such as beverage packaging, reliance on static documentation often leads to the accumulation of tacit knowledge. This experiential knowledge, retained by veteran operators, is difficult to transfer to new or temporary employees [30]. The resilience pillar specifically addresses this vulnerability by promoting process continuity that is independent of individual operator presence.

The literature examining the relationship between Lean methodologies and Industry 4.0 technologies (often termed "Lean 4.0") supplies this technology layer. Buer et al. [30] argue that Industry 4.0 technologies should be regarded not as replacements for Lean Production, but as enablers that confront the inherent limitations of established continuous improvement tools. Tortorella and Fettermann [31] demonstrate that manufacturers integrating digital assistance tools with Lean practices achieve significantly higher operational performance than those employing either approach independently. In machine setups, digitalising procedures ensures that external preparation tasks and internal mechanical adjustments are performed with consistent accuracy across shifts and teams [32].

A common misconception about automation in manufacturing is the belief that the ultimate objective is a fully autonomous, human-free shop floor. This is precisely the misconception Industry 5.0 corrects. Romero et al.'s [33] "Operator 4.0" typology - a skilled worker who collaborates with

robots and is supported by cognitive and physical assistance systems - is cited within the European Commission's own Industry 5.0 report as a direct conceptual antecedent of its human-centricity pillar [29].

Changeovers in high-speed packaging lines involve complex decision-making, particularly when assessing differences between current and subsequent SKUs, such as identifying which format parts and guide rails require adjustment. Providing operators with digital decision-support tools significantly reduces cognitive load. Fast-Berglund et al. [34] classify this as "cognitive automation" and observe that delivering dynamic, context-aware information to shop-floor workers reduces human error and accelerates task completion. Rather than relying on manual comparison and memory, digital support tools algorithmically specify the required parameters, thereby standardising the procedure.

The final and arguably most challenging phase of the 5S methodology is Shitsuke (Sustain). Academic discourse indicates that operational improvements often deteriorate over time if new standards are not fully embedded into daily workflows. Digital SOPs mitigate this degradation by replacing static, frequently overlooked paper manuals with interactive, phase-based guidance [35].

Erol et al. [36] observe that digital assistance systems can deliver step-by-step visual media and real-time validation, consequently bridging the gap between theoretical training and practical execution. In SMED, digital SOPs ensure strict enforcement of the separation between internal and external tasks through the software workflow. By formalising tacit knowledge within a digital logic engine, organisations can separate machine changeover efficiency from individual operator experience [37, 38]. This digitalisation offers a robust safeguard against operational disruptions resulting from workforce turnover and the pronounced seasonality characteristic of the brewing industry.

2.8 Engineering Design in Retrofitting

Operational methodologies such as SMED identify inefficiencies; however, addressing the equipment's physical limitations requires a comprehensive mechanical engineering strategy. In the beverage packaging industry, the substantial capital expenditure required to equip packaging lines makes it economically impractical to replace legacy machinery to meet newer high-variety demands. As a result, production optimisation often depends on retrofitting, which involves engineering modifications to existing systems to improve performance, increase flexibility, or automate manual processes while preserving the core machine architecture. This section establishes the context for how retrofitting bridges operational methodologies and engineering solutions.

2.8.1 Design for Changeover

To connect operational setup reduction with mechanical engineering, academic literature has introduced the concept of Design for Changeover (DFC). While classical SMED methodology primarily targets organisational and procedural improvements, it ultimately faces physical constraints

that must be addressed through design. Mileham et al. [39] argue that achieving world-class responsiveness requires manufacturing to progress by implementing direct physical modifications to equipment. Thus, DFC emerges as a mechanical engineering extension of operational strategies like SMED.

Formalised by researchers at the University of Bath [21, 39], DFC converts the operational objectives of SMED into concrete mechanical design guidelines. A key insight in DFC literature is the distinction between the setup phase, involving the physical exchange of parts, and the ramp-up phase, which consists of trial-and-error calibration to achieve full-quality production. Mileham et al. [39] report that industries often lose up to ten times as much production capacity during the ramp-up phase as during the actual setup. Consequently, DFC strongly promotes mechanical designs that inherently remove the need for post-setup adjustments.

In practical retrofitting, adherence to specific mechanical design rules is essential. The fundamental principles of DFC require the complete removal of continuous, infinitely variable adjustment mechanisms, such as threaded rods or friction clamps, in favour of discrete, exact-constraint locating points [39]. Additionally, DFC prescribes replacing standard threaded fasteners with quick-release mechanisms, quarter-turn fasteners, and captive hardware to eliminate inefficiencies associated with tool searching.

Recent studies have extended classical DFC by integrating it with contemporary Lean and ergonomic design frameworks. Braglia et al. [40] introduce Quick Changeover Design (QCD), a methodology that incorporates error-proofing Poka-Yoke principles directly into the mechanical structure of machines. By designing hardware interfaces that cannot be assembled incorrectly or adjusted outside of specifications, the mechanical design proactively prevents human error. In retrofitting legacy packaging equipment, the application of DFC and Poka-Yoke principles ensures that new mechanisms consistently reduce internal setup time and eliminate variability related to operator skill levels [40]. Mechanical Poka-Yoke at the level of individual fixtures and locating mechanisms is comparatively under-documented in peer-reviewed literature outside QCD's broader framework, with most available treatments appearing in trade and practitioner publications rather than academic venues [41, 42].

Research has expanded the design-stage focus to include packaging equipment. Götz et al. [43] propose a structured design approach for format-flexible packaging machines that integrates technical and economic evaluation directly into the development process. This addresses the challenges anticipated in this thesis, in which both legacy and new machinery are increasingly required to accommodate frequent format changes without reducing throughput. These findings indicate that integrating DFC principles with a retrofit-specific methodology aligns with current priorities in machine design research rather than addressing a historical concern.

This principle is rooted in established precision machine design theory. Slocum [44] presents exact-constraint design as locating a body using the minimum number of contact points required to eliminate each unwanted degree of freedom, thereby removing redundant, friction-dependent contact that causes continuously adjustable mechanisms to drift and exhibit operator-dependent variance.

The requirement for quick-change mechanisms extends beyond beverage packaging and originates from the industrial context in which SMED was first developed, as Shingo's initial applications focused on reducing die-change time for stamping presses [17]. Quick die change practices in this sector have evolved into a specialised engineering discipline that addresses the same fundamental challenge discussed in this section: replacing slow, tool-dependent fastening with mechanisms such as hydraulic and magnetic clamps, positive locating stops, and wedge-actuated draw-bars, all of which enable rapid release and repeatable, self-locating positioning.

2.8.2 Automated and Self-Positioning Adjustment Systems

A distinct technological class addresses changeover by removing manual adjustment from the operator's responsibilities. Motorised actuators, closed-loop position feedback, and format-indexed setpoints replace graduated scales and handwheels. In industrial literature, this class is commonly referred to as self-positioning, servo-adjustable, or automated format-change technology.

At the mechanism level, patented implementations already demonstrate the core principle. For example, an early system automates carton glue-head height adjustment using servomechanisms that move directly to predetermined positions corresponding to carton size, thereby removing operator fine-tuning from the changeover process [45]. At the systems level, commercial positioning modules that combine a brushless motor, gearbox, absolute-encoder feedback, and bus-based self-monitoring are supplied as standardised components for this purpose, enabling format changeover at the push of a button [46]. Equivalent functionality is reported using servo drives that automatically calculate the electronic cam profile for the selected format [47]. Industrial sources report approximately 50% reductions in changeover time when migrating from cam-driven to servo-driven adjustment on comparable equipment [48].

Two observations are directly relevant to the positioning of this thesis's contribution. First, nearly all available literature on servo or self-positioning systems, including patents, original equipment manufacturer documentation, and trade press, describes systems engineered into new, clean-sheet machine designs, where the servo axis and its spatial envelope are specified from the outset. Second, peer-reviewed or technical discussions of the retrofit case (adding equivalent automated positioning to legacy, non-servo equipment that was never designed to accommodate it, within fixed spatial envelopes, abrasive operating environments, and unmodifiable structural frames) are essentially absent from the surveyed literature.

2.8.3 Systematic Design in Constrained Environments (VDI 2221)

To mitigate unguided trial-and-error, the German engineering community formalised the design process through the VDI 2221 standard, "Systematic Approach to the Development and Design of Technical Systems and Products" [49]. This framework delineates four sequential macro-phases: Clarification of the Task, Conceptual Design, Embodiment Design, and Detail Design (Figure 2.5). These phases structure the design activities described in Chapter 7. Pahl et al. [49] further classify engineering projects as Original, Variant, or Adaptive Design. Retrofitting legacy packaging

machinery constitutes Adaptive Design, in which the machine's core solution principle, such as the kinematic transport of cardboard cutouts, remains unchanged. However, specific sub-systems, such as manual adjustment mechanisms, must be re-synthesised to satisfy new performance requirements.

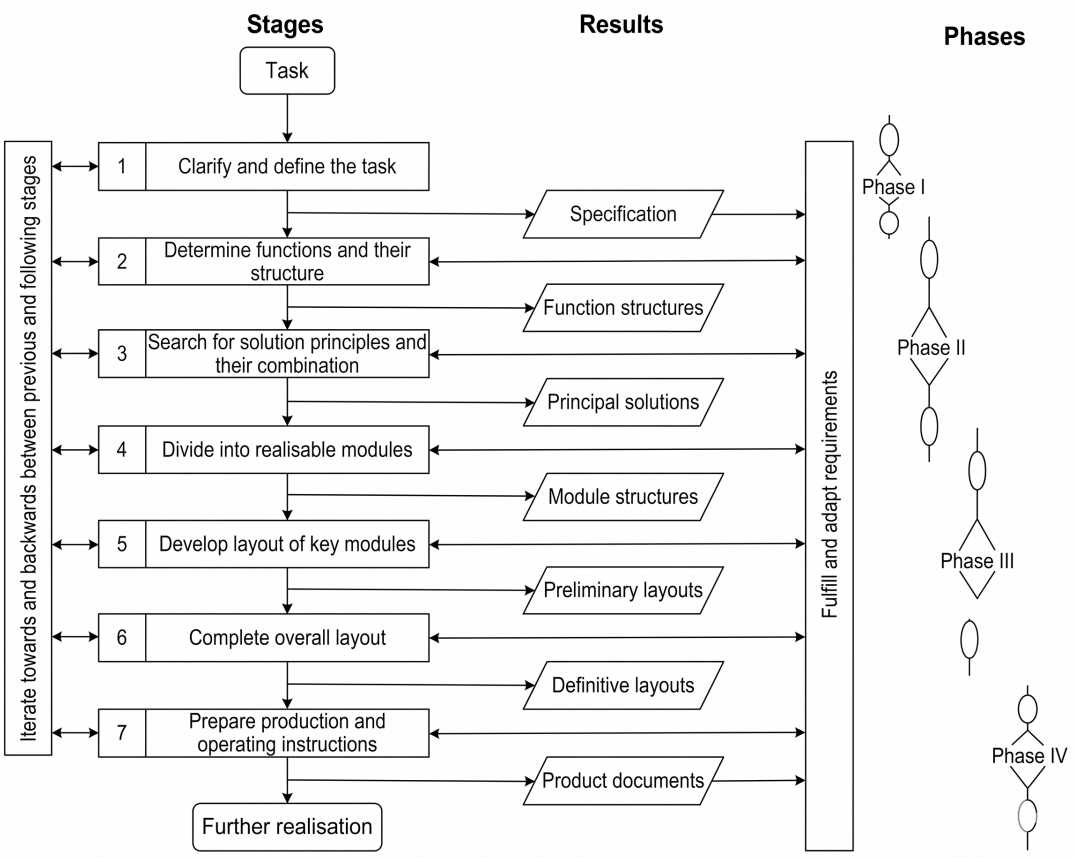


Figure 2.5: VDI 2221 Design Methodology Flowchart [50]

The application of VDI 2221 to adaptive retrofitting is particularly challenging during the Clarification of the Task phase. In contrast to original design, retrofitting provides no spatial or mechanical flexibility. Otto and Wood [51] contend that the process must therefore commence with rigorous reverse engineering. Prior to synthesising a new mechanism, the designer must map the legacy architecture, available spatial envelopes, reverse-calculated torque requirements, and transmission coupling interfaces. This approach is essential because Otto and Wood [51] identify spatial interference as the primary failure mode in adaptive design. Since the machine frame cannot be altered, new components such as motor brackets, belts, or hard-stops must be engineered to accommodate existing cross-members and moving parts. The systematic structure of VDI 2221, grounded in this reverse-engineering foundation, enables these constraints to be evaluated methodically, thereby reducing the risk of geometric conflict or mechanical binding.

2.8.4 Environmental Constraints in Beverage Packaging

Beyond kinematic constraints, end-of-line packaging modules (especially cartoners and shrink wrappers) operate in highly abrasive environments characterised by the accumulation of cardboard dust, the use of hot-melt adhesives, and deep-cleaning processes. These environmental conditions impose significant mechanical and biological limitations that must guide the embodiment design phase. The presence of cardboard dust fundamentally alters the tribological requirements of the machine's moving parts. Stachowiak and Batchelor [52] highlight the catastrophic effects of particulate contamination on wet-lubricated kinematic joints, where ambient dust binds with the lubricant and rapidly transforms into a highly abrasive paste that accelerates wear, degrading the machinery's dimensional tolerances. To counteract this, modern mechanical design is compelled to produce dry-running tribological systems that use self-lubricating engineering polymers, sealed bearings, or synchronous timing belts that inherently resist particulate buildup [52].

Additionally, mechanical design must meet rigorous hygienic and maintenance standards. Hot-melt glue applicators often lose calibration, causing mechanical brackets and guide rails to accumulate hardened adhesive. According to hygienic design principles described by Lelieveld et al. [53], food packaging equipment must be constructed to endure intensive physical sanitation procedures. Removing hardened adhesive requires aggressive mechanical scraping by maintenance personnel. Lelieveld et al. [53] note that such surface degradation is unacceptable in food packaging because the resulting micro-crevices trap abrasive debris and biological contaminants.

2.8.5 Research Methodology: Design Science Research and Action Research

In addition to the domain-specific methodologies discussed previously, this thesis is guided by an overarching research paradigm. Design Science Research (DSR) serves this function. As Hevner et al. [54] explain, rather than focusing on developing theories to explain organisational behaviour, design science aims to enhance human and organisational capabilities by constructing and evaluating new artefacts that address identified problems. Peffers et al. [55] formalise DSR as a six-phase process: problem identification, definition of solution objectives, design and development, demonstration, evaluation, and communication. This framework provides a structured template for design-oriented engineering research.

While DSR guides the abstract development and evaluation of an artefact, Action Research (AR) directs its implementation within a real organisational context. Susman and Evered [56] define AR as a cyclical process comprising diagnosing, action planning, action taking, evaluating, and specifying learning. This approach generates actionable knowledge through collaborative intervention rather than detached observation. Furthermore, Coughlan and Coghlan [57] demonstrate that AR is particularly effective in production environments where solutions require iterative refinement with operators.

These two frameworks operate at a higher level than the domain-specific tools, and this distinction shapes the structure of the thesis. DSR and AR determine how problems are identified and how solutions are evaluated, whereas TPM, SMED, and VDI 2221 are applied as tools within their

respective phases. Specifically, TPM and SMED time studies inform the problem-identification phase of DSR, VDI 2221 supports the design and development phase, and AR governs the demonstration phase when an artefact is deployed with operators. This hierarchical arrangement, with DSR as the overarching framework, AR as the implementation methodology within the demonstration phase, and TPM, SMED, and VDI 2221 as supporting tools, more accurately reflects their interrelationships than treating them as parallel approaches.

2.9 Research Gaps and Methodological Synthesis

A comprehensive review of the literature clearly delineates the distinction between operational management and physical machine design. To rigorously justify the technical interventions proposed in this thesis, it is necessary to evaluate the limitations of current methodologies combined with alternative manufacturing strategies. Table 2.2 summarises the main characteristics of each method discussed earlier in this chapter.

Table 2.2: Comparative Analysis of Engineering Design Paradigms for Retrofitting

Methodology & Authors	**Core Paradigm**	**Suitability**	**Limitations**
Design for Changeover (DFC) Mileham et al. [39]	Physical modification of equipment to intrinsically increase flexibility, eliminating threaded fasteners in favour of discrete, exact-constraint hard stops	High. Provides specific mechanical rules to eliminate ramp-up calibration time	Prescribes design rules but gives no cost-benefit threshold for when mechanical investment is justified over procedural SMED alone
Quick Changeover Design (QCD) Braglia et al. [40]	Integration of Poka-Yoke into machine architecture, so hardware cannot be assembled out of specification	High. Prevents operator variance	Explicitly ranks mechanisation last among its own strategies [40]; assumes organisational SMED has already been exhausted

Continued on next page...

Table 2.2 – Continued from previous page

Methodology & Authors	Core Paradigm	Focus	Limitations
Adaptive Design (VDI 2221) Pahl & Beitz [49]; Otto & Wood [51]	Modification of sub-systems while retaining the core solution principle, beginning with reverse engineering to map spatial and torque constraints	Mandatory. Ensures retrofit integrates without geometric interference	Gives no guidance on whether automated/servo positioning is feasible within the mapped constraints
Self-Positioning / Servo-Adjustable Systems	Removal of manual adjustment via motorised, closed-loop positioning, discretising continuous adjustment into automatically actuated and locked setpoints	Conditional. Well-documented for new-build machines; retrofit is the gap this thesis addresses	Literature assumes a clean-sheet design; spatial envelope, drive electronics, and structural frame are not pre-constrained as in retrofitting

As summarised in Table 2.2, operational tools and physical redesign paradigms have distinct boundaries. Prior to implementing a mechanical retrofit, a rigorous engineering evaluation should determine whether lower-risk operational approaches can resolve changeover inefficiency. In many cases, physical redesign is not economically justified. For low-to-medium-speed lines or standardised, low-variety portfolios, classical SMED and 5S methodologies may be sufficient, and reducing a changeover from 15 minutes to 2 minutes through automation may not justify the capital investment. Macro-level operations research provides a software-based alternative: sequence-dependent scheduling groups similar formats together, treats changeover times as fixed constants, and maximises uptime through scheduling logic, thereby avoiding capital expenditure, installation downtime, and technical risks associated with hardware modification [23, 27]. Retrofits are inherently disruptive because they require halting the production line and replacing simple manual mechanisms with mechatronic components, thereby increasing long-term maintenance complexity and potentially introducing new failure modes in abrasive or contaminated environments.

A physical retrofit is viable only under specific conditions: when line capacity is sufficiently high that trial-and-error ramp-up adjustments result in significant revenue loss; when just-in-time (JIT) constraints and high format diversity preclude scheduling major changeovers; and when the required geometric precision of a format adjustment surpasses the repeatable capability of a manual operator, thereby introducing permanent process instability.

This delineation reveals a central research gap. The operational school, which includes classical SMED, 5S, and digitalised SOPs, is scalable and low-capital but treats equipment as a fixed constraint. Once changeover reaches the physical limits of a machine's original kinematics, procedural adjustments alone cannot eliminate the need for trial-and-error calibration. The mechanical school, represented by DFC, QCD, and VDI 2221, modifies hardware directly but evaluates interventions as isolated mechanical tasks, neglecting operational dynamics such as sequence-dependent scheduling and operator cognitive load. These two domains operate independently, and the literature lacks a unified framework to integrate them. The design ceiling, defined as the point at which procedural tools are exhausted and a transition to mechanical redesign is warranted, is typically assumed rather than empirically demonstrated. The existing literature does not provide a systematic method for identifying this threshold within a specific industrial context using measurable evidence. Furthermore, current practice does not specify how micro-level algorithmic optimisation should influence physical layout, or how digital cognitive support should sustain engineered hardware changes over time.

Accordingly, this dissertation aims to address this disconnect. Rather than treating lean management and mechanical retrofitting as competing alternatives, it proposes a combined framework that integrates the organisational logic of SMED with the technical rigour of a highly constrained retrofit. This approach establishes a repeatable and balanced method for transforming legacy machinery into flexible, software-defined manufacturing assets.

Chapter 3

Initial Considerations and Methodology

Before addressing the proposed problem, a comprehensive understanding of production floor operations, team structures, and machine descriptions was required. An initial period of continuous Gemba Walks was conducted to observe changeover processes and the shop-floor dynamics. Following this, the framework adopted for the SMED methodology is explained, along with the initial results and conclusions.

3.1 Production Floor Organisation

SBG's production is organised into several lines, differentiated by container type: one-way kegs (OWK), returnable kegs (RK), one-way glass bottles (OWGB), returnable glass bottles (RGB), or cans. These lines differ not only in the container type produced, but also in capacity, size, and the machines included. Tables 3.1 and 3.2 present the line distribution throughout SBG.

Table 3.1: Technical Specification of Bottle and Can Packaging Lines at SBG

ID	Container type	Capacity (units/hour)
1	OWGB	60,000
2	OWGB	60,000
3	RGB	60,000
5	OWGB/RGB	80,000
6	OWGB/Cans	50,000 / 35,000
L	Cans	35,000

Table 3.2: Technical Specification of Keg Packaging Lines at SBG

ID	**Container type**	**Capacity (units/hour)**
4	RK	600
7	OWK	130
9	RK	173
Sebastião	OWK	50

As the project focused on the Mead and Kisters packaging machines dedicated to producing boxes, packs, trays, and shrink packages, Lines 4, 7, 9, and Sebastião were excluded since they produce only kegs. Line 3 was also excluded because it produces only RGB, which is packaged in crates of various sizes depending on the container type. Additionally, Line L, the specific line for packaging aluminium cans, was under construction and testing for most of the project timeline and was therefore not directly studied through the SMED analysis.

In terms of team structures, there are two blocks relevant to this project: Block 123, comprising the teams from Lines 1, 2, and 3, and Block 56L, comprising the teams working on Lines 5, 6, and L. Each block is managed by an Industrial Supervision Senior Engineer, who oversees four Team Leaders (Teams A, B, C, and D), each managing 14-18 operators across the three lines in each block (Figure 3.1). This division is mainly driven by the continuous-shift system implemented at the SBG production plant and by the need for four to six workers per Line, depending on the production plan and the line's requirements. During the project, there was daily direct contact with the teams from each Block, which was the main channel for understanding the processes carried out on the lines.

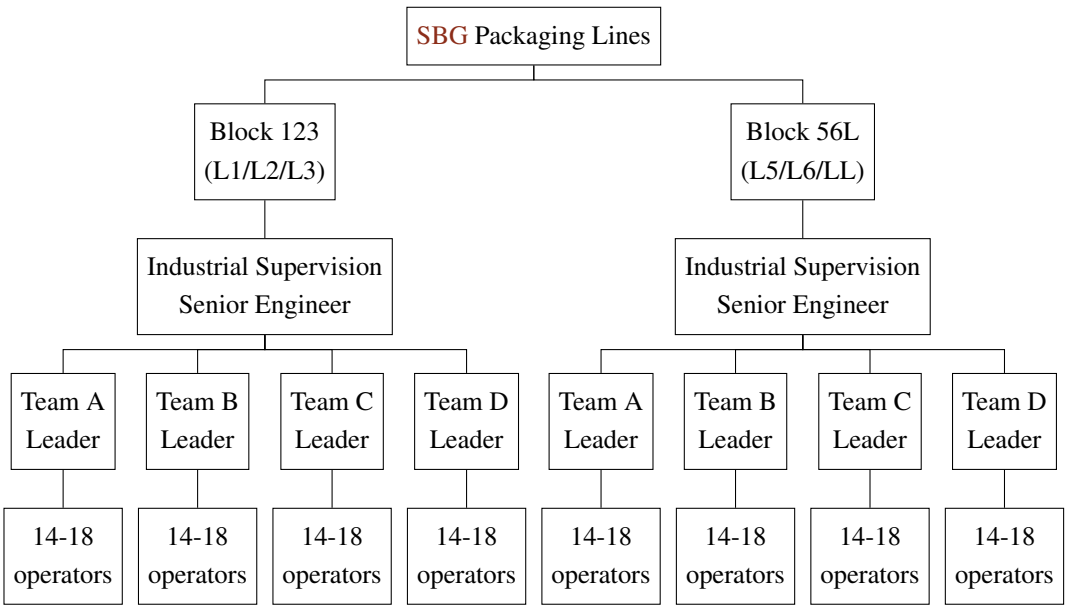


Figure 3.1: Organisational Team Structure for SBG's Packaging Lines

3.2 Technical Description of the Equipment

To establish a clear foundation for the application of the SMED methodology, this section details the mechanical architectures, modular configurations, and kinematic flows of the primary packaging lines under analysis.

3.2.1 Kisters

The KHS Innopack Kisters Wrap-Around Shrink Packers (Figure 3.2) and their variations, referred to internally at SBG as Kisters (from the original company, Kisters Maschinenbau GmbH), are packaging machines (cartoners) that serve as critical end-of-line components in beverage filling operations. Their primary function is to transition from primary packaging (such as glass bottles and aluminium cans, which directly contact and protect the beverage) to secondary packaging (such as boxes and trays, which group primary packages to provide commercial presentation, logistical protection, and ease of transport). These machines group individual containers into specific configurations and wrap them in cardboard supports, ranging from simple trays to wrap-around boxes and shrink-pack solutions.

Positioned as the final machine before the palletiser and logistics interface, the cartoning machine plays a decisive role in determining line flexibility. In an industry characterised by increasing product diversity to meet varying market and consumer demands, the ability of this machine to transition rapidly between configurations is essential. Therefore, a comprehensive understanding of its operation and changeover procedures is a prerequisite for the effective application of the SMED methodology.

The architecture of the Innopack line machines is inherently modular, enabling synchronisation of various processes in either continuous or intermittent mode, depending on the specific configuration. Operation relies on the convergence of three main flows: the product flow (beer containers), the packaging material flow (cardboard cutouts), and, optionally, the plastic film flow.



Figure 3.2: Innopack Kisters WSP Advanced Wrap-Around Shrink Packer [58].

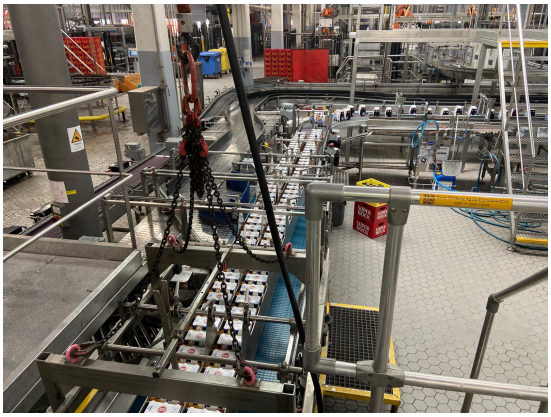
The module designations (M01–M09) are the manufacturer's internal references and do not follow the process-flow sequence. The modules are presented below in order of material flow.

M01 - Product Feeding Module

The overall process begins with introducing containers or container packs into the machine. During this stage, the system aligns and distributes the product flow across multiple paths, creating consistent rows of products for insertion into the packages. Accumulation sensors monitor inlet pressure to maintain the required product supply. This module (Figure 3.3) is mainly composed of feeding conveyors, guide rails, speed-regulation sensors, incorrect-product sensors, and a pneumatic actuator to eliminate product blockages.



(a) Row Divider Section



(b) Crane View

Figure 3.3: M01 - Product Feeding Module (Line 2)

M02 - Formatting Module

After the product is split into the predetermined number of lanes, group separation or the formation of the packaging matrix (for example, 4×6 for a box of 24 loose bottles or 2×2 for a tray of four 6-packs) is achieved using separating fingers or scroll systems and the product is then pushed by the upper conveyor belt's bar. These mechanisms isolate the precise quantity of product required for each packaging unit without interrupting the system's kinematic flow. This module (Figure 3.4) is mainly composed of guide rails, the separation system, and the conveyor belts.



(a) Lateral Guides



(b) Separation System

Figure 3.4: M02 - Formatting Module (Line 2)

M09 - Cardboard Cutouts Feeding Module

This module (Figure 3.5) is responsible for the intake of cardboard cutouts, their storage, and their subsequent release to the transportation system, which transports them directly to the Folding Module. Operators manually load stacks of corrugated blanks onto the roller conveyor, which automatically replenishes the hopper unit based on consumption demand. The cutout storage keeps the cutouts flat, and doses them to the transportation system when requested by the machine. This module maintains active communication with the previous two modules to ensure a cutout is available whenever bottles are being formatted, but cuts off the supply when none are. The main components of this module are the roller conveyors, dosing station, guide rails, cutout storage unit, and transportation system.



(a) Roller Conveyor (b) Transportation System (c) Cutouts Storage Unit

Figure 3.5: M09 - Cardboard Cutouts Feeding Module (Line 2)

M03 - Folding Module

At this stage, the packaging structure begins to take shape. Once the containers are positioned precisely on the cutout, closure is achieved using a hot-melt adhesive application system. The box or tray goes through a series of guide rails and bars, and spray units apply lines of glue to designated points on the flaps, which are then held under pressure by dynamic compression guides in the upper and lower hardening stations until the adhesive cures. When producing boxes, this is the last stage of the process, as it assumes its final form. For trays and shrink packages, the cardboard part assumes its final form, but the package still needs to go through the film-retracting process. This module (Figure 3.6) is mainly composed of the folding conveyors, folding supports, guide rails and bars, and the hot glue station.



(a) Outside View (b) Folding Station

Figure 3.6: M03 - Folding Module (Line 2)

M05 - Rotation Module

This module (Figure 3.7) has a simple operating principle: it rotates the product 90° when needed. The product conveyor belt moves the package at a certain speed, while a rubber conveyor line along its edge moves at a higher speed, creating relative motion and causing the box to spin to its side. Then a bar from the upper conveyor pushes the package into its transverse position. This module consists of the product conveyor belt, the rubber conveyor line, and the upper conveyor system.

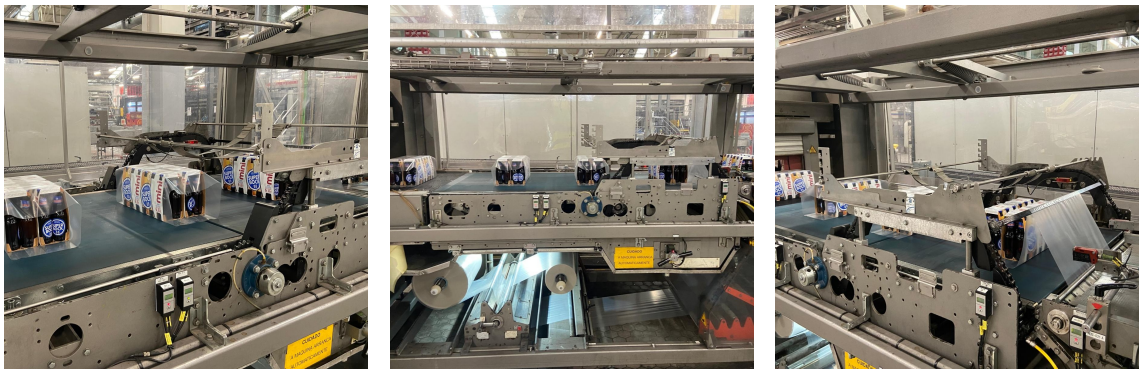


Figure 3.7: M05 - Rotation Module (Line 2)

M04 - Film Module

This module (Figure 3.8) applies LDPE (low-density polyethene) film around the product grouping, whether it is a cardboard tray or a collection of loose packs. This step ensures unitary cohesion prior to thermal sealing. The film is unwound and kept under constant tension by a

compensation roller, and a rotary knife cuts it to the required length. Wrapping bars guide the film around the moving package, creating a bottom overlap that is temporarily held by the products' weight until the next stage.



(a) Left View (b) Main View (c) Right view

Figure 3.8: M04 - Film Module (Line 2)

M07 - Retraction Module

This is the final stage before the product exits the machine, responsible for thermal finishing. Here, the film attains its final rigidity and adheres to the entire surface through heat application in the tunnel. The unit enters the tunnel (Figure 3.9), where electrical heating elements heat the air, and internal fans circulate it uniformly around the package. The heat causes the polyethene film to contract, conforming to the product's geometry and simultaneously fusing the overlapping layers at the base to seal the package. Upon exiting the tunnel, cooling fans accelerate film solidification, ensuring the package can be handled and palletised safely and immediately without loss of tension.

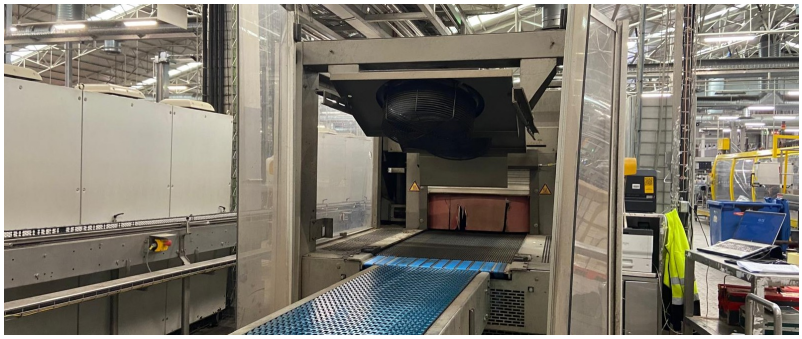


Figure 3.9: M07 - Retraction Module (Line 2)

Overall functioning and synchronisation

The correct operation of the Kisters machines relies on precise kinematic synchronisation between all modules rather than on a series of independent actions. The system ensures that the flows of product, cardboard, and film converge with millisecond precision, avoiding material waste or line inefficiency. From this project's perspective, this interdependence and complexity

make the transition between formats challenging. Because all the modules are mechanically and electronically linked, an adjustment in one area requires coordinated reconfigurations in the entire machine.

3.2.2 Mead

The WestRock Cluster-Pak EVOTECH SN 169 (Figure 3.10), referred to internally at SBG as Mead (from the original company, MeadWestVaco Corporation), is a highly automated, servo-driven packaging machine that functions as an intermediate cartoning component within beverage filling lines. In contrast to downstream end-of-line machines that process bulk boxes and shipping trays, the EVOTECH's primary function is to produce initial consumer-facing multipacks. This machine bridges the gap between primary packaging, such as non-returnable glass bottles or cans, and the final stages of secondary packaging. It accomplishes this by grouping individual bottles into specific multipack configurations, including 4-, 6-, and 10-pack formats, and securely wrapping them in compact cardboard cutouts.



Figure 3.10: WestRock Cluster-Pak EVOTECH [59]

Positioned upstream of the final case packers and palletisers, this machine plays a decisive role in determining overall line flexibility and throughput. Because its output directly feeds the subsequent secondary packaging machines, any downtime or inefficiency during its setup cascades through the rest of the line.

Comparable to the Kisters, the EVOTECH architecture depends on the precise convergence of material flows. This machine primarily merges two parallel, synchronised paths: the bottle circuit and the carton circuit. Cardboard blanks are synchronously positioned over grouped bottles, folded downward, and mechanically locked at the base, eliminating the need for hot-melt adhesive.

The architecture of the EVOTECH SN 169 is also modular and uses advanced servo-motor technology to precisely synchronise its continuous processes at up to 50,000 bottles per hour. The following section presents and describes the WestRock EVOTECH's primary process modules to facilitate a clearer understanding of its operational principles.

Product Infeed and Selection Module

The product flow begins with a single infeed conveyor that continuously supplies bottles from upstream machines. Sensors monitor the flow to detect fallen or defective bottles at the entrance. Symmetrical left and right starwheels regulate the product flow before the bottles reach the grippers. The gripper section selects and separates the bottles into the precise groupings required for the specific format. A synchronised lower double-chain then transfers these grouped bottles into the packaging guides.

Carton Magazine and Feeding Module

Operating in parallel with the bottle flow, this module stores and precisely doses the cardboard blanks. The hopper provides automatic gravity feeding of cartons, assisted by a fixed vibrator beneath the lower guides. The feeder uses vacuum suction cups mounted on dual-motion rotary shafts to extract the blanks. A rotary distributor (vacuum breaker) alternates between vacuum suction to pick up the blank and air blowing to release it. A synchronised double chain then lowers the angled cardboard directly onto the selected group of bottles.

Tucker and Overhead Boom Chains Module

Once the carton is placed over the bottles, the packaging takes its initial shape. The Tucker module, driven by servo motors and articulated fingers, simultaneously folds the lateral sides and end panels of the carton downwards. At the same time, the overhead boom chains, synchronised with the lower chains, maintain the cartons' positions and advance them over their respective bottle groups.

Bottom Folding and Locking Section (EFTAP)

Unlike machines that use hot glue, the EVOTECH relies on mechanical locking. As the packages advance, static bottom folders (rods and plates) fold the lower flaps under the bottles, closing the female flap first, then the male flap. The locking section uses pairs of pulling blocks mounted on a double chain. These blocks insert into the carton's pulling holes to align the flaps. Finally, a finger wheel pushes the locking tabs securely into their designated slots to finalise the pack.

Divider-Rotator Module

Once the packages are sealed, they enter the Divider-Rotator module. Equipped with a double chain synchronised with the machine's outfeed, this section features blocks adapted to the specific packaging type. Utilising fixed cams, the blocks can rotate the finished packs 90° if required by the configuration. Furthermore, a dual-cam shifting block system divides the output into single or multiple lines to feed the customer's downstream conveyors.

Overall Functioning and Synchronisation

The correct operation of the EVOTECH SN 169 relies heavily on its servo-driven architecture. This ensures that the bottle circuit and the carton circuit run in absolute parallel. The dual chains for the lower bottles, the overhead boom for the cartons, and the locking section must be aligned to ensure the cardboard is deposited and folded flawlessly at high speeds.

3.3 Format Setup Changeover

Optimising setup efficiency through the SMED methodology requires a comprehensive audit of reconfigurations dictated by a change in SKUs. This section details the mechanical actions, adjustable topologies, and tool-swapping protocols required to transition each asset between production formats.

3.3.1 Kisters

For the Kisters machine, the transition from one SKU to another, such as from a box of 24 loose 0.20L bottles to a tray of four 6-packs of 0.33L bottles, requires a complete reconfiguration and adjustment. This process is not linear and differs significantly between SKUs. The following section outlines the mechanisms that may be involved in a specific change.

Prior to any mechanical adjustments, a mandatory step involves the Human-Machine Interface (HMI). The operator selects the changeover mode and the program for the next SKU. This action adjusts various non-physical machine parameters, such as glue temperature, injection time, nominal speeds, shrink tunnel temperature, and film cutting time. Additionally, for safety, the machine is switched from operation mode to maintenance mode, allowing access for the operator. The Impulse mode function enables the machine to move slowly, providing access to all parts during the changeover process.

Format parts

During a typical format changeover, certain physical format tools cannot be adjusted between formats and must be replaced entirely. These tools, referred to as Format Parts, are specific to a number of products. For the Kisters machine, format parts may correspond to container size (e.g., 0.20L, 0.25L, 0.33L, 1L), packaging size (e.g., 12/15, 20/24, 30/35 bottles) or packaging type (trays, boxes, film). These components mainly include guide rails or their combinations in a trolley, separating system tools, pneumatic actuators, or folding supports. The fixing methods range from quick-release mechanisms to threaded fasteners, offering opportunities to reduce setup time through SMED methodology.

Adjustable points

For this machine, most structural elements are adjustable rather than interchangeable, due to its size and the number of components. As a result, there are significantly fewer format parts compared to many machines, such as the filler. This design can reduce changeover setup time by minimising component replacement, but can result in a longer ramp-up time due to fine-tuning. The 49 total adjustable points can be categorised into three types, as described below.

For the spindle adjustment points, the available tools include locking elements, detachable handwheels, detachable crank handles, and fixed-mount handwheels. These tools rotate the shaft, converting rotary motion into linear motion through transmission systems that may use gears, universal joints, rack-and-pinion mechanisms or linear guides. This mechanism is generally used to adjust sensitive parameters of specific machine components.

For linear adjustment points, which are simpler adjustments, such as lateral guide bars that move only inwards or outwards, a graduated metric scale is used. The guide can slide in or out and is secured by quick-release handles. This approach is effective for simple movements that still need a range of adjustment values.

For position selector adjustment points, only a limited number of positions are available. Adjustments are made exclusively at these designated positions, using quick-release handles with rings to lock the part in place, a coupled bar serving as a position scale, or indexing plungers. This method can also be applied within certain parts of the format to facilitate adaptation.

Identification system and adjustment value indicators

A major advantage of the machine during the transition phase is the instrumentation that supports this process. To ensure efficient and precise changeovers, the machine is equipped with a structured identification system and digital position indicators. These features facilitate a clear understanding of the machine configuration.

Every adjustable point in the machine is identified by a tag containing an alphanumeric code structured according to the following principles:

- Prefix: Indicates the module where the adjustment point is located (**M01**-061A - Product Feeding Module)
- Code: Number indicating the specific adjustment point (M01-**061**A - Lateral Guide Rails at the entrance of the M01 Module)
- Suffix: When relevant, the letters A or B indicate if the adjustment point is that of the operation side or the non-operation side (M01-061**A** - operation side)

In addition to the identification system, digital position indicators are key for managing complex changes. These devices are distributed throughout the machine, either on or near the adjustment point, and are marked with the corresponding code representing each adjustment point (Figure 3.11). While the devices are standardised, their operation varies depending on the type of adjustment needed.



Figure 3.11: Digital Position Indicator and Name Tag

The nominal value indicators correspond to format parts, linear adjustment points, and position selector adjustment points. After the program is changed in the machine interface, the relevant number for the new format part, the value for the metric scale position, or the setting of the position selector appears below the current value on the device's LCD screen. Once the format part is replaced or the adjustment is made, the operator confirms completion by pressing a button, which changes the LED from red to green, signalling that the adjustment is finalised.

The position indicators are related to the spindle adjustment points. Similarly to the nominal value indicators, after the program is updated in the machine interface, two numbers are displayed on the LCD screen. In these instances, the top value indicates the target setting, while the bottom value shows the current setting, monitored in real time by sensors. Illuminated arrows indicate the required direction of rotary adjustment. Once the correct position is reached using the appropriate tool, the LED changes from red to green, confirming that the adjustment is complete.

3.3.2 Mead

For the Mead, transitioning between SKUs requires comprehensive mechanical adjustments and part replacements across both the bottle and carton circuits. Because this machine uses advanced servo controls, the changeover process combines physical tool swaps with automated spatial reconfigurations.

Before physical intervention, the operator selects the new configuration on the machine's control panel. Unlike on the Kisters, the process of spatial and volumetric adjustments is fully automatic. This triggers several automated adjustments and changes the machine's parameters for the new format. Safety protocols are strictly enforced for physical access through sliding interlocking doors and emergency stops.

Automated Adjustable Points

Unlike older mechanical machines that rely heavily on manual spindles, the EVOTECH reduces changeover time by employing motorised assemblies for height and width adjustments. This

contrast is directly relevant to the research gap identified in Chapter 2. Contrary to the Kisters' complete manual adjustment system, the Mead exemplifies the new-build, servo-positioned machine architecture documented in industry and patent literature.

For height adjustments, when a new program is selected in the control panel, the machine automatically adjusts the carton feeder height, the overhead boom chains, and the rotator chains to match the new configuration. For width adjustments, sections such as the Selection Assembly and Side Lug Chains are adjusted laterally using integrated servo reducers and indexer rulers.

Format Parts

Besides the automatic adjustments, the remaining tasks involve swapping Format Parts between SKUs. Because of mechanical locking and precise folding mechanisms, several format parts are dedicated to specific bottle diameters and carton configurations and must be fully swapped. These include the following.

- Hopper Racks: Specific bottom guide racks are required for different cardboard blanks.
- Infeed Stars: The starwheels regulating bottle flow must perfectly match the bottle diameter.
- Grippers: Dedicated gripper sets are required for both the bottle diameter and the matrix size.
- Tucker Cams and Chains: Distinct folding assemblies are used depending on the matrix to ensure correct flap folding.
- Locking Section Components: Elements such as the locking stars vary based on pitch requirements.

To enable rapid exchange of many format parts, the machine relies heavily on manual quick-release hardware. Format parts in the RPM guides, EFTAP assemblies, and locking sections are secured with specific locking pins and indexer brakes. This design lets operators quickly uncouple, slide out, and replace stars and rails without heavy external tooling, providing strong baseline conditions for faster changeovers.

3.4 Changeover Analysis Methodology

This section sets out the methodology used to characterise the current-state changeover process before any intervention is proposed. The analysis is structured in three complementary parts, each addressed in a dedicated subsection.

3.4.1 SKU Portfolio and Setup Typology

To establish a robust baseline for applying the SMED methodology, the initial phase of this study involved systematically identifying and categorising the product portfolio produced by the packaging lines. In complex manufacturing environments, setup time depends not only on machine

mechanics but also on the degree of variance between successive SKUs. Consequently, a comprehensive assessment of the current production landscape was necessary to understand the underlying logic of changeover.

The primary data source for this characterisation was the SAP enterprise resource planning (ERP) system. Production orders for the entire plant were retrieved for the previous 24 months to ensure a statistically representative sample of production frequency and variety. This process went beyond simple data retrieval and required a substantial data-cleaning phase to ensure alignment with current operating conditions. The next step was to audit the obsolete materials, excluding SKUs that remained in the system but were no longer active in the commercial portfolio to minimise data noise. After that, the SKUs were mapped to their respective production lines, enabling a localised understanding of where each SKU was primarily being produced. For consistency in describing changeover events throughout this thesis, each observed Kisters changeover was classified into one of the types summarised in Table 3.3, each following its own specific procedural sequence.

Table 3.3: Kisters Changeover Classification

Code	Description
Z	No change at all
A	Box to Box, same container volume, same box type, different bottle count
B	Box to Box, same container volume, different box type
C	Box to Box, different container volume, same box type
D	Box to Box, different container volume, different box type
E1	Box to Tray of Packs
E2	Tray of Packs to Box
F1	Box to Tray of 1L Bottles
F2	Tray of 1L Bottles to Box
G1	Box of Loose Bottles to Box of 6-Packs
G2	Box of 6-Packs to Box of Loose Bottles
H	Cross-format transition, 6P bottle quantity
I	Tray of Packs to Tray of 1L Bottles (and vice-versa)

It was concluded that Line 2 produces the greatest variety of SKUs, including the majority of the alternative beers and ciders (all the different Somersby flavours, SB Stout, SB Green, etc.), which means the changeover process will be dominated by the Filler's CIP procedures, in the majority of changeovers. Line 5 produces, in the vast majority of cases, different box sizes for SB Original in large production orders, specifically the mini and 0.33 formats, which means the

changeover bottleneck will likely be the Kisters. Line 1, similarly to Line 2, produces a wide variety of SKUs but lacks the Mead machine, so it does not produce packs. Line 6 produces the majority of Carlsberg products and all 1L formats, and was, until recently, also producing every aluminium-can SKU.

3.4.2 SMED

The preliminary stage of applying the SMED methodology involves understanding and evaluating the as-is state. To achieve this, detailed observation and measurement of the setup process are required. For many changeovers on the Kisters, standard linear observation proved insufficient. The processes involve multiple operators performing different tasks simultaneously, sometimes individually and sometimes in pairs, making a simple sequential list inadequate. Observations needed to account for these parallel workflows to illustrate task overlap and team coordination during setup. This complexity introduces some limitations in observation accuracy, as the timing of certain tasks may vary by a few seconds. Consequently, Gantt charts were employed for critical changeovers, along with spaghetti diagrams and, less frequently, video recordings of specific tasks.

To ensure broad coverage of the sample, efforts were made to observe as many changeover procedures and typologies as possible, across all available teams and lines. Operational constraints, namely the continuous shift schedule and unpredictable equipment breakdowns, introduced significant scheduling variations that restricted the real-time observation of certain rare changeover typologies. Consequently, some highly specific procedures were documented on a single shift team. A total of 33 changeover procedures were recorded between February and May 2026 (Table A.1), with observations distributed across all four studied lines (Line 1: 9; Line 2: 5; Line 5: 10; Line 6: 9) and all four shift teams (Team A: 10; Team B: 7; Team C: 6; Team D: 10). The sample included 10 of the 13 typology codes defined in Table 3.3; the three codes not observed during the collection period either required no physical adjustment (Z) or represented low-frequency transitions (G1 and G2) structurally similar to already observed cases. This distribution provides a balanced cross-section of lines and shift teams for baseline structural analysis, despite variations in sequential execution order due to shop-floor conditions. Another key factor that distinguishes this analysis from a typical SMED application is that, although all Meads (Lines 2, 5, and 6) are very similar, the Kisters differ across lines due to age differences and the purpose of each line.

3.4.3 Adjustment Values Case Study

Initial Gemba observations uncovered a persistent issue during Kisters changeovers. Although newer machines (Lines 1 and 2) are equipped with digital adjustment value indicators to expedite adjustments, operators often bypass these systems. There is widespread distrust of the adjustment values stored in the programs; believing them unreliable, operators bypass the system entirely. Instead, they rely on physical box cutouts as shims to adjust machine components. This practice extends changeover times and delays the final ramp-up phase. To address this challenge, a

targeted study was initiated to evaluate the accuracy of current adjustment values, update system parameters, and implement a sustainable procedure for future modifications.

Line 1 was chosen as the case study because it incorporates the latest Kisters model and shows the highest functional rate of digital position indicators. Two digital indicators in the Cardboard Cutouts Feeding Module produced inaccurate readings due to frequent exposure to dust and water. Maintenance orders were issued to address these isolated hardware failures while the broader study proceeded. Data collection began in Week 15, immediately after the annual three-week maintenance stoppage. This timing provided a controlled baseline, helping ensure the machine was assessed in its optimal mechanical condition.

A tracking framework was established to monitor adjustment values for each SKU produced. At the start of each week, a production spreadsheet (Appendix B) was generated. Throughout the week, the adjustment values were recorded and compared to the system's nominal values. Data collection was subjected to a specific constraint. While the instantaneous position values for spindle adjustment points could be tracked on the machine's operation screen, the nominal values for the physical graduated scales depended on the machine's operational status. Because protective sliding doors obstructed the scales in modules M02 and M03 (Formatting and Folding), only the values from the M01 module (Product Feeding) could be recorded during operation. For those in the restricted modules, manual readings were only conducted during scheduled line stoppages or changeover procedures. This did not represent a critical constraint in the methodology because these adjustment points are purely mechanical and, once set, have no reason to drift between observations.

Over the eight-week data collection window, adjustment values were logged for seven distinct box-type programs (001, 002, 007, 008, 009, 013, and 015), for a total of 27 individual readings. Sampling frequency varied by program according to production frequency during the window: Programs 001 and 002 were recorded on seven occasions each; Program 007 on six; Program 008 on three; Program 015 on two; and Programs 009 and 013 on a single occasion each. Results for Programs 009 and 013, sampled only once, should accordingly be read as indicative rather than conclusive. This distribution reflects the actual production mix during the study period rather than a deliberate sampling design.

Chapter 4

Analysis of the Current-State Production System

4.1 Classification of Critical and Non-Critical Changeovers

The first step in analysing changeovers in the Kisters and Mead was to assess how an individual machine's changeover affected the overall process and the duration of the entire production line setup. As discussed in Chapter 2, the filler is usually the most critical machine when designing a new line. However, during setup changeovers, the critical machine can change depending on the products produced before and after. The total line changeover time is dictated by the machine that takes the longest to set up.

When changing container size or beer type between SKUs, the filler typically dominates the changeover because its procedures become complex. For example, when transitioning from Super Bock Original $0.33L \times 24$ to Somersby Blackberry $0.20L \times 15$ Pull-Off, changes occur not only in container size (0.33L to 0.20L) but also in beer type (SB Original to Somersby cider) and closure type (from crown to pull-off tab). In this case, the filler requires a 180-minute CIP procedure, followed by a setup changeover of approximately 245 minutes. This changeover is dominated by the filler, as every other machine in the line affected by this setup change (pasteuriser, labeller, Mead, or Kisters) has a much shorter changeover time. While this example illustrates an extreme case, such situations occur regularly in daily operations.

For changeovers where the main modifications involve packaging rather than the product itself, the line changeover time is dominated by the packaging machines, particularly the Kisters. For instance, when shifting production from Super Bock Original 0.20L x 24 to Super Bock Original 0.20L x 35, the filler continues operating since the container and beer type remain unchanged. Even with additional labels for external markets or minor subsequent changes, the Kisters requires the most time to change because it is the only machine that perform a setup changeover in this specific case. In cases where the SKU changes from box to pack, such as from a box of 24 loose bottles to a tray of four six-packs (Super Bock Original 0.20L x 6*4 Tray), the Kisters remain the critical machine, as the Mead machine (responsible for producing the packs) would have already

been adjusted. Mead changeovers are generally longer because they involve setting up numerous format parts, despite requiring fewer manual adjustments and less fine-tuning. Because most SKUs consist of boxes with loose bottles, Mead is rarely the critical machine in line changeover. Typically, it has several days or even weeks to complete the changeover between pack SKU production.

Based on these observations, changeovers were categorised as either critical or non-critical. This distinction is independent of the SKU-transition typology established in Table 3.3. A given typology code, such as Type A, may occur as either a critical or non-critical event depending on the specific production line and SKU sequence. During critical changeovers, most or all line staff are assigned to the Kisters to achieve the most efficient process. These changes can be quicker and simpler, such as altering box sizes and formats, or more complex when changing from box to pack or shrink and vice versa. In non-critical changeovers, there is more time available for execution, and the process is usually performed by one or two operators after the critical machine completes its setup. Although less critical to the overall line changeover, these processes also require optimisation.

Analysis of 24 months of SAP production-order data quantitatively confirms this pattern: 35.2% of Line 1 changeovers, 15.6% of Line 2 changeovers, 47.8% of Line 5 changeovers, and 41.6% of Line 6 changeovers were classified as Kisters-critical. Line 2's markedly lower share is consistent with its high variety of beer types, which more frequently shifts the critical bottleneck to the filler's CIP procedures. Lines 1, 5, and 6 each show a substantially higher critical-changeover share (35% to 48%), confirming that these three lines are the appropriate focus for Kisters-specific SMED interventions. Notably, over the same 24-month period, the Mead was identified as the line-critical machine only five times (three on Line 2, two on Line 5, and none on Line 6), confirming that Mead changeovers are reliably absorbed within available production windows and rarely constrain overall line throughput.

4.2 SMED Analysis

The preliminary stage of the SMED methodology consists of observing and documenting each changeover. Subsequently, the notes collected from each changeover were reviewed. These included detailed Gantt charts for critical changeovers, mapping the time each operator spent on the most complex tasks (an example presented in Figure A.1), visual observation notes, and time measurements for specific tasks to estimate their impact on the changeover procedure. As previously explained, the observation phase differs from a typical single-operator SMED analysis, as these changeovers are significantly more complex, may involve up to five operators performing tasks simultaneously, and cannot be recorded or observed as straightforwardly.

Across all observed changeover procedures, it was evident that most operators have comprehensive knowledge of their machines and are adept at addressing operational challenges. This expertise is a valuable asset that should be preserved and leveraged when modifying processes or introducing new tools for optimisation. Although not without imperfections, the critical changeovers

are generally well coordinated. Operators remain engaged in their designated tasks for nearly the entire duration, with minimal stoppages due to dependencies on other operators. However, variations in task duration and the clustering of tasks within each module or by operator inevitably result in brief waiting periods.

The first stage of SMED implementation concludes with mapping each observed task to its respective machine module and classifying it as either internal or external. Tables A.2 and A.3 provide a comprehensive inventory of tasks for both machines, organised according to the most complex changeover scenario. Although not every task is necessary for each SKU transition, the structure enumerates all possible tasks.

The Kisters inventory consists of 25 tasks: 2 external and 23 internal. Several module clusters, specifically M04, M05, M07 in their entirety, and three of the five M03 tasks, are relevant only to Lines 2, 5, and 6. Line 1 does not include the upstream Mead machine and therefore cannot produce pack or shrink formats.

The Mead inventory includes 27 tasks: 2 external and 25 internal. Since the mechanical configuration of the Mead is consistent across Lines 2, 5, and 6, this inventory is uniformly applicable without the need for a line-specific breakdown.

This mapping also revealed that task dependencies are confined almost entirely to individual modules, with negligible cross-module propagation observed across the studied changeovers. This diagnostic output serves as the foundation for the interventions developed in the latter part of this thesis, which focus on converting internal tasks to external ones and streamlining the remaining tasks.

4.3 Lack of Standardisation

Optimising industrial processes, particularly within high-speed packaging lines and continuous labour environments involving multiple teams, requires operational stability to implement SMED methodology effectively and sustainably. However, analysis of the current state of changeovers revealed significant variability in both procedures and part identification across production lines and team groups. This lack of homogeneity contradicts the principles of Lean Manufacturing and 5S. The absence of standardisation shows that format changes are based on empirical, fragmented knowledge rather than a systematic approach.

The absence of SOPs throughout the manufacturing unit directly contributes to workforce inflexibility. In an industry characterised by seasonal consumption, rapid adaptation and labour allocation are essential management requirements. The lack of standardised processes restricts operator versatility and hinders the seamless transfer of skills between lines. As a result, the integration period for new and temporary employees is significantly extended, creating operational constraints that prolong internal setup times and limit these workers' ability to perform substantive tasks.

4.3.1 Format Part Identification

As outlined in Section 3.3.1, and in contrast to the filler, the Kisters requires relatively few changes to format parts, with most adjustments handled through machine settings. Despite this, the processes would benefit from a standardised identification system. Packaging lines currently contain obsolete parts from SKUs not in production (such as the 0.50L and 0.208L format parts) and employ mixed identification systems depending on the line. Line 1 uses an informal numbering system that has never been formally documented or standardised. Line 2 features more format parts and adjustment points, with a colour and number system in place; however, most workers do not use it. Lines 5 and 6 face greater challenges, as older machines lack digital adjustment indicators for the desired position or format part for the next program. Identification in these lines relies almost exclusively on colour grading and, in some cases, handwritten text, resulting in the accumulation of obsolete parts and inconsistent systems across lines. Additionally, identification techniques are not uniform even within the same line.



Figure 4.1: Examples of Inconsistent or Absent Identification Systems

4.3.2 Changeover Procedures

No formal SOPs exist on the shop floor, resulting in each team following its own sequence of tasks. For experienced permanent operators, this lack of standardisation is largely invisible because accumulated tacit knowledge makes part selection intuitive and conceals underlying inefficiencies. The issue becomes evident when junior or temporary operators are integrated during peak seasons, as they are unable to execute changeovers independently without standardised procedures.

In practice, this challenge is managed informally rather than addressed systematically: these operators are assigned to simpler, low-risk tasks such as refilling consumables. This workaround further restricts the workforce's flexibility at times when seasonal demand is highest.

4.4 Adjustment Values Case Study Observations

The data retrieval phase of the case study lasted eight weeks. Data were organised by individual box-type programs to facilitate analysis of potential fluctuations in adjustment values. Subsequently, the data were thoroughly analysed to determine whether the operators' concerns regarding system reliability were justified. This analysis yielded several conclusions.

Although most adjustment values remained internally stable over time, they nonetheless deviated significantly from the documented nominal values for each program. Additionally, certain adjustment points exhibited substantial variation between production orders. All such instances were located within the M09 module, with the greatest variance observed at the M09-060 adjustment point (Table 4.1).

Table 4.1: Range of Adjustment Values at M09-060 by Box Program

Adjustment Point	**Box Program**	**Value**	
		Min	**Max**
M09-060	001	373.89	452.67
	002	362.15	391.75
	007	345.75	457.84

Further investigation identified the underlying issue. Specifically, the adjustment of the M09-060 point involves not only the spindle-driven carriage motion (a degree of freedom analogous to the equivalent M09-061 point on the opposite side) but also an extendable slider unique to this side. This slider introduces a third degree of freedom into the system that operators often overlook. The cutouts transportation system can be mapped onto a one-dimensional spatial coordinate system (Figure 4.2).

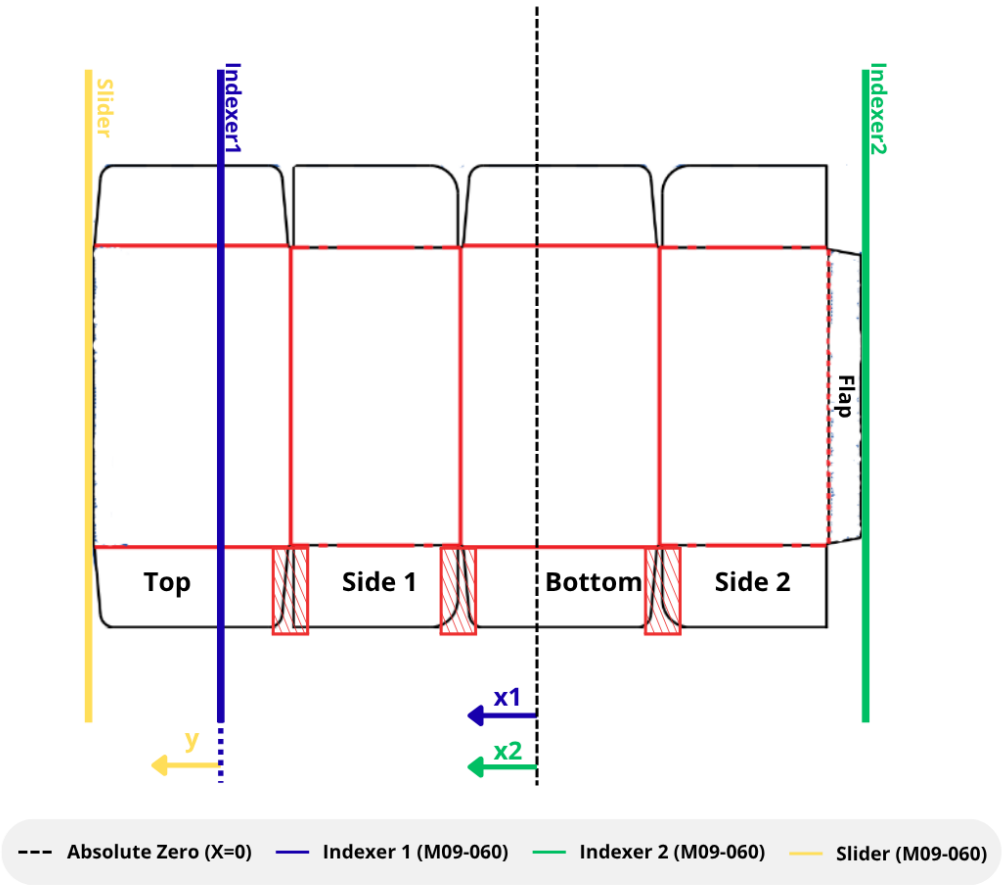


Figure 4.2: Spatial Coordinate System of the Cutout Transportation Mechanism

The absolute origin ($X = 0$) is set at the physical centre of the mechanism (represented by the central dashed line). This static section houses one of the two chains with guide fingers that move the cardboard cutout through the system. In the 12/15 and 30/35 box configurations, the centre of the bottom panel aligns with the machine's centre (arranged in rows of three and five, respectively). For the 20/24 configurations, the centre of the bottom panel shifts to the right (arranged in rows of four, towards side 2). This shift occurs because the Formatting and Product Feeding Modules have five paths for bottle flow, as shown in Figure 4.3.

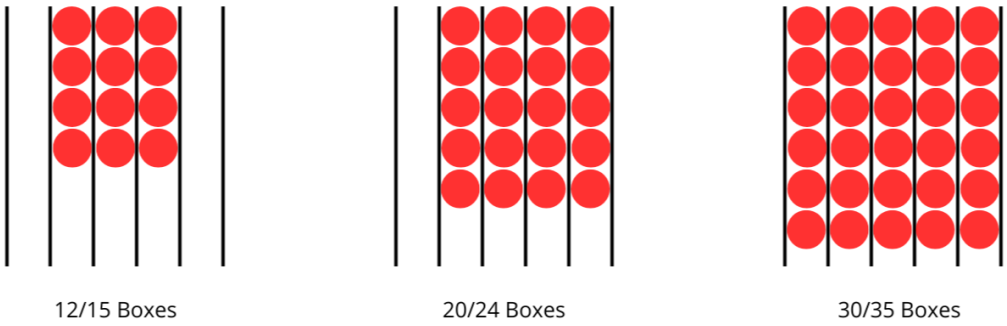


Figure 4.3: Bottle Configurations by Box Type

In the nomenclature that follows, adjustment point M09-061 corresponds to Indexer 2 (right side), while M09-060 comprises Indexer 1 together with the Slider (left side). The right guide rail directs the cutout's flap on the right side of the machine, with its position adjusted by Indexer 2. The left guide rail directs the cutout's top on the left side, and its position is controlled by both Indexer 1 and the Slider. Indexer 1 is positioned relative to the machine's absolute centre, similar to Indexer 2, but the Slider's position depends on Indexer 1's movement, extending an additional distance based on the box type. The Slider mechanism consists of three components, which, together with an indexing plunger in the guide, create a three-configuration system intended to optimise adjustments for various box sizes. Despite the presence of this system, no specific configurations are set; operators adjust it at their discretion (Figure 4.4).

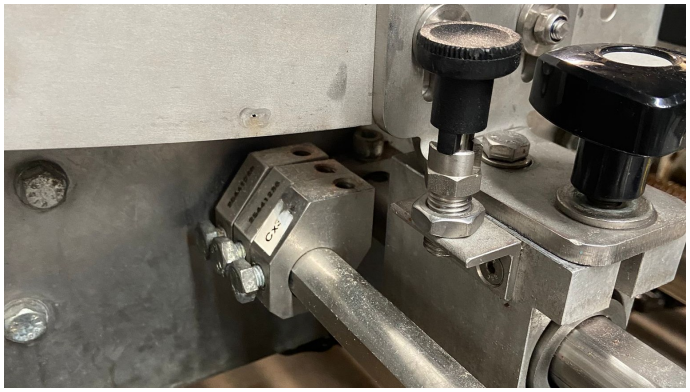


Figure 4.4: Absence of Defined Slider Configurations

This practice is primarily due to an additional constraint imposed by the cutout geometry. The first guide finger is fixed at the static centre of the machine, while the second finger moves laterally with Indexer 1. Neither finger may be placed in the creases between parts of the cutout (represented by the prohibited zones), as doing so causes deviation in the cutout's path and results in breakdowns. As a result, operators adjust Indexer 1 and the Slider without a defined method, leading to suboptimal system performance. This practice, combined with the fine-tuning period required after adjustment due to the module's precision requirements, extends changeover times.

The extent of this variance is more apparent when considered relative to Indexer 1's total physical travel range, which spans 380 mm (from 150 mm to 530 mm in absolute machine coordinates). Program 001's recorded range of 78.78 mm represents approximately 21% of the total travel, while Program 007's range of 112.09 mm accounts for approximately 30%. Thus, nearly one-third of the mechanism's adjustment range was effectively undefined for Program 007. In contrast, Program 002's narrower range (29.60 mm, approximately 8% of the total travel) indicates that the severity of the issue is influenced more by box geometry than by consistent operator imprecision.

Although the observation data did not isolate the exact time costs attributable specifically to Indexer 1 and Slider adjustments, the broader unreliability of the M09 module fine-tuning is supported by stoppage-frequency data collected during the observation stage of SMED. Among the 33 changeovers observed, 29 required fine adjustment within this module before production could resume reliably. This recurrence rate aligns with an unstructured, trial-and-error adjustment process rather than a deterministic approach. The inability to quantify the precise time cost of this specific sub-task is recognised as a limitation of the current diagnostic dataset.

Chapter 5

Proposed Solutions

This chapter addresses the findings detailed in Chapter 4. The proposed solutions to reduce changeover time are implemented following three standard stages to systematically minimise machine downtime. First, internal and external tasks are separated by categorising activities as either performed while the machine is stopped or while it is running. Next, internal tasks are converted to external tasks. Finally, all operations are streamlined by optimising the duration and execution of the remaining internal tasks and the newly externalised activities.

5.1 Separation of Tasks

After completing the preliminary SMED stage, it is necessary to separate internal and external tasks. The first SMED stage formalises the separation of internal and external tasks. The complete task inventory for both machines, its mapping to the machine modules, and the finding that task dependencies remain confined within individual modules were established in Section 4.2 . This section acts on that baseline. The few existing external tasks are already executed efficiently in most changeovers (Section 5.2). The analysis therefore concentrates on the internal tasks: those that can be converted to external time (Stage 2, Section 5.2) and those that can be streamlined to reduce both internal and external setup times (Stage 3, Section 5.3).

Although there are only a few external tasks they are already executed efficiently in most changeovers, as detailed in Section 5.2.

This stage is also essential for identifying internal tasks that could be externalised in stage 2 of SMED and for determining internal or external tasks that can be streamlined to reduce both internal and external setup times in the final stage of SMED.

5.2 Externalisation of Internal Tasks

The second stage of SMED implementation involves identifying internal tasks that can be performed concurrently with, or prior to, machine-stopped operations. Externalisation is already successfully applied to the few existing external tasks, specifically those related to replenishing

the line's only consumables: cardboard cutouts and hot-melt glue. An external logistics service provider ensures timely delivery of pallets with new cutouts to a holding area. Subsequently, a production operator uses a small forklift to position these pallets adjacent to the Cardboard Cutouts Feeding Module on the Mead and Kisters machines and unloads them for use while the previous SKU continues to run. Glue container refilling follows the same external process. This established practice demonstrates that externalisation is operationally viable on the shop floor. The objective of this section is to extend externalisation to additional internal tasks.

5.2.1 Mead

For the Mead machine, most changeover activities involve replacing Format Parts alongside the machine's automatic adjustment features. As a result, few tasks were identified as suitable for externalisation. These parts are organised either in dedicated trolleys near the machine (Lines 2 and 5), which are moved closer during changeover to minimise operator movement, or in dedicated shelves and accessible storage on both sides of the machine, depending on the location required (Line 6).

No further externalisation opportunities were identified for the Mead beyond the existing trolley and shelf-based storage described previously. Due to the Mead's relatively low criticality across the studied lines and its effective format-part organisation, the externalisation effort in this thesis focused on the Kisters, where higher changeover criticality and a greater proportion of internal tasks indicated a more substantial potential impact.

5.2.2 Kisters

Although adjustments in the Kisters machine are not automatic as in the Mead, they still constitute the majority of changeover tasks. Since these adjustments require the machine to be stopped, only a few simple internal tasks were identified as potentially optimisable during this phase of SMED. These tasks are discussed in the following paragraphs.

Adjustment of the guides inside the trolley in Product Feeding Module

On Lines 2, 5, and 6, the presence of the Mead machine upstream in the production line enables the production of various formats beyond boxes, including product packs. As a result, the trolley in the Product Feeding module must be changed between configurations for loose bottles, different pack arrangements, and, additionally for Line 6, trays and boxes for 0.66 and 1L bottles. Due to the trolley's weight (approximately 250 kg), an operator must use a crane to move it from the machine to the designated storage area. After assembling the new trolley, the guide rails must be adjusted, a task currently performed internally during changeover.

While changing the trolley cannot be externalised, adjusting the guide rails can be performed externally. It is proposed that guide rails be adjusted for the next production order either immediately after the current changeover or prior to the subsequent changeover. For instance, if the Kisters is producing trays of packs and the next SKU is a box of loose bottles, the trolley should be adjusted for the specific configuration of loose bottles before it is reassembled on the machine.

This adjustment can be completed after the current changeover for SKUs scheduled within the same week, or before the next changeover if it is scheduled further in advance. Implementing this practice is expected to save 2 to 3 minutes per changeover, depending on the trolley used.

Format Parts Retrieval

Most tasks related to Format Parts are already external or have been streamlined. For example, the M09-090 Row Separator Guides are placed on a workbench adjacent to their position on the machine. This allows the operator to switch parts according to the SKU being produced and store the removed part after the changeover. This is particularly relevant because each part weighs from 25 to 30 kg.

It was observed that the operator does not bring the Separation System toolset to the Formatting Module before the machine stops. Although the tools are located within 20 m, meaning the direct travel-time savings from earlier retrieval are minimal, the primary justification for this change is verification rather than speed: retrieving the tools while the machine is still running allows the operator to confirm their presence and condition before the changeover begins. Identifying a missing or broken tool at this stage allows time to source a replacement without halting the line; discovering the same issue only after the machine has stopped turns a preventable delay into unplanned mid-changeover downtime. Since these tools must be replaced for each container size or package type, the procedure was revised so that the operator retrieves them before stopping the machine and places them on the workbench near the Formatting Module.

5.3 Streamlining Internal and External Tasks

In the context of streamlining existing internal and external tasks, one specific task was identified as a strong candidate for improvement. This task is notable because it requires an integrated approach that combines machine design principles with the inherent process characteristics outlined in the SMED methodology to redesign the current adjustment system. The subsequent section provides a detailed explanation of this task.

5.3.1 Redesign of the Folding Bracket Mechanical System

The first critical subsystem targeted for optimisation involves the assembly and disassembly of the Folding Bracket (Figure 5.1). This adjustment is mandatory during format changeovers between wrap-around boxes and alternative packaging types, though it is bypassed on Line 1, which is dedicated exclusively to standard box production. For wrap-around box production, the larger cardboard cutouts require these brackets to guide the folding of the Side 1 and 2 flaps (as shown in Figure 4.2) into the interior of the box. In contrast, for alternative product formats, the formatting rails at the entry of the Folding Module are swapped, requiring the complete removal of the Folding Brackets to prevent geometric interference with the newly installed guide rails.

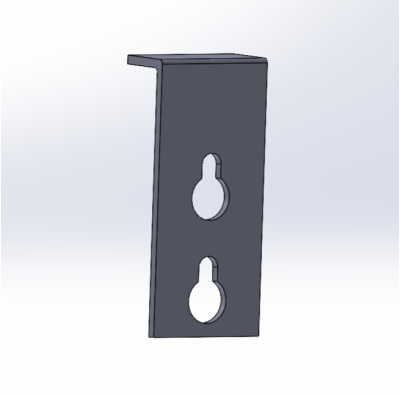
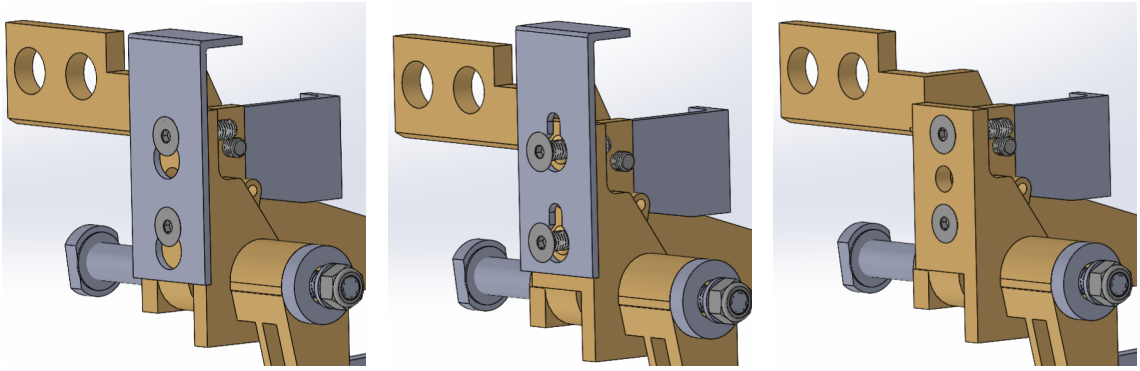


Figure 5.1: Folding Bracket Baseline Design

In the legacy configuration, operators must use a manual hex key to back out two threaded fasteners securing each bracket (Figure 5.2a). The bracket is then extracted via designated keyway slots (Figure 5.2b), after which the fasteners must be manually re-tightened to clear the slot area (Figure 5.2c). This inefficient process must be repeated for 24 independent supports (12 per side of the machine). Furthermore, the machine's structural layout requires operators to manually jog the drive transmission to access all mounting positions sequentially. The legacy disassembly sequence is illustrated in Figure 5.2, with the assembly process following the reverse procedure.



(a) Loosening the Screws (b) Bracket Removal (c) Tightening the Screws

Figure 5.2: Folding Bracket Legacy Disassembly Sequence

To address these inefficiencies, a DFC approach was adopted. The primary objective was to transition the bracket from a fully removable component to a captive, quick-adjust mechanism, eliminating the need for external tooling, preventing component misplacement, and reducing changeover windows.

The redesign was restricted by strict physical constraints: the machine's structural frame could not be permanently altered. Consequently, the new mechanical assembly had to integrate seamlessly with the existing mounting interface, using only pre-existing features: two M5 and one M8 threaded holes. Additionally, it was essential to preserve the bracket's functional inverted "L" profile, as the upper flange is critical to the cardboard folding process.

To achieve tool-less, captive adjustment within this restricted interface, the securing method was shifted from a static friction-clamped joint to a guided single-axis linear translation mechanism with positive discrete locking. Instead of completely detaching the bracket, the new component features an elongated vertical slot allowing it to slide downward into a non-interfering position.

The previously unused central M8 threaded hole was repurposed to house a spring-loaded indexing plunger. This plunger mates with a detent hole machined into the sliding bracket, establishing the active working position and mechanically guaranteeing positional accuracy along the X and Y axes without relying on operator alignment variables. Concurrently, the upper M5 fastener was replaced with a precision shoulder screw acting as the primary linear guide rail, passing through the bracket's vertical slot. When the indexing plunger is engaged, this upper shoulder screw constrains the remaining rotational degree of freedom (θ_z), achieving an exact-constraint kinematic state.

Initial design iterations considered using a secondary fixed guide pin in the lower M5 hole to establish a parallel rail system for pure translation. However, spatial interference analysis uncovered a critical geometric conflict regarding the machined features. Allowing the required vertical displacement of the bracket would necessitate a second elongated slot for the lower fastener. The guide pin's required trajectory in this lower slot would physically intersect the detent hole at its precise coordinate. Incorporating this lower slot would breach the closed profile of the detent hole, merging the two features and destroying the hole's ability to locate the indexing plunger pin. As a result, the lower secondary fastener was deliberately omitted. Although this exact-constraint design results in a single-point pivot during the brief translation phase (when the M8 plunger is manually retracted), the theoretical angular play is adequately mitigated by the components' tight tolerances.

5.3.1.1 Hardware Specification and Structural Baseline Selection

Selection of component hardware must ensure precise kinematics while adhering to the plant's standardised maintenance protocols. Standard threaded fasteners were excluded for the linear guide because their threaded profiles abrade machined slot walls, and inconsistent tightening torque leads to unpredictable sliding behaviour and premature loosening. Shoulder screws address these issues; however, the M5 ISO 7379 minimum shoulder length of 10 mm would result in 8 mm of unconstrained axial clearance with a standard sheet-metal bracket. Although custom screws could eliminate this gap, they would not meet the plant's standardised supply requirements. Consequently, a DIN 923 slotted-pan-head shoulder screw (M5 thread, ∅7 mm shoulder, 2.5 mm shoulder length L_s) was specified. The ∅7 mm shoulder also serves as a mechanical hard stop in the retracted position and provides sufficient shear area for the static resting load.

Positive locking is achieved using an Elesa+Ganter GN 717-5-M8-A-NI stainless-steel pull-ring indexing plunger (Appendix I). Its ∅5 mm, 5 mm-engagement pin maintains position even if the screw experiences micro-loosening. Material selection was determined by the Folding Module environment, in which the hot-melt applicator's drift deposits adhesive onto adjacent components,

requiring operators to remove it with aggressive scraping. On a durability-first basis, this environment would be expected to exclude engineering polymers such as POM-C, on the assumption that repeated adhesive scraping would cause gouging. The candidate material properties (Table 5.1) establish AISI 304 stainless steel as the baseline, as it has the highest elastic modulus and a surface hardness significantly greater than that of the 6061 alloy (170 vs 88 Brinell).

The bracket thickness was set to 2.5 mm to correspond with the DIN 923 shoulder length, resulting in an exact-constraint sliding fit. Since bending stiffness scales with t^3 ($I = \frac{bt^3}{12}$), this increase from the 2.0 mm legacy profile raises the second moment of area by a factor of $(2.5/2.0)^3 \approx 1.95$. This represents a 95% increase in stiffness, achieved solely by aligning with standard hardware dimensions.

Table 5.1: Comparison of Mechanical Properties for Candidate Bracket Materials [60–62].

Material (EN / US)	**Young's Modulus (GPa)**	**Hardness (Brinell)**	**Yield Strength (MPa)**
POM-C (Acetal Copolymer)	2.8	- [1], [2]	65
EN AW-6061 T6 (AA 6061-T6)	70.0	88	240
1.4301 (AISI 304 Stainless Steel)	200.0	170	230

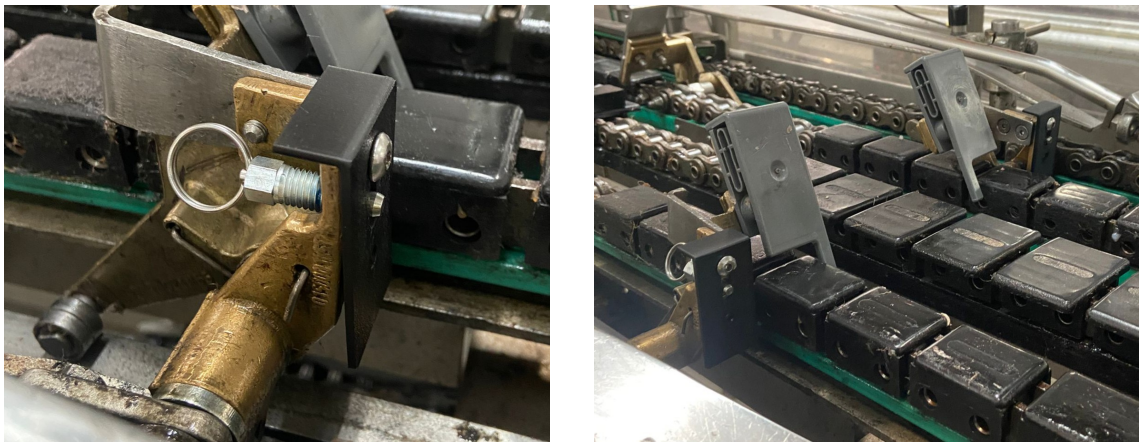
[1] Hardness values for metallic candidates are reported on the Brinell scale (ISO 6506-1). POM-C's hardness is not included for direct numerical comparison, as polymer hardness is conventionally measured via Ball Indentation Hardness (ISO 2039-1) or Rockwell M (ISO 2039-2) — scales with no standard conversion to Brinell.

[2] The Young's Modulus and Yield Strength comparisons, which use directly comparable units across all three candidates, remain the basis for the material screening in this section.

5.3.1.2 Empirical Prototyping, Dynamic Testing, and the Polymer Pivot

Prior to committing to final CNC machining and sheet metal forming, the kinematic viability and spatial clearances of the redesigned geometry were empirically validated. A functional prototype of the folding bracket was produced internally using Fused Deposition Modelling (FDM) 3D printing with Polyethylene Terephthalate Glycol (PETG) filament. PETG was selected for the prototype due to its low cost, rapid print turnaround times, and superior impact resistance compared to standard PLA.

A pair of these PETG prototypes was installed on the machine's Folding Module to conduct a physical interference study (Figure 5.3). Because the specified DIN 923 shoulder screws were unavailable during this preliminary phase, standard threaded fasteners were used as a temporary substitute for the primary upper guide and were manually tensioned to simulate a clearance fit. The lower fastener was removed, and the indexing plunger was fully implemented.



(a) Close-Up View (b) Position on the Kisters Machine

Figure 5.3: Rest-Position Interference Testing on the Active Production Line

The testing protocol was executed in two distinct phases. First, as a mechanical safety precaution against machine collision, the machine's drive chain was rotated manually in low-speed jog mode to confirm adequate static and low-speed spatial clearances. Following this validation, the machine was transitioned into standard dynamic production. Rather than limiting the trial to short-term checks, these polymer components were subjected to active, high-volume dynamic tray production. The prototype brackets were intentionally left in the resting position throughout the standard production cycle to monitor for vibration-induced displacement, harmonic resonance, or unforeseen dynamic clashes. This trial lasted two weeks and focused solely on tray production, providing real-time data regarding the prototype's industrial viability. The empirical testing yielded no interferences or functional failures, strongly supporting the geometric feasibility of the redesigned stroke length and the placement of the mechanical hard stop. After this, the prototype brackets were tested in their active working position to evaluate potential geometric conflicts and the prototype's strength.

Unexpectedly, the PETG brackets sustained the cyclic folding forces of the corrugated cardboard cutouts throughout the extended trial without exhibiting visible plastic deformation, localised creep, or structural degradation. While the Young's Modulus of PETG ($E_{PETG} \approx 2.1$ GPa) is orders of magnitude lower than that of steel, the actual flexural loads imposed by the cardboard folding process are small enough that the structural rigidity of the 2.5 mm-thick polymer geometry is sufficient for the deflection to fall well within acceptable operational limits.

This empirical outcome forced a critical design pivot. Because a 3D-printed part can be produced on-site at a fraction of the cost of a machined metal component, it can be treated as a highly economical consumable item. This realisation enabled a shift toward an engineered, additively manufactured polymer component as the final production solution.

5.3.1.3 Geometric Optimisation for Additive Manufacturing

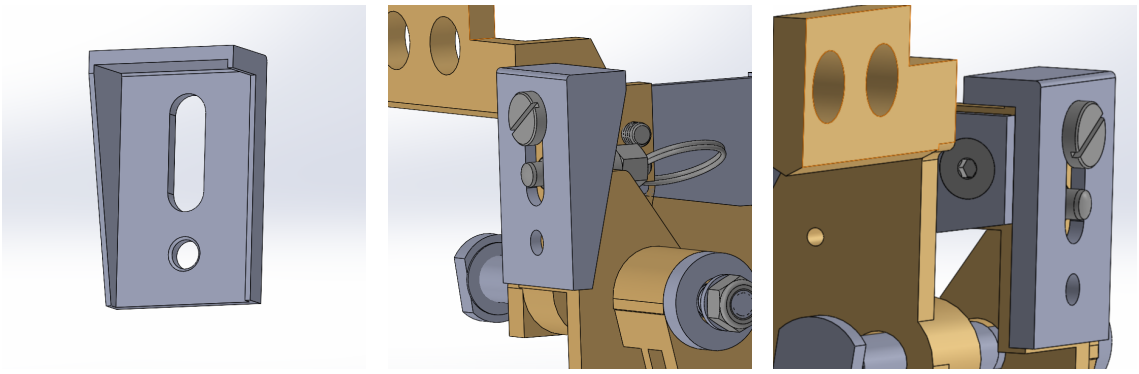
To leverage the geometric flexibility of additive manufacturing, the CAD model was optimised to address polymer material limitations and enhance the mechanism's kinematics through two main modifications.

Two reinforcing side ribs (gussets) were incorporated along the sides of the inverted "L" profile. In conventional subtractive manufacturing, machining such thin, localised reinforcing features causes significant tooling access challenges and increases production costs. In contrast, FDM additive manufacturing enables the integration of these ribs without additional tooling requirements. Structurally, these ribs increase the section modulus (Z) along the primary bending axis, converting bending moments into localised tensile and compressive stresses at their edges, ensuring geometric stability. Additionally, these ribs serve as a secondary kinematic constraint in the retracted rest position. When the indexing plunger is disengaged, the bracket is retained only by the upper shoulder screw, resulting in an unconstrained rotational degree of freedom (θ_z). To address this, the side ribs are toleranced to engage the fixed structural edge of the machine frame at the bottom of the downward stroke, serving as a mechanical alignment block that eliminates rotational play.

The reinforcing rib geometry is asymmetric due to spatial constraints imposed by the legacy machine frame. The unobstructed side of the bracket features a full-length, tapered gusset confined within a 1 mm width envelope. This configuration functions as a deep beam, shifting the neutral axis outward to maximise the section's resistance to the asymmetric loading imposed by the unobstructed mounting geometry.

By contrast, the opposite side is subject to strict interference from adjacent sheet metal components. Initial designs considered a symmetrical 2×2 mm triangular fillet at the inner vertex, but this feature acts merely as a stress-relief fillet with negligible global bending resistance. To maximise stiffness within the limited 1 mm clearance, an "L"-shaped edge was implemented, yielding an asymmetric cross-section. According to the parallel axis theorem ($I_x = \sum(I_{cx} + A \cdot d^2)$), distributing material continuously along the component's outer length significantly increases the global area moment of inertia. The final solution can be observed in Figure 5.4.

Also, the vertical profile of the bracket's main leg was substantially reduced. Previously, an extended vertical profile was necessary to accommodate the spacing between two clamping fasteners and the open-ended keyway slots. The redesign removes the lower-secondary M5 fastener, rendering the additional material unnecessary. Shortening the leg decreases the cantilevered mass and shifts the component's centre of gravity closer to the primary upper guide screw. This torque reduction minimises localised contact stresses within the guide slot, preventing binding or jamming during manual adjustment and increasing the clearance footprint in the resting position. The reduced length bracket final solution can also be observed in Figure 5.4.



(a) Ribs Design (b) Unobstructed Side (c) Obstructed Side

Figure 5.4: New Bracket Design

5.3.1.4 Engineered Slicing Parameters and the Mechanical Fuse Paradigm

To successfully transition the optimised folding bracket into a reliable end-use industrial component, the FDM process parameters were engineered using established optimisation matrices from the literature to counteract polymer anisotropy [63, 64]. The component was oriented flat on the build plate relative to its principal "L" profile, ensuring that primary bending stresses propagate along the continuous polymer strands of the $X-Y$ plane rather than inducing interlayer shear along the build axis (Z-axis) [64]. This orientation also enables more precise hole dimensioning, which will be discussed in this section.

Thermal parameters were optimised to maximise polymer chain diffusion across layer interfaces. An extrusion temperature of 245°C was specified; while literature notes that temperatures up to 270°C maximise fusion, the 245°C limit was chosen to eliminate risks of thermal degradation and severe viscosity drops that induce structural defects like stringing and oozing [63, 65]. Concurrently, the part cooling fan speed was restricted to 15% to maintain an elevated boundary temperature during deposition, prolonging the window for macromolecular entanglement.

The internal macrostructure was optimised based on established manufacturing frameworks that identify infill density as the primary statistical driver of the flexural rigidity of PETG components under bending loads [64]. Consequently, a 100% solid infill density was mandated. To fully exploit the structural "sandwich panel" effect - where the outermost fibres bear the highest localised bending stresses - the wall perimeter count was increased to 6 loops (yielding a 2.4 mm shell thickness), while using an alternating $\pm 45^{\circ}$ raster infill sequence. A layer height of 0.20 mm was selected as an optimised compromise between peak component density and deposition reliability. To mitigate the challenges posed by PETG's high hygroscopicity, which induces microvoids and the hydrolytic degradation of polymer chains during extrusion, the filament was pre-dried at 60°C for 4 hours prior to fabrication.

To realise the required precision mechanical fits directly off the build plate without secondary machining, specific toolpath compensation strategies were deployed. The vertical guide slot requires an exact sliding fit against the ∅7 mm shoulder screw, and the detent hole must firmly

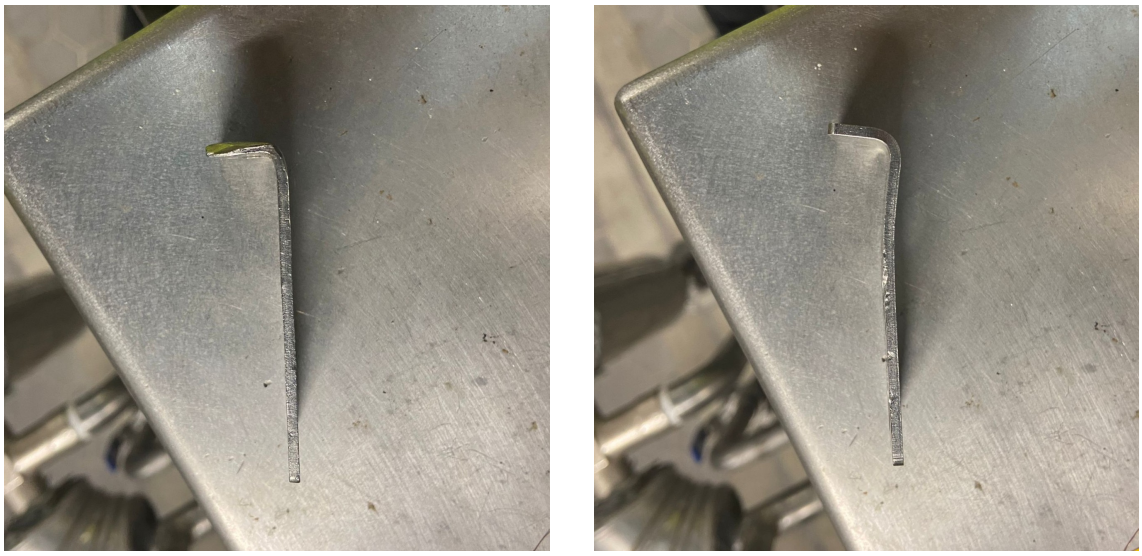
anchor the indexing plunger. According to the manufacturer's specifications, the GN 717 plunger pin has an effective physical diameter of 4.95 mm. To achieve locational clearance and minimise transverse backlash in the locked state, the target dimension for the detent hole was set to 5.00 mm, yielding an operational clearance range of at least 0.05 mm.

To counteract the well-documented phenomenon of internal hole shrinkage in FDM, driven by the centripetal drag of the molten polymer strand around radial trajectories, the slicing engine's "XY Size Compensation" tool was used to apply a positive radial offset to the toolpath contours [66]. This software-defined optimisation produced clean, ready-to-assemble 5.00 mm and 7.00 mm features directly from the build plate. Additionally, a 0.5 mm $\times$ 45° lead-in chamfer was integrated directly into the CAD model at the face of the detent hole. Generated seamlessly during layer deposition, this feature acts as a geometric funnel that guides the plunger pin cleanly into the tight-tolerance hole during format changeovers, preventing the tip from binding on a sharp edge upon release. The summarised printing parameters can be observed in Table 5.2.

Table 5.2: Engineered FDM Process Parameter Matrix for the Functional PETG Folding Bracket.

FDM Process Parameter	**Optimised Specification**
Material	PETG (Pre-dried at 60°C / 4 h)
Build Orientation	Flat (Parallel to "L" profile)
Extrusion Temperature	245°C
Layer Height	0.20 mm
Infill Density	100% (Solid)
Wall Perimeter Count	6 loops (2.4 mm shell)
Infill Raster Pattern	Alternating $\pm$45° sequence
Part Cooling Fan Speed	15%
Toolpath Optimisation	XY Size Compensation

Ultimately, shifting from a subtractively machined stainless steel assembly to an engineered polymer component introduces an operational advantage by establishing a deliberate *mechanical fuse* within the machine's kinematic chain. In high-speed packaging lines, operator errors—such as failing to retract the brackets before changing formatting rails—frequently cause severe mechanical collisions. If the folding brackets were manufactured from 2.5 mm stainless steel, an overload event would transmit massive impact forces directly through the mounting interface, inevitably damaging the machine's structural components or bending the brackets (Figure 5.5).



(a) Intact Bracket Side Profile (b) Warped Bracket Side Profile

Figure 5.5: Bracket's Side Profile Comparison

By manufacturing the brackets from PETG, the component is intentionally engineered to be the weakest link in the assembly. Extruding a pair of brackets requires approximately 10 grams of filament, translating to a raw material cost around 0.15 € and a print time slightly above 30 minutes (Figure 5.6), whereas an equivalent AISI 304 bracket incurs significant tool setup fees, machine-rate costs, and extended lead times. In the event of an operational clash, the polymer bracket undergoes elastic and plastic deformation, absorbing the impact's kinetic energy and failing sacrificially if needed. This substantially isolates the expensive machine frame from damaging stress concentrations, reducing a catastrophic multi-day maintenance breakdown into a trivial, low-cost component replacement cycle.

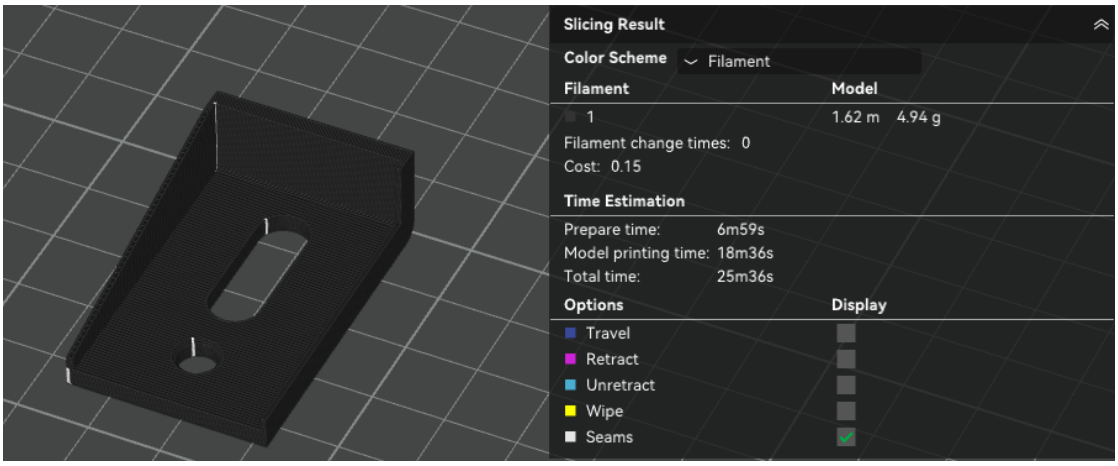


Figure 5.6: Slicer Results for the 3D-Printed Bracket

5.4 Adjustment Values Update and Box Configuration Optimisation

Building upon the diagnostic baseline established in Chapter 4, this section presents the deterministic engineering solutions and mathematical models implemented to mitigate changeover volatility.

5.4.1 Box Configuration Optimisation

5.4.1.1 Mechanical Constraints

To address the adjustment issue in the Kisters transportation system, an optimisation was conducted to determine the three most effective Slider configurations that minimise operator travel during point adjustments and reduce changeover time. This process required the establishment of relevant constraints.

The first mechanical complexity arises from the left-side guide rail, which features two degrees of freedom: Indexer 1 (I), serving as the primary carriage mechanism with a width of 90 mm and a physical travel bounded between 150 mm and 530 mm, and the Slider (S), a secondary mechanism mounted on Indexer 1 with a width of 45 mm and a maximum extension of 210 mm.

Unlike theoretical point-mass models, the total reach to the outer edge of the left guide rail must account for the physical thickness of the mechanisms. Therefore, the kinematic chain is defined in Equation 5.1.

$$Reach_{Total} = I + S + W_I + W_S = I + S + 135 \tag{5.1}$$

Furthermore, because the Slider is physically obstructed by the structure protecting the current transmission system at higher extensions (Figure 5.7), a structural boundary applies.

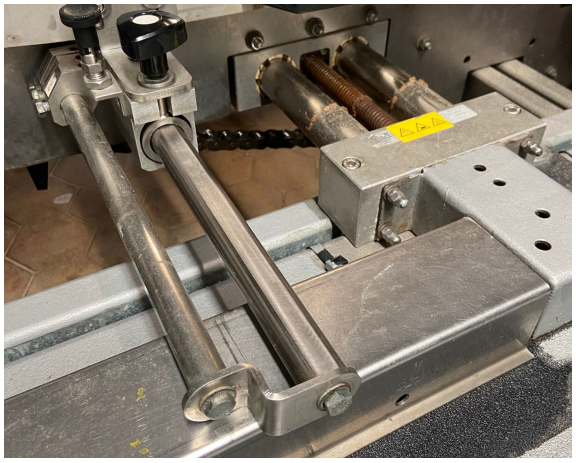


Figure 5.7: Structural Obstruction of the Slider

When Indexer 1 extends beyond 400 mm, the Slider loses its maximum extension capacity, creating a coupled mechanical limit

$$I + S \leq 610 \tag{5.2}$$

The right-side guide rail, in contrast, operates with a single degree of freedom: Indexer 2 (M09-061), which performs the same carriage function as Indexer 1 but without an equivalent Slider mechanism. Indexer 2 shares the same physical travel magnitude as Indexer 1, bounded between 150 mm and 530 mm from the machine's centre, though it operates on the opposite side of the absolute origin and is therefore expressed in negative coordinates. Because no Slider is mounted on this side, Indexer 2's positioning is governed by a simpler, single-term reach equation, without the coupled mechanical limit or structural obstruction constraints that apply to the left-side Slider.

To prevent machine faults and meet the system's precision requirements, strict positional constraints are enforced around the box creases. Initial calculations assumed a 30 mm safety clearance from any fold line. However, geometric analysis revealed that for smaller box formats (e.g., 20x15), combining a 30 mm clearance with the 90 mm width of Indexer 1 and its 150 mm origin bound creates a mathematically infeasible region, leading to a physical machine crash. Consequently, the safety clearance was relaxed to 25 mm.

As detailed in Section 4.4, the machine's coordinate system incorporates an asymmetrical datum that depends on the box configuration group. The machine centre aligns with the centre of the bottom panel for the 12/15 and 30/35 groups, whereas boxes in the 20/24 group are physically shifted toward Side 2 during operation. This shift is determined by the diameter of each bottle. The diameters of the 0.20, 0.25, and 0.33L bottles are 53 ± 1.2, 55 ± 1.2, and 58.9 ± 1.3 mm, respectively. For initial calculations, a shift of 27.5 mm (half of the 55 mm diameter bottle) is assumed. This geometric anomaly necessitates that the kinematic equations dynamically apply a positional offset by subtracting from the left-side reach and adding to the right-side reach to maintain spatial accuracy.

The geometric characteristics of the system and mechanical constraints are summarised in Table 5.3.

Table 5.3: Optimisation Problem Constraints

Constraint	**Value (mm)**	**Observations**
Indexer 1 Width	90	Primary left-side carriage footprint
Slider Width	45	Secondary mechanism mounted on Indexer 1
Crease Safety Zone	50	25 mm each side of the crease
Indexer 1 Travel	150 to 530	Absolute coordinates
Indexer 2 Travel	-150 to -530	Absolute coordinates
Slider Travel	0 to 210	From Indexer 1 position, towards Side 1

The 135 mm constant in Equation 5.1 is the sum of the Indexer 1 (90 mm) and Slider (45 mm) widths.

5.4.1.2 Optimisation Methodology and Formulation

To ensure standardised operation, the continuous Slider variable (S) is discretised into three fixed configurations ($c \in \{A, B, C\}$). The optimisation process determines the configuration lengths that minimise variance in Indexer 1 positions. This is formulated as a Minimax (Min-Span) objective, which minimises the absolute worst-case physical displacement boundaries.

$$\min(\max(I) - \min(I)) \tag{5.3}$$

The mathematical models were formulated in Python using the Pyomo algebraic modelling language and solved using the COIN-OR Branch and Cut (CBC) optimisation engine. CBC was selected over standard solvers (such as GLPK) due to its superior heuristic branching capabilities and computational efficiency when handling complex discrete constraints in Mixed-Integer Linear Programs. Two mathematical programming models were developed to evaluate the trade-off between theoretical machine boundaries and operational simplicity.

Model 1: Mixed-Integer Linear Programming (MILP)

Model 1 determines the absolute theoretical minimum travel span of the machine without operational grouping constraints by using an unconstrained clustering approach. When compared to standard clustering algorithms (e.g., K-Means), which only group data based on spatial proximity, the MILP approach was chosen because it guarantees the absolute mathematical minimum variance while strictly enforcing hard physical constraints and coupled mechanical obstructions.

The algorithm autonomously assigns each box b to a configuration c using a binary decision variable ($y_{b,c} \in \{0, 1\}$). Continuous spatial variables are converted into discrete assignment variables without introducing non-linearities through the application of a Big-M constraint method. The kinematic linkage is defined in Equations 5.4 and 5.5. The constant M represents an arbitrarily large value, and $Offset_b$ denotes the SKU-dependent datum shift.

$$I_b + S_c + 135 - (TargetReach_b - Offset_b) \leq M(1 - y_{b,c}) \tag{5.4}$$

$$I_b + S_c + 135 - (TargetReach_b - Offset_b) \geq -M(1 - y_{b,c}) \tag{5.5}$$

Additionally, because the 90 mm Indexer 1 must dynamically position itself either completely before or completely after specific creases depending on the box size, an auxiliary binary zone variable was introduced. This allows the solver to navigate the 25 mm safety clearance constraints without triggering a mathematically infeasible state.

Model 2: Name-Based Linear Programming (LP)

Model 2 was implemented to prioritise shop-floor standardisation while maintaining optimal variance limits. Although Model 1 achieves mathematical optimality, it imposes significant cognitive demands on operators due to the absence of logical nomenclature in algorithmic box assignments. Model 2 addresses this by introducing a predefined operational heuristic, mapping boxes to the configurations already in place (12/15, 20/24, and 30/35).

When compared to purely heuristic scheduling models or non-linear adjustments, this approach mathematically guarantees the tightest possible travel span within operational rules. Defining assignments a priori eliminates the binary assignment variable $y_{b,c}$, simplifying the problem from an MILP to a continuous LP. The Big-M inequalities are replaced with a single equality constraint mapped directly to the designated SKU group g.

$$I_b + S_g + 135 = TargetReach_b - Offset_b \tag{5.6}$$

This approach was selected to align mathematical optimisation with Lean Manufacturing principles. Assigning groups to SKU suffixes eliminates algorithmic ambiguity and enables operators to perform rule-based changeovers without consulting external documentation or reference sheets.

5.4.1.3 Results and Comparative Analysis

Table 5.4 establishes the comparison between both models.

Table 5.4: Comparison of Model 1 (Unconstrained Theoretical Optimum) and Model 2 (Deployed, Name-Based Configuration)

Metric	**Model 1 (MILP)**	**Model 2 (Name-Based LP)**
Grouping basis	Free assignment	Fixed a priori (12/15, 20/24, 30/35)
Slider configurations	A: 0.0 mm · B: 77.5 mm · C: 110.0 mm	Group_12_15: 0.0 mm · Group_20_24: 52.0 mm · Group_30_35: 108.0 mm
Worst-case travel span	82.0 mm	84.0 mm
Optimality gap vs. Model 1	—	2.0 mm (2.44%)

Model 2 assigns Slider values of 0.0 mm, 52.0 mm, and 108.0 mm to the Group_12_15, Group_20_24, and Group_30_35 configurations, respectively. This assignment results in an overall minimum Indexer 1 position of 292.0 mm, required by the smallest box in both the 12/15 group (20×15) and the 20/24 group (20×24). The overall maximum position is 376.0 mm, required by the largest box in the 30/35 group (25×30). Consequently, the worst-case travel span for Indexer 1 is 84.0 mm.

Model 1 assigns box programs to configurations without reference to operational naming, thereby establishing a theoretical minimum travel span of 82.0 mm. The difference between the two models is 2.0 mm (2.44%). Since Model 1 evaluates all possible clustering schemes for the eleven box programs into three configurations, this minimal gap indicates that no alternative

grouping scheme significantly outperforms the existing operational naming convention. The pre-existing 12/15, 20/24, and 30/35 groupings do not constitute a binding constraint relative to the unconstrained optimum.

This result clarifies the scope of the optimisation. It addresses the root cause identified in Section 4.4: the absence of a defined Slider configuration, which previously allowed operator discretion and resulted in substantially different values for nominally identical box programs across separate occasions. Assigning a fixed Slider value to each named group eliminates the need for this discretionary adjustment. The 84.0 mm travel span represents a system-wide property, specifically the total mechanical range Indexer 1 must support across the full portfolio.

5.4.1.4 Sensitivity Analysis

To assess the robustness of the deployed configuration, three sensitivity checks were performed on Model 2.

First, the 25 mm safety clearance, identified as the most consequential relaxed parameter in the formulation, was reverted to its original, more conservative value of 30 mm. Both Model 1 and Model 2 became infeasible under this stricter clearance. This outcome confirms that the relaxation to 25 mm is not a matter of convenience but a binding requirement for the existence of any feasible configuration.

Second, robustness to future product introductions was evaluated using a synthetic box format (20x40), constructed by extrapolating the dimensional scaling observed between existing programs within the 20/24 group. This scaling involved a growth of 0.25 mm per nominal unit, resulting in +4 mm adjustments to the dimensions relative to the 20x24 baseline. The synthetic format does not correspond to a confirmed future SKU and was used solely to stress-test the model's capacity. When incorporated into Group_20_24, the optimised configuration accommodated the new format without any change to the worst-case travel span (84.0 mm). This result indicates that the current configuration retains capacity for at least one plausible future format extension without requiring re-optimisation.

Third, sensitivity to the ±1.2 mm bottle-diameter manufacturing tolerance established in this work was assessed by varying the 27.5 mm datum-shift offset for Group_20_24 to its extremes (26.3 mm and 28.7 mm). In both cases, the worst-case travel span remained unchanged at 84.0 mm. Only the Group_20_24 Slider value adjusted (53.2 mm and 50.8 mm, respectively, compared to 52.0 mm at nominal tolerance), confirming that the optimised solution is robust to realistic manufacturing variation in bottle diameter.

5.4.2 Adjustment Values Update and Sustainability

After optimising the different box configurations, all the values taken from the case study were updated in the machine's software. To inform and educate the operators, structured training workshops were conducted across all four shift teams to explain the changes to the values and the new box configurations defined on the Slider.

Previously, privileges to modify program definitions were restricted to the maintenance team. Because production staff could not correct parameter drift as it emerged, erroneous values introduced during maintenance interventions persisted uncorrected through standard operation, accumulating over the years into the systematic misconfiguration documented in Chapter 4.

To decentralise control while maintaining system integrity, a new password-protected user profile was created for the Packaging Department. Access was limited to team leaders and line coordinators. This hierarchy preserved accountability and allowed the production team to update and maintain accurate adjustment values efficiently. A dedicated SOP was formalised and distributed to govern this access structure (Appendix C).

5.5 Development of the Digital Changeover Support Tool

As established in Chapter 4, the primary obstacle to efficient changeovers across all production lines is the lack of standardisation. Prior to the implementation of the digital tool, changeover management depended on operator experience and informal communication, resulting in two key process vulnerabilities.

The first vulnerability is the high variability in execution methods, task sequencing, and adjustment procedures across shifts, teams, and production lines. Additionally, the large number of changeover procedures and the absence of documented SOPs make it impractical for less-experienced or temporary operators, who are common during peak season, to learn and reliably execute these procedures. The second vulnerability is a lack of traceability. No historical records exist for changeover duration per specific equipment, adjustment values, machine parameters, or responsible personnel. In the absence of this data, continuous-improvement initiatives lack a measurable baseline.

The proposed solution is a digital support tool that converts the changeover from an experience-dependent process into a standardised, guided, and traceable one. It replaces informal routines with an enforced workflow that reduces process variation, lowers cognitive load, and automatically documents each changeover. The tool acts as a repository of digital SOPs covering every changeover across all lines, supported by line-specific images and videos of the relevant machine components, and structures preparation and mandatory steps to protect changeover time.

5.5.1 User Access and Context Initialisation

The system implements a two-level access structure that distinguishes shop-floor operations from data administration. The default operational profile limits users to the changeover workflow, allowing operators to execute guided procedures, initialise context, and validate SKUs. Operators are not permitted to modify master data, configurations, or any SOP. Access to administrative functions is provided via an ADMIN button and password validation, which grants entry to a separate menu.

Before executing any changeover logic, the production context must be established by the operator through three selections that define the current shop-floor state:

- **Production Line:** Six configurations are available (Lines 1, 2, 3, 5, 6, and L). Although Lines 3 and L are not included in the SMED analysis, they are incorporated to support plant-wide scalability. The selected production line filters all subsequent operations and determines which machine-specific format-part lists are generated during execution.
- **Team:** Four shift teams (A to D) are available. When combined with the production line selection, this serves as a relational key to retrieve the designated Team Lead/Coordinator, thereby establishing accountability.
- **Machine:** Kisters or Mead. This determines the rule set, changeover codes, and SOPs that the execution engine loads.

A live clock within the interface supports shift pacing and eliminates the need for manual logging. The initial interface is presented in Figure 5.8, and the dropdown menus are described in Appendix E.



Figure 5.8: Initial Menu

5.5.2 SKU Validation and Algorithmic Classification

Entry and validation. The interface includes two alphanumeric fields: SKU 1 (outgoing product) and SKU 2 (incoming target), each linked to the SKU code column, which serves as the primary key in the local database. When an entered code matches a record, the corresponding product description appears beneath the field, enabling the operator to cross-reference the physical packaging with the loaded record. If the code is incomplete or absent, a “SKU not found" message is displayed, and the OK button prevents progression until both fields correspond to valid records. This mechanism functions as a Poka-Yoke control at the data-entry layer, ensuring that non-existent or mistyped codes do not reach the classification engine and generate invalid outputs. The validation states are detailed in Appendix E.

Comparison and normalisation. Before rule evaluation, the records for SKU 1 and SKU 2 are transformed into a per-attribute comparison vector based on the four attributes that determine changeover type for both machines: Volume, Package Type, Bottle Quantity, and Box Type (Table 5.5). Non-mechanical variables, such as label design or liquid type, are excluded. Each attribute yields a binary result, indicating whether it is identical or different. The normalisation process removes formatting variations from text, applies an approximate-equality threshold to numeric fields, and resolves null entries. This ensures the engine detects genuine operational changes rather than data artefacts, such as differences in casing or numeric precision.

Table 5.5: SKU Database Schema and Attribute Specifications

Column Name	**Data Type**	**Permitted Domain**	**Role**
Product Code	TEXT	Alphanumeric product codes	SKU identification code
Material Description	TEXT	Product descriptions	Operator validation
Volume	REAL	0.20, 0.25, 0.33, 1.0 (Litres)	Container's capacity
Package Type	TEXT	Box, Tray, Shrink Film	Packaging archetype
Bottle Quantity	TEXT	4P, 6P, 10P, 12, 15, 20, 24, 30, 35	Container number and typology
Box Type	TEXT	Small, Medium, Large, Pack	Dimensional box size category

Rule engine. The engine processes the normalised attributes and comparison vector using a deterministic, first-match-wins rule set that implements the typology described in Table 3.3. Rules are defined for each machine (example for the Kisters in Table 5.6) and are evaluated sequentially from top to bottom. The first rule whose conditions are fully satisfied is assigned, and evaluation ceases. The condition syntax employs "=" or "dif" to test for attribute identity or difference; "=X" to require a specific value X; "A $\rightarrow$ B" for explicit state transitions; and "$\rightarrow$ B" or "A $\rightarrow$" for single-state constraints, treating the opposite side as a wildcard. Placing specific format-crossover rules (E1-I) above the broader box-to-box rules (A-D) ensures that specific transitions are not subsumed by general rules such as D.

The fallback mechanism is explicit and diagnostic: if a transition does not match any rule, the system returns a null classification and a "no matching rule" alert instead of assigning a default class. This approach highlights gaps in the transition matrix and notifies continuous-improvement engineers that a new rule is required.

Table 5.6: Kisters Machine Changeover Classification Rules

Code	Structural Condition Block
Z	__all__: =
A	Package Type = Box, Volume =, Box Type =, Bottle Quantity dif
B	Package Type = Box, Volume =, Box Type dif
C	Package Type = Box, Volume dif, Box Type =
D	Package Type = Box, Volume dif, Box Type dif
E1	Package Type: Box → Tray, Box Type: → Pack
E2	Package Type: Tray → Box, Box Type: Pack →
F1	Package Type: Box → Tray, Box Type: → Small
F2	Package Type: Tray → Box, Box Type: Small →
G1	Package Type = Box, Box Type: → Pack
G2	Package Type = Box, Box Type: Pack →
H	Package Type dif, Bottle Quantity = 6P
I	Package Type = Tray, Box Type dif, Bottle Quantity dif

After a valid code is assigned, the application retrieves the associated metadata, including the technical description of the changeover and the standard target time. It displays the attributes of both SKUs on a consolidated decision panel (Figure 5.9). This panel presents the two product states side by side, the assigned code and description, the format parts requiring adjustment, and the target duration. This provides operators with a direct visual reference and a benchmark for shift planning.

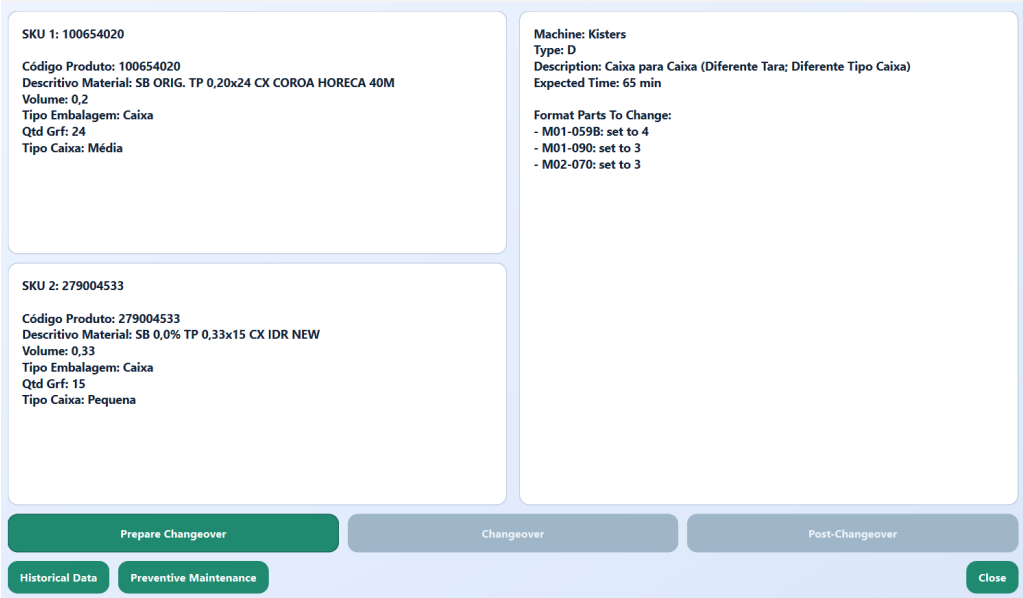


Figure 5.9: Consolidated SKU Comparison and Decision Panel

5.5.3 Guided Execution Workflow

The execution workflow consists of three sequential phases that correspond directly to the SMED methodology: Prepare Changeover (external tasks, machine running), Changeover (internal tasks, machine stopped), and Post-Changeover (external tasks, machine restarted).

Strict sequential navigation enforces phase progression. Initially, only the Prepare Changeover phase is enabled. The Changeover phase becomes accessible once all preparatory tasks are confirmed complete through a terminal action button ("Next Phase →"), while Post-Changeover remains inaccessible until the internal phase is validated. This structure ensures that external tasks are completed before machine stoppage, thereby reinforcing the SMED internal/external distinction on the shop floor, maximising preparation during runtime, and minimising downtime.

Task rendering and cognitive load. Tasks within each phase are organised by machine section or setup procedure and presented in one of three formats: collapsible groups, individual checklists, or mixed clusters (Appendix E). This approach serves as a cognitive filter tailored to the operator's experience. Routine or automated groups, such as HMI program selection, may be collapsed and confirmed with a single checkbox by experienced operators, or expanded into detailed sub-steps for less experienced personnel. In contrast, tasks that significantly affect quality, operational success, or safety are presented as granular checklists requiring individual confirmation, ensuring that critical steps are not bypassed regardless of operator experience.

Dynamic format-part instructions. In contrast to static task groups, the format-part group is generated at runtime based on component requirements determined by the classification engine. For each active line and SKU transition, the tool displays only those parts that require mechanical adjustment, using the format "Transition part [ID] from [SKU 1 state] to [SKU 2 state]"; parts that remain unchanged between products are omitted. Given the diversity of product portfolios,

maintaining a static transition matrix would be impractical. Generating the list dynamically from the backend eliminates the need for manual reference binders, reduces configuration errors, and expedites external preparation.

Media support. Text descriptions alone can be ambiguous when detailing mechanical calibrations such as guide-rail alignment or format-part assembly. Therefore, each step may include line-specific images and videos of the actual machine components, providing operators with an objective visual reference (Appendix E).

Internal timing and preventive maintenance. Since internal tasks determine machine downtime, a real-time timer is automatically initiated when the operator enters the internal phase, and the elapsed duration is recorded in the changeover log upon completion. This automation eliminates manual tracking errors and establishes an objective historical baseline necessary for ongoing SMED optimisation. To use extended stoppages effectively, a Preventive Maintenance module, accessible from the execution menu and built on the same checklist framework, provides routine cleaning, wear inspection, and condition verification tasks. Integrating this module into the changeover workflow transforms mandatory downtime into asset care without requiring a separate system, thereby supporting long-term equipment reliability.

5.5.4 Administrative Utilities and Data Governance

Data administration is strictly separated from routine tracking. Standard operators interact with a protected view, whereas product-data modifications are managed within a dedicated Administrator Mode, accessible via the ADMIN button and a password token. The Admin Menu contains three modules: Add SKU, Edit SKU, and Historical Data (Appendix E).

Add SKU. New products are entered using a form that enforces structural integrity prior to insertion. The Product Code and Description are entered manually, while technical attributes (Volume, Package Type, Bottle Quantity) are selected from dropdown menus. Box Type is not entered manually; instead, it is automatically derived from the bottle quantity using a fixed mapping.

$$f(\text{Bottle Quantity}) = \begin{cases} \text{Small}, & \text{if Bottle Quantity} \in \{12, 15\} \\ \text{Medium}, & \text{if Bottle Quantity} \in \{20, 24\} \\ \text{Large}, & \text{if Bottle Quantity} \in \{30, 35\} \\ \text{Pack}, & \text{if Bottle Quantity} \in \{4\text{P}, 6\text{P}, 10\text{P}\} \end{cases}$$

Enforcing this derivation is critical. Allowing free-text categorical entry would introduce variants such as “Média”, “media”, or “MED”, which disrupt exact-string matching in the rule engine and compromise downstream classification. Before insertion, a uniqueness check on the SKU code prevents duplicate primary keys.

Edit SKU. A load-edit-save workflow is used to maintain the portfolio over time. The administrator enters a code, loads the stored record into the form, modifies the attributes, and saves the changes. Box Type is recalculated using the same mapping to ensure consistency.

Historical Data. The third module displays a tabular log that aggregates each changeover into six metadata columns (Table 5.7). The current implementation merges predefined benchmark rows with live entries generated during the session. This approach provides immediate reporting capabilities and establishes the data architecture required for persistent automated logging in future iterations.

Table 5.7: Historical Data Table Schema and Captured Metrics

Column Name	**Metric Captured**
Date	Calendar date of the changeover event.
Start Time	Precise timestamp marking the start of the setup.
Team	Active shift group responsible for execution (A, B, C, or D).
Line	Line in which the changeover was executed.
Duration	Actual cumulative downtime duration.
Changeover Type	Resolved alphanumeric classification letter.

5.5.5 End-to-End System Data Flow

The complete changeover lifecycle is managed as a unified end-to-end pipeline rather than as a collection of isolated modules. The stages outlined in the preceding subsections (context initialisation, SKU validation, algorithmic classification, and phase-gated execution) are executed sequentially, with each stage consuming the output of its predecessor. This structure ensures that tracking metrics remain consistently linked, malformed data is prevented from reaching the classification engine, and external preparation activities do not coincide with the internal downtime window. The concurrent interactions among the operator, interface, classification engine, and persistence layer are illustrated in the system sequence diagrams in Figures 5.10 and 5.11.

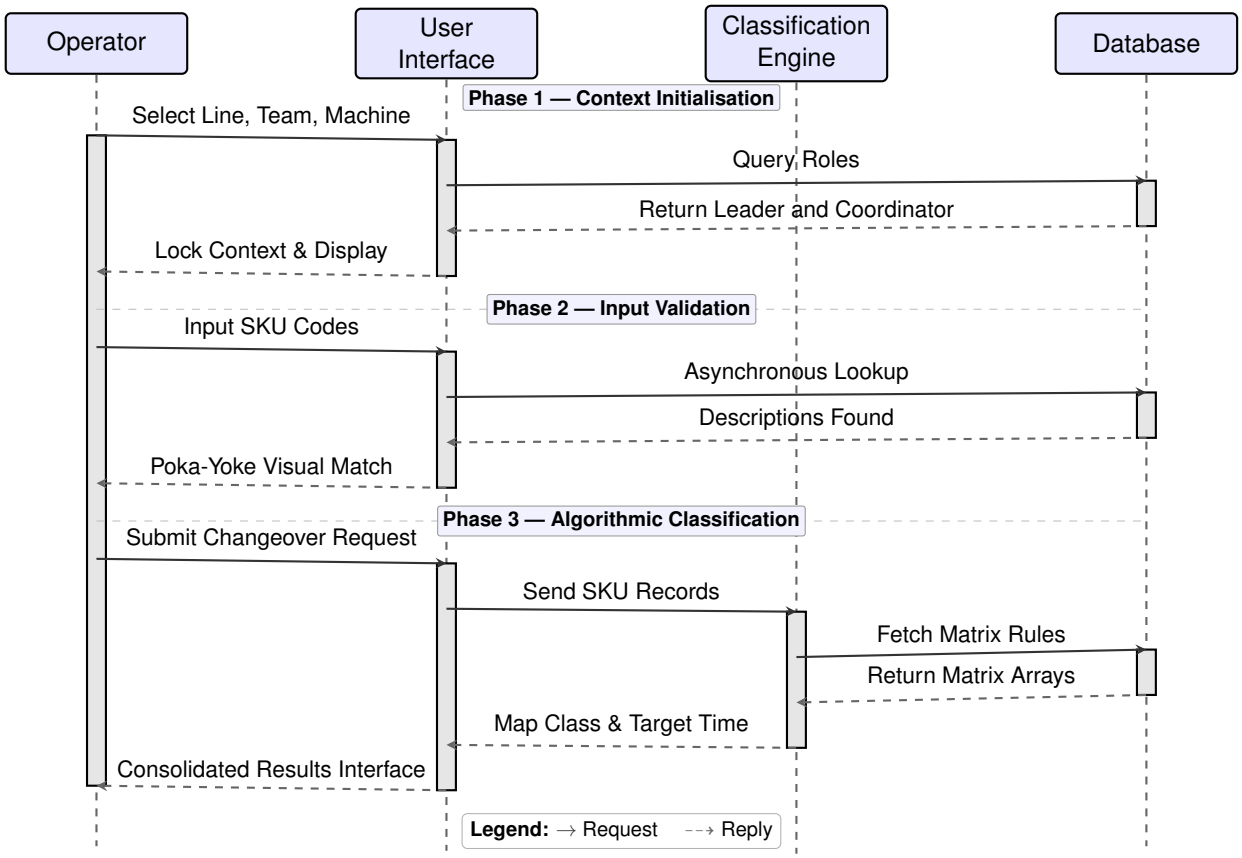


Figure 5.10: System Initialisation, Input Validation, and Algorithmic Classification Sequence

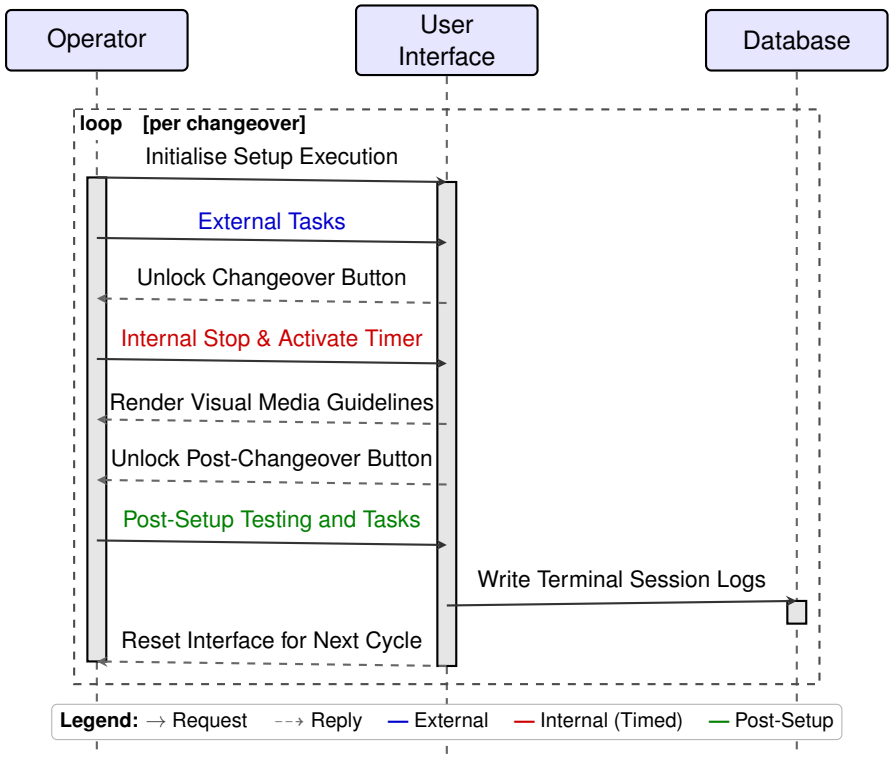


Figure 5.11: Guided SMED Execution Loop: Operator Workflow per Changeover

Chapter 6

Results and Discussion

6.1 Structure and Key Performance Indicators

This chapter provides an empirical validation, quantitative evaluation, and analytical discussion of the solutions implemented to optimise changeover procedures on the Mead and Kisters packaging lines. Building directly from the diagnostic findings in Chapter 4 and the engineering solutions proposed in Chapter 5, the performance of these interventions is evaluated against the primary objective of the SMED methodology and this thesis, the minimisation of non-productive machine downtime.

To guarantee a comprehensive assessment of the developed solutions, results are evaluated across multiple dimensions using time-and-motion data, kinematic validation, mathematical verification, and digital system logs. The impacts of these solutions are quantified using four core Key Performance Indicators (KPI):

- **Changeover Time Reduction:** The net time saved by converting internal setup steps into external operations and by streamlining manual adjustments.
- **Process Variance (σ^2):** The reduction of changeover execution variability across different shift teams (A, B, C, and D) and varying experience levels.
- **Operational Standardisation:** The reduction of cognitive load, data-entry errors, and procedural ambiguity through the implementation of programmatic control layers.
- **Structural and Economic Reliability:** The physical durability and cost-to-risk mitigation profile of the additively manufactured mechanical components.

The remainder of this chapter is structured to systematically evaluate each phase of the optimisation framework.

Section 6.2 evaluates the immediate time savings achieved by pre-adjusting the product feeding module's trolley guide rails and pre-staging the separation system toolsets.

Section 6.3 discusses the field results of the two-week active production trial of the 3D-printed PETG brackets, validating both their flexural integrity and their strategic utility as a mechanical fuse.

Section 6.4 verifies the shop-floor performance of the Name-Based Linear Programming (LP) model, confirming the reduction of the carriage mechanism's worst-case travel span to exactly 84.0 mm. Section 6.5 evaluates the digital support tool's field performance, analysing its impact on process standardisation, its Poka-Yoke data-entry layer, and the results of the proof-of-concept trials with inexperienced operators.

Section 6.6 consolidates these individual interventions into a final comparison, demonstrating the total reduction in line downtime and its broader implications for continuous improvement. Finally, Section 6.7 translates the consolidated time savings into an annual economic estimate, valuing the recovered line-time in both operating-cost and production-capacity terms.

6.2 Task Externalisation

The second stage of the SMED methodology aimed to convert internal setup activities into external operations performed while the machine being studied remains in operation. This section assesses the field performance and time-motion outcomes of two targeted externalisation measures implemented on the packaging lines: pre-adjustment of the Product Feeding Module's trolley guide rails and proactive retrieval of Format Parts, both on the Kisters.

6.2.1 Pre-adjustment of the Product Feeding Module's Trolley

The mechanical architecture of Lines 2, 5, and 6 enables integration with the upstream Mead machine, allowing these lines to shift between packaging configurations. As a result, changing the trolley and adjusting the respective guide rails significantly contribute to the changeover duration. Although the lengthiest task of physically mounting the trolley requires a crane and must remain an internal task, the guide-rail adjustment was converted into an external task completed before the machine stopped.

This practice was implemented across all three compatible lines, and field data were collected during a post-implementation observation period. In Line 5, no empirical data were recorded during the trial period because the production schedule consisted exclusively of continuous wraparound box SKUs, eliminating the need for trolley configuration changes. In Lines 2 and 6, 14 changeovers involving trolley reconfigurations were audited in detail (six on Line 2 and eight on Line 6).

To illustrate the change in time requirements for this task, Table 6.1 compares the empirical findings with the historical time-study baseline established in Chapter 4.

Table 6.1: Performance Comparison - Trolley Guide-Rail Pre-Adjustment

Production Line	**Monitored Events (n)**	**Historical Baseline Duration (min)**	**Post-Implementation Internal Duration (min)**	**Net Internal Time Saved (min)**
Line 2	6	4.0/4.5 min	0.0	4.0/4.5
Line 5	0	2.5/3.0	-	-
Line 6	8	3.0/3.5	0.0[1]	3.0/3.5

[1] One of the eight audited Line 6 events required a residual adjustment of approximately 12 seconds (0.2 min) instead of full elimination. The net time saved for this event was therefore approximately 0.2 min below the full baseline value. The remaining seven Line 6 events and all six Line 2 events achieved full elimination (0.0 min internal duration). The Line 5 baseline (2.5–3.0 min) is reported here for completeness, taken from the Chapter 4 time-study. No post-implementation comparison is available because no trolley reconfiguration occurred on this line during the observation window ($n = 0$).

Among the fourteen audited trolley reconfigurations, internal time for this task was reduced to 0.0 minutes in thirteen instances. In the remaining instance, on Line 6, a residual adjustment of approximately 12 seconds was required on one of the linear guides. In this particular situation, the operator confused two visually similar SKU configurations: 0.33L×24 and 0.25L×24. These configurations share the same packaging layout but require slightly different guide-rail values due to differing bottle diameters. This isolated case serves as a small-scale example of the discretionary value-confusion risk that the Slider optimisation and the digital decision-support layer are intended to address.

Given the binary nature of the intervention outcome, where the adjustment either remains fully on the internal timeline or it does not, the result is most appropriately expressed as a success rate rather than a mean reduction. Across the fourteen events, the exact (Clopper–Pearson) 95% confidence interval for full elimination is [66.1%, 99.8%]. This interval accurately reflects the presence of one observed exception, rather than suggesting a flawless outcome that the data do not support.

Beyond the direct time savings, this solution generated additional changeover benefits. Adjusting the guide rails prior to machine stoppage enabled the operator to perform concurrent internal tasks after assembling the trolley with the crane. This optimisation enhanced the line's parallel workflow, accelerated the overall changeover process, and reduced operator idle time.

6.2.2 Proactive Retrieval of Format Parts

Initial observations indicated that operators typically waited until the packing machinery stopped before walking to tool stations, located up to 20 m away, to retrieve the toolsets required for

changeover procedures. Although straightforward, this practice introduced unnecessary downtime during the machine-stopped phase. The proposed solution required operators to retrieve all necessary tools and Format Parts externally and pre-stage them before the line stops. The impact of this procedural change was evaluated across thirty changeover procedures distributed among four production lines: Line 1 (n = 6), Line 2 (n = 6), Line 5 (n = 10), and Line 6 (n = 8).

All thirty audited events had their internal downtime for tool retrieval reduced to 0.0 minutes (30/30; exact 95% CI [88.4%, 100%]), confirming this as a highly reliable outcome rather than a small-sample artefact (Table 6.2). The underlying per-line travel/retrieval durations are only available as a single pooled figure: a maximum of 1.5 minutes, observed across the thirty events combined.

Table 6.2: Performance Comparison – Proactive Retrieval of Format Parts

Production Line	**Monitored Events (*n*)**	**Historical Baseline Duration (min)**	**Post-Implementation Internal Duration (min)**	**Net Internal Time Saved (min)**
Line 1	6	0.5	0.0	0.5
Line 2	6	1.0	0.0	1.0
Line 5	10	1.0	0.0	1.0
Line 6	8	1.0/1.5	0.0	1.0/1.5

Beyond the time saved, the intervention provided a significant cognitive verification benefit: by retrieving tools during active production, operators could visually inspect and cross-reference tools against incoming SKU requirements before machine stoppage, eliminating the risk of delayed discovery during internal setup, such as identifying missing, broken, or incorrect tools, which had occasionally caused mid-procedure changeover delays.

Although each audited event achieved its time-saving objective, all thirty revealed a consistent shop-floor constraint. In the absence of a dedicated staging surface, tools were brought to the operational line and left on available surfaces such as the hot-glue unit, waste-bin lids, or stairs. This practice introduced risks related to safety, sanitation, and stability. Rather than being an incidental oversight, this issue represents a structural consequence of externalising the retrieval task without also externalising its staging logistics. Implementing a dedicated tool-placement zone or adopting trolleys, as currently used for the Mead on Lines 2 and 5, would maintain time savings while mitigating secondary hazards.

Together, these two Stage 2 interventions show that straightforward behavioural and organisational changes can reliably remove specific tasks from the internal changeover timeline: across the forty-four audited events, internal time for the targeted task was eliminated in forty-three (43/44; exact 95% CI [88.0%, 99.9%]), with a single quantified exception.

The magnitude of the benefit is line- and task-specific rather than uniform: on Line 2, where both measures were observed concurrently, total internal time removed from the critical path reached up to 5.5 minutes per changeover (4.0–4.5 minutes from guide-rail adjustment, plus up to 1.0 minutes from tool retrieval); on Line 6, the equivalent ceiling is up to 5.0 minutes (3.0 - 3.5 minutes plus up to 1.5 minutes). On Lines 1 and 5, where only tool retrieval was audited, the externalised time is bounded by the 1.0-minute maximum reported for that task alone. These figures should be read against the historical baselines established in the observation phase, which reflect a small number of time-and-motion observations per changeover type rather than a sampled distribution; the time-saved values reported in this section are therefore bounded estimates of task-level impact, not statistically tested mean differences.

The primary value of this stage is not the modest time savings, but rather the elimination of discretionary and easily disrupted manual steps from the internal critical path. This process stabilises the parallel operator workflow, which is essential for the success of subsequent, higher-impact interventions. Although this improvement is generally reliable, it remains sensitive to operator discretion and workspace organisation, as evidenced by both the single exception and the reproducible 5S staging gap.

6.3 Redesign of the Folding Bracket

The mechanical redesign of the Folding Bracket subsystem sought to replace an inefficient, tool-dependent legacy process with a more efficient and functional alternative. The redesigned process was subsequently prototyped and implemented. This section evaluates the quantitative time metrics, mechanical durability, cost-benefit profile, and human ergonomics associated with the proposed solution.

6.3.1 Quantitative Time and Motion Analysis

Under the legacy configuration, adjusting the 24 independent folding brackets was a significant changeover bottleneck. Because of the parallel tasks required across the different modules, this assignment was traditionally allocated to a single operator. This worker had to manually back out two threaded fasteners per bracket using a hex key, extract the bracket via the keyway slots, and re-tighten the fasteners.

Continuous timing observations were conducted 13 separate times throughout the study to establish a reliable baseline and monitor performance following implementation. Statistical analysis of this baseline indicates a mean execution time of 21 minutes and 14 seconds ($\mu = 1273.6$ s) with a standard deviation of 1 minute and 55 seconds ($\sigma = 114.6$ s). This elevated variance reflects the unpredictable nature of tool-based adjustments, where factors such as worn hex keys, over-tightened fasteners, and operator fatigue contribute to increased line downtime.

During initial trials on the Line 2 Kisters, a single pair of 3D-printed PETG brackets was installed for testing. To evaluate the pure manual handling of the component, the time to pull the indexing rings, slide the brackets down, and let them lock into the rest position was isolated. Over

15 controlled trials, the mechanism achieved an average adjustment time of 5.8 seconds per pair. This verified the kinematic efficiency of the tool-less design, excluding the fixed time required to jog the machine frame.

Following successful validation of the prototype for both the retracted and active positions, it was advanced to full-scale deployment, retrofitting all 24 bracket positions on the Line 2 and 5 Kisters machines with the engineered PETG solution. The complete task time, including manual manipulation, walking, and sequential machine chain jogging, was audited across 15 changeovers. This full-scale implementation resulted in a mean total task time of 4 minutes and 34 seconds ($\mu = 274.0$ s) with a standard deviation of 10 seconds ($\sigma = 9.8$ s).

Table 6.3 summarises the operational improvements resulting from the transition from the tool-driven legacy setup to the quick-adjust mechanism.

Table 6.3: Statistical Comparison of Total Task Execution Times for Folding Bracket Adjustment.

Metric	**Legacy Baseline Configuration**	**Redesigned Solution**	**Net Performance Change**
Sample Size (n)	13 changeovers	15 changeovers	—
Mean Time (μ)	21 min : 14 sec	4 min : 34 sec	16 min : 40 sec saved (78.5%)
Std. Deviation (σ)	1 min : 55 sec	0 min : 10 sec	91.4% reduction in σ; 99.3% reduction in variance (σ^2)

To confirm that this difference reflects a genuine effect rather than sampling noise, a Welch's two-sample t-test was applied (justified by the marked inequality of variances between groups). The difference was highly significant, $t(12.2) = 31.35$, $p < 0.001$, with a 95% confidence interval on the mean time saved of 15.50 to 17.82 minutes. The effect size is extremely large (Hedges' $g = 12.41$); this magnitude reflects the near-total collapse of post-intervention variance ($\sigma = 9.8$ s) as much as the shift in mean, since the toolless mechanism removes the operator-dependent variability that dominated the legacy task. Because the small sample sizes cannot fully verify the normality assumption underlying the t-test, an exact Mann-Whitney U test was also run as a distribution-free robustness check. The parameter U reached its maximum possible value for this sample size ($U = 195$, $p < 0.001$), meaning every individual legacy observation exceeded every individual redesigned observation, with zero overlap between the two distributions. The variance reduction was independently confirmed using an F-test ($F(12,14) = 136.8$, $p < 0.001$).

6.3.2 Empirical Structural and Mechanical Evaluation

A common concern when introducing additively manufactured polymer components into heavy industrial environments is their long-term structural survivability. To address this, the initial pair of PETG prototype brackets underwent a two-week continuous production trial on Line 2. Following the completion of the high-volume production trials, the components were extracted and subjected to detailed inspections.

- **Detent Holes Integrity:** The 5.00 mm detent holes were inspected for localised ovalisation, plastic creep, or micro-cracking caused by the repeated spring-loaded impact of the stainless-steel indexing plunger pin. No dimensional drift or structural degradation was observed.
- **Linear Guide Slot Wear:** The vertical slot paths showed no evidence of surface gouging or binding against the screws, confirming that the toolpath contours achieved using the slicing engine's compensation tool provided an optimal clearance fit directly off the build plate.
- **Adhesive Scraping Resilience:** Despite some exposure to stray hot-melt glue from adjacent applicator nozzles, the material withstood the mechanical scraping techniques employed by operators during scheduled cleanings. The solid infill matrix and 2.5 mm alternating $\pm 45^{\circ}$ wall shell provided sufficient surface hardness to maintain structural integrity without localised gouging.

Both Kisters units on Lines 2 and 5 were fully retrofitted with the PETG solution across all 24 bracket positions and monitored for an additional week of continuous production. No critical damage was observed at this broader scale. However, this result warrants careful interpretation. While the addition of components confirms the absence of early or widespread failure, it does not extend the temporal window of evidence beyond the initial trial. Breadth of deployment and length of service represent distinct considerations, and to date, only the breadth of deployment has been addressed.

This distinction is particularly relevant for additively manufactured parts. FDM components contain a dense network of layer-boundary discontinuities and inter-path voids, which serve as latent stress concentrators under cyclic loading. Because these parts do not behave as homogeneous bulk materials, standard analytical and finite-element fatigue models cannot reliably predict their long-term performance. Consequently, validation must be empirical and time-bound. The cumulative field exposure achieved to date, totalling three weeks across both trial phases, remains insufficient to establish extended durability.

This residual risk is addressed through a deliberate design contingency. The time-saving and standardisation benefits achieved result from the tool-less, quick-release kinematic principle of the redesigned bracket, rather than from the PETG material itself. If longer-term in-service monitoring reveals degradation inconsistent with continued safe operation, the original stainless-steel design (press-braked and laser-cut to form the same slot-and-hole geometry, and validated over years

of operation as the proven legacy solution) remains available as a direct drop-in replacement. Therefore, the SMED benefit achieved in this section depends on the broader mechanical principle shared by both material options, rather than on the polymer implementation alone.

6.3.3 Economic Viability and the Mechanical Fuse Paradigm

To justify manufacturing choices within lean manufacturing plants, it is necessary to evaluate cost and lead-time constraints. Acquiring or replacing custom mechanical components within the Portuguese industrial sector relies heavily on external workshops. The vast majority of large-scale manufacturing plants lack internal precision machining, laser cutting, or advanced metalworking infrastructure, as their core operational focus is high-volume production rather than equipment manufacturing.

Consequently, the production of custom components from materials such as stainless-steel must be outsourced to specialised vendors. Based on internal estimates derived from comparable outsourcing jobs previously commissioned by the company, typical turnaround times are expected to fall in the region of 3 to 4 weeks, exposing the plant to substantial out-of-pocket costs and the risk of extended downtime while awaiting delivery.

In contrast, the in-house 3D printing engineered solution bypasses external supply chains entirely. Using the optimised slicing matrix, a single bracket consumes approximately 5 g of filament, translating to a raw material cost of less than €0.15 per bracket. An even greater advantage is the lead time for the in-house solution: 8 brackets can be printed on-site in under 2 hours, and a complete machine set of 24 units can be fabricated in less than one operating shift.

The redesign also realises the mechanical-fuse advantage engineered. No collisions occurred during the trial period, but historical maintenance logs confirm that retract-failure incidents occasionally occur on these lines. Because the PETG bracket is deliberately the weakest link in the assembly, such an impact deforms a €0.15 component sacrificially rather than transmitting energy into the machine frame, turning what would otherwise be a lengthy, high-cost maintenance breakdown into a trivial replacement.

6.3.4 Operator Ergonomics and Qualitative Feedback

Post-implementation interviews and field monitoring across the different shift teams indicated highly positive feedback from operators and team leaders. While the tool-less design substantially reduced changeover time, it was also a significant ergonomic improvement. Accessing the legacy fasteners on the non-operator side of the machine required workers to maintain awkward, bent-over postures within the confined internal chassis of the Kisters unit while performing high-precision tool tasks. Eliminating the need for tools and introducing highly accessible pull-rings removed the physical strain associated with this task.

Among the 27 operators surveyed, only one expressed scepticism about the potential fragility of a plastic component in a heavy industrial environment, resulting in an acceptance rate of 96.3%.

All participants recognised the potential for time savings and improved work optimisation associated with the solution.

6.4 Adjustment Values Optimisation and Update

This section details the empirical results of updating adjustment values and implementing optimised slider configurations. Field validation was conducted on Line 1 Kisters, with setup durations tracked across four primary changeover types.

6.4.1 Shop-Floor Deployment and the Empirical Adaptation Window

Implementation of the mathematical programming outputs in the production environment required iterative adaptation and alignment. The deployment process comprised two primary steps: saving updated numerical parameters to the machine's HMI program and securing the slider mechanism into the three discrete, name-based configurations (12/15, 20/24, and 30/35 groups).

Initial field observations required minor millimetric calibrations to align the mathematical model with practical packaging constraints. In collaboration with senior operators, theoretical positions were adjusted for cardboard cutout clearance, material quality tolerances, and rail friction. Validation of extrapolated configurations indicated strong predictive validity. Following baseline alignment and minor clearance adjustments, all calculated configurations performed as anticipated, including low-production-volume packaging formats not tested prior to deployment, confirming robust boundary management. This outcome provides direct field confirmation of the robustness of the sensitivity analysis conducted in Section 5.4, where the optimised configuration was shown analytically to tolerate both a synthetic future SKU and the full ±1.2 mm bottle-diameter manufacturing tolerance without requiring re-optimisation; the absence of unexpected boundary failures during deployment is consistent with that theoretical result.

6.4.2 Quantitative Changeover Performance Evaluation

To evaluate the impact of eliminating trial-and-error fine-tuning, changeover durations on Line 1 were systematically tracked. Baseline data from observations conducted prior to parameter alignment were compared with post-implementation data using the updated standardised settings. The proactive tool-retrieval practice from Section 6.2 was already in place throughout both observation periods, so the comparison below isolates the effect of the slider optimisation specifically, without conflating it with the externalisation gains reported separately. Table 6.4 provides a statistical summary of these shop-floor performance metrics.

Table 6.4: Line 1 Changeover Duration Performance Metrics Before and After Software Optimisation

Changeover Type	**Baseline Observations (Minutes)**	**Post-Optimisation Observations (Minutes)**	**Mean Time Reduction**	**Net Efficiency Gain (%)**
Type A	30.0, 33.0 ($\mu = 31.5$)	24.0, 26.0 ($\mu = 25.0$)	6.5 min	20.6%
Type B	35.0, 28.0 ($\mu = 31.5$)	26.0, 27.0 ($\mu = 26.5$)	5.0 min	15.9%
Type C	38.0, 49.0 ($\mu = 43.5$)	35.0, 37.0 ($\mu = 37.5$)	6.0 min	13.8%
Type D	39.0, 39.0, 48.0 ($\mu = 42.0$)	35.0, 35.0 ($\mu = 35.0$)	7.0 min	16.7%

The results present a consistent reduction in changeover duration across all four observed types, with average time savings of 5.0 to 7.0 minutes per setup cycle and time improvements between 13.8% and 20.6%. Additionally, the intervention stabilised upper time limits: under baseline conditions, observed durations ranged from 28 to 49 minutes, whereas post-implementation, the range narrowed to 24 to 37 minutes. For Type C and Type D, baseline durations reached 49 and 48 minutes, respectively, mainly due to extended troubleshooting and machine readjustments. Implementation of the optimised minimum travel span eliminated these worst-case scenarios, reducing maximum downtime to 37 and 35 minutes.

Due to the limited number of samples for each individual changeover type (two or three per type), statistical significance cannot be established at the type level. This limitation arises from sample size rather than data quality. Pooling observations across all four types (baseline n=9, post-optimisation n=8) enables a more robust comparison, although this approach treats four distinct changeover types as a single population. The pooled analysis shows a mean reduction from 37.7 to 30.6 minutes (18.7%), with a large effect size (Hedges' g = 1.04). A Welch's t-test indicates a statistically significant difference ($t(14.5) = 2.30$, $p = 0.037$; 95% CI on the mean difference: 0.50 to 13.58 minutes), and tie-corrected Mann-Whitney U test yields a consistent result ($U = 57.5$, $p = 0.042$). Although the effect reaches conventional significance and is large and directionally consistent across all four changeover types, the small sample size and the heterogeneity introduced by pooling warrant caution: the result is best read as strong evidence of a genuine reduction rather than a definitive, per-type confirmation.

6.4.3 Shop-Floor Governance and Human Factors

In addition to mechanical and mathematical parameters, the long-term sustaining of a lean manufacturing process relies on effective data governance and sustained operator engagement.

The introduction of a password-protected user profile for the Packaging Department, restricted to Team Leaders and Line Coordinators, established a secure administrative gatekeeping mechanism. Although the long-term effectiveness of this control will be assessed over subsequent production seasons, no unauthorised or unlogged parameter adjustments were recorded during the observation period, a marked change from the previously open-access condition, where such adjustments were a known contributor to changeover variability.

Team leaders and line coordinators demonstrated exceptional proactivity during deployment, placing a high value on immediate improvements in line changeover performance and readily adopting the structured approach. Most operators responded positively to the standardised positions, noting that the name-based configurations simplified physical positioning and reduced reliance on subjective judgment. A minority remained sceptical about the universal applicability of the mathematical positions. This resistance diminished over time as successive standardised runs operated without issues, demonstrating that consistent objective data can reshape established shop-floor practices.

6.5 Digital Changeover Support Tool

Developing a digital changeover support tool was a primary strategic objective for this project. The goal was to transform uncodified, operator-dependent knowledge into a standardised digital asset. Due to the complexity of changeover configurations across production lines and the technical challenges of integrating a custom app into the company's IT infrastructure, the tool has not yet been fully deployed plant-wide.

Instead, a rigorous alpha testing and field validation process was conducted on the shop floor. This enabled real-world UI testing, workflow validation, and feedback assessment on the shop floor.

6.5.1 Iterative Feedback Loop and Initial Perceptions

Rather than designing the software in isolation, the development process relied entirely on a hands-on feedback loop. This direct field checking was essential to fully understanding the line-specific details often omitted from a macro perspective. The main feedback loops involved verifying the exact order of changeover tasks, confirming that the photos and videos clearly illustrated the specific tasks and adjustment points, and gathering immediate user feedback on how the interface should function to be useful and meet the operational requirements.

Operator feedback was clearly divided by demographic and experience. The senior, more experienced workers were overall sceptical and expressed doubts about the software application's ability to fully capture and resolve changeover inefficiencies, arguing that experience was the

only truly determining factor for quicker changeover procedures. On the other hand, younger and temporary workers were fully supportive of this tool as they would benefit greatly from it. They identified the solution as a powerful learning tool that would also help avoid mistakes in setup procedures, leading to higher-quality operations.

This division shows that while senior staff rely on intuition and memory, the digital tool may play a different role for newer or temporary workers, who lack that accumulated experience. This raises the practical question tested directly in the following section.

6.5.2 Proof-of-Concept

To assess whether the digital tool could guide inexperienced workers through a setup procedure without relying on prior procedural knowledge, two trials were conducted on Line 1, chosen for its relatively simple changeover operations. Two temporary workers participated, each with about seven weeks of general shop-floor experience but no familiarity with this specific procedure. Both received an informal, 15-minute orientation to the application's interface, but no instruction on the changeover procedure itself. This focused the trial on whether the app's guidance alone could substitute for the procedure-specific experience. An experienced coordinator was present solely for safety and did not intervene.

The application automatically records internal setup time, measured from the start of the changeover to the end of the internal phase. The two trial operators completed the procedure in 51 and 57 minutes, respectively. For comparison, an experienced shift team completed the same changeover type (Type A) in 30 and 33 minutes under normal conditions, as reported in Table 6.4. However, this comparison is not a direct speed test due to two key differences. First, the trial aimed to determine whether an unaided, inexperienced operator could complete the changeover independently, not to match experienced-team speed. The longer duration, about 1.6 to 1.9 times greater, reflects the expected gap in task-specific experience, not a shortcoming of the application's guidance. Second, the reference times likely represent a team-based effort, with logistics tasks such as retrieving pallets handled in parallel by other operators. In contrast, the trial required the temporary worker to complete all setup tasks alone, including logistics. A fair speed comparison would require testing inexperienced solo operators with and without the app, which was beyond the scope of this trial.

Three additional limitations constrain these results. First, no error rate could be determined because the application does not log interaction-level events, and the straightforward changeover process provided few opportunities for procedural error. Second, repeatability cannot be established from a single trial per operator; although the two recorded times (51 and 57 minutes) are similar, this observation is descriptive rather than evidence of consistency. A statistically robust assessment remains a subject for future research. Finally, both changeovers were followed by a ramp-up phase that, according to informal observation, appeared to last somewhat longer than usual, although precise durations were not documented.

This final point highlights the distinction between procedural compliance and achieving optimal outcomes. While the application can guide operators through the correct mechanical steps, it

does not yet provide the tacit, experience-based judgment required to verify that the setup yields acceptable output. This skill continues to be developed only through repeated ramp-up practice.

6.6 Overall Discussion

The solutions developed during this project were not designed as a single, abstract system; instead, each was created to solve a specific, practical bottleneck identified during the shop-floor diagnostic phase. While some solutions operated completely independently, others relied on one another to be effective. Table 6.5 provides an overview of the operational shift from an unstandardised, experience-dependent environment to a data-driven, structured workflow, comparing pre- and post-implementation states.

Table 6.5: Master Synthesis of Operational States and Key Outcomes Across Chapters 5 and 6

Intervention Area	**Baseline State (Before)**	**Optimised State (After)**	**Key Operational Outcome**
Task Externalisation (6.2)	Trolley guide-rail adjustment and tool/format-part retrieval performed only after the machine stopped.	Both tasks shifted to the external, machine-running window across all compatible lines.	Internal time eliminated in 43 of 44 audited events (97.7%); modest per-event savings (0.5–6.0 min depending on line); a parallel 5S staging gap was identified as a structural side-effect.
Folding Bracket Mechanism (6.3)	Tool-dependent fastener adjustment; mean 21:14, highly variable (σ=114.6 s).	Tool-less quick-release mechanism; mean 4:34, near-constant (σ=9.8 s).	78.5% task-level time reduction; 99.3% variance reduction; statistically conclusive (Welch's t, exact Mann–Whitney, Hedges' g=12.41) — the project's strongest single result, though not directly comparable to whole-changeover literature benchmarks.

Continued on next page

Adjustment Values & Slider Optimisation (6.4)	Continuous adjustment scale; manual guessing; changeovers up to 49 minutes.	Three discrete, name-based slider configurations; mathematically optimised and HMI-synchronised.	13.8–20.6% whole-changeover time reduction (Line 1) — the chapter's only directly verified, literature-comparable result.
Process Control & Security (6.4.3)	Parameter editing restricted to the maintenance team alone, creating a bottleneck that contributed to accumulated misconfiguration over time.	Access decentralised to a password-protected Team Leader and Line Coordinator profile, with a dedicated SOP governing the new structure.	No unauthorised or unlogged parameter changes recorded during the observation period under the new access model.
Digital Support Tool (6.5)	Paper manuals largely ignored; tribal, experience-dependent knowledge.	Phase-gated mock-up support tool, tested in two proof-of-concept trials.	Enabled procedure-inexperienced operators to complete a setup independently, though not yet matching experienced-team speed or ramp-up quality; plant-wide deployment still pending.

Individual evaluation of these interventions reveals their unique contributions and varying evidentiary strength. The externalised tasks, although modest when considered separately, consistently eliminated specific steps from the internal timeline. This established the procedural discipline necessary for the effectiveness of subsequent, higher-impact interventions. The folding bracket redesign yielded the most substantial and statistically robust result in this chapter; however, it pertains to a single task rather than an entire changeover, a distinction discussed in the following section.

The principal benefit of these combined solutions is the reduction of operational uncertainty. In production environments, although average changeover times are significant, predictability is equally vital for effective scheduling and overall line efficiency. Replacing subjective operator intuition with fixed mechanical settings and validated software data has converted an unpredictable process into a more standardised, deterministic routine across the production lines studied.

The 78.5% reduction achieved by the folding bracket at the task level is not directly comparable to published case studies, which typically report reductions for the entire changeover process rather than for individual sub-tasks. A more appropriate comparison is provided by Line 1's slider optimisation, which resulted in a 13.8% to 20.6% reduction in total changeover duration, depending on the changeover type. This is the only directly verified result in this chapter that aligns with the scope commonly reported in SMED literature, as Line 1 does not employ the folding bracket mechanism and thus isolates the effect of the slider optimisation on the entire changeover.

A complementary, although explicitly unverified, analysis can be conducted using the historical changeover log presented in Appendix A. Four changeover types recorded prior to implementation (E1, E2, F1, and F2) involve all three interventions: trolley guide-rail pre-adjustment, proactive retrieval of format parts, and the folding bracket redesign. When restricting this analysis to Lines 2 and 6 (excluding Line 5 due to the absence of measured trolley procedures), the log provides usable baseline observations only for E1 (n=3) and E2 (n=4). F1 and F2 are represented by a single event each, which is insufficient for drawing any conclusions.

For E1 and E2, the documented task-level savings from previous sections provide achievable improvement, assuming these savings are additive and independent. Table 6.6 presents this calculation.

Table 6.6: Illustrative Ceiling Estimate for Combined Stage 1/2 Interventions, Lines 2 and 6.

Line	**Type**	**Historical Baseline (min)**	**Theoretical Combined Saving (min)**	**Theoretical After (min)**	**Implied Max. Reduction**
L6	E1	75	21.2	53.8	28.2%
L6	E1	80	21.2	58.8	26.5%
L2	E1	64	21.9	42.1	34.2%
L6	E2	77	21.2	55.8	27.5%
L6	E2	68	21.2	46.8	31.1%
L6	E2	54	21.2	32.8	39.2%
L2	E2	71	21.9	49.1	30.9%

Across these seven events, the implied maximum reduction ranges from 26.5% to 39.2%, pooling to approximately 30.6%. This value exceeds Line 1's verified result and aligns with the expected outcome that three interventions would have a greater cumulative effect than two. However, this figure represents only an upper bound rather than a validated outcome, as it assumes that the documented savings transfer directly to these specific historical events, without interaction effects between tasks or execution friction. Confirming this estimate would require direct

post-implementation timing of the E1 and E2 changeovers on Lines 2 and 6, which constitutes a logical next step beyond the scope of this thesis.

When benchmarked against published SMED case studies, which report a wide range of whole-changeover reductions - from 18% to 33% in a plastic injection-moulding case [67] - to more than 45% in a turning-line case [68], to 55.55% reported by McIntosh et al. [69], and up to Shingo's original benchmark cases averaging approximately 94% [17]; Line 1's verified result of 13.8% to 20.6% falls at the lower end of this spectrum. It closely overlaps the lower-bound case study, rather than falling below it. This situates the result credibly within established SMED practice: it is robust and field-validated, positioned at the more conservative end of documented outcomes, and consistent with the limited scope of a single optimisation intervention rather than a comprehensive overhaul. The theoretical ceiling estimated for Lines 2 and 6 would, if confirmed by direct measurement, fall within the middle of this range. This reflects the larger effect anticipated when three more significant interventions are combined rather than two.

The digital support tool represents a distinct category of evidence. Its two-subject proof of concept demonstrated that operators without prior procedural experience could complete a full changeover unaided. However, the trials also revealed a significant limitation of procedural guidance: both were followed by a modestly extended ramp-up phase. This suggests that the tacit, experience-based judgement required to verify setup quality cannot yet be fully replicated by the tool.

This boundary also delineates the scope of the remaining work in this thesis. Procedural and organisational improvements, corresponding to Stages 1 and 2 of the SMED methodology, have measurably reduced both the duration and variability of changeover operations across all studied lines. Nevertheless, the results converge on a fundamental limitation: even with optimised target values and guided execution, adjustment of the Kisters still relies on manual fine-tuning, the quality of which varies with operator judgement and experience. This residual source of downtime and ramp-up variability cannot be fully eliminated through further refinements to procedural, training, or digital guidance, as the limitation is physical rather than informational. An operator manually setting a value, regardless of the quality of the instruction, remains constrained by manual dexterity and visual judgement.

This represents the design ceiling identified by McIntosh et al. [21], where procedural SMED improvements must transition to technical redesign. Chapter 7 addresses this by applying Stage 3 of the SMED methodology, which involves streamlining the remaining internal operation through mechanisation and parallel execution, rather than further procedural adjustment, specifically to the M09 Module. This module is the logical focus for three independent reasons established throughout this thesis: it contains the highest density of spindle-type adjustment points on the machine; it is the same physical system whose target values were mathematically optimised in Section 5.4 and empirically validated in Section 6.4, making automation a direct extension of prior work; and it is the primary source of fine-tuning-related stoppages observed during this study. While Sections 5.2 through 5.5 standardised the correct adjustment value and designated personnel, Chapter 7 addresses the final variable: the individual performing the adjustment and

the method employed.

6.7 Economic Analysis

The operational gains described in Sections 6.2 through 6.5 are consolidated into an aggregate estimate of their annual economic value to SBG. This estimate is based on the line's approximate hourly operating cost for labour and utilities, excluding depreciation, of €300/hour. Recovered time is also quantified as production capacity, using each line's nominal filling rate 60,000 bottles/hour for Lines 1 and 2, 80,000 bottles/hour for Line 5, and 50,000 bottles/hour for Line 6. During the capacity-constrained periods that predominate throughout the operating year, each recovered hour translates directly into additional saleable output.

Changeover frequencies were annualised over the 49 productive weeks that follow the three-week preventive-maintenance stoppage. For Lines 2, 5, and 6, frequencies were scaled from an eight-week observation window (weeks 15 to 22), which covers the transition from the spring shoulder period into the May production ramp-up. This period is considered broadly representative of the year, rather than a low-season sample. The frequency for Line 1 was derived from its weekly changeover average. Based on these calculations, the lines perform approximately 250 (Line 1), 410 (Line 2), 239 (Line 5), and 263 (Line 6) changeovers annually.

Each intervention is credited only when its time saving reduces the overall line changeover duration. The folding-bracket and trolley savings are fully credited, as these tasks occur during changeovers, when the Kisters machine is the critical constraint. The slider-optimisation and format-part-retrieval savings are credited only to the Kisters-critical share of each line (35 to 48 %), as these occur during product changeovers that can be dominated by the filler or other equipment. This approach is deliberately conservative. On non-critical changeovers, the saved time is not lost; instead, the Kisters completes its setup earlier and releases skilled operators to assist the critical workstream. Since the overall changeover duration is determined by the slowest parallel task, this earlier release can further reduce the total changeover time. Therefore, the values presented below represent a lower bound, with the uncredited portion contributing to parallel-workflow capacity that cannot be directly quantified with the available data. Trolley reconfigurations are treated as coinciding with folding-bracket changeovers, consistent with their observed correlation.

Table 6.7 presents the resulting annual estimate.

The implemented interventions are projected to recover approximately 73 hours of line time per year, which corresponds to an estimated 4.7 million bottles of annual production capacity and an operating-cost value of roughly €22,000 per year. The majority of this benefit is realised on the higher-throughput, higher-frequency lines, with Line 2 alone accounting for nearly half of the recovered capacity.

The capital investment required to achieve these gains is minimal. The folding-bracket solution requires less than €4 in filament per 24-position machine set, plus a small portion of an existing €700 printer already allocated for other purposes. The slider and trolley improvements are procedural and do not incur any capital costs. Two additional measures are not included in

Table 6.7: Consolidated Annual Economic Impact of Deployed Interventions

Intervention	**Line(s)**	**Events/yr**	**Saving/event**	**Hours/yr**	**Value/yr (≈€300/h)**
Folding-bracket redesign	2, 5	159	16.7 min	44.3	€13,300
Slider optimisation	1	88*	6.7 min	9.8	€2,950
Trolley pre-adjustment	2, 5, 6	248	2.5–4.0 min	14.0	€4,190
Format-part retrieval	1, 2, 5, 6	376*	0.5–1.0 min	5.5	€1,660
Total (deployed)				**≈73.6**	**≈€22,000**

*credited only at the Kisters-critical share of the line.

this calculation: integration of the digital changeover tool into the plant IT environment, estimated at €2,000 and further reduced by in-house implementation, and a recommended 5S staging zone, estimated at €1,000. Even when these costs are fully allocated against the recovered value, the payback period remains under three months. The mechanical and procedural interventions responsible for the majority of the benefit achieve payback within days of deployment.

A limitation should be noted regarding this estimate. The per-event savings for the externalisation measures are bounded task-level estimates rather than statistically validated means (Section 6.2). Therefore, these figures should be interpreted as a defensible order-of-magnitude assessment of realised benefit, rather than as a formal financial audit. Valuing recovered time at the operating cost represents a deliberately conservative approach. Since these lines operate to meet demand for most of the year, an hour recovered during the high season equates to foregone saleable production, the value of which significantly exceeds the €300 per hour operating rate. The economic justification for the capital-intensive intervention discussed in Chapter 7 is based on this distinction and is further developed using the same hours-and-capacity framework.

Chapter 7

Case Study: Design of an Automatic Adjustment System

This chapter presents the systematic engineering design process for the automatic adjustment system. The process integrates the SMED methodology framework, which supports the thesis, with a classical mechanical engineering approach to demonstrate the complementary relationship between these disciplines. The following sections document the development of the machine, including clarification of boundary conditions, generation and objective evaluation of conceptual layouts, analytical validation of mechanical components, and final specification of the system architecture.

7.1 Design Methodology Execution

As established in Chapter 2, the mechanical retrofitting of the Kisters Cardboard Cutouts Feeding Module constitutes an Adaptive Design problem. To prevent unguided trial-and-error, the development of the automated shaft adjustment system strictly follows the VDI 2221 framework. Rather than reiterating the theoretical framework, this section documents the practical execution of the four VDI 2221 macro-phases applied directly to the Kisters packer:

1. **Phase 1: Clarification of the Task:** The boundary conditions of the legacy machine are physically mapped. This includes measuring the available spatial envelopes around the transmission elements to keep, reverse-calculating the required rotational torque to overcome stiction, and establishing the environmental constraints dictated by the abrasive cardboard particulate. The result is a rigorous requirements list tailored to the machine's existing footprint.

2. **Phase 2: Conceptual Design:** The functional architecture of the retrofit is synthesised. In this phase, competing actuation methods and power transmission systems are objectively evaluated using weighted decision matrices to select an optimal solution for each part.

3. **Phase 3: Embodiment Design:** The selected conceptual layout is translated into a physical architecture. Iterative CAD modelling is used to size the mechanical components, design

the modular offset bracket geometries, and ensure the kinematic chain respects strict spatial bottlenecks, such as the machine's absolute floor clearance limits.

4. **Phase 4: Detail Design:** The final spatial integration is validated and prepared for manufacturing. This stage focuses on Design for Manufacture and Assembly (DFMA) by specifying standard Commercial-Off-The-Shelf (COTS) components (e.g., DIN/ISO fasteners and bearings) and defining precise manufacturing tolerances (such as H8 locational clearance fits) to guarantee the physical viability of the automated adjustment system.

Application of this structured execution framework ensures that all mechanical, spatial, and electrical decisions are objectively validated against the reality of the shop floor before any physical prototyping or capital expenditure occurs.

7.2 Clarifying the Task

As stated in the previous chapters, most of the Kisters changeover is achieved by adjusting parts of the machine to fit the different size packages. This task requires the operators to manually adjust the graduated metric scales or spindle adjustment points. For the latter case, this requires a high level of precision for the operator to correctly adjust the machine in order to ramp-up and start production smoothly. Because of this, this task is present in every type of changeover from the quickest and easiest to the most complex and lengthiest. If these adjustment points could be adjusted automatically and simultaneously this is expected to reduce the changeover time substantially. Therefore, incorporating a machine design case study within the SMED project is expected to yield significant benefits.

Line 1 was selected for this case study for the reasons outlined in Section 3.4.3. Additionally, following the completion of the study on adjustment parameters, these parameters were updated and now represent the most accurate values. The main goal is to study the feasibility of developing an automatic adjustment system for the precise spindle adjustment points throughout the machine, in order to reduce changeover time.

In order to start the design process it was necessary to understand where this system would be implemented. For this, the adjustment points of the machine were studied to understand if there was a way to streamline the focus of the project. The spindle adjustment points are distributed throughout the machine as observed in Table 7.1.

Table 7.1: Spindle Adjustment Points Distributed Across the Machine's Modules

Module	**Spindle Adjustment Points**	**Spindle/Total**
Product Feeding Module (M01)	020	1/16
Cardboard Cutout Feeding Module (M09)	001/010/012/021/025/060/061	7/7
Formatting Module (M02)	030/040/076/160	4/15
Folding Module (M03)	140/213/230	3/11
Total		15/49

As it can be observed in the Table 7.1, not every module has the same type and number of adjustment points. The Cardboard Cutout Module represents the most favourable characteristics which makes it the most suitable candidate to host this project. Firstly it has by far the greatest number of spindle adjustment points of any other module and all of its adjustment points are of this type. This allows this module to be fully automated not requiring any format piece change or scale adjusting. Secondly this is the module where precision is most critical. Due to the delicate nature of the tasks relative to cardboard handling and distribution and the material rigidity, there is an inherent precision requirement throughout this whole module, especially due to moving through roller conveyors, being pushed by forks and being slid through belts. When these precision requirements are not fully fulfilled, errors throughout the module occur, stopping production, as can be observed in Figure 7.1.

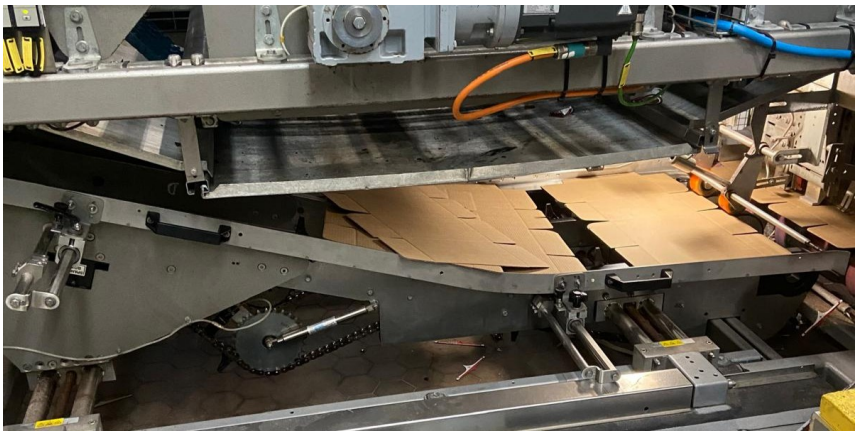


Figure 7.1: Example of Cardboard Cutout Overlapping Error Due to Poor Adjustments

In addition to inaccurate adjustments by the operator, errors introduced by the cardboard manufacturer must also be considered. Occasionally, incorrectly cut cardboard pieces with dimensional deviations of several millimetres cause the Kisters to jam and malfunction (Figure 7.2). These issues typically arise when defective pallets are mixed with standard ones, resulting in significant disruptions to production.



Figure 7.2: Defective Cardboard Cutout

Finally, due to cardboard characteristics and the complexity of the adjustment system, the ramp-up process of the machine is highly dependent on these adjustments. From the changeover observation notes, incidents and stoppages were accounted for the ones relative to the Cardboard Cutout Feeding Module. These results are presented in Figure 7.3.

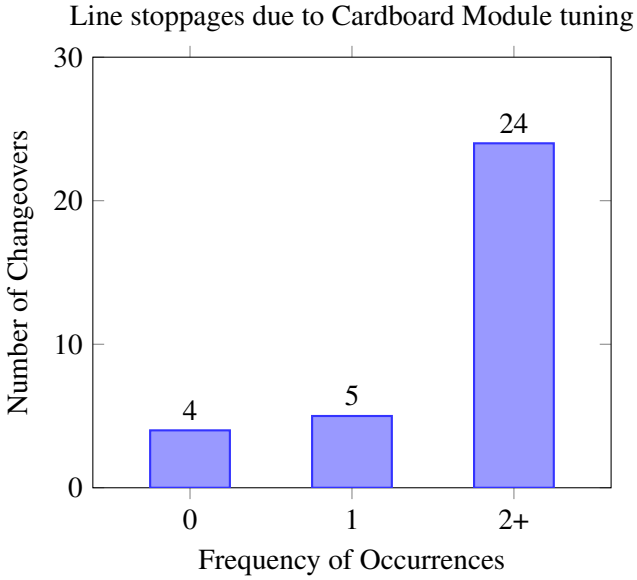


Figure 7.3: Distribution of Occurrences Across the Universe of Observed Changeovers

The graph above illustrates that most changeovers were delayed by stoppages resulting from incidents or the requirement for finer adjustments within this module. Among the 29 changeovers interrupted for these reasons, 24 experienced multiple stoppages. Notably, four changeovers did not require finer adjustments; these involved boxes of the same type and containers of identical volume. In such cases, the critical lateral guides remain unchanged, as the box only increases in

length to accommodate more bottles (for example, from 20 to 24 bottles). These specific adjustments are simpler and rarely result in operational issues.

For the changeovers in which these occurrences were observed, a box plot was generated to depict the time distribution for both scenarios (Figure 7.4). The median fine-tuning duration is 6 minutes for changeovers with a single stoppage, rising to 14 minutes for changeovers with two or more stoppages. These incidents frequently extend the ramp-up process, thereby delaying the initiation of subsequent production orders and increasing overall changeover times.

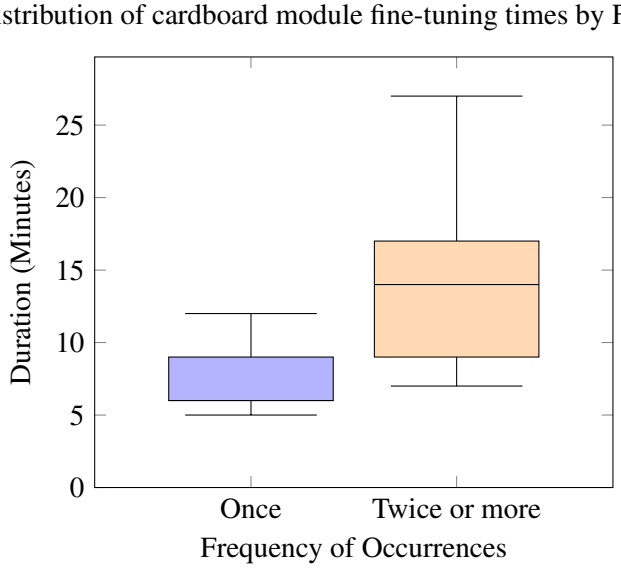


Figure 7.4: Time Distributions of Observed Changeovers Based on Their Frequency of Occurrence

It was decided that the project would narrow its scope to the automation of the Cardboard Cutout Feeding Module changeover. Given the time and resource constraints inherent to the project, narrowing the focus to a single, more critical system ensured a better project development and further feasibility of implementation.

At this phase of the project, the system's functional requirements must be defined as well as the division of the project in sections which represent best the division between integrated components.

A critical factor when trying to implement a major change in operation of a previously designed system is understanding the level of change that can realistically be implemented. In the beverage industry, where machines produce continuously there is no real opportunity to change the basis of a machine. Changing structural elements and many other parts of the machine must be avoided as this would mean greater stoppages and the project would have to be robust and flexible enough to deal with the associated constraints of the industry.

In order to design a solution it is essential to understand how these adjustment points work. Due to the functioning and area of actuation, the problem should be divided into three sections: the Cardboard Cutouts Transportation System (M09-060/061), the Roller Conveyor (M09-001) and the Cardboard Cutouts Storage Unit (M09-010/012/021/025). M09-001 is relative to the transverse

adjustment of the guide rails to the roller conveyor. M09-060/061 are both relative to adjusting the guide for the transportation system which takes the cardboard cutouts directly to the folding module. M09-010/012/021/025 are relative to adjustments in the cardboard cutout storage unit before they enter the transportation system. They are relative to the transverse adjustment of the stop, the transverse adjustment of the separator, height adjustment of the separation wedges and longitudinal adjustment of the rear skid, respectively.

For the Transportation System to achieve the correct movement on the guide rails, the system uses 3 linear guides with lead screw drive, with a static centre point and a moving anchor on each side with independent control, relative to the different adjustment points (060 relative to the operation side and 061 relative to the opposite side). These 3 guides are spaced along the guide rails to maintain uniform motion throughout the guide and prevent deflection. Figure 7.5 illustrates the distribution, highlighting the linear guides in green and the M09-060 adjustment point in yellow. This uniform motion is guaranteed by a transmission system of bevel gears, shafts, universal joints, and spur gears such that, when either adjustment point is rotated, the guides move simultaneously and uniformly. There is a functional requirement that all these linear guides must move simultaneously and in the same way to guarantee the correct adjustment of the rails.



Figure 7.5: M09-060 Adjustment Point and Related Linear Guides

The adjustment mechanism for the roller conveyor's transverse guide is simpler yet fundamentally similar to that of the transportation system. This system employs two identical linear guides with a screw drive, comparable to those in the transportation system but featuring only one travel anchor for the entire travel distance. The guides are arranged symmetrically around the centre to ensure even load distribution across the guides' geometry. The transmission system also resembles that of the transportation system, providing a single adjustment point for the operator. This point allows simultaneous adjustment of both guides, using the same types of components, though arranged differently (Figure 7.6).



Figure 7.6: Cardboard Roller Conveyor and Transverse Guide Adjustment Mechanism

The final adjustment in the M09 module involves the Cardboard Storage Unit (M09-010 /012/021/025), where cardboard is temporarily stored before transfer to the Folding Module via the Cardboard Transportation System. The unit has four adjustment points (stop, separator, separating wedges, and rear wedge) that control its operation. These points function similarly to those in other parts of the module, converting the operator's spindle movement into linear motion via a transmission system and lead screws. Unlike other components, these mechanisms were custom-designed by the machine manufacturer (Figure 7.7).

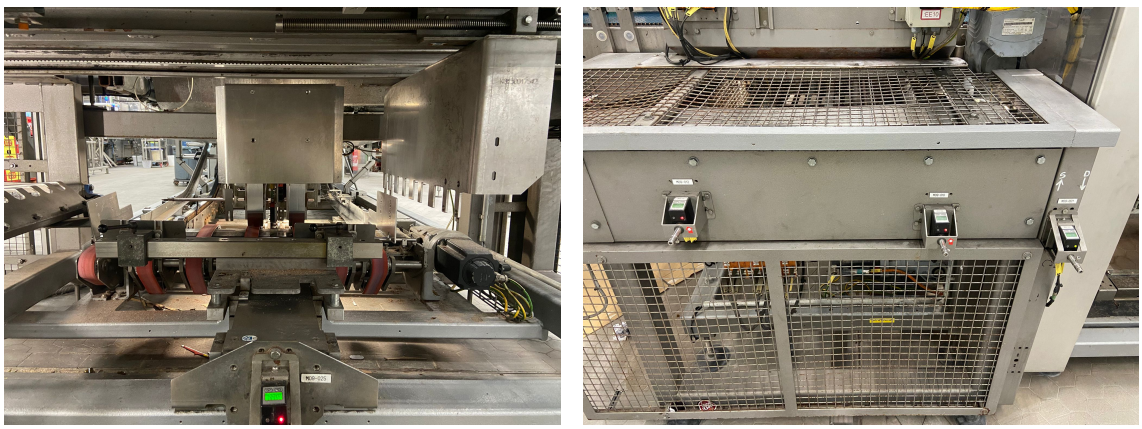


Figure 7.7: Cardboard Storage Unit and Respective Adjustment Points

Having characterised how each of these three subsystems is currently adjusted, the next step is to translate this understanding into an explicit, measurable requirements list - the targets the automated solution must satisfy before any concept can be evaluated against them.

Before specifying the mechanical and torque requirements for each subsystem, it is necessary to establish comprehensive quantitative functional specifications. Additionally, understanding the

system's expected operating requirements during changeover is essential. The primary requirements are as follows:

- The system must allow adjustment in both directions of movement and remain compact, without requiring modifications to the machine's main structural or functional components.
- The process must be fully automated and capable of adjusting each position to a predetermined point, defined by the size of each box, with high precision.
- The changeover procedure should be straightforward for the operator and, if feasible, integrated into the existing machine software.
- The system must also include a manual adjustment mode, enabling the operator to select the desired adjustment point for fine tuning. This mode serves as a fail-safe fallback to the pre-retrofit procedure in the event of an automation fault.

In contrast to continuously operating production equipment, this retrofit functions at a notably low duty cycle. For Line 1, which is the focus of this case study, changeovers occur at most once per day, with an average frequency of 5.1 occurrences per week. Considering the line's annual three-week maintenance stoppage, this results in approximately 49 production weeks per year. Multiplying this by the average weekly frequency yields the value shown in Equation 7.1.

$$n_{year} = 5.1 \times 49 \approx 250 \text{ actuation cycles/year} \tag{7.1}$$

This low usage rate, rather than a generic industrial benchmark, forms the basis for the reliability targets defined below.

Table 7.2 summarises the quantitative performance criteria, operational reliability, and project boundaries that define the scope of the automated redesign.

Table 7.2: Global Functional and Project Specifications

Category	Specification Metric	Target Design Value
Performance	Maximum Adjustment Time	≤ 60 s per changeover
	Required Positioning Accuracy	± 0.5 mm
	Positioning Repeatability (worst case)	$\leq \pm 0.2$ mm
Reliability	Annual Actuation Frequency	≈ 250 cycles/year
	Target Calendar Design Life	≥ 10 years
	Availability / MTBF	N/A - substituted by calendar life (see discussion)
	Fault Response	Graceful fallback to manual mode
Financial	Cost Objective	Minimised, no fixed ceiling
	ROI / Payback	Not Defined

The required Adjustment Time is determined kinematically based on the system's design parameters, rather than by selecting an arbitrary target. The calculation uses the largest spindle thread pitch present in the module ($p = 5$ mm) and a conservative continuous-duty speed of $n = 300$ RPM (selected to remain within the high-torque region of the curve). The resulting linear speed is $v = n \cdot p \cdot i = 1500 \cdot i$ mm/min $\approx 25 \cdot i$ mm/s. For a worst-case single-axis travel of $\Delta x_{max} = 84$ mm, defined by the optimisation problem in Section 5.4, applying a 50% margin for acceleration/deceleration ramps and controller settling, and assuming a direct drive system ($i = 1$) yields an adjustment time of around 5 seconds. The ≤ 60 s target therefore already carries substantial margin; it remains, in any case, an order of magnitude below the duration of the remaining (non-automated) changeover tasks, which is the system's true functional constraint and is not itself binding.

The ± 0.5 mm accuracy target reflects the defined permissible cardboard blank's tolerance to guide misalignment and is the structural driver for the selection of the actuator later in this Chapter. This value is not actuator-limited because the linear unit's rated positional accuracy is ±0.1 mm per 300 mm of travel (Appendix I), so reaching the ±0.5 mm bound would require a travel length exceeding 1.5 m, which is far beyond any travel present in this system. The rated accuracy therefore sits comfortably within the target across every adjustment point.

$$\Delta x = \frac{1.8^\circ}{360^\circ} \cdot p = \frac{1}{200} \cdot 5 \text{ mm} = 0.025 \text{ mm} = 25\ \mu\text{m} \tag{7.2}$$

This calculated linear resolution provides a comfortable margin of precision and accuracy for the intended material-handling application. The governing error source is the inherent axial back-

lash at the linear unit's lead screw/nut interface, which occurs whenever the direction of travel reverses. Taking the manufacturer's specified backlash for the RK Rose+Krieger linear units (Appendix I) of ±0.1 mm as the worst-case bound, a repeatability target of $\leq \pm 0.2$ mm is adopted for bidirectional motion. This figure can be tightened to near step-resolution levels by enforcing a unidirectional final-approach strategy in the control logic, always completing the final positioning move in the same direction of travel, which eliminates backlash-induced error without requiring an anti-backlash nut variant.

Given the established usage rate, the classical hour-based mean time between failures (MTBF) is not a meaningful metric. The cumulative active running time amounts to only a few hours annually, which is several orders of magnitude below the rated cycle life of commercial off-the-shelf actuators and transmission components. Consequently, mechanical fatigue is not expected to be life-limiting at this duty cycle. Instead, the primary failure modes are environmental factors such as corrosion, dust ingress, and stiction creep. For this reason, the IP64 sealing strategy at critical points and the selection of corrosion-resistant materials are prioritised over additional mechanical margin. A calendar-based design life of at least 10 years is therefore adopted as the governing reliability metric, with annual preventive maintenance as the rest of the machine. Rather than specifying an availability percentage without field data, the binding reliability requirement is qualitative and structural: any single-cycle failure of the automated system must degrade gracefully to the pre-retrofit manual procedure (already specified as a mandatory operating mode), ensuring that a fault does not result in net downtime exceeding the pre-retrofit baseline. Empirical measurement of the automatic-mode success rate is identified as a future work item, to be collected after system deployment.

As this is an exploratory feasibility project, no external budget ceiling is imposed. Instead, cost is treated as a minimisation objective alongside reliability, primarily achieved by selecting standard components and using common parts and materials across subsystems. As a result, no a priori return on investment (ROI) or payback target is established.

7.3 Conceptual Design

After defining the three subsystems, the design components required at each were identified as follows:

- **Actuation:** Components generating the rotational torque required to adjust position, critical for precision and, where required, holding torque.
- **Power Transmission and Coupling:** The mechanical adaptation between motor and spindle, necessary because the motor rarely connects directly to the shaft when retrofitting a compact space where structural changes are forbidden.
- **Control Logic:** The dedicated architecture required to automate the system, built around a Programmable Logic Controller or equivalent.

- **Others:** Additional components such as mounting plates or brackets, which may have to be custom-made for each point.

The system must also withstand the harsh conditions of its operating environment. Because the entire module handles cardboard, it is chronically contaminated with dust and cutout debris (Figure 7.8). Weekly cleanups mitigate this, but the design must not depend on human perfection.



Figure 7.8: Cardboard Debris Present Throughout the M09 Module

7.3.1 Actuation

The actuation solution must suit a specific operating envelope: low duty cycle, low-to-moderate speed, a peak breakaway torque to overcome initial static friction, and the ability to hold position accurately without external mechanical brakes. Four working principles were evaluated against this envelope: open-loop stepper, AC induction (VFD and encoder), AC/DC servomotor, and closed-loop stepper. Their full working-principle trade-offs are compiled in Appendix F; the selection itself is formalised below.

To eliminate subjectivity in weight assignment, the evaluation criteria in Table 7.4 were weighted using the pairwise comparison method from Saaty's Analytic Hierarchy Process [70, 71], applied directly to the criteria and aligned with the engineering requirements established earlier. Each pair was compared on a 1–9 scale, where 1 indicates equal importance, 5 strong dominance, and 9 extreme importance.

The evaluation logic defines a clear design hierarchy, with functional performance taking precedence over spatial and economic constraints. Torque and reliability are assigned the highest, equal priority, as they are essential for initiating movement and preventing desynchronisation or manual fallback. These outrank geometric footprint, which, while a hard constraint, is secondary because all candidates were pre-screened for spatial feasibility. Cost is given the lowest priority, as the project has no strict budget limit and financial impact is treated as a minimisation objective rather than a binding constraint.

Table 7.3: Pairwise Comparison Matrix for Actuation Selection Criteria

	Torque	Reliability	Footprint	Cost
Torque	1	1	3	5
Reliability	1	1	3	5
Footprint	1/3	1/3	1	3
Cost	1/5	1/5	1/3	1

Applying the row geometric mean method, the normalised priority vector is:

$$\mathbf{w} = [0.39,\ 0.39,\ 0.15,\ 0.07] \tag{7.3}$$

The consistency ratio of the comparison matrix is $CR = 0.016$, well below the $CR \leq 0.10$ threshold conventionally accepted for AHP judgements [71], confirming the pairwise comparisons are internally consistent.

Table 7.4: Weighted Decision Matrix for Actuation Selection (AHP-Derived Weights)

Criterion	**Weight**	Open-Loop	AC Ind.	AC/DC Servo	Closed-Loop
Breakaway Torque	0.39	4 (1.56)	3 (1.17)	4 (1.56)	5 (1.95)
Positional Reliability	0.39	2 (0.78)	4 (1.56)	5 (1.95)	5 (1.95)
Compact Footprint	0.15	5 (0.75)	1 (0.15)	3 (0.45)	4 (0.60)
Integration Cost	0.07	5 (0.35)	2 (0.14)	2 (0.14)	4 (0.28)
Weighted Total	–	**3.44**	**3.02**	**4.10**	**4.78**

To verify that the selection is not an artefact of the specific weight set, the matrix was re-evaluated under an unweighted (equal-priority) scheme as a robustness bound.

Table 7.5: Robustness Check: Equal-Weight Re-Evaluation

	Open-Loop	AC Induction	AC/DC Servo	Closed-Loop
Total	16	10	14	**18**

The Closed-Loop Stepper remains the top-ranked candidate under both the weighted and the equal-priority schemes, despite a reordering among the non-selected alternatives. The selection

is therefore driven by the candidate's consistent strength across criteria rather than by the specific weights chosen, addressing the risk that the matrix merely formalises a pre-existing decision. The closed-loop stepper is retained for its high low-speed breakaway torque and stable holding characteristics, combined with a closed-loop drive that detects physical stalls and corrects lost steps without the low-speed "hunting" of a servo.

7.3.2 Transmission System and Coupling

The transmission system bridges the spatial gap between actuator and spindle while setting the mechanical reduction ratio, which in turn defines the required motor torque. Six transmission principles were evaluated against the module's spatial and environmental constraints; their full trade-offs are compiled in Appendix F, and their governing verdicts in this environment are summarised below:

- **Metallic spur gears:** require wet lubrication, which combines with cardboard dust into an abrasive paste, forcing a sealed enclosure that violates the compact-retrofit constraint.
- **Polymer spur gears:** run dry, but fixed centre distances and dust packing into the tooth roots risk binding and fracture under the breakaway load.
- **Friction belts (V/flat):** require high pre-tension (large radial bearing loads) and exhibit creep incompatible with multi-turn positional accuracy.
- **Synchronous timing belts:** no lubrication, bridge variable centre distances, and near-zero-slip positional accuracy, at the cost of moderate radial pre-load and a tensioning provision.
- **Rigid direct coupling:** viable only with near-perfect alignment; misalignment induces cyclic bearing fatigue, and the collinear layout protrudes axially.
- **Flexible elastomer jaw coupling:** absorbs some misalignment, runs dry, near-zero backlash; its limitation is the axial length it adds in a confined envelope.

Because the three subsystems differ substantially in axial offset and available spatial envelope, no single transmission architecture is imposed across the module. Each principle above is evaluated against the specific geometry of each subsystem, with the final selection made independently for the Roller Conveyor, Cardboard Storage Unit, and Transportation System.

7.4 Embodiment Design

For this part of the design, a sequence from simplest to most complex is followed: Roller Conveyor, Storage Unit and Transportation System.

7.4.1 Cardboard Feeding Roller Conveyor

The Cardboard Feeding Roller Conveyor was the simplest part of the M09 module so it will be the first step in the Embodiment Design stage.

7.4.1.1 Torque Requirements

In the cardboard roller conveyor, two RK Rose+Krieger EP-II 40 linear units (7914010A1AA1420) control the movement of the guide stop according to the size of the cardboard. Currently, both linear units are linked to a single manual adjustment point. The operator rotates the spindle in the required direction until the desired position is reached. The motion is transmitted from this adjustment point to the two linear guides through a transmission system, as illustrated in Figure 7.9. Table 7.6 summarises the most relevant characteristics of the guide, and the specifications manual is provided in Appendix I.

Table 7.6: RK Rose+Krieger EP-II 40 Linear Unit Specifications

Technical Specification	**Value**
Height (mm)	63
Width (mm)	180
Spindle Thread	Trapezoidal
Lead Screw Nominal Diameter (mm)	20
Lead Screw Pitch (mm)	4
Travel Length (mm)	1300
Shafts' Diameter (mm)	12
Shafts' Length (mm)	38
Key Slot	$4 \times 4 \times 32$

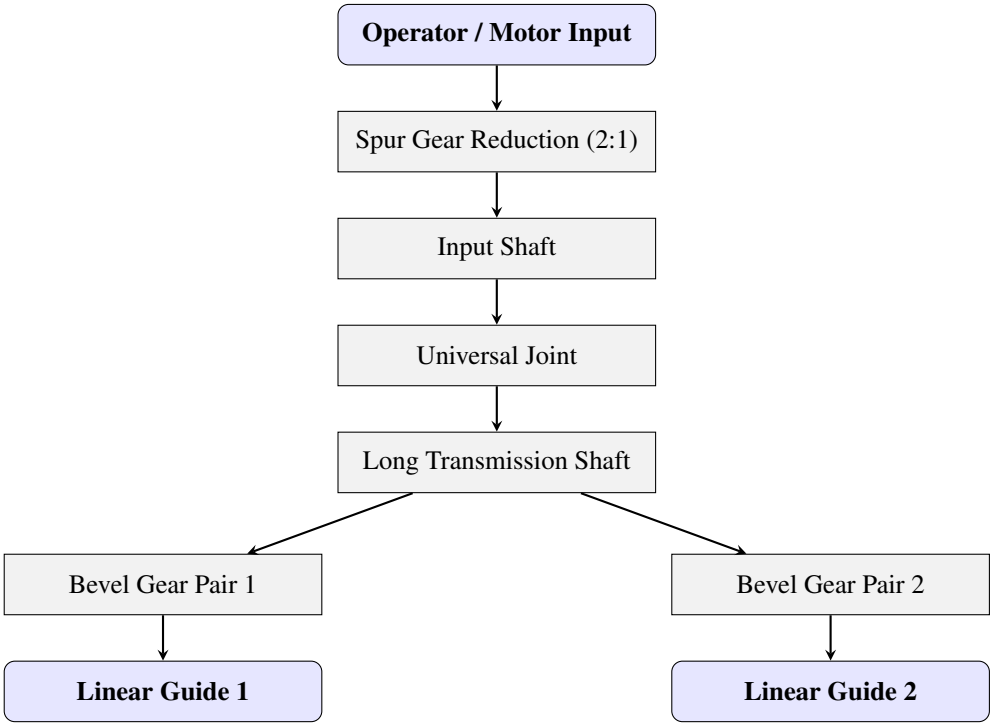


Figure 7.9: Roller Conveyor Transmission: Parallel Power Distribution to the Two Linear Guides

In this module, the guide stop measures 4800 mm in length, with its weight symmetrically distributed across the two linear units, each positioned 1600 mm from the guide centre. Torque was measured using the same methodology, assumptions, and values for efficiency of transmission components as in previous analyses. Cardboard dust does not present as significant a challenge in this module as it does in the transportation system. However, debris accumulated over several years can result in increased torque requirements following the breakaway torque. Calculations similar to those in the previous section were conducted to determine the torque required for each linear unit, as shown in Equations 7.4 to 7.11.

Before the transmission system separates for the two linear units, the movement goes through a spur gear with a reduction ratio of $i = 2$ to a small shaft that redirects the movement through a universal joint to the bigger connection shaft in the machine's adjustment point.

$$T_{mainshaft} = T_{measured} \cdot i \cdot \eta_{sg} \cdot \eta_{uj} \tag{7.4}$$

$$T_{main} = 4.8\ \text{Nm} \cdot 2 \cdot 0.95 \cdot 0.85 = 7.752\ \text{Nm} \tag{7.5}$$

Each linear unit is connected to the shaft by similar bevel gears, with one gear positioned at the beginning and another at the end of the shaft. The shaft measures approximately 3200 mm in length and is supported by two bearings to accommodate its own weight. Although Bevel Gear Pair 2 is situated approximately 3,000 mm further along the transmission shaft than Pair 1, this

separation does not result in a measurable decrease in transmission efficiency or phase lag. Torsional deflection ($\theta = \frac{T \cdot L}{J \cdot G}$) becomes significant primarily under high dynamic loads. However, the system operates under low-torque boundary conditions and at low rotational velocities, resulting in quasi-static operation. Under these parameters, inertial loads and acceleration spikes are negligible, and the shear stiffness of the steel tubing greatly exceeds the applied torsional forces. As a result, the elastic wind-up of the shaft is minimal, permitting the entire 3,000 mm length to be accurately modelled as a rigid body. Therefore, it will assumed that the only difference in the torque needed at each point is the presence of bearings which support the shaft.

- Branch 1: Spindle 1 is connected only through a bevel gear.

$$\eta_1 = 0.95 \tag{7.6}$$

- Branch 2: The efficiency of the bearings supporting the shaft must be considered in addition to the bevel gear pair.

$$\eta_2 = \eta_{cg} \cdot \eta_b \cdot \eta_b = 0.95 \cdot 0.98 \cdot 0.98 = 0.9124 \tag{7.7}$$

The total 7.752 Nm on the main shaft must supply enough torque to satisfy T_s across all branches.

$$T_{main} = \frac{T_s}{\eta_1} + \frac{T_s}{\eta_2} \tag{7.8}$$

$$7.752 = T_s \left(\frac{1}{0.95} + \frac{1}{0.912} \right) \tag{7.9}$$

$$T_s = 3.61 \text{ Nm} \tag{7.10}$$

Active rust and cardboard dust contamination on the linear guides increase the baseline friction coefficient, as noted in the mechanical design literature [72], reflecting poor lubrication and surface oxidation. To address the additional startup torque needed to overcome stiction on rusted tracks, a Safety Factor of $S_f = 1.5$ was applied to the final torque requirement, meeting the minimum guidelines set by linear unit manufacturers [73, 74] for contaminated industrial environments.

$$T_{motordesign2} = 3.61 \cdot 1.5 = 5.42 \text{ Nm} \tag{7.11}$$

Actuating the linear units on the roller conveyor requires a mechanical transmission system capable of delivering 5.42 Nm of torque to the input shaft. In contrast to the transportation system, which is subject to strict geometric boundaries and high-precision tolerances, this sub-system operates with more relaxed spatial constraints and moderate precision requirements.

Nevertheless, as the system is fully exposed to the operational environment rather than enclosed within a machine, its design is strictly constrained by environmental and lifecycle considerations. The system must achieve an IP64 rating to ensure complete protection against dust

ingress and resistance to low-pressure water jets from any direction, to protect itself during general cleaning procedures on the shop floor. Furthermore, the assembly must remain maintenance-free throughout its operational lifecycle, eliminating the need for periodic relubrication or mechanical adjustments due to wear.

To satisfy the system's requirements, two architectures were evaluated: a high-ratio geared system and a direct-drive system.

Architecture A

This architecture uses a more compact stepper motor combined with a precision planetary gearbox to increase torque output.

The main mechanical advantages of using a gearbox are high efficiency, torque multiplication, and effective inertia matching. This type of transmission mechanism can achieve up to 98% efficiency at high ratios such as 10:1 or 15:1, ensuring alignment between the input and output shafts. The gearbox also reduces the load inertia reflected to the motor shaft by the square of the gear ratio, as described by $J_{reflected} = \frac{J_{load}}{i^2}$. This configuration results in a stable dynamic system with increased resistance to stalling. Additionally, the assembly maintains a compact radial footprint.

Using a planetary gearbox increases the solution's mechanical complexity and introduces backlash. To satisfy the maintenance-free requirement, the gearbox must be lubricated for its entire operating life, which substantially raises component costs. From an environmental sealing perspective, achieving IP64 standards is possible, as multiple static seals are used at both the motor-to-gearbox and gearbox-to-linear-unit interfaces, also increasing the costs.

Architecture B

This solution eliminates the mechanical transmission stage by using a higher torque stepper motor coupled directly to the linear guide's input shaft via an internal flexible coupling. The absence of intermediate gear assemblies ensures almost zero mechanical backlash and eliminates gear-tooth wear, thereby meeting the maintenance-free requirement. Additionally, achieving IP64 protection is simplified, as the design requires only a single sealed structural interface, such as a stainless steel housing. From a cost perspective, generating the required 5.42 Nm of torque by upgrading the motor is more economical than employing precision planetary gears.

The primary disadvantage of the direct-drive configuration is its spatial requirement. Direct-drive systems inherently experience inertia mismatch, as the motor must directly overcome the full inertia of the linear guide's carriage and lead screw assembly (J_{load}). However, the low-speed and infrequent actuation of this module make these dynamic risks, such as resonance or stalling during acceleration, negligible. As a result, the operational drawbacks are limited to increased volume and mass. Achieving the required torque electromagnetically requires a substantial amount of copper windings and electrical steel, resulting in a motor with a significantly larger radial footprint and greater mass than geared alternatives.

To assist the decision, Table 7.7 compares the most important indicators for this solution.

Table 7.7: Architecture Evaluation Matrix for the Roller Conveyor Actuation Solution

Evaluation Criteria	**Geared (Small Stepper)**	**Direct-Drive (Large Stepper)**
Torque Delivery	Met (via mechanical reduction)	Met (via electromagnetic scale)
Maintenance Profile	Low (Lubricated-for-life)	Lowest (Frictionless transmission)
IP64 Integration	More Complex	Simpler
Dimensions	Compact	Bulky
Cost	High	Moderate

For this section of the module, the direct-drive solution was selected. To implement this solution, it is necessary to conduct motor sizing, dynamic inertia matching, and coupling specification.

Motor Sizing

Following the establishment of the closed-loop topology, the appropriate physical frame size for the stepper motor must be determined. The continuous required torque of 5.42 Nm already incorporates the Sf = 1.5 safety factor, which accounts for rust and cardboard dust progressively degrading the linear unit's lubrication over its service life. Selecting a motor rated precisely at this value is nonetheless insufficient, since stepper motors experience torque reduction as speed increases. Stepper motor selection practice recommends an additional design margin of 1.25 to 2.5 times the calculated load torque at this stage [75]. A factor of Ka = 1.25, at the lower bound of this range, is adopted here. As the dominant source of mechanical uncertainty in this system, load-side degradation from the linear unit, is already covered by $S_f = 1.5$, so a larger value would only compound margin onto margin, inflating torque, inertia, and structural loads through the rest of the design chain without addressing a distinct physical risk. The motor sizing torque is given by the following Equations.

$$T_{\text{motor}} \geq T_{\text{required}} \cdot K_a \tag{7.12}$$

$$T_{\text{motor}} \geq 5.42 \cdot 1.25 = 6.78 \text{ Nm} \tag{7.13}$$

Considering the 6.78 Nm peak breakaway torque requirement of the packaging module, the selection process was limited to some standard industrial frame sizes: NEMA 23, NEMA 24, and NEMA 34. The choice of motor frame determines both the spatial constraints at each adjustment point and the standard shaft diameter.

A comparative analysis of the three motor frames is presented below:

Table 7.8: Comparative Specifications of Standard NEMA Stepper Motor Frames

Motor Frame	**Flange Dimensions (mm)**	**Shaft Diameter (mm)**	**Holding Torque (Nm)**	**Average Mass (kg)**
NEMA 23	57×57	6.35 / 8.0	1.2 – 2.4	≈ 1.0
NEMA 24	60×60	8.0 / 10.0	2.4 – 4.0	≈ 1.5
NEMA 34	86×86	12.7 / 14.0	3.6 – 9.6	≈ 3.0

As observed, the NEMA 34 or larger frame size stepper is required because it is the only one capable of handling the torque requirement. NEMA 34 stepper motors typically have standard torque ratings between 3.6 to 9.6 Nm for industrial applications, which satisfies the calculated torque requirement. For the design process, an IP64 NEMA 34 Closed-Loop Stepper Motor with a 9.33 Nm rating and encoder is selected (ASA8618L95-W1 from Nanotec Electronic GmbH). The specifications for this motor are provided in Table 7.9 and complete datasheet and technical drawings are presented in Appendix I and I.5.

Table 7.9: Roller Conveyor NEMA 34 Stepper Motor Specifications

Technical Specification	**Value**
Specification	NEMA 34 / 86 mm
Protection	IP64
Holding Torque (Nm)	9.33
Length (mm)	155
Shaft's Length (mm)	35
Shaft's Diameter (mm)	∅14
Key	-
Rotor Inertia (g·cm^2)	3,000
Encoder Signal Type	SSI (Absolute)
Encoder Resolution	17 Bit Single-Turn / 16 Bit Multi-Turn Absolute
Encoder Operating Voltage (V)	4.75–15.00

Coupling Specification

The mechanical interface between the stepper motor and the linear unit requires a flexible coupling mechanism. This component must reliably transmit torque without introducing backlash, whilst compensating for inevitable manufacturing and assembly misalignments.

Rigid couplings are strictly precluded, as perfect shaft concentricity is physically unattainable and rigid connections convert minor geometric deviations into cyclic radial loads, accelerating bearing fatigue. While metallic bellows couplings offer high torsional stiffness, they are structurally sensitive and transmit the high-frequency micro-vibrations inherent to stepper motors directly to the load. Consequently, a reduced-backlash elastomer jaw coupling is selected. The coupling uses a geometrically oversized, pre-stressed polyurethane elastomeric insert (spider) between two metallic hubs. This spider functions as a mechanical low-pass filter, damping the motor's torque ripple and accommodating shaft misalignment while maintaining an almost zero-backlash, fail-safe torque transmission.

The component selected to physically bridge the shafts was a modular Ringfeder GWE 5104 elastomer jaw coupling. Although the more compact Ringfeder GWE 5113 model was evaluated because it would occupy less space inside the housing, it was not long enough to securely fix both shafts. The mechanical integration of this coupling must address a fundamental hardware asymmetry: the existing linear guide input features a 12 mm shaft with a standard DIN 6885 parallel key (4x4), whereas the stepper motor has a smooth output shaft with a diameter of 14 mm. Specifically, GWE 5104-19 was chosen because it was capable of handling the torque and the shaft's dimensional requirements. The primary specifications are presented in Table 7.10, while additional details are provided in Appendix I.

Table 7.10: GWE 5104 Coupling Specifications

Technical Specification	**Value**
Coupling Series	GWE 5104
Size	19
Input Bore Diameter d_1 (mm)	14 (without keyway)
Output Bore Diameter d_2 (mm)	12 (with keyway)
Transmissible Torque T (Nm)	17
Maximum Rotation Speed $n_{\max}$ (revolution/min)	11,000
Total Moment of Inertia J ($\mathrm{kg \cdot m^2 \times 10^{-3}}$)	0.036
Radial Misalignment ΔK_r (mm)	0.06
Angular Misalignment ΔK_w (°)	0.9
Axial Misalignment ΔK_a (mm)	+1.2 / -0.5

While parallel keys provide excellent positive locking, they introduce mechanical hysteresis upon torque reversal due to the necessary geometric clearance fit. To eliminate this backlash, a hybrid radial-clamping architecture is employed. For the stepper's shaft, the coupling hub is

specified as a smooth-bore radial clamp. By elastically deforming the thick-walled aluminium collar via a transverse screw, a high-friction interference fit is generated, transmitting torque purely through surface adhesion. For the linear unit's shaft, the coupling hub is specified as a radial clamp with an integrated DIN keyway. As the clamping screw is torqued, the hub's elastic deformation clamps the internal keyway walls directly against the existing steel key, eliminating the clearance gap.

This hybrid configuration ensures that the primary torque transmission across the entire assembly is governed by reduced-backlash friction, while the retained steel key on the linear guide serves as a mechanical failsafe against frictional slip (Figure 7.10).

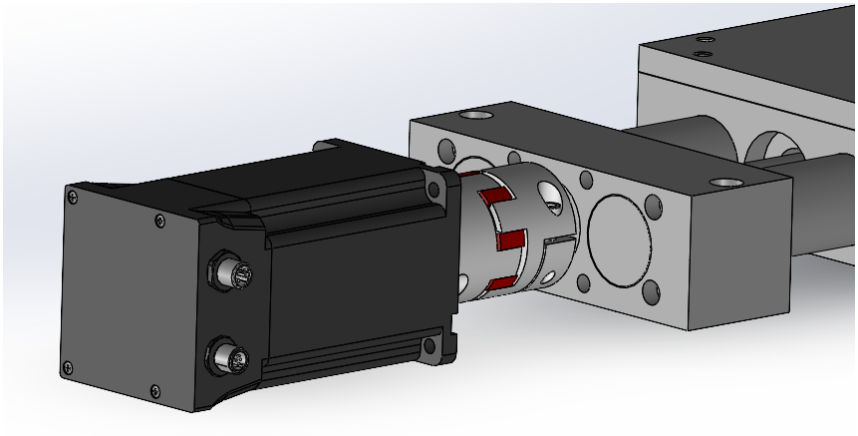


Figure 7.10: Roller Conveyor Direct-Drive Architecture: Stepper Motor, Coupling, and Housing Assembly

Dynamic Inertia Matching

Although this is a low-speed application, calculating the inertia ratio is essential to demonstrate dynamic stability. Significant mismatches can result in resonance and missed steps. For direct-drive stepper motors, the recommended inertia ratio is $\leq 10:1$ [76, 77].

To determine the total load inertia (J_{load}) reflected to the motor shaft, the rotational inertia of the linear guide's screw (J_{screw}) is summed to the translational inertia of the moving mass (J_{trans}). For a lead screw, the moment of inertia is calculated using the material density (ρ), screw length (L), and outer diameter (D), as shown in Equation 7.14. The mass of the metallic guide is converted into rotational inertia based on the screw's pitch, requiring the mass of the guide (m_{load}) and the screw pitch (p), as indicated in Equation 7.15. The inertia ratio is then calculated using Equation 7.16, with the motor inertia J_{motor} obtained from the manufacturer's datasheet.

$$J_{screw} = \frac{\pi \cdot \rho \cdot L \cdot D^4}{32} \tag{7.14}$$

$$J_{trans} = m_{load} \cdot \left(\frac{p}{2\pi}\right)^2 \tag{7.15}$$

$$Ratio = \frac{J_{screw} + J_{trans}}{J_{motor}} \tag{7.16}$$

Because the exact load of the metallic guide pushed by the linear units is unknown, it is necessary to estimate the mass moment of inertia without relying solely on the torque value. While breakaway torque determines the required static holding power, dynamic stability in the closed-loop system depends on the inertia mismatch during acceleration. The 6.78 Nm empirical measurement primarily reflects static friction and stiction, and therefore cannot be reliably used to determine the mass moment of inertia (J_{load}).

Instead, the load inertia is evaluated using geometric methods. In precision screw-driven linear systems, the reflected inertia of the translating mass (J_{trans}) is reduced by the square of the screw pitch, so the solid steel screw (J_{screw}) constitutes the majority of the system's total rotating inertia. Thus, J_{load} is approximated using geometric formulas for a solid rotating cylinder. This approach ensures that, even with a conservative overestimation of the carriage mass, the system maintains a load-to-rotor inertia ratio (J_{load}/J_{motor}) of $\leq 10:1$, confirming that the direct-drive motor will most likely not experience control loop resonance or loss of synchronisation when overcoming static friction.

Dynamic stability verification of the direct-drive configuration is conducted using the geometric and material properties of the system components. The linear unit incorporates a solid steel screw ($\rho_{\text{steel}} = 7850\ \text{kg/m}^3$) with a diameter $D = 0.020$ m and length $L = 1.30$ m. From Equation 7.14, the rotational inertia of the screw shaft is calculated as:

$$J_{\text{screw}} = \frac{\pi \cdot 7850 \cdot 1.30 \cdot (0.020)^4}{32} = 1.603 \times 10^{-4}\ \text{kg} \cdot \text{m}^2 \tag{7.17}$$

To account for secondary carriage geometries, an upper-bound width of 0.50 m is specified for the 10 mm thick stainless steel plate ($\rho_{\text{ss}} = 8{,}000\ \text{kg/m}^3$). The total mass of this bounding plate geometry is:

$$m_{\text{total}} = 0.010 \cdot 4.80 \cdot 0.50 \cdot 8{,}000 = 192.00\ \text{kg} \tag{7.18}$$

Because the load is shared equally between two parallel linear units, the mass per axis is $m_{\text{load}} = 96.00$ kg. For a screw pitch $p = 0.004$ m, the reflected translational inertia is calculated via Equation 7.15.

$$J_{\text{trans}} = 96.00 \cdot \left(\frac{0.004}{2\pi}\right)^2 = 3.891 \times 10^{-5}\ \text{kg} \cdot \text{m}^2 \tag{7.19}$$

Including the manufacturer-specified inertia of the Ringfeder GWE 5104 coupling ($J_{\text{coupling}} = 3.600 \times 10^{-5}\ \text{kg} \cdot \text{m}^2$), the total load inertia (J_{load}) at the motor shaft interface is:

$$J_{\text{load}} = 1.603 \times 10^{-4} + 3.891 \times 10^{-5} + 3.600 \times 10^{-5} = 2.352 \times 10^{-4}\ \text{kg} \cdot \text{m}^2 \tag{7.20}$$

Given the selected motor's rotor inertia $J_{\text{motor}} = 3{,}000 \times 10^{-4}\ \text{kg} \cdot \text{m}^2$, Equation 7.16 yields the system inertia ratio:

$$\text{Ratio} = \frac{2.352 \times 10^{-4}}{3{,}000 \times 10^{-4}} = 0.784 : 1 \tag{7.21}$$

The resulting inertia ratio of $0.784 : 1$ satisfies the industrial design guideline of $\leq 10 : 1$. The 4 mm lead screw pitch isolates the motor from the translating mass, ensuring control-loop stability and eliminating the requirement for a mechanical gear reduction stage.

Although the manufacturer ratings for the stepper motor and coupling assume continuous-duty thermal steady state, the system's actual operation is highly intermittent. The EP-II 40 linear units are self-locking, with friction alone maintaining position after each move, eliminating the need for motor holding current. At the intended usage (≈ 250 moves/year ≤ 60 seconds per move), the effective electrical duty cycle is below 1%, ensuring the motor operates well within its thermal envelope. This negligible duty cycle also prevents hysteresis self-heating in the coupling's polyurethane spider, requiring no temperature derating ($S_\vartheta = 1.0$ up to 30°C). Furthermore, the resulting load reversals over the design life fall several orders of magnitude below the threshold at which elastomeric fatigue becomes a limiting factor. Thermal and cyclic-duty effects are therefore not expected to limit the performance of the actuator or coupling subsystem, and component ratings are applied without derating.

Housing Protection and Alignment Layout

The final architectural requirement involves the physical integration of the stepper motor, flexible coupling, and linear guide, while ensuring a continuous IP64 environmental boundary. Although the primary stator housing of the selected motor is IP64-rated, the front output shaft region is only rated to IP54, which necessitates an enclosure face seal on the installation side. A custom stainless-steel bell housing is specified to establish this protection boundary, maintain structural coaxiality between the driving and driven axes, and enforce axial standoff spacing.

To prevent shaft-to-shaft interference within the internal cavity, the housing length is determined based on the component dimensions. The GWE 5104-19 coupling has a total length of $L = 66$ mm and a rated hub engagement depth of $C_1 = 25$ mm, resulting in a central 16 mm pocket for the elastomeric spider. When the $\varnothing$14 mm $\times$ 37 mm motor shaft and the $\varnothing$12 mm $\times$ 38 mm linear guide shaft are engaged to their full 25 mm design depths, 12 mm and 13 mm of unengaged shaft length remain exposed, respectively. The sum of these segments establishes the absolute face-to-face housing length baseline:

$$L_{\text{housing}} = 12\ \text{mm} + 66\ \text{mm} + 13\ \text{mm} = 91\ \text{mm} \tag{7.22}$$

Unlike other adjustment points throughout this module, which have strict envelope constraints, the Roller Conveyor's adjustment points have no comparable structure within reach of the housing's projected extension. The housing length derived above is therefore governed entirely by

internal component geometry rather than by an external spatial boundary, and no further envelope verification is required at this point.

This dimensional constraint ensures maximum hub engagement and isolates the shaft tips from the internal damping spider. Radially, although the nominal hub diameter is ∅40 mm, the manufacturer-specified clearance diameter (H) for the size 19 clamping assembly is ∅46 mm to accommodate the clamping hardware. These spatial boundaries define the geometric framework for the metrological fits, static seals, and structural fastening interfaces described in the subsequent stage.

7.4.2 Cardboard Storage Unit

This section details the embodiment configuration for the four adjustment points of the Cardboard Storage Unit (M09-010, M09-012, M09-021, and M09-025). To enforce strict component standardisation across the machine, these four points directly reuse the direct-drive layout, coupling selection, and structural housing principles validated for the Roller Conveyor (Section 7.4.1); the material, sealing, and mounting deviations specific to this module are detailed below.

7.4.2.1 Torque Requirements

Torque was measured at each adjustment point using the same methodology and assumptions as in the preceding section. Figures 7.11, 7.12, and 7.13 illustrate the transmission architectures for M09-025, M09-021, and M09-010/012 respectively (the latter two points sharing an identical configuration). Table 7.11 presents the measured values. For M09-021, the measured torque fell below the 1.0 Nm floor of the torque wrench, so 1.0 Nm was adopted as a conservative bound.

Table 7.11: Torque Measured at the Cardboard Storage Unit Adjustment Points

Adjustment Point	**Torque (Nm)**
M09-010	1.2
M09-012	1.2
M09-021	1.0
M09-025	1.4

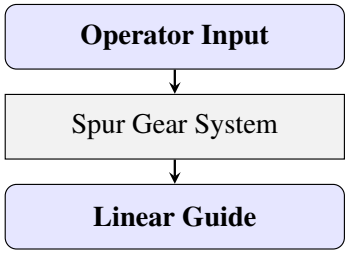


Figure 7.11: M09-025 Transmission: Direct Spur-Gear Drive to a Single Linear Guide

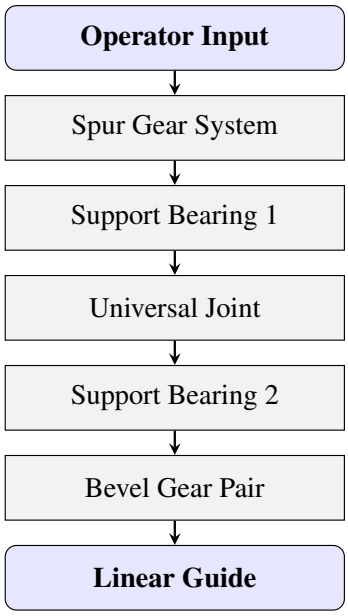


Figure 7.12: M09-021 Transmission: Sequential Drivetrain with Dual-Bearing-Isolated Universal Joint

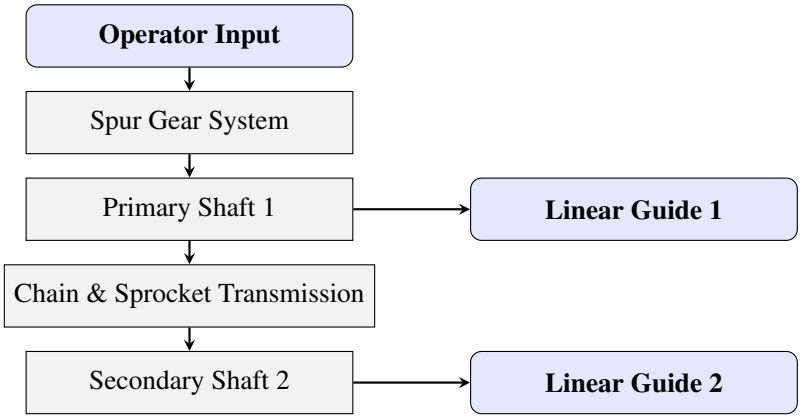


Figure 7.13: M09-010/012 Transmission: Parallel Chain-and-Sprocket Drive to Two Linear Guides

The automation redesign replaces only the legacy manual handle and its initial input spur-gear stage; the motor then couples to the same entry shaft the operator previously turned by hand.

Because the torque was measured at precisely this interface, the reading already incorporates every loss downstream of it - the retained bearings, universal joints, and chain-and-sprocket elements that remain in service - so no separate downstream efficiency accounting is required. This differs from the Roller Conveyor (Section 7.4.1), where the measurement and actuation points sat on opposite sides of the retained drivetrain and the downstream losses therefore had to be tracked forward explicitly. Here, sizing reduces to extrapolating the measured torque across only the *removed* spur-gear stage ($i = 2$, $\eta_{\text{sg}} = 0.95$) to recover the baseline delivered to the entry shaft, then applying the same Safety Factor $S_f = 1.5$ and Application Factor $K_a = 1.25$ used previously. The resulting motor-sizing torques are summarised in Table 7.12; the full per-point derivations are provided in Appendix F.3.

Table 7.12: Cardboard Storage Unit Torque Sizing Results

Point	T_{measured} **(Nm)**	T_{entry} **(Nm)**	T_{motor} **(Nm)**	**Architecture**
M09-025	1.4	2.66	4.99	Direct-to-spindle
M09-021	1.0	1.90	3.56	Retained sequential drivetrain
M09-010 / M09-012	1.2	2.28	4.28	Retained chain-driven (parallel)

Motor and Coupling Specification

All four points use the same NEMA 34 stepper family as the Roller Conveyor to unify plant inventory and control-loop profiles. Because the torque demands here are lower, a more compact, lower-power variant is selected, delivering a selection margin of $S_{sel} = 5.94/4.99 = 1.19$ at the most demanding point (M09-025). Table 7.13 summarises this motor.

Table 7.13: Cardboard Storage Unit NEMA 34 Stepper Motor Specifications

Technical Specification	**Value**
Frame Specification	NEMA 34 / 86 mm × 86 mm
Chassis Protection Class	IP64
Holding Torque (M_{H})	5.94 Nm
Longitudinal Body Length (L_{motor})	125 mm
Shaft Length (l_{s})	35 mm
Shaft Diameter	∅14 mm (Smooth)
Shaft Keyway Profile	None (Smooth Surface)
Rotor Inertia (J_{motor})	1900 g · cm^2
Encoder Signal Type	SSI (Absolute)
Encoder Resolution	17-Bit Single-Turn / 16-Bit Multi-Turn
Encoder Operating Voltage	4.75 V – 15.00 V

Power transmission reuses the reduced-backlash GWE 5104 Size 19 elastomeric jaw coupling verified for the Roller Conveyor, including its misalignment ratings and the thermal and duty-cycle justification of Section 7.4.1; all four points share the same part number, actuation profile, and non-derated spider rating. Because the legacy entry shafts at all four points share the identical ∅12 mm diameter and DIN 6885 parallel keyway, the coupling interface is identical to the Roller Conveyor's — a smooth ∅14 mm radial-clamp hub on the motor side and a ∅12 mm keyed radial-clamp hub on the machine side - and is not re-derived here.

Dynamic Inertia Matching

The Cardboard Storage Unit manipulates significantly lighter guide-plate structures than the Roller Conveyor, so the reflected translational inertia is minimal and total load inertia is dominated by the fixed rotational inertia of the internal screws. Applying the same cylinder approximation (Equation 7.14) to the longest screw present gives $J_{\mathrm{screw}} = 8.015 \times 10^{-5}$ kg·m^2.

Unlike the Roller Conveyor, the M09-010, 012, and 021 points retain their legacy bearings, universal joints, and chain-sprocket components downstream of the motor coupling. Rather than disassembling these to characterise each contribution, a deliberate contingency factor $K_J = 2.0$ is applied directly to the screw inertia. This is an engineering judgement, not a standard-derived value: doubling the estimate biases conservatively in the direction that protects the governing $\leq$ 10:1 stability guideline [76, 77], since underestimating J_{load} is the failure direction that risks resonance or lost steps.

$$J_{\text{screw,real}} = J_{\text{screw}} \cdot K_J = 8.015 \times 10^{-5} \cdot 2.0 = 1.603 \times 10^{-4}\ \text{kg·m}^2 \tag{7.23}$$

Against the selected motor's rotor inertia ($J_{\text{motor}} = 1900\ \text{g·cm}^2$), the worst-case inertia ratio is $1603/1900 = 0.844$:1, well below the ≤ 10:1 limit and confirming the direct-drive solution.

Environmental Protection and Alignment

To balance component standardisation with cost-engineering principles, the environmental sealing and structural mounting architecture is divided into two tiers according to the physical location of the adjustment points, their structural foundations, and their exposure to cleaning operations:

M09-025 (IP64 Enclosure): Because it is located in the lower, fully exposed region of the module, this point requires strict protection against accidental low-pressure liquid jets during floor washdowns and high volumes of abrasive carton dust. The structural layout must incorporate a compact, custom-machined housing fixed directly to a custom adapter plate mounted on the linear unit's block face. This solution is functionally identical to the one implemented for the Roller Conveyor adjustment points, requiring the exact same concentric housing profile and internal sealing paths. The only minor modification is geometric, as the mounting flange on the linear unit side is tailored with a specific hole array to match the unique threaded fixation holes of the storage unit's spindle block face.

M09-010 and M09-012: Both points are positioned high within the structural frame of the machine and consist of legacy shafts that protrude directly through a heavy structural 6 mm thick steel enclosure panel on the side of the module. The solution removes the initial manual spur-gear stage associated with the legacy manual adjustment points, while leaving the core internal transmission elements completely unchanged, as required by the project's constraints.

Because these points are isolated from floor-level fluid washdowns due to their elevated position, they prioritise mechanical shielding over liquid tightness, omitting O-rings entirely to minimise component and machining costs. The structural housing for these points features an expanded base flange that aligns directly with the machine panel's pre-existing threaded holes. Because these two points share the same hole arrangement, they use an identical machined housing component.

M09-021: This adjustment point is also located in the higher elevation zone and shares the identical housing specifications to the previous two points. However, because this is a different, slender plate, the pre-existing threaded fixing points at this location use a different spatial arrangement, so the housing must be tailored to this configuration.

Structural Rigidity Validation

Unlike the M09-025 solution, which bolts directly to a rigid linear guide block face, the upper nodes feature floating transmission shafts that protrude directly out of the 6 mm thick steel side

panels without local internal structural backing blocks. These points are supported by bearings and similar components which are connected to other structural elements of the machine, inside the unit. It is therefore necessary to structurally validate the safety of mounting the custom housing and the 3.4 kg cantilevered motor mass directly to the plate.

A 6 mm thick medium-carbon structural steel plate has a high area moment of inertia, providing substantial local and global bending stiffness. Under the combined mass of the assembly and the maximum dynamic torque reaction ($M_{\mathrm{H}} = 5.94$ Nm) generated, the localised deflection of the plate is negligible, ensuring that structural panel flexing cannot induce shaft bending stresses or throw the coupling out of alignment.

Furthermore, threading the housing's structural steel mounting bolts directly into the pre-existing holes provides a thread engagement depth of exactly 6 mm. For an M8 fastener interface, this engagement length equals $0.75 \cdot D$. For a standard metric internal thread, the theoretical pitch diameter line where the bolt and plate threads mesh together is defined by Equation 7.24.

$$d_2 = d - 0.649519 \cdot P = 8.00 \text{ mm} - (0.649519 \cdot 1.25 \text{ mm}) = 7.188 \text{ mm} \tag{7.24}$$

The thread engagement length within a joint must provide sufficient shear area to guarantee that the fastener limits are governed by tensile yielding rather than catastrophic thread stripping [72, 78]. The internal thread stripping shear area (A_{si}) for standard metric 60-degree coarse threads is evaluated using the geometric boundary equations compiled in the literature [79], where the internal shear path accounts for thread pitch diameter variations.

$$A_{\mathrm{si}} = \pi \cdot d \cdot L_{\mathrm{e}} \cdot \left[0.5 + \frac{1}{\sqrt{3}} \cdot \frac{(d - d_2)}{P} \right]$$

$$A_{\mathrm{si}} = \pi \cdot 8.00 \text{ mm} \cdot 6.00 \text{ mm} \cdot \left[0.5 + \frac{1}{\sqrt{3}} \cdot \frac{(8.00 - 7.188)}{1.25} \right] = 131.95 \text{ mm}^2$$

The maximum force required to physically tear the threads straight out of the 6 mm steel plate is the product of the total shear area and the material's shear strength:

$$F_{\mathrm{strip}} = A_{\mathrm{si}} \cdot S_{\mathrm{us}} = 131.95 \text{ mm}^2 \cdot 330 \text{ N/mm}^2 = 43,543.5 \text{ N}$$

Comparing the structural stripping limit directly against the high installation assembly preload tension gives:

$$SF_{\mathrm{strip}} = \frac{F_{\mathrm{strip}}}{F_{\mathrm{preload}}} = \frac{43,543.5 \text{ N}}{14,500 \text{ N}} \approx 3$$

This depth provides a substantial shear area that safely exceeds the minimum threshold required to resist thread stripping under full assembly preloads. The joint behaves as a rigid friction lock, confirming that the machine's existing 6 mm steel plate serves as a safe, highly stable mounting foundation, eliminating the need for auxiliary internal reinforcement frames or complex bracket extensions.

7.4.3 Transportation System

The three RK Rose+Krieger EPX-II 40 linear units (7944031A1AA1292) will continue to transmit motion to the guide rails. Their specifications are provided in Appendix I, and the transmission layout is shown in Figure 7.14.

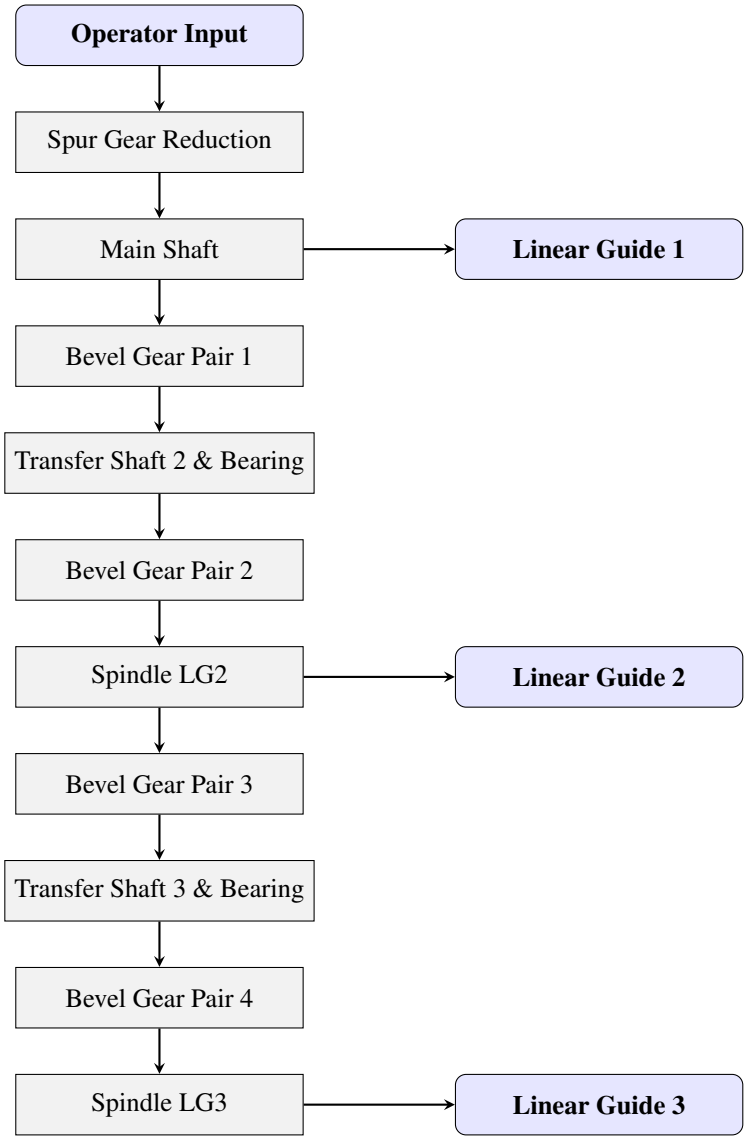


Figure 7.14: Transportation System Transmission: Three-Point Asymmetric Parallel Layout

The torque necessary to move the guide rails was measured at the input point with a VANPO torque wrench (1-25 Nm) because this was the only available option without disassembling the machine, which was strictly forbidden. The measured torque included both the breakaway torque, typically the highest value due to static friction, and the dynamic torque. Due to rust buildup and contamination from cardboard dust and particles (Figure 7.15), the dynamic torque could be significantly higher than anticipated, as was indeed observed.



Figure 7.15: Rust buildup and Cardboard Dust

In order to understand the torque distribution, the calculations in Equations 7.25 to 7.33 were used. All the calculations were made assuming the guide rail behaves as a rigid element that does not bend in this particular scenario so that the actual physical load is split equally, meaning each spindle requires a pure torque of T_s. The transmission efficiencies were taken from handbooks and academic estimations [72, 80]. For these calculations it will be assumed the following efficiencies: Spur Gears ($\eta_{sg} = 0.95$), Bevel Gears ($\eta_{cg} = 0.95$), Bearings ($\eta_b = 0.98$), Universal Joints ($\eta_{uj} = 0.85$ for angles between $30° - 45°$) and Chain Drives ($\eta_c = 0.98$).

Before the transmission system separates into the 3 branches, the movement goes through a spur gear with a reduction ratio of $i = 2$, in the machine's adjustment point.

$$T_{mainshaft} = T_{measured} \cdot i \cdot \eta_{sg} \tag{7.25}$$

$$T_{main} = 9.2\ \text{Nm} \cdot 2 \cdot 0.95 = 17.48\ \text{Nm} \tag{7.26}$$

Next, it is necessary to map the cascading branch efficiencies.

- Branch 1: Spindle 1 is directly driven by the main shaft.

$$\eta_1 = 1.0 \tag{7.27}$$

- Branch 2: Power leaves the main shaft through a bevel mesh, a shaft bearing, and another bevel mesh into Spindle 2.

$$\eta_2 = \eta_{cg} \cdot \eta_b \cdot \eta_{cg} = 0.95 \cdot 0.98 \cdot 0.95 = 0.884 \tag{7.28}$$

- Branch 3: Power leaves Spindle 2 through another bevel mesh, another shaft bearing, and

another bevel mesh into Spindle 3.

$$\eta_3 = \eta_2 \cdot (\eta_{cg} \cdot \eta_b \cdot \eta_{cg}) = 0.884 \cdot (0.95 \cdot 0.98 \cdot 0.95) = 0.782 \tag{7.29}$$

The total 17.48 Nm on the main shaft must supply enough torque to satisfy T_s across all three branches.

$$T_{main} = \frac{T_s}{\eta_1} + \frac{T_s}{\eta_2} + \frac{T_s}{\eta_3} \tag{7.30}$$

$$17.48 = T_s \left(\frac{1}{1.0} + \frac{1}{0.884} + \frac{1}{0.782} \right) \tag{7.31}$$

$$T_s = 5.13 \text{ Nm} \tag{7.32}$$

Similarly to the previous sections, a Safety Factor $S_f = 1.5$ was applied due to the current degradation of the linear units and the environment in which they operate and an Application Factor $K_a = 1.25$ for the motor sizing.

$$T_{motordesign} = 5.13 \cdot 1.5 \cdot 1.25 = 9.62 \text{ Nm} \tag{7.33}$$

Before evaluating the spatial layout, the feasibility of a direct-drive coupling between the actuator and each spindle must first be checked. Applying the same factors S_f and K_a yields a required motor-sizing torque of 9.62 Nm at the spindle interface under a 1:1 coupling assumption. This value exceeds the rated holding torque of the largest stepper motor already qualified for this project by approximately 3% ($S_{sel} = \frac{9.33}{9.62} = 0.96985$). Torque amplification between the actuator and the spindle is therefore established as a binding requirement independent of, and in addition to, the spatial constraints developed below.

Geometric Constraints

A fundamental requirement of the conceptual design phase is the rigorous mapping of the spatial envelopes available. Because the retrofit must be integrated into the existing structural frame of the Kisters packaging module without requiring major modifications, the physical volume surrounding each of the three linear guides dictates the permissible size and orientation of the motors and transmission components. An initial geometric audit of the machine frame revealed significant spatial disparities among the three adjustment units.

Rather than designing three bespoke transmission systems, the conceptual strategy prioritised identifying the most restrictive geometric bottlenecks. These bottlenecks established the maximum allowable dimensions for a universal, standardised drive architecture capable of fitting into all three locations.

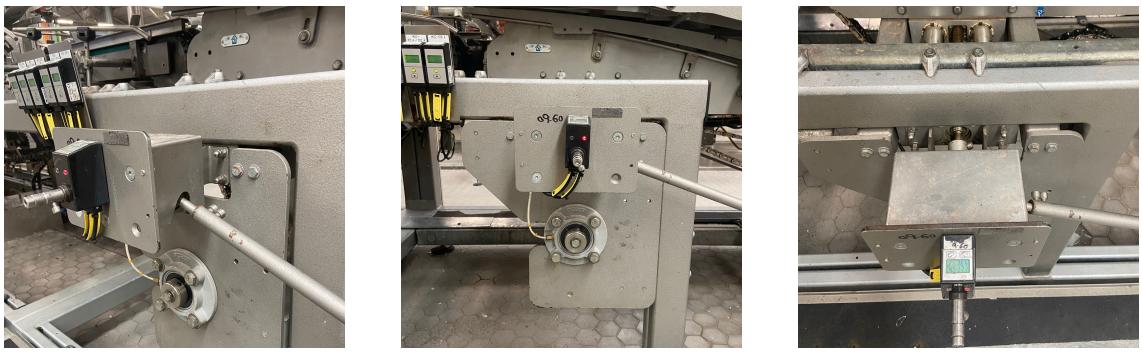
The most critical geometric boundary governing the entire transmission architecture is the floor clearance of the two lower linear guides. The existing guide blocks measure exactly 63 mm in height, placing the central axis of the threaded spindle exactly 31.5 mm above the machine floor. To prevent the timing belt and pulley from grinding against the machine chassis, the radius

of the driven pulley (including the timing belt) cannot exceed this 31.5 mm limit. Consequently, this bottleneck dictates the maximum kinematic reduction achievable via the belt drive, thereby changing the actuator's requirements.

The surrounding spatial envelopes for each specific guide were mapped to determine the solution's placement and orientation.

Linear Unit 1

This axis is suspended above the machine floor and benefits from a highly unconstrained spatial envelope. The available mounting volume extends 112 mm below the block, 260 mm above the block, and 165 mm from the front of the unit's block (Figure 7.16).



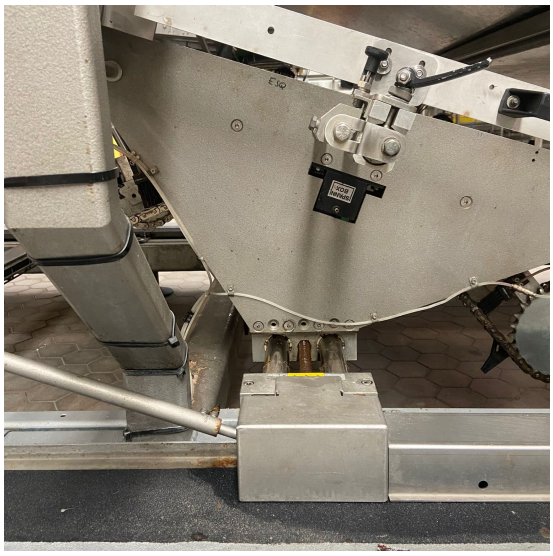
(a) Side View (b) Front View (c) Top View

Figure 7.16: Linear Unit 1 Spatial Envelope and Surrounding Clearances

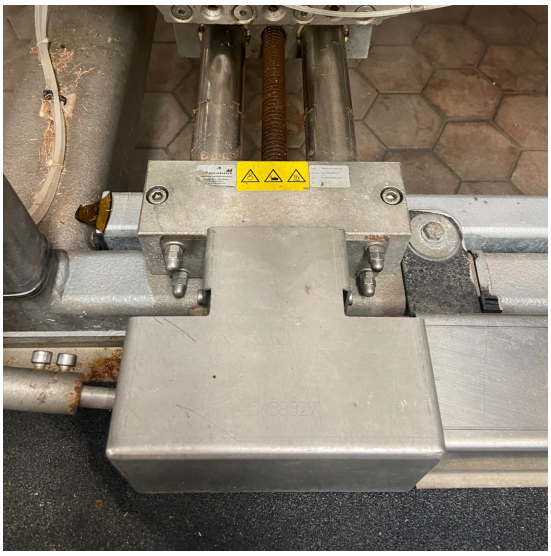
This envelope allows for multi-directional mounting of the motor bracket without risk of collision with structural cross-members.

Linear Unit 2

Subject to the 31.5 mm floor bottleneck, this axis is strictly bounded by the machine chassis on the left (60 mm) but is almost completely unconstrained to the right. It affords 230 mm of vertical clearance and 310 mm of front clearance (Figure 7.17). The optimal orientation for this envelope is a vertical, top-mounted alignment, which maximises the use of the available vertical space while maintaining a narrow horizontal footprint.



(a) Front View



(b) Top View

Figure 7.17: Linear Unit 2 Spatial Envelope and Surrounding Clearances

Linear Unit 3

Also subject to the floor bottleneck, this axis represents the most severe packaging challenge. It is bounded vertically to just 80 mm of top clearance (above the top face of the block) due to the sliding guide, making a vertical motor mount geometrically impossible. However, the envelope affords 88 mm of clearance to the left, 350 mm to the right, and 310 mm to the front (Figure 7.18). To satisfy these constraints, the motor must be mounted in a horizontal orientation extending toward the right or left side of the machine.

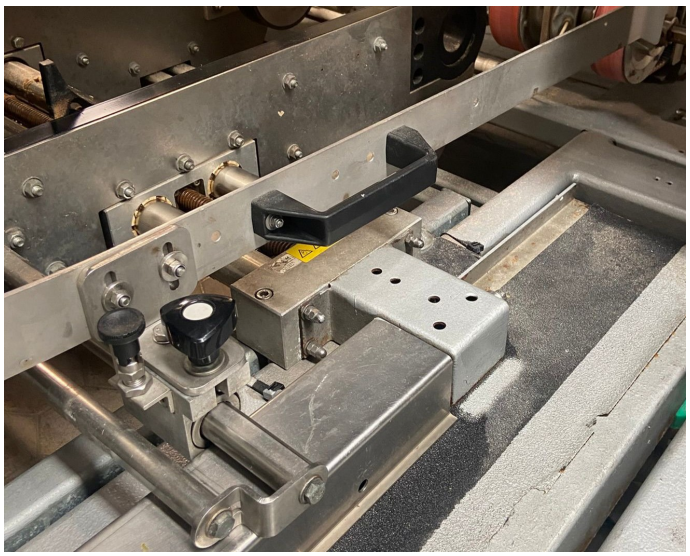


Figure 7.18: Linear Unit 3 Spatial Envelope, Side View

Despite the varying spatial constraints, the design aims to produce a universal bracket and power transmission solution adaptable across the entire transportation system.

With the torque requirement and spatial envelope now established, the chosen architecture must balance high torque transmission, fine positional synchronisation, and a compact spatial layout. Following the discussion presented in the Conceptual Design section, a timing belt and pulley system will be employed, specifically because there is no need for regular maintenance and lubrication, while also having good precision characteristics as required.

7.4.3.1 Kinematic Configuration and Geometrical Constraints

The automated drive system within the Transportation System is constrained by rigid structural interfaces. To ensure component uniformity throughout the machine, the actuation will be guaranteed by the same NEMA 34 stepper motor used for the Cardboard Storage Unit's solution (Table 7.13).

To comply with DFMA principles, a parallel mounting configuration was implemented, aligning both the motor and linear unit shafts in the same direction. The motor's chassis length of 125 mm, compared to the linear unit's bearing block length of 60 mm, results in an axial offset of 85 mm between the motor flange face and the block face. This geometric separation precludes the use of a traditional single-stage coplanar pulley arrangement. Combined with the 31.5 mm floor clearance established above, this rules out a single-stage coplanar pulley of any meaningful diameter. To address these spatial constraints without altering the machine frame, a two-stage synchronous belt transmission system with an intermediate jackshaft is required.

In high-stiction positioning applications, timing belt failures are predominantly attributed to tooth root shear or tooth cam-out (ratcheting). To determine the optimal belt tooth geometry, standard industrial profile families were qualitatively assessed with respect to these primary failure modes, as summarised in Table 7.14.

Table 7.14: Comparative Analysis of Synchronous Belt Tooth Profiles for High-Stiction Applications

Belt Profile	**Root Stress Distribution**	**Shock Load Capacity**	**Positional Accuracy**
Metric Trapezoidal (e.g., T5, AT5)	Moderate (Sharp profile corners create internal stress concentrations)	Poor (Prone to riding up pulley walls and ratcheting)	Moderate (Inherent backlash clearances required for meshing)
Modified Parabolic (e.g., STD S5M)	Good (Broader tooth root distributes forces more evenly)	Good (Smooth tooth engagement mitigates impact wear)	Good (Low backlash clearance; reduced operating noise)
Curvilinear (HTD) (e.g., HTD 3M/5M)	Excellent (Uniform shear distribution across smooth root arc)	High (Deep tooth engagement physically prevents jumping)	High (Near-zero backlash engagement for closed-loop encoders)

Classical metric trapezoidal profiles are unsuitable for this application because their sharp root transitions serve as geometric stress concentrators under shock loading. Although modified parabolic profiles present significant improvements, the High Torque Drive (HTD) curvilinear profile was selected. The HTD profile's fully rounded, deep-tooth geometry maximises the shear cross-section and ensures a uniform distribution of tangential loads, enabling the reduced backlash synchronisation required to use the motor's absolute encoder.

To determine the optimal pitch module, an initial evaluation applied the compact HTD 3M series (3 mm pitch). To maximise mechanical advantage within the 63 mm floor constraint, the largest standard catalogue HTD 3M pulley was selected for the driven spindle shaft ($Z = 44$). This pulley has a maximum outer diameter (d_{outer}) of 48 mm, providing a 7.5 mm radial clearance to the floor, and a pitch diameter (d_{pitch}) calculated in Equation 7.34.

$$d_{\text{pitch}_3\text{M}} = \frac{Z \cdot p}{\pi} = \frac{44 \cdot 3 \text{ mm}}{\pi} = 42.02 \text{ mm} = 0.04202\text{m} \tag{7.34}$$

The critical failure metric for the pitch module is the maximum tangential force (F_u) imposed on the belt fibres during peak load events. Evaluating this loop under the required application torque ($T_{\text{spindle}} = 5.13 \cdot 1.5 = 7.70$ Nm) yields the results presented in Equation 7.35.

$$F_{\text{u}_3\text{M}} = \frac{2 \cdot T_{\text{spindle}}}{d_{\text{pitch}_3\text{M}}} = \frac{2 \cdot 7.70 \text{ Nm}}{0.04202\text{m}} = 366.49\text{N} \tag{7.35}$$

Empirical manufacturing catalogue data [81], in accordance with ISO 13050, indicate that a standard 15 mm wide HTD 3M belt has a baseline static allowable force limit of approximately

290N. The calculated operational force of 366.49 N exceeds this threshold by 26%. At full motor stall capacity ($T_{\text{motor}} = 5.94$ Nm), this force would increase further, leading to tensile cord elongation, tooth root fracture, and belt ratcheting. Therefore, the HTD 3M profile was deemed structurally inadequate. To accommodate the load profile without exceeding the shaft length limits, the larger HTD 5M profile (5 mm pitch) must be employed.

However, even if the axial placement of the components is disregarded, a single-stage HTD 5M layout could not satisfy the spatial limits. Using a smaller 14-tooth pulley on the motor to achieve reduction reduces the solid aluminium hub wall thickness around the ∅14 mm keyway to an unsafe 1.27 mm, causing torsional hub failure. Conversely, scaling up the pulleys to ensure hub integrity forces the driven-spindle pulley to exceed the 63 mm diameter limit, thereby striking the floor structure. Distributing the reduction across a two-stage intermediate jackshaft simultaneously resolves these boundary conditions.

In an initial design iteration, a compact baseline pulley set was proposed to minimise volume (full specification in Appendix G). Verified at the motor's absolute stall torque, this baseline produced a tangential force at the motor driver pulley of $F_{u1} = 2 \cdot 5.94/0.03501 = 339.33$ N, exceeding the motor's rated radial bearing limit (220 N) by 54.2%. Operation would cause rapid bearing fatigue and premature motor failure, so the baseline was rejected.

To physically force the motor's radial bearing load below the 220N threshold without increasing the housing width, the pitch diameters of the primary stage were upscaled. Increasing the pitch diameter of the driving pulley increases the mechanical lever arm, thereby reducing the net tangential belt tension required to transmit the equivalent torque. To minimise component proliferation, the stage 2 pulleys were frozen at their baseline specification of 22T ($Z_3 = 22$) and 28T ($Z_4 = 28$), while Stage 1 was modified to a 32T $\rightarrow$ 52T configuration also using standard components and keeping the same belt width. The finalised, optimised four-pulley dataset is compiled in Table 7.15.

Table 7.15: Technical Specifications of the Finalised, Load-Optimised Two-Stage HTD 5M System

Technical Specification	**Pulley 1** (Z_1)	**Pulley 2** (Z_2)	**Pulley 3** (Z_3)	**Pulley 4** (Z_4)
Manufacturer Sourcing	Norelem	Madler	Norelem	Norelem
System Role	Motor Driver	Jackshaft Input	Jackshaft Output	Spindle Driven
Number of Teeth (–)	32	52	22	28
Belt Width (mm)	15	15	15	15
Pitch Diameter (mm)	50.93	82.76	35.01	44.56
Maximum Outer Flange Diameter (mm)	55	-	39	50

This optimised distribution shifts the local transmission ratios to $i_1 = \frac{52}{32} = 1.6250$ and $i_2 =$

$\frac{28}{22} = 1.2727$, expanding the total system mechanical advantage to $i_{\text{total}} = 2.0682$. Sizing the optimised loops under the peak permissible torque ($T_{\text{motor}} = 5.94$ Nm) at an efficiency of $\eta = 0.95$ per stage yields the following operational torque progression:

$$T_{2\text{max}} = T_{3\text{max}} = 1.625 \cdot 5.94 \cdot 0.95 = 9.17 \text{ Nm}, \quad T_{4\text{max}} = 1.2727 \cdot 9.17 \cdot 0.95 = 11.09 \text{ Nm} \tag{7.36}$$

The resulting maximum tangential forces (F_u) at each pulley are evaluated from Equation 7.37 to 7.40.

$$F_{\text{u1max}} = \frac{2 \cdot T_{1\text{max}}}{d_{\text{pitch1}}} = \frac{2 \cdot 5.94 \text{ Nm}}{0.05093 \text{ m}} = 233.26\text{N} \tag{7.37}$$

$$F_{\text{u2max}} = \frac{2 \cdot T_{2\text{max}}}{d_{\text{pitch2}}} = \frac{2 \cdot 9.17 \text{ Nm}}{0.08276 \text{ m}} = 221.61\text{N} \tag{7.38}$$

$$F_{\text{u3max}} = \frac{2 \cdot T_{3\text{max}}}{d_{\text{pitch3}}} = \frac{2 \cdot 9.17 \text{ Nm}}{0.03501 \text{ m}} = 523.85 \text{ N} \tag{7.39}$$

$$F_{\text{u4max}} = \frac{2 \cdot T_{4\text{max}}}{d_{\text{pitch4}}} = \frac{2 \cdot 11.09 \text{ Nm}}{0.04456 \text{ m}} = 497.76 \text{ N} \tag{7.40}$$

As a result of the diameter optimisation, the motor's radial load under full stall torque is $F_{u1max} = 233.26$ N. Nanotec's datasheet (Appendix I) rates the permissible radial force at $F_r = 220$ N at a reference distance of 20 mm from the motor face. Because permissible radial load scales inversely with the load's distance from the support bearing [82], and the pulley centreline sits at 17 mm from the face - fixed by the pulley hub width and mounting geometry established in the housing layout, not selected to clear the limit - the allowable load at the installed plane is $F_{r,17} = 220 \times 20/17 \approx 258.8$ N, giving a verified margin of approximately 11% even under full stall. This worst case is itself conservative: F_{u1max} assumes the motor at its absolute stall torque (5.94 Nm), whereas the system's continuous design torque - the operational load including the $S_f = 1.5$ degradation allowance - is $T_{\text{operational}} = \frac{5.13 \cdot 1.5}{2.0682 \cdot 0.95^2} = 4.12$ Nm, corresponding to a normal-operation radial load of only $F_{u1} \approx 161.9$ N and a margin of over 37%. The spindle radial load ($F_{u4max} = 497.76$ N) is adequately supported by the linear unit's heavy-duty internal bearings (1800 N) regardless of operating condition.

The resulting maximum tangential force of the system occurs in Pulley 3. Against the allowable static threshold for a 15 mm wide HTD 5M belt (535 N [81]) establishes a peak belt safety margin of $S_{belt} = 535/523.85 = 1.021$ under full motor stall. This is a slim margin, and the tightest in the system, though it applies only to the stall fault condition and not to normal operation.

Under the continuous design torque rather than stall, the Stage 2 tangential force scales down by the operational-to-stall torque ratio, $Fu3(continuous) = 523.85 \cdot (4.12/5.94) = 363.3$ N, raising the belt margin to $S_{\text{belt(continuous)}} = 535/363.3 = 1.47$. The governing 1.021 margin is therefore specific to the stall fault condition; in normal duty the belt carries a comfortable 47% reserve.

The adoption of a wider 25 mm belt at this loop, which would directly raise the stall-condition margin, was evaluated and deliberately deferred for three reasons. First, the 1.021 margin arises exclusively under the actuator's absolute electrical stall torque, a fault condition; under the continuous design torque that governs normal duty, the 15 mm belt already carries a 47% reserve. Moreover, since the selected closed-loop stepper drives permit software-based current limiting, the delivered torque can be capped below the absolute stall value at commissioning, making the 1.47 continuous-duty margin the effective governing case. Second, the 15 mm width is spatially coupled to the Linear Unit 2 envelope: the net enclosure depth presented toward the 60 mm lateral boundary is the sum of the belt width, flange profile clearances, and wall thickness (Section 7.4.3.2), and a 25 mm belt would add approximately 10 mm to this dimension, eroding a clearance margin that is itself flagged for verification against production mockup tolerances. Third, retaining the 15 mm width preserves the frozen Stage 2 baseline pulleys and the commonality of standard catalogue components across all three drivetrain cores. The wider belt therefore remains the recommended first action of any future design revision, once the mockup-validated envelope clearance is confirmed, rather than a change adopted at this stage against an unverified spatial margin.

With the centre distances fixed at $C_1 = 120$ mm and $C_2 = 90$ mm and the teeth-in-mesh requirement satisfied (TIM ≥ 6 at both stages), the required belt lengths and idler tensioning travel were derived geometrically (full derivation in Appendix G). Stage 1 adopts a standard 475 mm pitch-length belt and Stage 2 a 350 mm belt. Because all three shaft centres are fixed to preserve housing rigidity and IP64 sealing, pretensioning is achieved entirely through adjustable idlers: the active calibration travel required to reach full pretension is $\Delta x_1 = 5.26$ mm (Stage 1) and $\Delta x_2 = 3.94$ mm (Stage 2). These travel values define the idler slot geometry specified in the detail design (Section 7.5.3).

Universal Envelope Strategy

Rather than developing three independent transmission architectures, the embodiment design pursues a single universal drivetrain core (stepper motor, two-stage pulley train, intermediate jackshaft, and idler tensioning bracket) applied identically at all three linear units. This trades a marginally larger footprint at the least-constrained station (Linear Unit 1) for a single qualified design, eliminating component variety and the need to re-validate three separate load paths.

To guarantee this is geometrically valid everywhere, the housing's external envelope is dimensioned against the three most restrictive boundary conditions identified in the geometric audit: the 60 mm lateral clearance to the left of Linear Unit 2, the $80 + 63 = 143$ mm vertical clearance above Linear Unit 3's floor and the 250 mm clearance from Linear Unit 2's block face to the sliding protections of the machine. Because these limits act along different axes at different stations, the drivetrain core is packaged so that its constrained cross-sectional dimension never exceeds the tighter of these three values, while its long axis (motor-to-spindle direction) is free to use whichever generous clearance is locally available. Following the geometrical constraints, the solution adopts a vertical, top-mounted orientation at Linear Unit 2, while Linear Units 1 and 3

share a horizontal orientation.

The idlers rotate on integrated dual rolling-element ball bearings, which are supported by an integrated cantilevered pin shaft machined with the mobile adjustment bracket plate as a single structural element. This bracket includes parallel linear guide slots that enable manual positional adjustment. After achieving the desired belt pretension (F_{preload}), the bracket is securely locked in position.

As the transportation system functions as a bi-directional positioning drive, the tension profile across the belt spans alternates dynamically during reversing cycles. During drive reversal under conditions of maximum stiction or fault stall, the idler-bearing spans become the high-load tight side of the transmission drivetrain. The wrap angles formed along the triangular paths result in peak forces that attempt to move the adjustment brackets backward along their tracking slots. The critical operational loading is localised at the Stage 2 idler bracket, where the combined vectors produce a maximum perpendicular sliding force of $F_{\text{idler\_slip}} = 485.50\text{N}$.

To guarantee absolute immobilisation of the bracket under alternating dynamic shock loads without causing material failure within the adjacent structural housing, the retention architecture utilises specific fastener combinations tailored to the independent local wall thicknesses of the machine frame. The clamping interfaces must fulfil the static friction constraint:

$$F_{\text{friction\_holding}} = n \cdot (\mu \cdot F_{\text{screw\_preload}}) \geq F_{\text{idler\_slip}} \cdot S_{joint} \tag{7.41}$$

Where $\mu = 0.74$ [79] is the dry static friction coefficient established between the raw machined bracket face and the housing frame wall, and $S_{joint} = 1.50$ is the minimum structural safety factor defined against tracking loss.

Because both idler brackets are clamped using existing screws drawn from neighbouring joints rather than dedicated fasteners, each stage relies on a single shared bolt (n=1) rather than the dedicated two-bolt pattern used elsewhere in this chapter. At Stage 1, the bracket is captured by the same ISO 4762 M6 socket head cap screw (A4-70 stainless steel) that secures the stepper motor to the housing, configured as a through-bolt locked by a nut on the motor flange's far face; per the preload established for this fastener class previously ($F_{\text{screw\_preload}} \approx 7.8$ kN at 9.5 Nm):

$$F_{\text{hold,1}} = 1 \cdot (0.74 \cdot 7800) = 5772 \text{ N}, \qquad S_{\text{clamp,1}} = 5772/485.50 = 11.88 \tag{7.42}$$

At Stage 2, the bracket is captured by the same ISO 4762 M8 counterbore socket head cap screw (A4-70 stainless steel) that secures the housing to the linear unit, threaded into the linear unit's existing tapped interface; per the preload established for this fastener class ($F_{\text{screw\_preload}} \approx 14.5$ kN at 22.0 Nm):

$$F_{\text{hold,2}} = 1 \cdot (0.74 \cdot 14500) = 10730 \text{ N}, \qquad S_{\text{clamp,2}} = 10730/485.50 = 22.10 \tag{7.43}$$

Both stages satisfy the governing constraint ($F_{\text{hold}} \geq F_{\text{idler\_slip}} \cdot S_{\text{joint}} = 728.25$ N), with Stage 1 carrying the tighter margin despite Stage 2 nominally experiencing the higher belt-induced load

- a consequence of the smaller M6 fastener and lower preload available at that node, not of the applied load itself. Because each shared screw's preload is generated independently along its own tensioned shank, no reduction in clamping capacity results from its dual mounting/retention duty.

7.4.3.2 Spatial Envelope Verification

The governing rotating element is Pulley 2 ($d_{\text{outer},2} = d_{\text{pitch},2} = 82.76$ mm, radius $r_2 = 41.38$ mm, flangeless), mounted on the jackshaft at $Y_{2,3} = 59.92$ mm above the floor. The top of the assembly reaches its maximum vertical boundary via Equation 7.44:

$$Y_{\text{top}} = Y_{2,3} + r_2 = 59.92 \text{ mm} + 41.38 \text{ mm} = \mathbf{101.30} \text{ mm} \tag{7.44}$$

At Linear Unit 3 (the governing station), the 80 mm clearance limit is measured directly above the block's top face, which sits at an elevation of 63 mm above the floor datum. The structural ceiling and corresponding safety headroom margin are evaluated in Equation 7.45:

$$Y_{\text{limit,LU3}} = 63 \text{ mm} + 80 \text{ mm} = 143.00 \text{ mm}, \qquad \text{Margin} = 143.00 \text{ mm} - 101.30 \text{ mm} = \mathbf{41.70} \text{ mm} \tag{7.45}$$

The universal core clears the worst-case station with 41.70 mm of vertical headroom to spare. Note that the 82.76 mm pulley diameter must not be compared directly against the raw 80 mm clearance figure: the 80 mm value is an incremental clearance measured above the already-elevated 63 mm block face, not an absolute ceiling height from the floor. Evaluated against the correct reference plane, the assembly clears with the margin shown above.

At Linear Unit 2, the 60 mm spatial envelope restriction acts laterally, while the generous 230 mm vertical clearance comfortably accommodates the 101.30 mm peak assembly height. The physical dimension presented toward the 60 mm lateral boundary is the net depth of the enclosure housing (representing the sum of the belt width, flange profile clearances, and wall thickness allowances perpendicular to the pulley pitch plane), estimated between 35 mm and 40 mm. This provides a safe operating margin, though it is recommended to verify this thickness against final production mockup tolerances. Linear Unit 1's open envelope constraints are satisfied automatically without structural modification.

7.4.3.3 Environmental Protection and Enclosure Strategy

The Transportation System drivetrain achieves full IP64 compliance using a single-piece monolithic stainless steel housing body that locates and encloses both synchronous belt stages. The enclosure is sealed by a protective lid that contains the primary machined jackshaft bearing seats to complete the sealed boundary envelope. Because the intermediate jackshaft is entirely contained internally and never penetrates the exterior housing walls, the requirement for dynamic rotational shaft seals is eliminated.

Fluid and dust protection is restricted to static sealing boundaries: the continuous body-to-lid perimeter joint, sealed using a liquid silicone (RTV) sealant applied as a continuous bead within the machined face channel, selected over a compressed gasket given the joint's infrequent disassembly, and the two external flange interfaces mounting the motor and linear unit. These mounting points reuse the twin-O-ring face-seal strategy validated for the Roller Conveyor module, since the rotating boundary at each node is isolated by the motor's and linear unit's native internal seals. The perpendicular idler tensioning shaft access constitutes the only additional penetration through the housing wall; this interface is locked using a sealed-plug configuration, which is structurally appropriate given that the tensioner is an infrequently accessed calibration interface rather than a continuously moving component.

7.4.3.4 Integrated Jackshaft and Bearing System Design

The jackshaft carries the transmitted torque between Stage 1 (driven pulley, oriented $+70^\circ$ from vertical) and Stage 2 (driving pulley, -55° from vertical), an inverted-V arrangement matching the physical layout of Linear Units 2 and 3. Torque is conserved across the shaft ($T_{2max} = T_{3max} = 9.17$ Nm). Resolving the resulting belt forces by orientation and applying the continuous belt-tension factor ($b = 2.0$ [83]) yields bearing reactions of $R_A = 793.4$ N (governing) and $R_B = 296.8$ N; the full vector resolution is provided in Appendix G.

The shaft adopts a symmetric, double-shoulder profile in which each pulley is positively located by shoulders on both faces rather than by circlips or set screws, since synchronous belt drives impose negligible axial thrust when properly aligned [72, 79] and the shoulders are therefore required only to locate the pulleys during assembly. Journal and shoulder diameters ($d_1 = 10$ mm, $d_2 = 14.5$ mm, $d_3 = 18$ mm) follow directly from the SKF 6,000-family bearing's catalogue abutment limit; the resulting axial layout is given in Table 7.16, with keyway positions offset from adjacent shoulders to satisfy standard minimum-clearance guidance [72].

Table 7.16: Jackshaft Axial Geometry and Coordinate Map

Shaft Element / Feature	**Start Z (mm)**	**End Z (mm)**	**centre Z (mm)**	**Target Dia. (mm)**
Left Bearing Support (A)	-4.0	4.0	0.0	10.0 (h6 fit)
Standoff	4.0	9.0	–	14.5
Pulley 3 Journal (Keyway)	9.0	35.0	22.0	14.5
Central Locating Shoulder	35.0	74.5	54.75	18.0
Pulley 2 Journal (Keyway)	74.5	104.5	89.5	14.5
Standoff	104.5	105.5	–	14.5
Right Bearing Support (B)	105.5	113.5	109.5	10.0 (g6 fit)

Given the purely radial load profile and low operating speed ($<$ 500 RPM), an **SKF 6,000-Z** deep groove ball bearing is specified ($C_{0r} = 1.96$ kN, $C_r = 4.75$ kN); the single-shield variant is sufficient since the jackshaft is fully enclosed within the sealed housing and the shield's role is limited to lubricant retention. Verified against the governing reaction R_A, the static safety factor is $s_0 = C_{0r}/R_A = 2.47$, and the basic dynamic rating life exceeds the project's 10-year design-life target by several orders of magnitude, confirming that bearing fatigue is not life-limiting at this duty cycle. Full reaction-force and life-calculation derivations are provided in Appendix G.

The shaft material is AISI 4140 chromium-molybdenum steel, quenched and tempered (42CrMo4 in the KISSsoft material database; $R_m = 655$ MPa, $R_e = 415$ MPa). The governing section is the Pulley 3 journal ($Z = 22.0$ mm, $d = 14.5$ mm), where the combined bending and torsional stress, amplified by the DIN 6885 keyway's stress-concentration factors ($K_t = 2.14$, $K_{ts} = 3.0$ [72]), yields a von Mises equivalent stress of 148.06 MPa against the material's yield strength, giving a static safety factor of $S_f = 2.80$.

Fatigue cycle counting must reflect the shaft's loading physics: as a rotating shaft under stationary bending loads, the jackshaft experiences one fully reversed bending stress cycle per revolution, not per adjustment actuation. Each actuation displaces the guide rail by at most the 84 mm worst-case travel span established in Section 5.4; at the linear unit's 4 mm screw lead and the Stage 2 ratio i = 28/22, this corresponds to at most 27 jackshaft revolutions per actuation. At the established usage rate (250 actuations/year), the shaft therefore accumulates $\approx 6.7 \times 10^4$ stress reversals over its 10-year design life - a deliberately conservative count, since most changeovers traverse only a fraction of the worst-case span. This remains more than an order of magnitude below the 10^6-cycle threshold that defines the infinite-life fatigue regime, so the governing fatigue check is evaluated at finite life, conservatively rounded up to N = 10^5, using the standard Basquin high-cycle relation [84], giving a modified-Goodman safety factor of $SF_{fatigue} = 1.77$.

For reference, evaluating the same stresses against the infinite-life endurance limit would give $SF_{fatigue,} = 1.35$, a lower bound the design satisfies regardless of the cycle-count basis. The full Marin/Basquin derivation is provided in Appendix G. The central locating shoulder was checked using the same method and does not govern (Sf = 5.62, $SF_{fatigue}$ = 3.51).

Angular deflection at the bearing supports, evaluated by superposition of both applied loads, reaches $\theta_A \approx 0.068°$ (governing) - nearly an order of magnitude below the bearing manufacturer's 0.5° misalignment limit.

To cross-validate the hand calculation, the shaft geometry, load case, and material were reproduced in KISSsoft (Table 7.17). Agreement on the bearing reaction force, static safety factor, and dynamic life is within 1%. The larger discrepancy in angular deflection (32%) reflects the hand calculation's conservative simplification of the shaft as a uniform-diameter section, whereas KISSsoft's stepped-geometry model captures the added stiffness of the central shoulder; both values remain comfortably within the manufacturer's limit. A dedicated KISSsoft fatigue cross-check was not pursued, as KISSsoft's fatigue module defaults to the infinite-life regime and is therefore not directly applicable to this duty cycle; the DIN 743 finite-life hand calculation above is retained as the governing fatigue check.

Table 7.17: Hand Calculation vs. KISSsoft Cross-Validation

Metric	**Hand Calculation**	**KISSsoft**	**% Difference**
Governing reaction force (R_A)	793.4 N	794.0 N	0.08%
Static safety factor (s_0, Bearing A)	2.47	2.467	0.1%
Basic rating life (L_{10h}, Bearing A)	11,920 h	11,874 h	0.4%
Angular deflection (θ_A)	0.068°	0.046° (0.805 mrad)	32%
Fatigue safety factor (SF_{fatigue}, DIN 743, finite-life $N = 10^5$)	1.77	-	N/A

7.5 Detail Design

The final stage of the design process involves providing a comprehensive explanation of the remaining elements required to implement the solution. These elements may include specifications for machined parts, assembly instructions, technical drawings, exploded view diagrams, or other relevant documentation.

7.5.1 Roller Conveyor

7.5.1.1 Geometric and Structural Configuration

The custom coupling housing is designed as a single-piece, asymmetrical machined component that connects the geometric configurations of the linear guide and the stepper motor. The housing comprises three distinct zones: a linear-side mounting flange, a central clearance cylinder, and a stepper-side mounting flange.

The linear unit interface incorporates a $60 \times 60 \times 5$ mm square flange. The spindle axis of the linear guide is positioned at a vertical height of 31.5 mm from the reference base plane. Given that the block face has a total height of 60 mm (with its geometric centre at 30 mm), the central bore of the housing flange is machined with a 1.5 mm vertical offset relative to its outer profile. This asymmetrical offset maintains collinearity with the driving screw axis and prevents the lower edge of the housing from breaching the machine chassis's structural mounting plane.

The central cylindrical body consists of a machined cylinder with an internal diameter of 48 mm and an external diameter of 50.5 mm, yielding a nominal wall thickness of 1.25 mm. The internal diameter is strictly bounded by the ∅46 mm maximum rotational sweep of the GWE 5104-19 coupling clamping hardware, maintaining a 1.0 mm radial air gap to eliminate dynamic friction. The external diameter of 50.5 mm (radius 25.25 mm) is governed by the installation constraints of the four linear-side M8 mounting bolts. These fasteners are arranged in a square pattern spaced 46 mm apart, positioning each bolt centre at a radial distance of:

$$r_{\text{bolt}} = \sqrt{23^2 + 23^2} \approx 32.53 \text{ mm} \tag{7.46}$$

Given that a standard ISO 4762 M8 socket head cap screw features an outer head diameter of 13 mm (radius 6.5 mm), the innermost boundary of the bolt head counterbore profile is located at:

$$r_{\text{head\_inner}} = 32.53 \text{ mm} - 6.5 \text{ mm} = 26.03 \text{ mm} \tag{7.47}$$

Setting the cylinder exterior at a radius of 25.25 mm provides a precise 0.78 mm clearance, which allows tool access for torqueing the M8 hardware while maintaining adequate wall thickness. The cylinder extends longitudinally for 77.5 mm to separate the two mounting interfaces. The housing ends at the motor interface with an $85.85 \times 85.85 \times 8.5$ mm square flange that matches the physical envelope of the NEMA 34 frame. This flange incorporates four ∅6.6 mm clear holes arranged on a 69.5×69.5 mm pattern to accept through-bolts.

7.5.1.2 Structural and Displacement Validation (FEA)

To verify that the housing geometry withstands the system's governing load case, particularly the 1.25 mm nominal wall thickness of the central cylindrical body, a static linear FEA study was performed in SolidWorks Simulation on the finalised housing geometry.

Boundary Conditions

The four through-holes on the linear unit's side mounting flange were fixed in position, replicating the structural restraint provided by the linear unit's block face and screws. The 9.33 Nm maximum motor stall torque was applied as a moment about the bore axis on the stepper-side flange face. The motor's mass was represented as a remote load of $m \cdot g = 4.6 \cdot 9.81 = 45.13$ N, applied at an offset point corresponding to the motor's actual centre of mass rather than at the flange face directly, to correctly capture the cantilevered moment arm (Figure 7.19). The housing was modelled in AISI 316 Annealed Stainless Steel Bar ($R_e = 137.9$ MPa), and the mesh was refined to the finest standard scale.

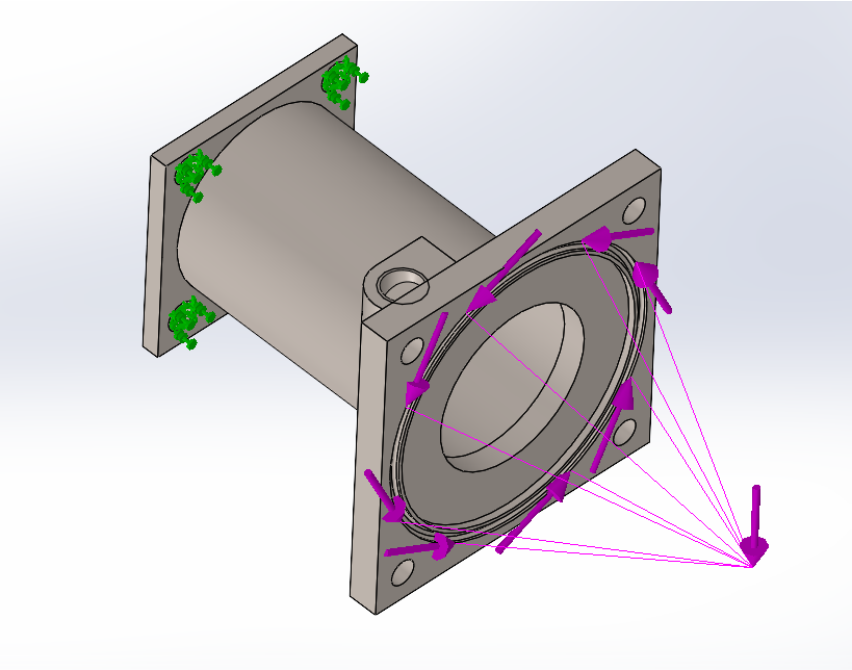


Figure 7.19: Boundary Conditions Established for the Roller Conveyor Housing FEA Validation

Stress Results

The resulting peak von Mises stress reaches a maximum of $\sigma_{vm} = 10.41$ MPa, located at the bore of the M12 threaded access port. This is the same feature that is reinforced by the local thickening boss previously stated (Figure 7.20). Despite this local geometric discontinuity, the governing stress yields an elevated static safety factor, confirming that the housing, including its thinnest cross-section, carries the governing load case with substantial margin.

$$S_f = \frac{137.9}{10.41} \approx 13.25 \tag{7.48}$$

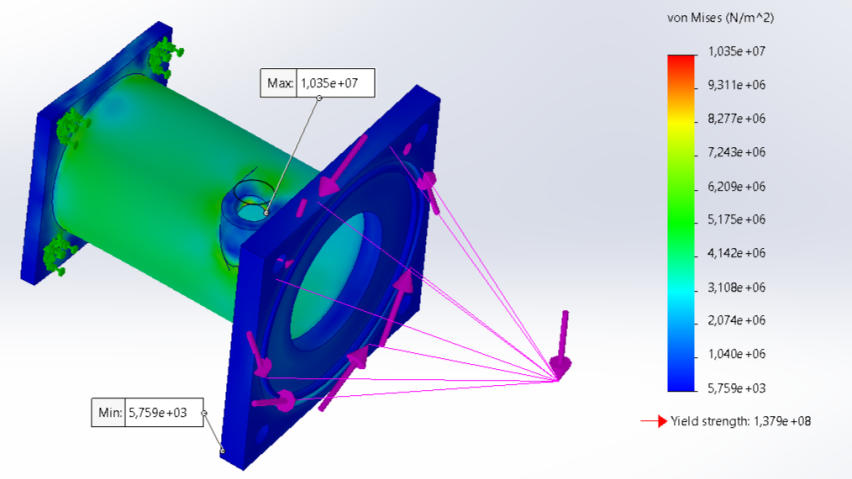


Figure 7.20: Von Mises Stress Results from the Roller Conveyor Housing FEA Simulation

Displacement Results

The resultant displacement (URES) reaches a maximum of 8.107×10^{-3} mm at the free end of the assembly, which is the point most distant from the fixed constraint (Figure 7.21). This displacement is subsequently included as an additional, independent factor in the overall radial misalignment budget.

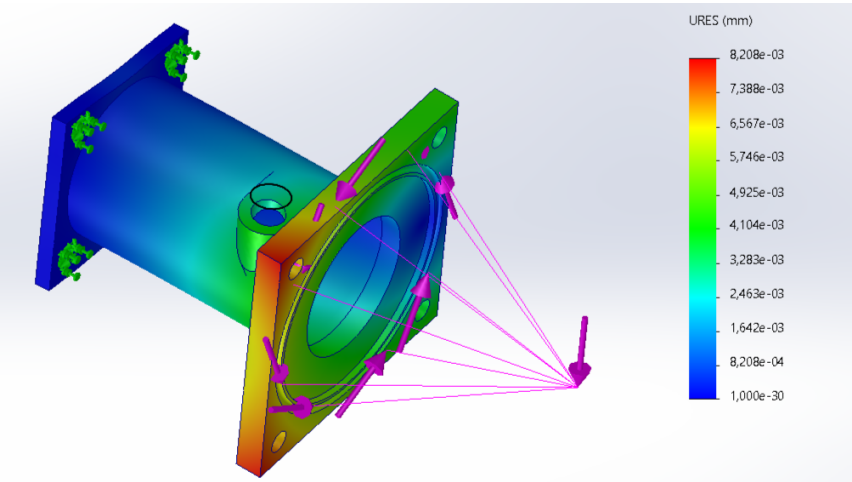


Figure 7.21: Displacement Results from the Roller Conveyor Housing FEA Simulation

7.5.1.3 Metrological Specifications and Fit Selection

To mitigate cyclic radial loading and prevent accelerated bearing wear in both the motor and the linear guide, strict locational clearance fits and geometric dimensioning and tolerancing (GD&T) principles are applied. The linear unit's side interface incorporates a male alignment spigot machined to an ISO f7 tolerance (∅39.950 mm to ∅39.975 mm). This spigot couples with the existing female locating bore of the linear guide, which is specified to an ISO H8 tolerance

(∅40.000 mm to ∅40.039 mm). This arrangement establishes a deterministic locational clearance fit ranging from 0.025 mm to 0.089 mm, ensuring repeatable concentric alignment during mounting. The stepper's side flange incorporates a female counterbore designed to accept the male pilot register of the motor ($\varnothing 73.025 \pm 0.025$ mm). The internal counterbore is machined to a tolerance of ∅73.055 mm to ∅73.074 mm, which limits the maximum structural eccentricity across the joint.

To maintain system collinearity, the metrological datums are defined relative to the central axis established by the ∅40 h6 spigot (Datum A). The primary geometric controls are defined as follows:

- **Coaxiality:** The ∅73.000 mm female motor counterbore must be coaxial to Datum A within a cylindrical tolerance zone of ∅0.02 mm.
- **Perpendicularity:** The axial mating faces of both the linear-side flange and the motor-side flange must be perpendicular to Datum A within a tolerance zone of 0.03 mm to eliminate angular cocking of the shafts upon bolt tensioning.

The radial misalignment budget at the coupling is determined by summing three independent contributions: the linear-side spigot fit (h6/H8, worst-case eccentricity 0.0275 mm), the motor-side register fit (custom-limit bore against the motor's stated pilot tolerance, 0.037 mm), and the housing's internal coaxiality callout (0.02 mm, 0.01 mm). The worst-case arithmetic sum is 0.0745 mm, which exceeds the coupling's rated radial capacity of 0.06 mm. However, since these error sources arise from independent, uncorrelated variations in manufacturing and fit rather than a single common-cause deviation, a statistical root-sum-square combination, incorporating the housing's own FEA-derived elastic deflection as a fourth, independent contributor, yields a more accurate estimate of ($\sqrt{0.0275^2 + 0.037^2 + 0.01^2 + 0.0081^2} \approx 0.048$ mm). This approach offers a 20% margin relative to the 0.06 mm rated capacity. The statistical method is preferred over worst-case stacking because any exceedance results in a gradual increase in the spider restoring force, rather than an abrupt functional failure.

The angular and axial misalignment budgets are not limiting factors. The 0.03 mm perpendicularity callout over the 85.85 mm flange face corresponds to approximately 0.02°, which is two orders of magnitude below the coupling's 0.9° rated angular capacity. The axial position is constrained by the engagement-depth geometry specified in Section 7.5.1, remaining well within the +1.2/0.5 mm rated axial allowance.

7.5.1.4 Environmental Sealing Design

To meet the IP64 environmental criteria for dust ingress and low-pressure shop-floor washdowns, the housing employs twin static elastomeric face seals conforming to ISO 3601-1. On the linear unit's interface, an O-ring with an internal diameter of 43 mm and a nominal cross-sectional diameter (d_2) of 3.0 mm is specified. The matching rectangular gland groove is machined into the

60×60 mm flange face with a depth of 2.35 ± 0.05 mm and a width of 4.10 mm. Under nominal metal-to-metal contact, this geometry enforces a constant axial squeeze of:

$$S_{\text{linear}} = \frac{3.0 \text{ mm} - 2.35 \text{ mm}}{3.0 \text{ mm}} \times 100\% \approx 21.6\% \tag{7.49}$$

On the stepper motor interface, an O-ring with an internal diameter of 75 mm and a nominal cross-sectional diameter (d_2) of 2.0 mm is specified. The face groove is machined to a depth of 1.55 ± 0.04 mm and a width of 2.80 mm, yielding an axial compression of:

$$S_{\text{stepper}} = \frac{2.0 \text{ mm} - 1.55 \text{ mm}}{2.0 \text{ mm}} \times 100\% = 22.5\% \tag{7.50}$$

Both compression values are within the required 15% to 25% elastomeric threshold necessary to establish a continuous fluid-tight seal against low-pressure water jets and to avoid material degradation. To prevent fluid bypass through micro-capillary paths, the mating faces and groove roots are specified with a surface roughness of $R_a \leq 1.6$ μm.

7.5.1.5 Design for Manufacture and Assembly (DFMA) and Access Optimisation

Since the coupling assembly is fully enclosed within the 47 mm internal bore of the cylinder, direct blind installation is not feasible. The validated assembly sequence requires the coupling to be fixed to the linear unit spindle first, followed by installation of the housing body. The stepper motor shaft is then inserted axially into the open hub of the coupling until the motor flange contacts the housing face. To torque the motor-side coupling hub clamp screw after the motor is seated, a single radial access port is integrated into the cylinder wall. The port is positioned at an axial distance of 15.5 mm from the stepper-side flange face and a radial distance of 14.5 mm from the shaft centreline, aligning perfectly with the internal M4 clamping hardware. The port is machined with an M12 $\times$ 1.5 metric fine thread to accept a specialised Wiska ESVS 12 stainless steel stop plug. The Wiska plug features a thread length of 5 mm and an external head diameter of 14 mm embedded with a native O-ring face seal to maintain local IP66/IP68 protection. Because the nominal cylinder wall thickness is only 1.25 mm, it cannot support the thread profile. To provide sufficient engagement, a flat external boss is milled onto the cylinder exterior, increasing the local wall thickness and providing a smooth landing zone for the plug head. The stepper motor is axially secured with four ISO 4762 M6 socket head cap screws passing through the flanges, locked with standard washers and ISO 4032 nuts on the back. Because the mounting holes sit on a 69.5×69.5 mm pattern, the bolt circle radius is 49.15 mm. This places the through-holes entirely outside the $\varnothing$75 mm face O-ring groove (radius 37.5 mm), ensuring the holes penetrate only the unsealed atmospheric zone. The radial clearance between the $\varnothing$50.5 mm cylinder outer wall (radius 25.25 mm) and the M6 bolt centers is:

$$C_{\text{tool}} = 49.15 \text{ mm} - 25.25 \text{ mm} = 23.90 \text{ mm} \tag{7.51}$$

This distance ensures sufficient spatial clearance for standard deep-well sockets or open-ended wrenches to secure the nuts during structural tensioning.

The coupling hub is therefore fitted to the linear-unit shaft before the housing is engaged over it, with the motor installed last so that its output shaft enters the coupling's open hub through the access port; this order allows the internal clamp screw to be torqued and visually verified before the port is sealed with its plug, completing the IP64 boundary.

7.5.1.6 Fastener Selection and Fastening Torque Matrix

To minimise galvanic corrosion cells across the machined structural interfaces during washdown procedures, all structural fasteners, washers, and nuts are specified as high-grade A4-70 stainless steel ($\sigma_y = 450$ MPa). The structural adequacy of the selected fastener diameters is verified by evaluating the relationship between the installation clamp loads and the operational machine loads. For the linear unit interface, the ISO 4762 M8 fasteners feature a tensile stress area $A_s = 36.6$ mm^2. Tightening each screw to the target torque of 22.0 Nm utilises approximately 65% of the material yield strength, generating a nominal axial preload force of 14.5 kN per bolt. Across the four-bolt pattern, this establishes a total structural clamping force of:

$$F_{\text{clamp\_linear}} = 4 \times 14.5 \text{ kN} = 58.0 \text{ kN} \tag{7.52}$$

The primary operational load acting on this joint is the peak motor holding torque of 9.33 Nm. At the bolt circle radius of 32.53 mm, the resulting rotational shear force attempting to induce slip across the flange face is:

$$F_{\text{shear\_operational}} = \frac{9.33 \text{ Nm}}{0.03253 \text{ m}} = 286.81 \text{ N} \tag{7.53}$$

Because the friction force generated by the 58.0 kN static clamp load heavily exceeds the 286.81 N operational shear force, the joint operates strictly under a friction-locked condition. Consequently, the M8 fasteners are not expected to experience meaningful cyclic shear stress on their threads during operation. For the stepper motor interface, the ISO 4762 M6 fasteners feature a tensile stress area $A_s = 20.1$ mm^2. Torquing these fasteners to 9.5 Nm induces an axial preload of approximately 7.8 kN per bolt, creating a combined clamping force of 31.2 kN against the motor flange face. The external static load applied to this joint consists of the cantilevered mass of the NEMA 34 motor (≈ 4.6 kg), which exerts a vertical gravitational force of 45.13 N. Since the clamping force (31.2 kN) is several orders of magnitude greater than the cantilevered gravitational force (45.13 N), joint separation or structural relaxation under operation is not a credible failure mode. Table 7.18 outlines the definitive engineering specifications and tightening torque values required to maintain joint pre-load without yielding the components.

Table 7.18: Roller Conveyor Fastening and Joint Specification Matrix

Interface Joint	**Fastener Standard**	**Material Grade**	**Qty**	**Target Torque**
Linear Unit Mount	ISO 4762 M8 × 25 Screw	A4-70 Stainless Steel	4	22.0 Nm
Stepper Motor Mount	ISO 4762 M6 × 20 Screw	A4-70 Stainless Steel	4	9.5 Nm
Stepper Motor Nut	ISO 4032 M6 Hex Nut	A4-70 Stainless Steel	4	-
Stepper Motor Washer	ISO 7089 M6 Plain Washer	A4-70 Stainless Steel	4	-
Access Port Plug	Wiska ESVS 12 (M12 × 1.5)	Stainless Steel 1.4305	1	5.0 Nm
Coupling Hub Clamp	Integrated M4 Hex Screw	High-Tensile Steel	2	4.9 Nm

7.5.1.7 Final Solution and Technical Documents

The final 3D CAD assembly is shown in Figure 7.22. The complete set of engineering and manufacturing drawings can be observed in Appendix J.

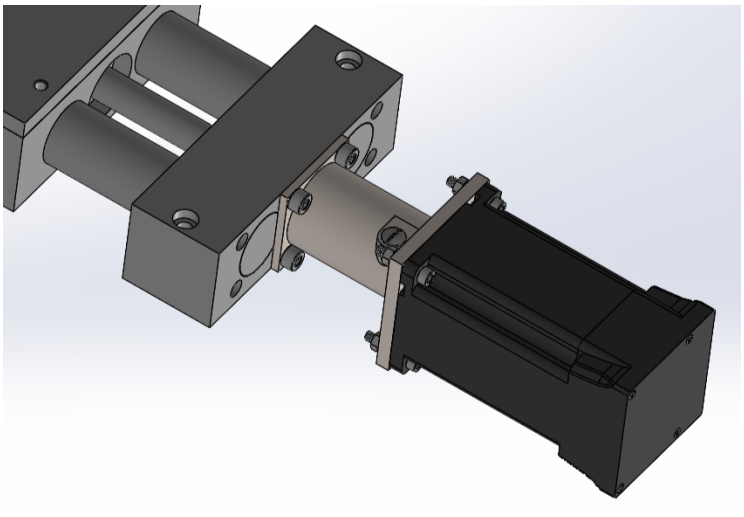


Figure 7.22: Final 3D CAD Assembly for the Roller Conveyor Solution

7.5.2 Cardboard Storage Unit

The four Cardboard Storage Unit housings reuse the detail design method validated for the Roller Conveyor (Section 7.5.1) - the concentric housing architecture, the GD&T and fit scheme, the

coupling family, and the fastener strategy. Only the material, sealing, and mounting deviations specific to this module are detailed below; the full FEA result fields for all four points are provided in Appendix H.1.

7.5.2.1 Geometric and Structural Configuration

The housings employ a split-material strategy tailored to local exposure. The M09-025 housing is fabricated from AISI 316 stainless steel to resist the wet, chemically aggressive zone it occupies. The three upper points (M09-010, M09-012, M09-021) are machined from Aluminium AW-6082-T6 to reduce mass on the structural panel and lower material and machining cost.

For M09-025, the axial envelope is constrained to 260 mm from the linear unit's block face to the sliding mesh guard. The global axial stack-up is:

$$L_{\text{assembly}} = L_{\text{motor}} + L_{\text{Housing}} = 125 + 35 + 35 + 2 + 16 = 213 \text{ mm} \tag{7.54}$$

giving 47 mm of positive clearance to the guard. M09-010, M09-012, and M09-021 face no axial boundary - they extend toward the unused side of the machine - so their housing length is governed solely by coupling and shaft-engagement geometry.

Because the three upper points register directly against the panel's pre-existing threaded holes rather than a machined locating feature, their through-holes are oversized, allowing the installer to compensate for the legacy panel's positional tolerance during fitting. This removes the build-tolerance budget that governs the spigot-located nodes, and is the reason their alignment is validated directly against the coupling capacity rather than via an RSS stack (below). To simplify machining, the central body of all four housings uses a rectangular outer cross-section with a cylindrically machined internal cavity, rather than the circular profile of the Roller Conveyor.

On M09-025, the metrology is identical to the Roller Conveyor: the same ∅40 mm H8 locating bore, f7 spigot, custom-limit ∅73.055–73.074 mm motor-side register, and 0.02 mm coaxiality callout. The Roller Conveyor's validated misalignment budget therefore applies directly to M09-025 without re-derivation.

7.5.2.2 Structural and Displacement Validation (FEA)

Static linear FEA was performed on the three distinct housing geometries (M09-025; the shared M09-010/012 design; and M09-021), using the boundary-condition convention validated for the Roller Conveyor: the linear-unit- or panel-side flange fixed, the motor stall torque applied about the bore axis on the stepper-side flange, and the motor mass applied as a remote load at its centre of mass. The M09-025 model used AISI 316; the aluminium housings were modelled in a 6061-T6 proxy, with safety factors reported against the specified AW-6082-T6 yield ($R_e = 260$ MPa). Table 7.19 summarises the results; the full boundary-condition, stress, and displacement fields are provided in Appendix H.1.

Table 7.19: Cardboard Storage Unit Housing FEA Results

Housing	**Material**	**Peak σ_{vm} (MPa)**	**R_e (MPa)**	**S_f**	**Peak displ. (mm)**
M09-025	AISI 316	5.284	137.9	26.1	1.917×10^{-3}
M09-010 / 012	AW-6082-T6	14.45	260	18.0	3.794×10^{-2}
M09-021	AW-6082-T6	10.77	260	24.1	3.199×10^{-2}

For M09-025, the peak displacement (1.917×10^{-3} mm) is smaller than the Roller Conveyor's FEA-derived deflection (8.107×10^{-3} mm) already absorbed in the validated 0.048 mm RSS misalignment budget; since the metrology and coupling family are shared, the Roller Conveyor's $\approx 20\%$ margin conservatively applies here without a separate re-derivation.

For the three upper housings, no build-tolerance budget applies (installer-aligned through oversized holes), so displacement is compared directly against the GWE 5104 coupling's rated 0.06 mm radial misalignment capacity: the M09-010/012 deflection leaves $\approx 37\%$ margin and M09-021 $\approx 47\%$. This single-term comparison is deliberately not equivalent to the combined RSS budget used for the sealed nodes, since no independent fit-based error sources exist at these installer-aligned points.

The upper housings deflect roughly an order of magnitude more than M09-025 or the Roller Conveyor. This follows from two compounding factors captured directly in the simulated geometry: the lower elastic modulus of aluminium (≈ 69 GPa versus ≈ 193 GPa for steel), and the reduced local bending stiffness introduced by the milled service-access window in the housing's top face. Both housings nonetheless retain substantial margin against both yield and the coupling's misalignment limit.

7.5.2.3 Environmental Sealing and Access Architecture

The environmental sealing architecture is separated into two functional tiers based on local exposure risks.

Node M09-025 (IP64 Critical Zone): To seal the internal coupling cavity against liquid ingress and cardboard particulate contamination, the housing incorporates two NBR O-rings conforming to ISO 3601-1. These are the same ones used in the Roller Conveyor's solutions, and the same dimensions grooves are also machined in the same part of the component to fight the harsh environment.

To clamp the internal coupling hub hardware during field assembly, a single radial access port is integrated into the flat top wall of the rectangular housing profile. In contrast to the Roller Conveyor's solution, the rectangular outer profile greatly simplifies machining process and component durability as it is much simpler to insert a threaded hole. Due to the expanded flat surfaces of the

rectangular body, this access port is upgraded to an M20×1.5 metric thread to accept a heavy-duty, brass nickel-plated blanking plug manufactured by Weidmüller Interface GmbH & Co. This plug incorporates an integrated NBR O-ring to ensure a certified IP68 protection rating. The expanded M20 opening maximises tool visibility and provides wide clearance for T-handle hex keys to torque the internal coupling clamp screws.

Nodes M09-010, M09-012, and M09-021: Since the three upper adjustment points are isolated from fluid exposure, compression O-rings and threaded blanking plugs are not included in their housing design. To address the risk of galvanic corrosion at the aluminium-to-steel interface with the carbon steel machine panel, the Aluminium AW-6082-T6 housing bodies receive a specialised Type III Hardcoat Anodised surface treatment. This electrochemical process forms a dense, non-conductive ceramic layer of aluminium oxide, which electrically isolates the dissimilar metals and prevents galvanic cell formation.

A large rectangular service window is milled through the top face of the aluminium housing body in place of a threaded port. This access window is covered by a thin, flat lid, which is structurally secured to the housing body with a single M3 button-head screw on each side. This arrangement enables quick maintenance access when necessary and serves as an effective mechanical barrier against airborne coarser particles. This lid can either be fabricated from sheet metal or 3D-printed in-house to meet the required specifications.

7.5.2.4 Fastener Sizing and Structural Preload Matrix

Because all four housings share the stepper-flange and housing-flange specifications, the M8 housing-to-machine fasteners reuse the identical screws, washers, and nuts validated for the Roller Conveyor (Section 7.5.1), maintaining a common stock. Table 7.20 lists the module's fastening specification.

Table 7.20: Cardboard Storage Unit Joint Fastening Specification Matrix

Interface Joint Location	**Fastener Standard**	**Material / Type**	**Qty**	**Target Torque**
Machine Flange Mount	ISO 4762 M8 × 25 Cap Screw	A4-70 Stainless Steel	4	22.0 Nm
Machine Flange Washer	ISO 7093 M8 Large Series Washer	A4-70 Stainless Steel	4	-
Stepper Motor Flange Mount	ISO 4762 M6 × 20 Cap Screw	A4-70 Stainless Steel	4	9.5 Nm
Stepper Motor Flange Nut	ISO 4032 M6 Hex Nut	A4-70 Stainless Steel	4	-
Stepper Motor Washer	ISO 7089 M6 Plain Washer	A4-70 Stainless Steel	4	-
M09-025 Access Port Plug	Weidmüller VP M20 (M20 × 1.5)	Brass, Nickel-Plated (IP68)	1	12.0 Nm
Upper Access Cover Screws	ISO 7380-1 M3 × 6 Button Screw	A4-70 Stainless Steel	2	1.2 Nm
Coupling Hub Clamp Screw	Integrated M4 Hex Clamp Screw	High-Tensile Carbon Steel	2	4.9 Nm

7.5.2.5 Final Solution and Technical Documents

Figure 7.23 presents the final 3D CAD assembly layouts and geometrical configurations developed for the four automation points of the Cardboard Storage Unit. The comprehensive manufacturing blueprints, dimensional tolerances, and detailed assembly drawings are provided in Appendix J.

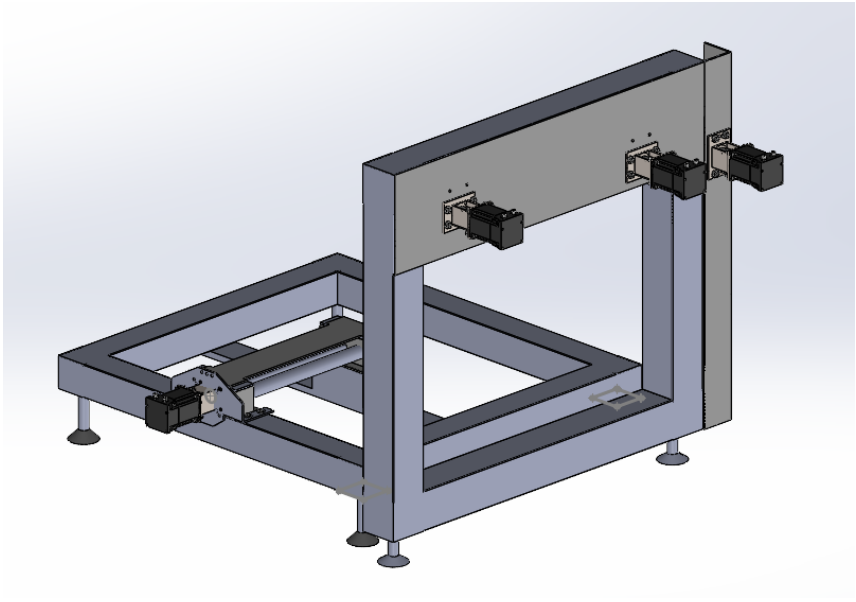


Figure 7.23: Cardboard Storage Unit CAD Assembly

7.5.3 Transportation System

7.5.3.1 Geometric and Structural Configuration

The housing is realised as a CNC-machined AISI 316 stainless steel body closed by a matching lid, selected for corrosion resistance given the risk of washdown fluid and broken glass ingress inside the Kisters frame. The cavity is divided into two functional zones, each inheriting a different wall thickness dictated by the loads it carries: the **Stage 1 wall** (motor side) is 3 mm, supporting the motor mounting interface and the Stage 1 idler bracket; the **Stage 2 wall** (linear-unit side) is 5 mm, supporting the structural mounting bolts to the linear unit's block face and the Stage 2 idler bracket.

The three shaft bores are positioned per the cross-sectional geometry established in Embodiment Design: the motor-interface bore at $Y_1 = 38.93$ mm above the housing floor, the jackshaft bores at $Y_{2,3} = 59.92$ mm, and the spindle-interface bore at $Y_4 = 31.5$ mm, with horizontal offsets $\Delta Z_{12} = 118.15$ mm and $\Delta Z_{23} = 85.40$ mm resulting from the fixed centre distances $C_1 = 120$ mm and $C_2 = 90$ mm.

The jackshaft's two support bearings are not split across the body/lid joint. Each is a complete bore: Bearing 1 is machined into the body's back wall, and Bearing 2 is machined into the lid. The jackshaft sub-assembly - shaft, both pulleys, both circlips, and Bearing 1 pre-installed - is built externally and lowered into the body as a single unit; closing the lid brings Bearing 2 into engagement and constrains the shaft's free end.

The motor-interface bore reuses the established NEMA 34 mounting pattern (69.5×69.5 mm bolt circle, ∅73 mm H7 pilot register) validated for the Roller Conveyor and Storage Unit. The spindle-interface bore reuses the ∅40 mm H8 bore / f7 spigot pairing from the same family.

Each belt stage carries its own tensioning idler, implemented as a linear sliding bracket rather than a pivoting arm: two elongated slots accept the retention screw, allowing the bracket to translate along the slot axis until the belt slack established in Embodiment Design ($\Delta x_1 = 5.26$ mm, $\Delta x_2 = 3.94$ mm) is taken up, after which the screw is torqued to lock the position. As established in Section 7.4.3.1, each bracket is retained by an existing screw shared with a neighbouring joint - the Stage 1 motor-mount M6 and the Stage 2 linear-unit-mount M8, respectively - rather than by dedicated hardware. Slot width is set to 6.4 mm (Stage 1) and 8.4 mm (Stage 2), matching the close-fit clearance diameter for each screw. Slot length is sized to accommodate this travel plus the screw's clearance-hole diameter and assembly margin:

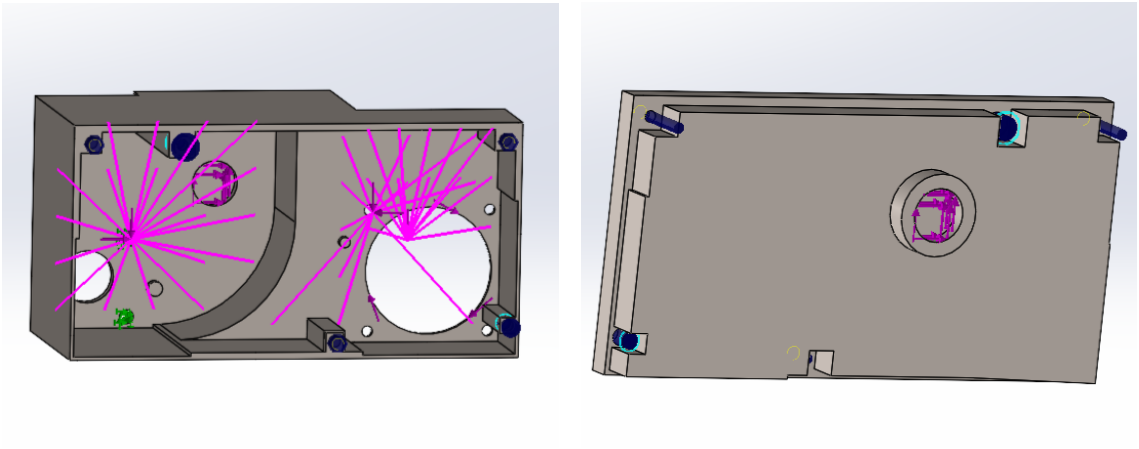
$$L_{\text{slot}} = d_{\text{clearance}} + \Delta x + 2 \times 1 \text{ mm} \tag{7.55}$$

giving $L_{\text{slot},1} \approx 14.3$ mm for the Stage 1 M6 screw ($d_{\text{clearance}} = 7$ mm, ISO 273 coarse series) and $L_{\text{slot},2} \approx 15.9$ mm for the Stage 2 M8 screw ($d_{\text{clearance}} = 10$ mm, ISO 273 coarse series), specified on the bracket drawing with a +0.3/0 mm tolerance to guarantee the full travel is never undersized. Brackets are specified in AISI 316 stainless steel to match the housing material and maintain corrosion compatibility within the sealed cavity.

7.5.3.2 Structural and Displacement Validation (FEA)

Unlike the single-body housings validated for the other subsystems, the Transportation System housing is a two-part assembly (body and lid) joined by bolted connectors and registration features. The FEA study was therefore constructed at the assembly level, explicitly modelling the body–lid interface rather than treating the pair as a single continuous solid.

Boundary conditions: The four through-holes on the linear-unit-side flange were fixed, per the convention established for the other housings. The body–lid interface was modelled with a No-Penetration contact condition at the parting line, allowing the joint to resist compression and transmit shear through friction and the dowel pins while remaining free to separate under tension, rather than treating the two parts as continuously bonded. The two dowel pins were represented as Pin connectors; the Motor Mount (M6), Linear Unit Mount (M8), and Body–Lid Perimeter (M5) fasteners as Bolt connectors preloaded to the Table 7.21 torques. Four load groups, each derived earlier in this chapter, were applied simultaneously to represent the governing fault condition: the motor's absolute stall torque and weight at the motor-side flange; the jackshaft bearing reactions R_A and R_B at the Bearing 1 (body) and Bearing 2 (lid) bores; and the idler slip force ($F_{\text{idler\_slip}} = 485.50$ N) at each stage, oriented toward the pre-tensioned end of travel (Figure 7.24). Gravity was applied per each station's mounting orientation. The housing and lid were modelled in AISI 316 stainless steel ($R_e = 137.9$ MPa, $R_m = 550$ MPa). The complete stress and displacement fields for both orientations are provided in Appendix H.



(a) Housing-Side View (b) Lid-Side View

Figure 7.24: Boundary Conditions of the Housing Assembly in the Transportation System

Stress results. The governing peak stress is located at the lid, at the counterbore floor beneath one of the Body–Lid Perimeter M5 screws, reaching $\sigma_{vm} = 101.5$ MPa - the tightest static margin in this chapter ($S_f = 137.9/101.5 \approx 1.36$). This peak arises under the actuator's absolute electrical stall torque combined with bearing reactions computed using the conservative $b = 2.0$ shaft-load factor (itself heavier than the ≈ 1.5 predicted by rigorous tension-ratio vector summation [83]), so the true physical stress is likely lower. Because motor stall is a fault condition distinct from the ≈250-cycle/year duty, this is a single-event static overload check rather than a fatigue-relevant load; the margin against ultimate strength - the more relevant criterion for a confined, ductile, single-event overload at a localised notch - remains substantial ($S_{f,\text{ult}} = 550/101.5 \approx 5.42$). The housing's peak, at the filleted transition adjacent to the M8 tapped boss, reaches 50.31 MPa ($S_f \approx 2.74$).

The two mounting orientations were evaluated separately. The governing peak locations and values are essentially invariant with orientation (lid $S_f \approx 1.36$, housing $S_f \approx 2.74$ in both), because the governing peaks are set by the jackshaft bearing reactions, idler slip force, and motor stall torque - none of which vary with orientation - while gravity, acting only on the motor and housing self-weight, perturbs only the field minima. The horizontal orientation is confirmed as the governing case for stress, though the two are effectively equivalent.

Displacement results. The vertical orientation produces the larger deflections and therefore governs the alignment budget. At the jackshaft bearing bores it reaches 1.363×10^{-2} mm (body) and 1.975×10^{-2} mm (lid), against 1.175×10^{-2} mm and 1.565×10^{-2} mm in the horizontal case; at the motor and spindle-interface bores it reaches 3.019×10^{-2} mm and 3.792×10^{-4} mm, also elevated relative to the horizontal orientation. These vertical-orientation values are carried forward as inputs to the alignment budgets in Section 7.5.3.3.

7.5.3.3 Metrological Specifications, Fit Selection, and Alignment

Center-distance alignment. Belt tracking accuracy is governed by the maximum permissible axial face misalignment between mating pulleys, limited to 0.5% of centre distance:

$$\Delta a_{\max} \leq 0.005 \cdot C \tag{7.56}$$

$$\Delta a_{\text{limit},1} = 0.005 \times 120.00 = 0.600 \text{ mm} \quad \text{(Stage 1)} \tag{7.57}$$

$$\Delta a_{\text{limit},2} = 0.005 \times 90.00 = \mathbf{0.450} \text{ mm} \quad \text{(Stage 2, governing)} \tag{7.58}$$

The housing's bore positioning and pulley mounting faces must collectively respect the 0.450 mm governing budget.

Bore position and parallelism. The spindle-interface bore is taken as Datum A, registering directly to the existing, unmodifiable linear unit. The motor-interface bore is positioned relative to Datum A within ± 0.05 mm, and all bore axes are held parallel to Datum A within 0.02 mm over the bore depth tighter than the tracking budget above, leaving margin for component-level tolerance stack-up.

Body–lid bearing coaxiality. Because Bearing 1 (body) and Bearing 2 (lid) support opposite ends of the same jackshaft, two ∅6 mm DIN 7 dowel pins register the lid to the body, holding the lid's Bearing 2 bore coaxial to Bearing 1 within ∅0.03 mm - a positive location rather than relying on perimeter bolt-hole clearance.

This analysis assumes ∅6 mm DIN 7 dowel pins, press-fit into the body at P7 tolerance (5.988 to 5.998 mm) and slip-fit into the lid at H7 tolerance (6.000 to 6.012 mm) [79]. This configuration represents a standard captured-pin arrangement, consistent with the assembly sequence, in which the lid is closed over pins already seated in the body. Since the body-side interface is rigidly fixed by the press fit, only the lid-side slip fit contributes to positional clearance, resulting in a worst-case radial value of 0.004 mm. This value is combined in a root-sum-square manner with a ∅0.015 mm position tolerance specified on each part's bearing bore relative to its own dowel-hole datum pair, compared against an allowed radial deviation of 0.015 mm (which is half of the ∅0.03 mm coaxiality target). This analysis confirms that the target is achievable with an approximate 24% margin, provided that the tighter-than-default position tolerance and the distinction between press and slip fits are explicitly specified on the respective manufacturing drawings.

$$\Delta_{\text{radial}} = \sqrt{0.0075^2 + 0.0075^2 + 0.004^2} \approx 0.0113 \text{ mm} \tag{7.59}$$

Pulley retention - radial (torque transmission). All four pulleys are positively keyed to their shafts via DIN 6885-1 parallel keys: Pulley 1 and Pulley 4 use the 14 mm and 12 mm shaft keyways; Pulleys 2 and 3 use a matched key on the custom jackshaft. Keyway surface pressure is verified against the DIN 6892 (Method C) allowable limit ($p_{\text{allowable}} = 80$ MPa) under full motor stall torque:

$$p = \frac{2T_{\text{stall}}}{d \cdot l \cdot t_2} \tag{7.60}$$

At the motor shaft (⌀14 mm, $T_{\text{stall}} = 5.940$ Nm, $l = 15$ mm, $t_2 = 2.3$ mm):

$$p_1 = \frac{2 \times 5.940}{0.014 \times 0.015 \times 0.0023} = 24.59 \text{ MPa} \rightarrow S_{kp1} = 3.25 \tag{7.61}$$

At the spindle shaft (⌀12 mm, stall torque propagated through the two-stage reduction, $T_{\text{stall}} = 11.087$ Nm, $l = 15$ mm, $t_2 = 1.8$ mm):

$$p_4 = \frac{2 \times 11.087}{0.012 \times 0.015 \times 0.0018} = 68.44 \text{ MPa} \rightarrow S_{kp4} = 1.17 \tag{7.62}$$

Both remain below the allowable surface pressure; the spindle-side keyway runs the tighter margin and is the priority interface to revisit if a dimension changes.

Pulley retention - axial. Pulley 1 and Pulley 4 are secured via dual ISO 4029 M5 cup-point set screws ($\geq 0.3 \cdot d_{\text{screw}} = 1.5$ mm edge clearance), with thread engagement set by the hub radial wall thickness:

$$L_{e,\text{spindle}} = \frac{30.5 - 12}{2} = 9.25 \text{ mm}, \qquad L_{e,\text{motor}} = \frac{38 - 14}{2} = 12.00 \text{ mm} \tag{7.63}$$

both exceeding $L_{\min} \geq 1.5 \cdot d_{\text{screw}} = 7.5$ mm. Pulleys 2 and 3, mounted on the custom jackshaft, are instead captured between a shaft shoulder and a DIN 471 retaining circlip - a positive geometric stop immune to the slip risk inherent to a set-screw interface.

Incorporating the FEA-derived bore displacements of Section 7.5.3.2, the governing case is the vertical orientation (Linear Unit 2), which produces larger displacements than the horizontal case at both the bearing bores and the belt-interface bores. The conservative difference between the body and lid bearing-bore displacements yields $\Delta = 1.975 \times 10^{-2} - 1.363 \times 10^{-2} = 6.12 \times 10^{-3}$ mm, a margin of approximately 80% against the 0.03 mm coaxiality budget. The same conservative bound at the motor- and spindle-interface bores, $\Delta = 3.019 \times 10^{-2} - 3.792 \times 10^{-4} \approx 2.981 \times 10^{-2}$ mm, sits at approximately 93% margin against the 0.450 mm belt-tracking budget. Both checks pass comfortably under the governing orientation, confirming the design is robust across the full range of mounting configurations adopted across the three linear units.

7.5.3.4 Environmental Sealing Design (IP64)

The motor and linear-unit flange interfaces reuse the twin-O-ring face-seal geometry validated for the Roller Conveyor (ISO 3601-1, 15–25% squeeze). The body/lid parting line - an irregular perimeter rather than a simple circular face - is sealed with a continuous O-ring channel following the joint outline, sized to the same squeeze target. Two sealed access ports (Wiska ESVS, M12 × 1.5, one per idler stage) close the only remaining penetrations, reused directly from the established family.

7.5.3.5 Design for Manufacture and Assembly (DFMA)

Because the jackshaft's far bearing (Bearing 2) is only constrained once the lid is fitted, the jackshaft sub-assembly - shaft, both pulleys, and Bearing 1 - is built externally and lowered into the body, and both belts are routed over their respective pulleys before the lid closes. Because the idler-retention screws are shared with the motor and linear-unit mounting joints rather than dedicated to the brackets (Section 7.4.3.1), belt slack must be removed and each bracket positioned against its locating pin before those joints are brought to final torque, which simultaneously fixes the motor/housing position and locks the idler bracket in place.

7.5.3.6 Fastener Selection and Fastening Torque Matrix

Linear unit mount (M8×20, existing tapped holes): one of the four screws at this interface additionally retains the Stage 2 idler bracket, per Section 7.4.3.1.

$$A_{si} = \pi \cdot 8 \cdot 20 \cdot \left[0.5 + \frac{1}{\sqrt{3}} \cdot \frac{8 - 7.188}{1.25}\right] = 440.0 \text{ mm}^2 \tag{7.64}$$

$$F_{\text{strip}} = 440.0 \times 330 \text{ MPa} = 145{,}200 \text{ N}, \qquad S_f = \frac{145{,}200}{14{,}500} = 10.0 \tag{7.65}$$

Motor mount: four ISO 4762 M6 through-bolts with ISO 4032 nuts on the back, reusing the Roller Conveyor scheme exactly - the through-bolt arrangement makes thread engagement in the thin Stage 1 wall irrelevant to this joint's strength. One of these four screws additionally retains the Stage 1 idler bracket, configured as a through-bolt locked by a nut on the motor flange's far face.

Idler bracket retention (both stages): as established above, neither idler bracket uses dedicated fasteners; each is clamped between its respective screw head/nut and the housing wall, using the Motor Mount (Stage 1) and Linear Unit Mount (Stage 2) screws described above. The resulting friction-clamping margin against the idler slip load ($F_{\text{idler\_slip}} = 485.50$ N) is verified in Section 7.4.3.1, yielding $S_{\text{friction\_clamp}} = 11.88$ (Stage 1) and 22.10 (Stage 2). Because retention is achieved through bearing pressure at the screw head/nut rather than thread engagement in the housing wall, no thread-stripping check or thread insert is required at either location.

Bearing pressure under the idler screw heads. Because each idler bracket is clamped between an existing screw head/nut and the housing wall through an elongated slot rather than a round clearance hole, the bearing footprint is reduced relative to a standard washer calculation: the slot's straight edges remove a full band through the washer's circular footprint, rather than only the small central bore a round hole would remove. For a washer of diameter D_w and a slot of width W_s, the bearing area is:

$$A_{\text{bearing}} = 2\left[\left(\frac{D_w}{2}\right)^2 \arccos\left(\frac{W_s/2}{D_w/2}\right) - \frac{W_s}{2}\sqrt{\left(\frac{D_w}{2}\right)^2 - \left(\frac{W_s}{2}\right)^2}\right] \tag{7.66}$$

Evaluated against the bare screw head ($D_k = 10$ mm M6 / 13 mm M8) and a standard ISO 7089 washer, the resulting pressures (168.1 MPa, 160.8 MPa) exceed the AISI 316 bracket's yield strength established elsewhere in this chapter (137.9–172.4 MPa), as the slot's geometric penalty largely offsets the washer's benefit. A standard ISO 7093 (large series) washer is therefore specified at both locations – consistent with the washer standard already adopted for the Storage Unit's M8 mount – restoring the bearing pressure to $p_{M6} = 55.1$ MPa and $p_{M8} = 56.9$ MPa, a margin of approximately 59–60% against yield at both stages.

Idler Pin Bending Verification. The idler mounting pin is subjected to cantilever bending due to the idler slip force ($F_{\text{idler\_slip}} = 485.50\,\text{N}$). The inner ring of the idler bearing is fixed at the boss, while the outer ring and pulley body rotate freely. For a conservative estimate, the resultant force is assumed to act at the axial midpoint of the bearing pair, located 11 mm from the root where the $\varnothing 8$ mm pin interfaces with the $\varnothing 10$ mm boss:

$$M = F_{\text{idler\_slip}} \times 11 = 485.50 \times 11 = 5{,}340.5\ \text{N·mm} \tag{7.67}$$

$$\sigma_b = \frac{M}{\pi d^3/32} = \frac{5{,}340.5}{50.27} = 106.2\ \text{MPa} \tag{7.68}$$

No deliberate fillet is specified at this root. Consequently, the governing factor is the sharp shoulder fillet category ($K_t = 2.7$, $r/d \approx 0.02$) [72], which represents the practical minimum radius produced by standard milling, rather than an idealised zero-radius corner:

$$\sigma_b' = K_t\,\sigma_b = 2.7 \times 106.2 = 286.7\ \text{MPa} \tag{7.69}$$

Because the pin remains stationary, the applied load does not reverse direction. This scenario constitutes a static yield check rather than a fatigue case, which aligns with the low actuation frequency established in Section 7.2. For an as-machined 316 (annealed) pin, the calculated local stress would exceed the yield strength ($S_f < 1$). Therefore, the pin is specified as **17-4 PH stainless steel, Condition H900** (per ASTM A564, minimum certified $R_{p0.2} \geq 1{,}000\,\text{MPa}$), resulting in:

$$\text{S}_f = \tfrac{1{,}000}{286.7} \approx 3.49 \tag{7.70}$$

This margin already accounts for the governing sharp-corner case; therefore, no additional fillet specification is structurally required at this feature.

Table 7.21: Transportation System Fastening Specification Matrix

Interface	**Fastener**	**Material**	**Qty**	**Torque**
Motor Mount (Stage 1)	ISO 4762 M6 + ISO 4032 nut + ISO 7093 Large Washer	A4-70 Stainless Steel	4	9.5 Nm
Linear Unit Mount (Stage 2)	Existing M8×20 tapped + ISO 7093 Large Washer	A4-70 Stainless Steel	4	22.0 Nm
Body–Lid Perimeter	ISO 4762 M5	A4-70 Stainless Steel	Per perimeter	5.5 Nm
Body–Lid Registration	DIN 7 dowel pin, ∅6 mm	Stainless Steel	2	-
Access Port Plug	Wiska ESVS, M12×1.5	Stainless Steel	2	5.0 Nm

7.5.3.7 Final Solution and Technical Documents

The final 3D CAD assembly for the Transportation System solution is shown in the appended figures. Complete engineering and manufacturing drawings, including bore coordinates and bracket slot geometry, are provided in Appendix J. The verification in this chapter is analytical and numerical throughout; the absence of physical prototype validation is discussed as a limitation of this work in Chapter 8.

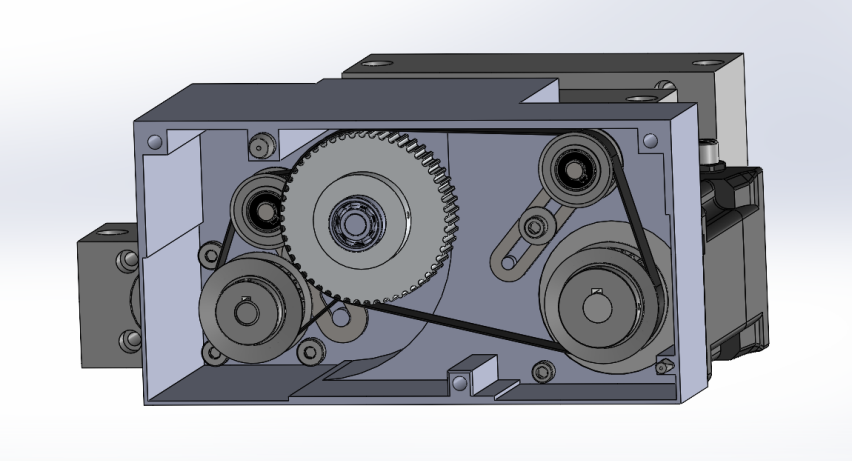


Figure 7.25: Transportation System Solution CAD Assembly

7.5.4 Global Safety Factor Synthesis

The preceding embodiment and detail design sections established a safety factor or displacement margin at every structurally significant interface across the three subsystems. This section compiles those results into a single comparative view, distinguishing checks performed under normal operational load from those performed under the actuator's absolute stall torque, which represents a fault condition rather than the duty-cycle load. Since the structural safety of an assembly is determined by its weakest verified link, not by the average strength of its components, the objective of this synthesis is to explicitly identify the governing minimum. While the tables below indicate that most components are comfortably oversized, this observation alone does not constitute the primary design conclusion.

Table 7.22: Safety Factor Synthesis Matrix - Complete System Overview

Component / Interface	**Failure Mode**	**SF / Margin**	**Load Case**
1. Roller Conveyor Subsystem			
Housing (M12 port bore)	Yield (von Mises)	13.25	Stall torque
Coupling radial alignment	Misalignment vs. rated capacity	1.25 (20%)	Build tolerance
Linear Unit Mount (M8×4)	Joint slip (friction-locked)	≈202	Stall torque
Stepper Motor Mount (M6×4)	Joint separation	≈691	Static (gravity)
Dynamic inertia ratio	Resonance / lost steps	12.8:1 margin (0.78:1 vs. 10:1)	Acceleration
2. Cardboard Storage Unit Subsystem			
M09-025 Housing	Yield (von Mises)	26.1	Stall torque
M09-010/012 Housing	Yield (von Mises)	18.0	Stall torque
M09-021 Housing	Yield (von Mises)	24.1	Stall torque
M09-010/012/021 Panel Mount (M8)	Thread stripping	3.00	Installation preload
M09-010/012 Coupling alignment	Misalignment vs. rated capacity	1.58 (37%)	Stall torque (FEA)

Continued on next page

M09-021 Coupling alignment	Misalignment vs. rated capacity	1.88 (47%)	Stall torque (FEA)
Motor selection margin (M09-025)	Holding torque vs. demand	1.19	Continuous duty
Dynamic inertia ratio	Resonance / lost steps	10.9:1 margin (0.84:1 vs. 10:1)	Acceleration
3. Transportation System Subsystem			
HTD 5M belt (Stage 2, Pulley 3)	**Tooth shear / tensile cord**	**1.021**	**Stall torque**
HTD 5M belt (Stage 2, Pulley 3)	Tooth shear / tensile cord	1.47	Continuous duty
Spindle keyway (Pulley 4)	**Surface (bearing) pressure**	**1.17**	**Stall torque**
Lid (perimeter M5 boss)	**Yield (von Mises)**	**1.36**	**Stall torque**
Motor radial bearing load	Bearing overload	1.11	Stall torque
Motor radial bearing load	Bearing overload	1.375 (37.5%)	Continuous duty
Lid (perimeter M5 boss)	Ultimate tensile (single-event)	5.42	Stall torque
Housing (M8 boss fillet)	Yield (von Mises)	2.74	Stall torque
Jackshaft, Pulley 3 journal	Static yield (von Mises)	2.80	Stall torque
Jackshaft, Pulley 3 journal	Fatigue (finite-life, $N = 10^5$)	1.77	Mean operating torque
Jackshaft, central shoulder	Static yield (von Mises)	5.62	Stall torque
Jackshaft, central shoulder	Fatigue (finite-life, $N = 10^5$)	3.51	Mean operating torque
Bearing A (jackshaft)	Static (DIN ISO 76)	2.47	Peak reaction
Bearing A (jackshaft)	Dynamic life (ISO 281)	several orders of magnitude vs. 10-yr life	Peak reaction

Continued on next page

Motor-side keyway (Pulley 1)	Surface (bearing) pressure	3.25	Stall torque
Linear Unit Mount (M8)	Thread stripping	10.0	Installation preload
Idler bracket retention, Stage 1	Friction-clamp slip	11.88	Idler slip force
Idler bracket retention, Stage 2	Friction-clamp slip	22.10	Idler slip force
Idler screw bearing pressure (both)	Local yield under washer	2.42–2.50 (59–60%)	Idler slip force
Jackshaft bearing-bore coaxiality	Belt tracking loss	4.90 (80%)	FEA, governing orientation
Motor/spindle bore belt-tracking	Belt tracking loss	15.1 (93%)	FEA, governing orientation
Angular deflection at bearings	Bearing misalignment	7.35 (86%)	Superposed loads

The minimum safety factor across the mechanical design is governed by the HTD 5M synchronous belt at the Stage 2 loop of the Transportation System, with $S_{\text{belt}} = 1.021$ against tooth shear under full motor stall torque. When evaluated at the system's continuous operating torque ($T_{\text{operational}} = 4.12$ Nm), this margin increases to $S_{\text{belt}} \approx 1.47$. This result confirms that the belt is not subjected to excessive stress during normal duty-cycle operation, and that the lower margin is specific to the fault condition. This value, along with the second- and third-tightest margins identified above (spindle-side keyway surface pressure $S = 1.17$ and housing lid's yield margin at the perimeter fastener boss $S = 1.36$), shares two notable characteristics. First, all three are located within the Transportation System, which is the most geometrically and torque-constrained of the three subsystems, rather than being distributed throughout the design. Second, all three are evaluated under the actuator's absolute electrical stall torque, representing a fault condition rather than the duty-cycle load experienced during normal operation. None of these margins governs the system's day-to-day reliability, which is instead determined by the substantially larger margins reported under continuous-duty and finite-life fatigue loading in the table above.

The global safety factor of this design is therefore reported as $SF_{\text{global}} = 1.021$, which occurs exclusively under full motor stall and is governed by belt-tooth shear.This is not a comfortable margin in absolute terms, and is flagged here as the single component most deserving of attention in any future revision of this design, most directly by re-evaluating a wider belt (25 mm in place of 15 mm) at this loop. The rationale for retaining the 15 mm belt at this design stage is set out in Section 7.4.3.1. This would not alter any upstream torque value already established in this chapter,

though it would require minor corresponding adjustments to the pulley flange width and housing internal clearance at this loop alone.

7.6 Automation and Control Logic

This section details the PLC-based control architecture developed for the seven adjustment points automated in this chapter and presents the corresponding verification results. In alignment with the project's feasibility study scope, no physical PLC, drives, or HMI panel were installed. Instead, the architecture was developed and verified exclusively within Siemens TIA Portal.

7.6.1 Hardware and Network Architecture

The system operates under the control of a Siemens CPU 1515T-2 PN (S7-1500T), chosen for its integrated motion-control kernel. This kernel presents individual axes to the user program as Motion Control Technology Objects, rather than as raw encoder or drive signals. Communication is established via PROFINET IO over the CPU's X1 interface. The X2 interface remains structurally unconnected to isolate motion-relevant cyclic traffic from potential future non-deterministic network usage.

Each of the 12 actuators described in the previous sections requires a dedicated drive. The mechanical design specifies the Nanotec N6-2-10-1 (PROFINET, PROFIdrive, 6A rated current), which is compatible with the closed-loop stepper motors' integrated SSI encoder feedback. In the TIA Portal verification model, this drive is represented by the Siemens SINAMICS S210 PROFIdrive object. Both drives provide an equivalent telegram-based interface to the CPU's Technology Objects, and the S210 is available natively in the TIA Portal catalogue, eliminating the need for a third-party device-description import. Operator interaction is facilitated by a SIMATIC HMI KTP700 Basic PN panel. Table 7.23 presents the resulting network configuration.

Table 7.23: PLC Network Devices and IP Addressing

Device	**Role**	**IP Address**
CPU 1515T-2 PN	IO Controller	192.168.0.1
SINAMICS S210 (M09-060, LU1/2/3)	IO Device $\times 3$	.10–.12
SINAMICS S210 (M09-061, LU1/2/3)	IO Device $\times 3$	.13–.15
SINAMICS S210 (M09-001, LU1/2)	IO Device $\times 2$	.16–.17
SINAMICS S210 (M09-010/012/021/025)	IO Device $\times 4$	.18–.21
KTP700 Basic PN	HMI	.30

7.6.2 Motion Control Technology Object Architecture

The seven adjustment points require twelve actuators; however, not all actuators operate independently. M09-060 and M09-061 each distribute motion across three linear units that support a single rigid guide rail, while M09-001 distributes motion across two linear units supporting the Roller Conveyor's guide stop. In these configurations, the supported rail will rack or bind unless its support points move synchronously. Therefore, these axes must follow a common position profile in real time, rather than simply reaching the same endpoint. In contrast, the four Cardboard Storage Unit points (M09-010, M09-012, M09-021, M09-025) are unconstrained and move independently.

This architecture is implemented by assigning a Virtual Axis Technology Object to each synchronised group. The Virtual Axis serves as a software-based position generator without a physical drive or encoder, and the group's real axes are geared to it at a 1:1 ratio via `MC_GearIn`. Employing a virtual master, rather than designating one real axis as the reference, prevents the propagation of a single motor's following error to adjacent axes. Table 7.24 enumerates the resulting fifteen Technology Objects.

Table 7.24: Motion Control Technology Object Architecture

Technology Object	Type	Geared To	Telegram
M09-060_Master	Virtual Axis	-	-
M09-060 LU1/2/3	Positioning Axis ×3	M09-060_Master	Standard Telegram 3
M09-061_Master	Virtual Axis	-	-
M09-061 LU1/2/3	Positioning Axis ×3	M09-061_Master	Standard Telegram 3
M09-001_Master	Virtual Axis	-	-
M09-001 LU1/2	Positioning Axis ×2	M09-001_Master	Standard Telegram 3
M09-010/012/021/025	Positioning Axis ×4	- (standalone)	Standard Telegram 3

Each real Positioning Axis is configured with PROFIdrive Standard Telegram 3, the position-controlled interface (setpoint, actual value, control word, status word), with position feedback supplied by the drive over PROFIdrive rather than read by the CPU directly from the motor's encoder.

7.6.3 Sequential State Machine

The control sequence is implemented as a `CASE`-driven state machine (Table 7.25), executed once per changeover and commanding every axis to its target position simultaneously.

Table 7.25: Sequence State Machine

State	Name	Function
0	IDLE	Waits for the start command; resets gearing execute memory to guarantee a rising edge on next entry to state 20.
10	POWER_UP	Enables the relevant virtual master and standalone axes via `MC_Power`.
20	GEAR_IN	Engages `MC_GearIn` on the group's real axes against their virtual master; advances once all report `InGear`.
30	MOVE	Commands `MC_MoveAbsolute` on the virtual master and standalone axes, using recipe-indexed target positions.
40	MONITOR	Drops `Execute` to allow the moves to run; advances to IDLE once all report `Done`, or aborts to IDLE on `Error`.

Only the M09-001 group, consisting of the virtual master and its two real axes, and the standalone M09-010 axis were configured and tested in TIA Portal. The remaining two groups and three standalone axes follow an identical, replicated pattern and were not constructed separately. The state machine described above does not yet incorporate a persistent, operator-acknowledged fault state or an electronic manual-jog mode, both of which are required by the fault-response and manual-fallback targets specified in Table 7.2. These features remain defined but unimplemented extensions of the current architecture.

The target positions used in state 30 are designed to be retrieved from a recipe data block (`Recipe_Memory`), which is an array of structures indexed by box format, with one field per axis. This data block is populated by the box-size optimisation model described in Section 5.4.

The SCL code was implemented in its specific Function Block, and can be observed in Appendix K.

7.6.4 Verification

The architecture underwent static verification. Figure 7.26 presents the completed PROFINET network, with all 12 drives and the HMI panel assigned as IO devices within the CPU's PROFINET IO system.

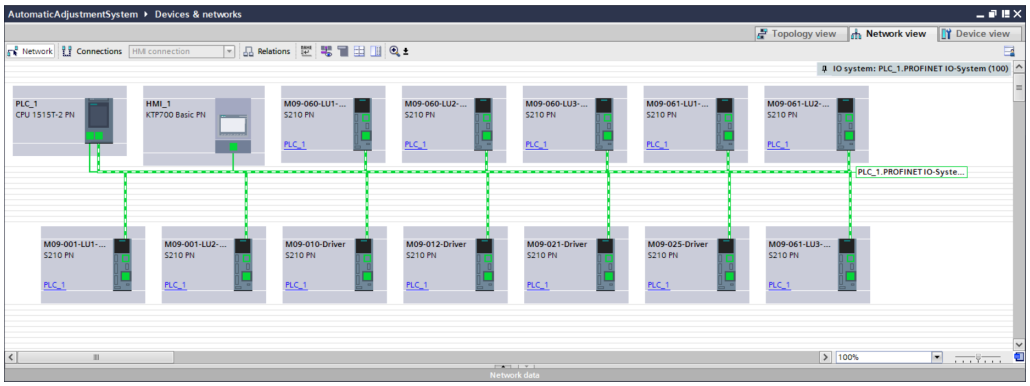


Figure 7.26: Completed PROFINET Network: CPU, HMI, and 12 Drives, All Assigned as IO Devices

Figure 7.27 illustrates the PROFIdrive Telegram 3 link configured on the M09-001 LU1 drive, with both data directions actively linked and mapped into the CPU's I/O memory.

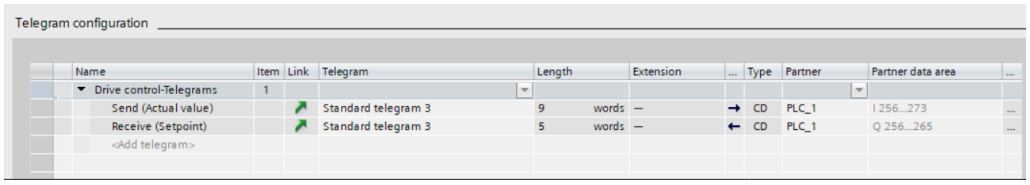


Figure 7.27: PROFIdrive Standard Telegram 3 Configuration, M09-001 LU1 Drive

Figure 7.28 depicts the corresponding Positioning Axis Technology Object configured for this drive interface.

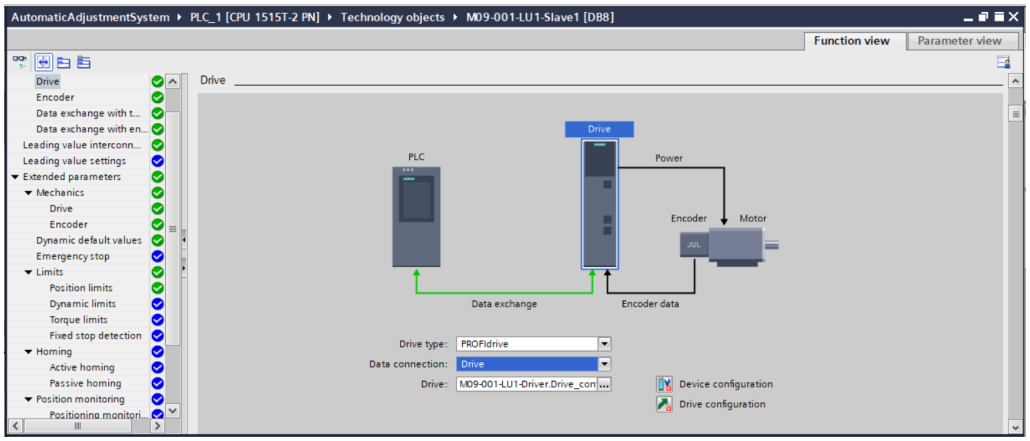


Figure 7.28: Positioning Axis Technology Object Hardware Interface Configuration, M09-001 LU1

Figure 7.29 demonstrates that the `FB_Motion_Sequence` compiles without errors or warnings.

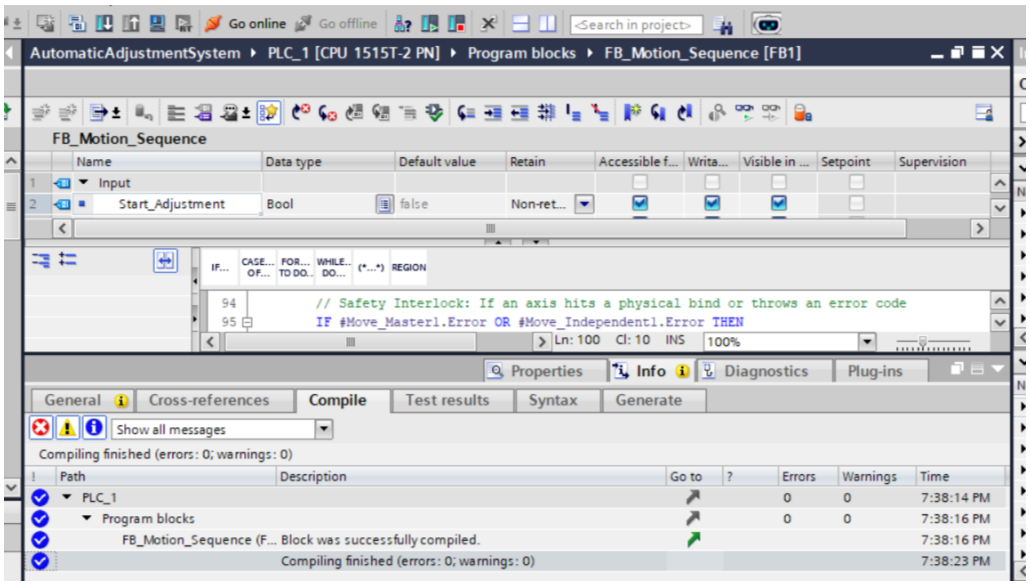


Figure 7.29: FB_Motion_Sequence, Compiled with Zero Errors and Zero Warnings

Dynamic verification using S7-PLCSIM was not conducted in this study. Due to the lack of a physical prototype for the mechanical subsystems, runtime commissioning was also not performed. Instead, the control logic was validated by manually tracing the state sequence during development. Consequently, the architecture has been confirmed at the levels of network configuration, Technology Object configuration, and static program compilation. However, dynamic closed-loop behaviour with a live or simulated CPU remains unverified.

7.7 Failure Mode and Effects Analysis (FMEA)

This Failure Mode and Effects Analysis (FMEA) focuses on the governing, lowest-margin items identified for each subsystem in the Global Safety Factor Synthesis (Section 7.5.4), rather than analysing every component listed in that table. Items with sufficient structural margins under all load cases are excluded from further analysis, as their risk has already been established. Severity (S), Occurrence (O), and Detection (D) are each rated on a 1 to 10 scale, and the Risk Priority Number (RPN $= S \times O \times D$) is used to rank items for recommended action. An RPN threshold of 80 is used to identify items that require a design or maintenance response; this threshold is selected for this analysis and is not based on a cited standard. No item in this system is rated at the highest level of severity (hazardous, without warning), as all considered failure modes result in mechanical malfunction or production stoppage rather than a credible hazard to personnel.

This mechanical FMEA addresses structural and mechanical failure modes of the primary, lowest-margin items. It does not yet include control and automation failures, such as sensor, drive, or PLC faults, as these require a physical prototype and will be covered in post-commissioning work described in Chapter 8.

Table 7.26: Failure Mode and Effects Analysis - Governing Items by Subsystem

Failure Mode	Effect	S	Cause	O	Detection	D	RPN
1. Roller Conveyor Subsystem							
Coupling radial misalignment exceeds rated capacity (SF=1.25)	Cyclic bending fatigue at motor bearing; eventual bearing seizure, lost positioning	6	Build-tolerance stack-up exceeding RSS estimate; assumption invalidated by long-term wear	2	No direct alignment monitoring; only inferred via stall/position-error once severe	7	84
Breakaway torque exceeds K_a margin from long-term stiction/rust accumulation	Lost steps / stall during adjustment move	5	Lubrication degradation or contamination exceeding the modelled baseline	3	Closed-loop encoder stall detection (immediate)	2	30
2. Cardboard Storage Unit Subsystem							
Motor torque margin insufficient at M09-025 under degraded friction (SF=1.19)	Lost steps / stall at the most demanding adjustment point	5	Narrowest motor margin in the subsystem; legacy transmission degradation	3	Closed-loop encoder stall detection (immediate)	2	30

Continued on next page

Table 7.26: Failure Mode and Effects Analysis (Continued)

Failure Mode	**Effect**	**S**	**Cause**	**O**	**Detection**	**D**	**RPN**
M09-010/012 coupling misalignment exceeds rated capacity (SF=1.58)	Premature spider wear; eventual backlash and positioning drift	5	Oversized through-holes, installer-aligned, no precision spigot - greater as-built variance than the spigot-located Roller Conveyor design	3	No direct sensing; manifests as gradual positioning drift, caught only at scheduled adjustment or annual maintenance	6	90
Galvanic corrosion at aluminium housing / steel panel interface (M09-010/012/021)	Gradual loosening of mounting interface; eventual loss of structural retention	6	Local anodised-coating damage at fastener contact points during installation	2	Not monitored by the control system; visual inspection only, via annual preventive maintenance	7	84
3. Transportation System Subsystem							
HTD 5M belt tooth shear, Stage 2 / Pulley 3 (SF=1.021 stall, 1.47 continuous)	Loss of Stage 2 drive; desynchronised linear units; guide rail racking	7	Full motor stall torque combined with the conservative $b = 2.0$ shaft-load factor	2	Closed-loop stall detection catches the triggering stall condition	3	42

Continued on next page

Table 7.26: Failure Mode and Effects Analysis (Continued)

Failure Mode	Effect	S	Cause	O	Detection	D	RPN
Motor radial bearing overload (SF=1.11, stall)	Accelerated bearing wear; eventual motor bearing failure	6	Full stall torque reached; radial load scales with the stall condition	2	No direct radial-load sensor; manifests as eventual stall or audible wear	6	72
Spindle keyway (Pulley 4) surface pressure exceeds allowable (SF=1.17)	Keyway peening; eventual loss of positive drive (pulley/shaft slip)	6	Full stall torque propagated through the two-stage reduction	2	No direct sensing; manifests as backlash increase over repeated stall events	7	84
Lid perimeter fastener boss local yield (SF=1.36, stall)	IP64 seal breach at the body-lid joint; accelerates other degradation modes	5	Full stall torque combined with bearing reaction loads	2	No direct sensing; caught by visible deformation or moisture ingress at maintenance	6	60

Four items exceed the RPN= 80 threshold: the Roller Conveyor coupling misalignment (84), the Cardboard Storage Unit's M09-010/012 coupling misalignment (90) and galvanic corrosion risk (84), and the Transportation System's spindle keyway surface pressure (84). Recommended actions:

- **Roller Conveyor coupling alignment:** add a periodic dial-indicator check during scheduled maintenance, since no continuous sensor monitors this parameter directly.
- **M09-010/012 coupling alignment:** specify a precision locating feature (dowel pin or spigot) at installation rather than relying on oversized through-holes and installer alignment alone, directly reducing as-built variance.
- **Galvanic corrosion risk:** add isolating washers or sleeves at the fastener-to-panel interface in addition to the anodised coating, since coating-only protection is vulnerable to local damage during installation.

- **Spindle keyway surface pressure:** already identified in Section 7.5.3 as the priority interface to revisit if a dimension changes; no new action beyond that existing recommendation.

A notable result of this analysis is that the highest RPN in the system (90) does not correspond to the lowest structural safety factor in the system (the Transportation System belt, SF=1.021, Section 7.5.4). The belt's risk is suppressed by two factors specific to it: it only approaches its governing margin under the motor's absolute stall condition, and a stall event is itself the trigger the closed-loop encoder is designed to detect. The M09-010/012 coupling, by contrast, degrades gradually under normal operating loads with no equivalent detection mechanism, relying entirely on scheduled maintenance to catch it before it becomes functionally significant. This indicates that detection capability, not structural margin alone, is the dominant risk driver for several of the system's components - a distinction the safety factor synthesis alone does not surface.

7.8 Economic Feasibility Assessment

The requirements outlined in Section 7.2 did not specify the financial return of the automatic adjustment system, instead considering cost as a minimisation objective rather than a fixed target. This section addresses that omission by providing a pro forma assessment. As the system was specified and analytically verified but not constructed, the investment is estimated based on quoted and catalogue prices, while the benefit is projected from the design rather than measured outcomes. Both figures are clearly identified as such.

Investment. The estimated bill of materials is presented in Table 7.27. The Siemens S7-1500T motion controller referenced in Section 7.6.1 is excluded, since an appropriate unit is already available at SBG. The twelve closed-loop stepper motors and the cabling are based on supplier quotations, while the remaining items are supplier estimates.

Projected benefit. The system addresses the manual fine-adjustment of the Cardboard Cutout Feeding Module, a task required at every changeover on the case-study line (Line 1). During the 33 observed changeovers, this adjustment imposed an average manual burden of approximately 11 minutes per changeover (Section 7.2). This figure, however, was measured before the slider optimisation of Section 5.4 was deployed; of those 11 minutes, 6.7 minutes correspond to the trial-and-error determination of the correct target value, a saving already credited to the slider optimisation in Section 6.7. To avoid double-counting, the benefit attributable to the present system is therefore evaluated on the residual base of approximately 4.3 minutes per changeover — the manual dexterity required to physically set an already-known value, identified as the residual task at the design ceiling — against a kinematically derived automated adjustment time of about 5 seconds. When applied to Line 1's approximately 250 annual changeovers, automation is projected to recover around 17.9 hours of line time per year, equivalent to roughly 1.1 million bottles of annual production capacity, valued at approximately €5,400 per year at the €300/hour operating

Table 7.27: Estimated Bill of Materials - Automatic Adjustment System

Item	Qty	Cost	Basis
Closed-loop stepper motors, integrated encoders	2 + 10	€5,302	quoted
PROFINET stepper drives (Nanotec N6-2-10-1)	12	€3,360	estimated
HMI panel (SIMATIC KTP700 Basic)	1	€500	estimated
Control cabinet, PSU, switch, wiring accessories	–	€2,000	estimated
Machined housings (2× AISI 316, 6× Al 6082-T6)	8	€2,200	estimated
Transmission (pulleys, HTD belts, jackshafts, bearings)	–	€600	estimated
Elastomer jaw couplings	12	€480	estimated
Cabling	–	€200	quoted
Brackets, O-rings, fasteners	–	€500	estimated
Installation labour	–	€3,500	estimated
Total		**≈€18,600**	

rate. Based on these figures, the estimated payback period is approximately 3.5 years, considering only the operating costs. For reference, if the system were deployed on a line without the prior slider optimisation, the full 11-minute burden would apply, yielding approximately 45 hours per year (€13,600) and a payback of approximately 1.4 years. These two interventions are sequential rather than additive: the slider optimisation eliminates the cognitive component of the task, while the present system eliminates its physical component.

Interpretation. When valued at operating cost and credited only with the residual benefit beyond the already-deployed procedural measures, the payback period is materially longer than that of the procedural interventions, which aligns with expectations for a mechanical retrofit and is consistent with literature cautioning that automating short manual tasks is justified only under specific conditions. Two additional factors further strengthen the case for the system, although they are not reflected in the figures above. First, the $300\,\mathrm{h}^{-1}$ basis values recovered time only at operating cost; during capacity-constrained high season, the same recovered capacity represents foregone saleable production of significantly greater value, which would substantially shorten the payback period. Second, the base case represents the lowest-throughput deployment: implementing the design on a higher-speed line, such as Line 5 at 80,000 bottles/hour, would recover proportionally more capacity per changeover and further reduce the payback period. Therefore, this assessment should be interpreted as a conservative estimate of the first-of-kind unit's potential rather than its maximum benefit.

7.9 Closing Synthesis

In accordance with the VDI 2221 phases outlined in Section 7.1, this chapter has advanced the automatic adjustment system from initial task clarification to a fully specified and analytically verified architecture. This encompasses the mechanical, control, and reliability aspects across all three subsystems of the Cardboard Cutout Feeding Module.

Section 7.2 established a baseline for manual fine-adjustment incidents, which recorded a median duration of approximately 6 minutes when occurring once per changeover. This duration increased to approximately 14 minutes when incidents occurred twice or more, a scenario observed in 24 of the 29 affected changeovers (Figures 7.3 and 7.4). In comparison, the automated system is designed for a kinematically-derived adjustment time of around 5 seconds (under direct-drive), against a design target of no more than 60 seconds. Measured against the manual baseline of 6 to 14 minutes per incident, this corresponds to a predicted reduction of roughly 70 to 170 times - more than an order of magnitude, approaching two. Because this figure is derived analytically rather than measured on a commissioned system, it is presented as a design projection; empirical confirmation is identified as future work. The projection directly addresses the primary changeover-time constraint identified in this case study.

Implementation and physical commissioning of the design were not completed within the timeframe of this thesis. Instead, verification was conducted through analytical and digital methods, including finite element analysis (FEA), hand calculations cross-validated with KISSsoft, and static and logical verification of the control architecture in TIA Portal. The FMEA in Section 7.7 identifies specific items requiring attention prior to any future build. The chapter's scientific contribution lies less in the individual mechanical calculations, which apply established engineering methods, than in demonstrating that a SMED-derived operational output - the target adjustment values optimised in Section 5.4 - can be carried, as direct design input, through a complete VDI 2221 retrofit under real spatial, torque, and environmental constraints. The implications of this project scope, and the steps necessary to transition from verified specification to a commissioned system, are discussed in the concluding chapter.

Chapter 8

Conclusions and Future Work

This dissertation aimed to reduce changeover time on SBG's beverage packaging lines, treating the associated ramp-up phase as a diagnostic indicator rather than a separately quantified target, beginning with the diagnostic premise outlined in Chapter 1: that these losses stem from two compounding root causes, one procedural and one physical, each requiring a distinct class of intervention. Chapter 4 empirically confirmed this premise by identifying the Kisters as the critical bottleneck on Lines 1, 5, and 6, and by highlighting both unstandardised task sequencing and persistent operator distrust of the machine's digital adjustment indicators. Chapters 5 and 6 subsequently implemented the SMED methodology (from task separation and externalisation to streamlining), value standardisation, and measured their effects in the field across multiple lines and shift teams.

The primary conclusion, as presented in Section 6.6, is that these procedural interventions approach a practical limit rather than eliminating the issue entirely. Even with optimised target values, guided execution, and access control, the fine adjustment of the Kisters remains dependent on manual dexterity and visual judgement. This constraint is physical rather than informational, and therefore cannot be addressed through procedure, training, or software alone. This limitation aligns with the design ceiling described by McIntosh et al. [21], in which further improvements via SMED require mechanical redesign rather than additional procedural refinement. Chapter 7 was developed in direct response to this finding. It focuses on the same Cardboard Cutout Feeding Module optimised in Section 5.4, applying the VDI 2221 systematic design methodology to structurally eliminate the manual task by specifying, dimensioning, and analytically validating an automatic adjustment system, although this system has not yet been physically implemented.

8.1 Fulfilment of Objectives

The first objective was to diagnose and classify the current-state changeover process. Chapter 4 quantified the Kisters' criticality share per line (35.2%, 15.6%, 47.8%, and 41.6% on Lines 1, 2, 5, and 6) using 24 months of SAP data, and identified the specific mechanism underlying the

adjustment-value distrust reported by operators: the unaccounted-for third degree of freedom at M09-060.

Objective 2 was to externalise and streamline internal tasks using SMED. Trolley guide-rail pre-adjustment and proactive format-part retrieval eliminated internal time in 43 of 44 audited events (97.7%, exact 95% CI [88.0%, 99.9%]), resulting in time savings of 0.5 to 5.5 minutes per changeover, depending on the line. The analysis also identified a 5S staging gap as a structural side-effect of externalisation, which should be considered alongside the observed gains.

Objective 3 focused on optimising and standardising adjustment values. The comparison between the unconstrained MILP (82.0 mm) and the deployed name-based LP (84.0 mm) indicates that the pre-existing box-format groupings incur only a 2.44% cost relative to the true global optimum. Three sensitivity checks (safety clearance, a synthetic future SKU, and bottle-diameter tolerance) confirm the robustness of the deployed configuration. The model's field-measured impact is positive. The bracket-comparable per-type reductions (13.8%-20.6%) cannot be tested individually due to small sample sizes, but the pooled analysis reaches conventional significance (Welch's $t(14.5) = 2.30$, $p = 0.037$; tie-corrected Mann–Whitney $U = 57.5$, $p = 0.042$; Hedges' $g = 1.04$). Given the small, heterogeneous sample, this result is characterised as strong supporting evidence of a genuine reduction rather than a definitive per-type confirmation.

Objective 4 was to develop a digital changeover support tool. The two-subject proof of concept demonstrated that operators without prior procedural experience could complete a changeover unaided, fulfilling the tool's core capability. The trials also exposed its boundary: the operators did not yet reach the ramp-up performance of an experienced team, and with n=2 the evidence supports a proof of concept rather than a validated plant-wide claim. Both the scale-up and the ramp-up gap are carried forward as future work.

Objective 5 was to identify the design ceiling and develop an automatic adjustment system in response to it. The ceiling is established empirically in Section 6.6 (converging evidence that procedural SMED had reached its practical limit), and Chapter 7 answers it by carrying the VDI 2221 process through Detail Design - dimensioning, component selection, FEA, hand-calculation cross-validated against KISSsoft, a finite-life fatigue treatment appropriate to the system's low duty cycle, a global safety-factor synthesis, and an FMEA. The design is validated analytically and computationally; physical prototyping and dynamic closed-loop commissioning are the identified next phase, consistent with an exploratory feasibility scope.

Performance across the five objectives was evaluated using the four KPIs defined in Section 6.1. Changeover time reduction, process variance reduction, and operational standardisation were each demonstrated using field data (Chapter 6). The statistical strength of these results varied by intervention: the folding-bracket redesign yielded conclusive evidence, while the pooled slider-optimisation result was suggestive. Structural and economic reliability were established through the analysis in Chapter 7 and the consolidated economic estimate. The deployed interventions recovered approximately €22,100 per year in operating value, with a payback period of less than three months. The proposed system required a pro forma investment of €18,600, with a projected payback period of approximately 3.5 years when credited only with the residual benefit beyond the

deployed slider optimisation (or approximately 1.4 years on a line without that prior intervention). The absence of a defined ROI target for the proposed system reflects the exploratory-feasibility scope, in which cost was treated as a minimisation objective rather than a fixed constraint.

8.2 Scientific and Industrial Contributions

The primary scientific contribution of this dissertation is the development of a structured methodology that facilitates the transition from operational optimisation to mechanical redesign for changeover reduction. While the existing literature typically addresses SMED-based operational improvement and formal machine design as distinct domains, this research defines and demonstrates the connection between them through a two-part approach.

The dissertation first demonstrates the transition from SMED-derived optimisation output, specifically the target adjustment values produced by the box-configuration optimisation in Section 5.4, to direct design input within a VDI 2221 mechanical retrofit (Chapter 7). These values populate the recipe memory that drives the automated adjustment system. This process establishes a concrete, data-driven link between operations-management tools and classical machine-design processes, rather than treating them as separate or competing domains. The necessity of this transition is established by the design-ceiling criterion described in the following section.

Second, the dissertation establishes an empirically grounded criterion that determines when this transition becomes necessary, referred to as the design ceiling. Instead of presuming the existence of such a ceiling, the threshold is demonstrated through multiple, independently measured limitations: field gains that correspond to the lower end of the SMED literature range, a residual adjustment task that remains physically dependent on manual dexterity, and a digital tool that addresses the procedural gap but not the ramp-up gap. Collectively, the criterion and its practical application constitute a framework that, demonstrated in this retrofit, offers a transferable approach for transitioning from operational optimisation to mechanical redesign in changeover reduction, addressing a combination that the existing literature typically treats as two distinct fields.

Additionally, as a supporting methodological contribution, the dissertation introduces a rigorously validated optimisation formulation for the adjustment-value problem. An unconstrained-versus-named-grouping comparison reveals a 2.44% optimality gap, and three independent sensitivity analyses confirm that the deployed configuration is both close to globally optimal and robust under realistic operating variations.

These scientific contributions are distinct from, though demonstrated through, the industrial improvements delivered to SBG. The value of the latter is operational, and the value of the former is a transferable method. A tool-less quick-release mechanism was developed for the folding bracket, replacing hex-key fastener removal with a slide-and-lock indexing system. This solution statistically reduced task time by 78.5% and variance by 99.3% (Welch's t test, exact Mann–Whitney test, Hedges' g = 12.41). In addition, a sacrificial-material design choice (PETG versus stainless steel) was implemented for the same bracket by applying the mechanical fuse

principle. This approach addresses cost and downtime risk rather than nominal task time, converting collision damage from a multi-week, externally outsourced repair into a same-shift, in-house replacement at a cost under €0.15 per unit. These interventions, including trolley pre-adjustment, the redesigned bracket, and the optimised slider configuration, were field-validated and deployed on SBG's production lines, resulting in measured reductions in changeover time. Finally, the research provides a complete mechanical and control design for an automatic adjustment system, including CAD models, component specifications for standard commercial off-the-shelf parts, control architecture, and a structured Failure Mode and Effects Analysis (FMEA) that SBG can use directly in the prototyping phase. The dimensioning, component selection, and structural analysis in this package apply established engineering methods; their contribution is industrial rather than scientific, since the dissertation's novelty lies not in these calculations but in the transition methodology they serve.

8.3 Limitations

The empirical results presented in this dissertation were obtained within an active production environment, and their interpretation is limited by the specific conditions of that setting. Three primary constraints should inform any generalisation. First, the sample sizes are small because changeover events for a given format-transition type occur only as often as the production schedule dictates, resulting in several comparisons based on a limited number of observations. In some cases, such as the E1/E2 clusters in Table 6.6, only a single recorded event per type is available. Data collection was not structured as a controlled experiment; it was restricted to changeovers required by production planning, without randomisation, repetition on demand, or control over confounding variables such as shift team, product sequence, or concurrent line conditions. Second, the field results are primarily observational rather than experimental. Interventions were measured as implemented during normal operations, so observed differences reflect actual operating conditions but do not fully isolate the intervention from operational variability. Third, operational variability (including differences between operators, teams, ambient conditions, and machine wear states) introduces additional dispersion that cannot be adequately characterised given the available sample sizes. These limitations are not incidental but inherent to research conducted on a live production line. They delineate the boundary between what this study demonstrates (that the interventions yield measurable improvement under real conditions) and what it cannot yet establish (statistically confirmatory effect sizes for each individual intervention).

Within these constraints, statistical strength varies by intervention: the folding-bracket result is strongly significant, while the pooled Line 1 slider-optimisation result reaches conventional significance ($p = 0.037$) but rests on a small, heterogeneous sample and so is treated as indicative rather than a definitive per-type confirmation. The approximately 30.6% combined-intervention ceiling reported in Table 6.6 represents an unvalidated upper-bound estimate. This estimate assumes additive, independent savings without accounting for potential task-interaction effects and

is not confirmed by direct post-implementation measurement. Validation of the digital tool is limited to the two-subject proof of concept discussed above, with no quantitative usability metrics collected.

The automatic adjustment system described in Chapter 7 is subject to limitations related to its developmental stage. In the absence of a physical prototype and industrial trial, validation is limited to calculations, CAD models, and static control-logic verification. As a result, dynamic closed-loop control behaviour has not been verified. This limitation reflects the current maturity of the design rather than an inherent flaw. The lack of physical prototyping also affects the FMEA in Section 7.7, which relies on engineering judgement ratings rather than empirical field data or failure-rate statistics. Additionally, the analysis omits the control and automation failure layer due to the absence of physical validation.

8.4 Future Work

Future research should focus on implementing and commissioning a physical prototype of the automatic adjustment system to facilitate dynamic verification of the control logic using PLCSIM or a live CPU. Implementing this prototype will support industrial trials to assess adjustment time, repeatability, and fault-recovery performance relative to the targets specified in Table 7.2. Once operational, the FMEA Severity, Occurrence, and Detection ratings should be recalibrated based on empirical field data. Additionally, safety and reliability analyses should be expanded to include the control and automation layer as dynamic verification data are collected.

To enhance the statistical and empirical rigour of the production interventions, the Line 1 slider-optimisation field trial should be expanded to collect a larger sample for each changeover type. While the pooled comparison already reaches significance ($p = 0.037$), the individual per-type reductions (13.8%–20.6%) remain untested owing to small samples; a larger dataset would allow each type to be confirmed on its own rather than only in aggregate. Direct measurements of the combined-intervention changeovers (E1, E2, F1, and F2) should also be performed on Lines 2 and 6 to validate or update the ceiling estimate provided in Table 6.6. Furthermore, validation of the digital tool should progress from the initial two-subject proof of concept to a comprehensive, plant-wide trial that collects quantitative usability metrics.

The economic assessment presented in Chapters 6 and 7 valued recovered time at operating cost. A fuller financial treatment incorporating capacity-driven high-season value, Net Present Value, and formal ROI would strengthen the investment case for the Chapter 7 system.

References

[1] Li Liu et al. “Fermented beverage and food storage in 13,000 y-old stone mortars at Raqefet Cave, Israel: Investigating Natufian ritual feasting”. In: *Journal of Archaeological Science: Reports* 21 (2018), pp. 783–793. ISSN: 2352-409X. DOI: 10.1016/j.jasrep.2018.08.008. URL: https://www.sciencedirect.com/science/article/pii/S2352409X18303468.

[2] Ian S. Hornsey. *A History of Beer and Brewing*. RSC Paperbacks. Cambridge: Royal Society of Chemistry, 2003. ISBN: 9780854046300. DOI: 10.1039/9781847550026.

[3] Wolfgang Kunze. *Technology Brewing and Malting*. Ed. by Olaf Manger. 6th. Berlin: VLB Berlin, 2019. ISBN: 9783921690871.

[4] DIN. *DIN 8782: Beverage containers; terms for bottling plants and individual machines (Begriffe für Abfüllanlagen und einzelne Aggregate)*. German, English. Standard. Berlin, Germany: Deutsches Institut für Normung e.V., May 1984.

[5] Frank L. Härte. *Efficiency Analysis of Packaging Lines*. WBBM Report Series 33. Delft, The Netherlands: Delft University of Technology, Department of Mathematics and Computer Science, 1997.

[6] Stephen Bates and Jaime Jurado. “The Importance of Beer Packaging, Packaging Line Systems, and Personnel Management”. In: *Beer Packaging*. Ed. by Ray Klimovitz and Karl Ockert. St. Paul, Minnesota: Master Brewers Association of the Americas, 2014. Chap. 1, pp. 1–18.

[7] Gavin D. Smith. *Beer: A Global History*. Edible. London: Reaktion Books, 2014. ISBN: 9781780232607.

[8] KHS Indústria de Máquinas. *Conceito de Linha: Soluções para todas as áreas*. Material de Treinamento Técnico, KHS Indústria de Máquinas. Departamento de Treinamento. Abrange dimensionamento de linha, gráfico V e norma DIN 8782. São Paulo, Brasil, Fevereiro 2013.

[9] T. Ohno. *Toyota Production System: Beyond Large-Scale Production*. Taylor & Francis, 1988. ISBN: 9780915299140.

[10] J.P. Womack and D.T. Jones. *Lean Thinking: Banish Waste And Create Wealth In Your Corporation*. Simon & Schuster UK, 2013. ISBN: 9781471111006.

[11] Wellington Santos, Olivia McDermott, and Anna Trubetskaya. “Lean Six Sigma 4.0 Application in the Food & Beverage Industry: A Case Study”. In: *IEEE Engineering Management Review* PP (Jan. 2025), pp. 1–31. DOI: 10.1109/EMR.2025.3538268.

[12] Manoj Dora et al. “Operational performance and critical success factors of lean manufacturing in European food processing SMEs”. In: *Trends in Food Science & Technology* 31 (2013), pp. 156–164. DOI: 10.1016/j.tifs.2013.03.002.

[13] J. Liker. *The Toyota Way: 14 Management Principles from the World's Greatest Manufacturer*. McGraw-Hill, 2003. ISBN: 9780071392310.

[14] Luana Bonome Message Costa et al. "Lean, six sigma and lean six sigma in the food industry: A systematic literature review". In: *Trends in Food Science & Technology* 82 (2018), pp. 122–133. ISSN: 0924-2244. DOI: 10.1016/j.tifs.2018.10.002. URL: https://www.sciencedirect.com/science/article/pii/S0924224418301730.

[15] T. Osada. *The 5S's: Five Keys to a Total Quality Environment*. Asian Productivity Organization, 1991. ISBN: 9789283311164.

[16] Rod Gapp, Ron Fisher, and Kaoru Kobayashi. "Implementing 5S within a Japanese context: an integrated management system". In: *Management Decision* 46.4 (2008), pp. 565–579.

[17] A.P. Dillon and S. Shingo. *A Revolution in Manufacturing: The SMED System*. Taylor & Francis, 1985. ISBN: 9780915299034.

[18] Jugraj Randhawa and Inderpreet Ahuja. "5S implementation methodologies: Literature review and directions". In: *International Journal of Productivity and Quality Management* 20 (Jan. 2017), p. 48. DOI: 10.1504/IJPQM.2017.080692.

[19] S. Nakajima. *Introduction to TPM: Total Productive Maintenance*. Preventative Maintenance Series. Productivity Press, 1988. ISBN: 9780915299232.

[20] Diana Stella Rossi-Huamán, Billy Manfred Tecse-Villacorta, and Richard Nicholas Meza-Ortiz. "Enhancing Operational Effectiveness in a Beverage Bottling SME through SMED, 5S, and TPM Maintenance Practices". In: *SSRG International Journal of Industrial Engineering* 12.3 (2025), pp. 20–32. DOI: 10.14445/23499362/IJIE-V12I3P103.

[21] R. I. McIntosh et al. "A critical evaluation of Shingo's 'SMED' (Single Minute Exchange of Die) methodology". In: *International Journal of Production Research* 38.11 (2000), pp. 2377–2395.

[22] Mohammed Ali Almomani et al. "A proposed approach for setup time reduction through integrating conventional SMED method with multiple criteria decision-making techniques". In: *Computers & Industrial Engineering* 66.2 (2013), pp. 461–469.

[23] Ali Allahverdi. "The third comprehensive review on scheduling problems with setup times/-costs". In: *European Journal of Operational Research* 246.2 (2015), pp. 345–378. DOI: 10.1016/j.ejor.2015.04.004.

[24] Jakob Puchinger and Günther R. Raidl. "Combining Metaheuristics and Exact Algorithms in Combinatorial Optimization: A Survey and Classification". In: *Artificial Intelligence and Knowledge Engineering Applications: A Bioinspired Approach*. Vol. 3562. Lecture Notes in Computer Science. Springer, 2005, pp. 460–469. DOI: 10.1007/11499305_5. URL: https://doi.org/10.1007/11499305_5.

[25] Rui Xu and Donald Wunsch. "Survey of clustering algorithms". In: *IEEE Transactions on Neural Networks* 16.3 (2005), pp. 645–678. DOI: 10.1109/TNN.2005.845141. URL: https://doi.org.

[26] Yves Pochet and Laurence A. Wolsey. *Production Planning by Mixed Integer Programming*. Springer Series in Operations Research and Financial Engineering. New York, NY: Springer Science & Business Media, 2006. ISBN: 978-0-387-29959-4.

[27] Deisemara Ferreira, Reinaldo Morabito, and Socorro Rangel. "Solution approaches for the soft drink integrated production lot sizing and scheduling problem". In: *European Journal of Operational Research* 196.2 (2009), pp. 697–706. DOI: 10.1016/j.ejor.2008.03.035.

[28] Cláudio F. M. Toledo et al. “A relax-and-fix with adaptive large neighborhood search heuristic for production routing problems”. In: *Computers & Operations Research* 52 (2014), pp. 140–152. DOI: 10.1016/j.cor.2014.07.007.

[29] Maija Breque, Lars De Nul, and Athanasios Petridis. *Industry 5.0 – Towards a sustainable, human-centric and resilient European industry*. Policy Brief KI-BD-20-021-EN-N. Brussels, Belgium: Directorate-General for Research and Innovation, European Commission, 2021. DOI: 10.2777/308407.

[30] Sven-Vegard Buer, Jan Ola Strandhagen, and Felix T. S. Chan. “The link between Industry 4.0 and lean manufacturing: mapping current research and establishing a research agenda”. In: *International Journal of Production Research* 56 (2018), pp. 2924–2940. DOI: 10.1080/00207543.2018.1442945.

[31] Guilherme Luz Tortorella and Diego Fettermann. “Implementation of Industry 4.0 and lean production in Brazilian manufacturing companies”. In: *International Journal of Production Research* 56 (2017), pp. 2975–2987. DOI: 10.1080/00207543.2017.1391420.

[32] Fabiana Cifone, Matthias Holweg, and Alberto Portioli-Staudacher. “‘Lean 4.0’: How can digital technologies support lean practices?” In: *International Journal of Production Economics* 241 (Aug. 2021), p. 108258. DOI: 10.1016/j.ijpe.2021.108258.

[33] David Romero et al. “Towards an Operator 4.0 Typology: A Human-Centric Perspective on the Fourth Industrial Revolution Technologies”. In: *Proceedings of the 46th International Conference on Computers & Industrial Engineering (CIE46)*. Tianjin, China: Computers & Industrial Engineering, 2016.

[34] Åsa Fast-Berglund et al. “Cognitive automation in assembly systems for the aging workforce”. In: *Procedia CIRP* 7 (2013), pp. 258–263. DOI: 10.1016/j.procir.2013.05.044.

[35] Michele Gattullo et al. “Towards augmented reality manuals for industry 4.0: A methodology”. In: *Robotics and Computer-Integrated Manufacturing* 56 (Nov. 2018), pp. 276–286. DOI: 10.1016/j.rcim.2018.10.001.

[36] Selim Erol et al. “Tangible Industry 4.0: A Scenario-Based Approach to Learning for the Future of Production”. In: *Procedia CIRP* 54 (2016), pp. 13–18. DOI: 10.1016/j.procir.2016.03.162.

[37] Lorenz Hoerner, Markus Schamberger, and Freimut Bodendorf. “Using Tacit Expert Knowledge to Support Shop-floor Operators Through a Knowledge-based Assistance System”. In: *Comput. Supported Coop. Work* 32.1 (Sept. 2022), pp. 55–91. DOI: 10.1007/s10606-022-09445-4.

[38] Enzo Fenoglio et al. “Tacit knowledge elicitation process for industry 4.0”. In: *Discover Artificial Intelligence* 2 (Mar. 2022). DOI: 10.1007/s44163-022-00020-w.

[39] A. R. Mileham et al. “Rapid changeover – a pre-requisite for responsive manufacture”. In: *International Journal of Operations & Production Management* 19.8 (1999), pp. 785–796. DOI: 10.1108/01443579910274383.

[40] Marcello Braglia et al. “Quick changeover design: a new Lean methodology to support the design of machines in terms of rapid changeover capability”. In: *Journal of Manufacturing Technology Management* 34.1 (2023), pp. 84–114. DOI: 10.1108/jmtm-12-2022-0430.

[41] Iris D. Tommelein. "'Poka Yoke' or Quality by Mistake Proofing Design and Construction Systems". In: *Proceedings of the 16th Annual Conference of the International Group for Lean Construction (IGLC-16)*. Manchester, UK, 2008, pp. 195–206.

[42] Paul F. Dvorak. "Poka-yoke designs make assemblies mistakeproof". In: *Machine Design* 70.5 (1998), pp. 181–184.

[43] Georg Götz et al. "A design approach for the development of flexible production machines". In: *Production Engineering* 12.3-4 (2018), pp. 331–340. DOI: 10.1007/s11740-018-0804-5.

[44] Alexander H. Slocum. *Precision Machine Design*. Englewood Cliffs, NJ: Prentice Hall, 1992. ISBN: 978-0136909187.

[45] Dominick Formaro. *Apparatus and method for adjusting a hot melt adhesive gun dispenser nozzle assembly*. US Patent 6,413,315. July 2002.

[46] halstrup-walcher. *Fast, fully automated adjustment to different packaging formats with smart positioning systems: Case study with Gerhard Schubert GmbH*. Available at halstrup-walcher portal. 2019.

[47] Siemens / Packaging Strategies. "Driving Flexibility: Electronic Cam Profiles and Servo Automation in Modern Packaging Machines". In: *Packaging Strategies* 21.4 (2019), pp. 14–18.

[48] Packaging World. "How servo-driven adjustments slice machine changeover times by 50 percent". In: *Packaging World Magazine* (2020). Industrial Feature Report.

[49] Gerhard Pahl et al. *Engineering Design: A Systematic Approach*. 3rd. London, UK: Springer Science & Business Media, 2007.

[50] Verein Deutscher Ingenieure. *VDI 2221 Part 1: Design of technical products and systems - Model of product design*. Standard. Düsseldorf: VDI, 2019.

[51] Kevin N. Otto and Kristin L. Wood. *Product Design: Techniques in Reverse Engineering and New Product Development*. Upper Saddle River, NJ: Prentice Hall, 2001. ISBN: 978-0130212719.

[52] Gwidon W. Stachowiak and Andrew W. Batchelor. *Engineering Tribology*. 4th. Oxford, UK: Butterworth-Heinemann, 2013. ISBN: 978-0123970473.

[53] Huub L. M. Lelieveld, John Holah, and David Napper. *Hygiene in Food Processing: Principles and Practice*. 2nd. Cambridge, UK: Woodhead Publishing, 2013. ISBN: 978-0857094292.

[54] Alan R. Hevner et al. "Design Science in Information Systems Research". In: *MIS Quarterly* 28.1 (2004), pp. 75–105.

[55] Ken Peffers et al. "A Design Science Research Methodology for Information Systems Research". In: *Journal of Management Information Systems* 24.3 (2007), pp. 45–77. DOI: 10.2753/mis0742-1222240302.

[56] Gerald I. Susman and Robert D. Evered. "An Assessment of the Scientific Merits of Action Research". In: *Administrative Science Quarterly* 23.4 (1978), pp. 582–603. DOI: 10.2307/2392581.

[57] Paul Coughlan and David Coghlan. "Action research for operations management". In: *International Journal of Operations & Production Management* 22.2 (2002), pp. 220–240. DOI: 10.1108/01443570210417515.

[58] KHS Group. *Fully automatic wrap-around shrink packer*. Accessed: 2026-05-24. 2026. URL: https://www.khs.com/en/products/machines-equipment/detail/innopack-kisters-wsp-advanced-wrap-around-shrink-packer.

[59] Smurfit Westrock. *Multipack Sleeve Applicators | Cups, Tubs, Bowls, Bricks*. https://www.smurfitwestrock.com. Accessed: June 1, 2026. 2026.

[60] European Committee for Standardization. *EN 10088-2:2014: Stainless steels - Part 2: Technical delivery conditions for sheet/plate and strip of corrosion resisting steels for general purposes*. Tech. rep. Brussels, Belgium: CEN, 2014.

[61] European Committee for Standardization. *EN 485-2:2016+A1:2018: Aluminium and aluminium alloys - Sheet, strip and plate - Part 2: Mechanical properties*. Tech. rep. Brussels, Belgium: CEN, 2018.

[62] International Organization for Standardization. *EN ISO 527-2:2012: Plastics - Determination of tensile properties - Part 2: Test conditions for moulding and extrusion plastics*. Tech. rep. Geneva, Switzerland: ISO, 2012.

[63] Marcin Wikło, Bartłomiej Henryk Byczuk, and Kinga Skrzek. "Mechanical Characterization of FDM 3D-Printed Components Using Advanced Measurement and Modeling Techniques". In: *Materials* 18.4 (2025), p. 892. DOI: 10.3390/ma18040892.

[64] Dragos Valentin Iacob, Dragos Gabriel Zisopol, and Mihail Minescu. "Study on the Optimization of FDM Parameters for the Manufacture of Three-Point Bending Specimens from PETG and Recycled PETG in the Context of the Transition to the Circular Economy". In: *Polymers* 17.12 (2025), p. 1645. DOI: 10.3390/polym17121645.

[65] Ahmed H. Awad, Rehab Alaa Eldin Sayed, and Mohamed Atef. "Enhancing Mechanical Properties of PETG by Optimization of Process Parameters Using the Taguchi Method". In: *Journal of Physics: Conference Series* 3058.1 (2025), p. 012008. DOI: 10.1088/1742-6596/3058/1/012008.

[66] U. M. Dilberoglu et al. "Shrinkage compensation of holes via shrinkage of interior structure in FDM process". In: *The International Journal of Advanced Manufacturing Technology* 94.5–8 (2018), pp. 2115–2126.

[67] Rotan Kumar Saha et al. "Reduction of Changeover Time by Using the SMED Technique with the Assistance of Lean Manufacturing Tools in a Plastic Company". In: *Proceedings of the International Conference on Industrial Engineering and Operations Management (IEOM)*. Dhaka, Bangladesh, 2023.

[68] Ramazan Şahin and Aycan Koloğlu. "A Case Study on Reducing Setup Time Using SMED on a Turning Line". In: *Gazi University Journal of Science* 35.1 (2022), pp. 60–71. DOI: 10.35378/gujs.735969.

[69] Richard McIntosh et al. "Changeover Improvement: Reinterpreting Shingo's "SMED" Methodology". In: *IEEE Transactions on Engineering Management* 54.1 (2007), pp. 98–111. DOI: 10.1109/TEM.2006.889070.

[70] R. W. Saaty. "The analytic hierarchy process—what it is and how it is used". In: *Mathematical Modelling* 9.3 (1987), pp. 161–176. ISSN: 0270-0255. DOI: 10.1016/0270-0255(87)90473-8. URL: https://www.sciencedirect.com/science/article/pii/0270025587904738.

[71] T. L. Saaty. *The Analytic Hierarchy Process: Planning, Priority Setting, Resource Allocation*. McGraw-Hill International Book Company, 1980. ISBN: 9780070543713.

[72] Richard G. Budynas and J. Keith Nisbett. *Shigley's Mechanical Engineering Design*. 11th. McGraw-Hill Education, 2020. Chap. 8.

[73] THK Co., Ltd. *LM Guide Selection Guide*. Section: Static Safety Factor $(f_s), Table 10 : Guideline for the Static Safety Factor$. THK Co., Ltd. Tokyo, Japan, 2021. URL: https://www.thk.com.

[74] HIWIN Technologies Corp. *Linear Guideway Technical Information*. Section 1-3-1: Basic Static Load Rating, Table 1.1: Static Safety Factor. HIWIN Technologies Corp. Taichung, Taiwan, 2020. URL: https://www.hiwin.com.

[75] Anaheim Automation. *Selecting a Stepper Motor System*. https://anaheimautomation.com/blog/post/selecting-a-stepper-motor-system. Application engineering note. Accessed: 24 June 2026. 2024.

[76] Oriental Motor. *Motor Sizing Basics: Load Torque & Inertia*. Technical Application Note. Oriental Motor U.S.A. Corp., 2022.

[77] Kollmorgen. *Understanding Inertia Matching and Its Effects on Servo Performance*. Technical Publication. Kollmorgen, 2018.

[78] Verein Deutscher Ingenieure. *VDI 2230 Sheet 1: Systematic calculation of highly stressed bolted joints*. 2015.

[79] Industrial Press. *Machinery's Handbook*. 31st. Section: Thread Shear Area and Stripping Calculations. New York, NY: Industrial Press, 2020.

[80] Robert C. Juvinall and Kurt M. Marshek. *Fundamentals of Machine Component Design*. 7th. Hoboken, NJ: John Wiley & Sons, 2020. ISBN: 978-1119598148.

[81] norelem. *Indicações técnicas para correias dentadas 22062*. pt. Technical Data Sheet and Power Transmission Catalogue. norelem. URL: https://www.norelem.com.

[82] Johann Tang. *Motor Sizing Basics Part 4 - How to Calculate Radial Load and Axial Load*. https://blog.orientalmotor.com/motor-sizing-basics-part-4-radial-load-and-axial-load. Engineering Notes. Accessed: 24 June 2026. Oriental Motor U.S.A. Corp., 2024.

[83] SDP/SI (Stock Drive Products/Sterling Instrument). *Timing Belt Theory — Section 14: Belt Pull, Static Belt Pull, Shaft Load, and Bearing Load*. Technical Section T-58, Designatronics Inc. URL: https://www.sdp-si.com/D265/PDF/D265T058.pdf.

[84] Richard G. Budynas and J. Keith Nisbett. *Shigley's mechanical engineering design*. 10th. McGraw-Hill Education, 2015.

Appendix A

Changeovers Observations

Table A.1: Changeover Observations Log (February – May 2026)

Date	Time	Line	Shift Team	Type of Changeover	Duration
24/02/2026	09:09	L1	B	A	30 min
24/02/2026	16:28	L6	C	E1	75 min
25/02/2026	10:05	L2	D	D	38 min
26/02/2026	12:21	L6	A	F1	63 min
02/03/2026	17:03	L5	D	E2	84 min
04/03/2026	16:44	L1	D	C	38 min
09/03/2026	12:43	L5	A	E1	63 min
11/03/2026	13:05	L1	B	D	39 min
12/03/2026	15:03	L5	D	B	33 min
16/03/2026	10:16	L5	C	H	59 min
18/03/2026	11:27	L6	D	B	28 min
20/03/2026	16:51	L2	A	B	28 min
23/03/2026	11:06	L6	C	C	50 min
25/03/2026	10:00	L5	B	A	23 min
27/03/2026	14:54	L6	D	E2	77 min
31/03/2026	15:41	L1	B	A	33 min
01/04/2026	08:51	L6	A	E1	80 min
03/04/2026	11:50	L1	D	B	36 min
06/04/2026	15:42	L6	A	I	70 min

Continued on next page

Table A.1 – Continued from previous page

Date	Time	Line	Shift Team	Type of Changeover	Duration
08/04/2026	19:37	L6	C	E2	68 min
09/04/2026	10:18	L5	A	D	40 min
13/04/2026	13:21	L1	D	C	49 min
15/04/2026	13:57	L2	B	E1	64 min
17/04/2026	18:40	L1	D	B	28 min
21/04/2026	04:51	L6	A	E2	54 min
21/04/2026	11:33	L2	B	B	36 min
21/04/2026	14:15	L5	D	E1	68 min
24/04/2026	09:23	L2	B	E2	71 min
24/04/2026	11:43	L6	A	F2	80 min
24/04/2026	13:32	L1	A	D	39 min
28/04/2026	15:55	L5	A	E1	78 min
30/04/2026	16:13	L5	C	E2	85 min
01/05/2026	15:34	L1	C	D	48 min

Table A.2: Clusters of Kisters' Tasks by Module

Module	Task	Expected Duration (min)	Lines Included
External (Before)	Trazer as paletes com os novos recortes de cartão e reabastecer a estação de cola quente	5	L1/L2/L5/L6
General	Esvaziar a máquina	2-5	L1/L2/L5/L6
	Alteração do programa	1	L1/L2/L5/L6
M01	Regulação da altura e número de alavancas do sensor de produto incorreto	**2**	L1/L2/L5/L6
	Substituição do conjunto de guias de divisão em filas	3	L1/L2/L5/L6
	Substituição do carrinho de guias de entrada (estrutura de substituição)	15	L2/L5/L6

Continued on next page

Table A.2 – Continued from previous page

Module	**Task**	**Expected Duration (min)**	**Lines Included**
	Substituição do atuador pneumático de vibração para não encravamento de garrafas	4	L1/L2/L5/L6
	Regulação transversal das calhas de guia no módulo de entrada	3-6	L1/L2/L5/L6
M02	Troca do jogo de ferramentas do Sistema de Separação	10	L1/L2/L5/L6
	Ajuste das guias laterais	1	L1/L2/L5/L6
	Ajuste da distância entre correntes de transporte	1	L1/L2/L5/L6
M09	Ajustes no armazém de cartão	5	L1/L2/L5/L6
	Montar as guias laterais do recorte no interior/exterior	8	L1/L2/L5/L6
	Ajustes do transporte de recortes	3	L1/L2/L5/L6
M03	Substituição das guias de formatação	3	L2/L5/L6
	Substituição das pás	12-14	L2/L5/L6
	Substituição dos esquadros de encosto	17-20	L2/L5/L6
	Ajustes nas pistolas de aplicação de cola quente	1-3	L1/L2/L5/L6
	Ajustes de largura, altura e comprimento do produto final	6-8	L1/L2/L5/L6
M05	Regulação da largura da mesa giratória	2	L2/L5/L6
M04	Regulação da detecção da marca impressa	1	L2/L5/L6
	Ajuste da altura da curva de impacto	2	L2/L5/L6
M07	Regulação transversal dos bocais de injeção de ar na entrada / saída	1	L2/L5/L6

Continued on next page

Table A.2 – Continued from previous page

Module	**Task**	**Expected Duration (min)**	**Lines Included**
	Regulação da altura do deflector de ar na entrada / saída	1	L2/L5/L6
External (After)	Descartar os recortes e produtos antigos que sobraram	3-5	L1/L2/L5/L6

Table A.3: Clusters of Mead's Tasks by Module

Module	**Task**	**Expected Duration (min)**
External (Before)	Trazer as paletes com os novos consumiveis de packs e colocá-los na plataforma de alimentação de packs	3
General	Mudar programa na máquina	1
	Iniciar sincronização	10
Product Infeed and Selection Module	Ajustar altura do detector de garrafas (A1)	1
	Colocar/Trocar guias (K2)	2–3
	Mudar/Trocar guia inferior de corrente (H)	4-6
	Colocar/Retirar Guia de gargalo à vista (K5)	5-10
	Troca de Estrelas (D1)	6-10
	Trocar tacos superiores (K)	10
	Troca de grippers (E1)	15
Carton Magazine and Feeding Module	Mudar Hopper	2-4
	Ajustar valores da altura da tremonha (B2)	2-3
	Ajustar valores da largura da tremonha (B3)	2-3
	Troca de ventosas (C)	5-6
Tucker and Overhead	Retirar/Colocar guia de dobragem de cartão (F2)	2-3

Continued on next page

Table A.3 – Continued from previous page

Module	**Task**	**Expected Duration (min)**
Boom Chains Module	Troca de correntes do alimentador de papel (F1)	4-5
	Colocar/Trocar guia de dobragem (G)	5-6
	Manuseamento de Tucker (G/G1)	13-15
Bottom Folding and Locking Section (EFTAP)	Retirar Bottle Locker (I)	5
	Manuseamento de "RPM" (I)	5
	Colocar/Ajustar/Trocar Bottle Locker (I)	14-15
	Trocar guia de "SABRE" (J)	10
Divider-Rotator Module	Ajuste lateral das guias na zona do divisor (N2)	3
	Troca de pás do divisor (N1)	5
	Trocar "Carro de cozido" (M)	8-10
	Troca de estrela de "Carro de cozido" (M)	8-10
External (After)	Descartar os consumiveis de cartão que sobraram	3

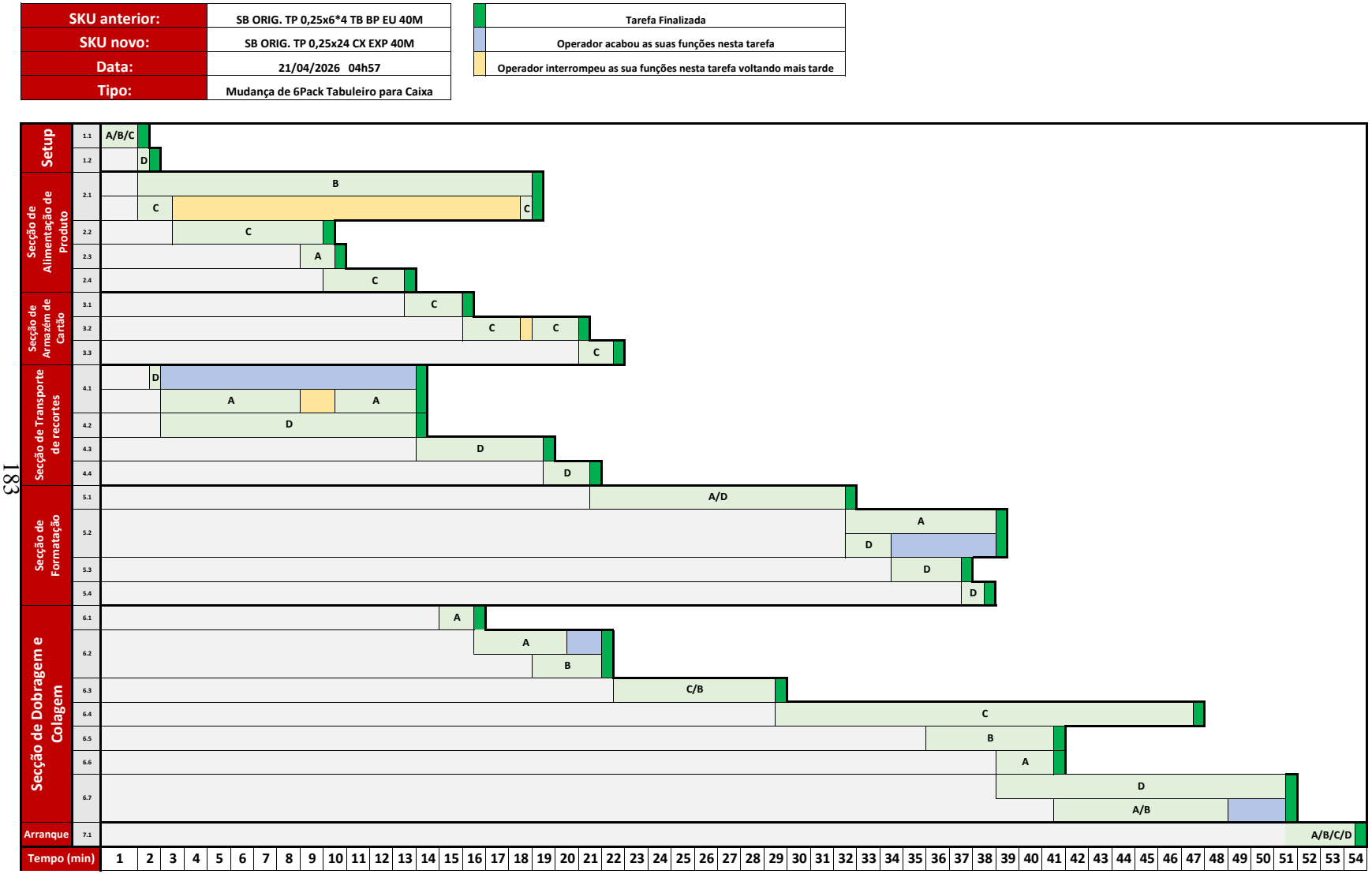


Figure A.1: Illustrative Gantt Chart of observed Changeover

Appendix B

Adjustment Values Spreadsheet

Número do Programa:						
SKU:						
Data:						
Assinatura:						

ID	Indexadores					
M01-020						
M01-010						
M01-011						
M01-090						
M01-050A						
M01-059A						
M01-051A						
M01-057A						
M01-058A						
M01-060A/061A						
M01-050B						
M01-059B						
M01-051B						
M01-057B						
M01-058B						
M01-060B-062B						
M09-060						
M09-061						
M09-025						
M09-012						
M09-010						
M09-021						
M09-001						
M02-0-81A/082A						
M02-090						
M02-101A/102A						
M02-108A						
M02-160						
M02-100A						
M02-030						
M02-040						
M02-076						
M02-070						
M02-020						
M02-081B/0282B						
M02-101B/102B						
M02-108B						
M02-100B						
M03-240						
M03-140						
M03-213						
M03-230						
M03215A						
M03-212A						
M03-211A						
M03-030						
M03-211B						
M03-212B						
M03-215B						

Appendix C

Standard Operating Procedures

Procedimento Operacional Standard			**Centro de Produção:** SUPER BOCK GROUP
Departamento: Enchimento	**Área:** Geral	**Categoria:** Máq./Oper.v	**Equipamento:** Kisters
Ajuste Valor nominal dos Indexadores L1			**Pág.** 1 **de** : 1 — **Data emissão:**

Início de Sessão:

1. Carregar no botão com o cadeado no canto inferior direito do ecrã.
2. Inicio de sessão do Operador
3. Escolher Operador
4. Pin: 1111
5. Sessão iniciada.



Alterar valor indexador

6. A partir da vista principal, selecionar o menu "Tipo"
7. Selecionar "Alteração guiada de formato"
8. Secionar "Configurações mecânicas"
9. Escolher o módulo a alterar (ex: alimentação de Produto).
10. Carregar no indexador.
11. Igualar o "Valor nominal" ao "Valor real".
12. Carregar "OK".
13. Para guardar carregar no botão com a disquete no canto superior direito.
14. Confirmar que pretende guardar os formato.





Documentos relacionados:													
Nº documento	**Formação sobre o POS**	Data:											
POS....		por:											
		para:											

Appendix D

Mathematical Optimisation Models

D.1 Model 1: Mixed-Integer Linear Programming (MILP)

Listing D.1: Volumetric MILP baseline model script.

```
import pyomo.environ as pyo

# ========================================
# MODEL 1: MILP BASELINE (Volumetric Digital Twin)
# ========================================
boxes_data = {
    "20x15": [163, 184, 161.5, 182.5, 35], "20x12": [164, 184, 162.5, 182.5,
        50],
    "25x12": [174, 195, 173.0, 194.0, 35], "33x15": [180, 228, 178.5, 226.5,
        35],
    "33x12": [180, 229, 178.5, 227.5, 35], "20x24": [216, 184, 214.5, 183.5,
        35],
    "25x20": [229, 192, 228.0, 191.0, 35], "25x24": [230, 193, 228.5, 191.5,
        35],
    "33x24": [239, 229, 237.5, 227.5, 35], "20x35": [269, 184, 268.0, 183.0,
        35],
    "25x30": [286, 192, 284.0, 191.0, 35]
}

boxes = list(boxes_data.keys())
configs = ["A", "B", "C"]
M = 2000

CLEARANCE = 25
INDEXER1_WIDTH = 90
SLIDER_WIDTH = 45

# 1. Asymmetric Datum Shift
box_offsets = {b: 27.5 if b in ["20x24", "25x20", "25x24", "33x24"] else 0 for
    b in boxes}

# 2. Crease Coordinates and Target Reaches
C1 = {b: (boxes_data[b][0]/2) - box_offsets[b] for b in boxes}
C2 = {b: (boxes_data[b][0]/2) + boxes_data[b][1] - box_offsets[b] for b in
    boxes}
target_reach = {b: C2[b] + boxes_data[b][2] for b in boxes}
indexer2_pos = {b: (boxes_data[b][0]/2) + boxes_data[b][3] + boxes_data[b][4] +
    box_offsets[b] for b in boxes}
```

```
31
32 model1 = pyo.ConcreteModel()
33 model1.B = pyo.Set(initialize=boxes)
34 model1.C = pyo.Set(initialize=configs)
35
36 # 3. Constrained Physical Variables
37 model1.Indexer1 = pyo.Var(model1.B, bounds=(150, 530),
       domain=pyo.NonNegativeReals)
38 model1.Slider = pyo.Var(model1.C, bounds=(0, 210), domain=pyo.NonNegativeReals)
39 model1.y = pyo.Var(model1.B, model1.C, domain=pyo.Binary)
40 model1.Zone_Var = pyo.Var(model1.B, domain=pyo.Binary)
41
42 model1.Indexer1_max = pyo.Var(bounds=(150, 530))
43 model1.Indexer1_min = pyo.Var(bounds=(150, 530))
44
45 def obj1_rule(model): return model.Indexer1_max - model.Indexer1_min
46 model1.Obj = pyo.Objective(rule=obj1_rule, sense=pyo.minimize)
47
48 # Trackers & Assignment
49 model1.Assign = pyo.Constraint(model1.B, rule=lambda m, b: sum(m.y[b, c] for c
       in m.C) == 1)
50 model1.MaxTrk = pyo.Constraint(model1.B, rule=lambda m, b: m.Indexer1_max >=
       m.Indexer1[b])
51 model1.MinTrk = pyo.Constraint(model1.B, rule=lambda m, b: m.Indexer1_min <=
       m.Indexer1[b])
52
53 # 4. Volumetric Kinematic Linkage
54 def link_upper(m, b, c): return m.Indexer1[b] + m.Slider[c] + INDEXER1_WIDTH +
       SLIDER_WIDTH - target_reach[b] <= M * (1 - m.y[b, c])
55 model1.LinkU = pyo.Constraint(model1.B, model1.C, rule=link_upper)
56
57 def link_lower(m, b, c): return m.Indexer1[b] + m.Slider[c] + INDEXER1_WIDTH +
       SLIDER_WIDTH - target_reach[b] >= -M * (1 - m.y[b, c])
58 model1.LinkL = pyo.Constraint(model1.B, model1.C, rule=link_lower)
59
60 # 5. Slider Obstruction Constraint (I1 + S <= 610)
61 def obstruction(m, b, c): return m.Indexer1[b] + m.Slider[c] <= 610 + M * (1 -
       m.y[b, c])
62 model1.Obstruction = pyo.Constraint(model1.B, model1.C, rule=obstruction)
63
64 # 6. Safety Clearance Constraints
65 def safe_c1(m, b): return m.Indexer1[b] >= C1[b] + CLEARANCE
66 model1.SafeC1 = pyo.Constraint(model1.B, rule=safe_c1)
67
68 def safe_c2_left(m, b): return m.Indexer1[b] + INDEXER1_WIDTH <= C2[b] -
       CLEARANCE + M * m.Zone_Var[b]
69 model1.SafeC2_L = pyo.Constraint(model1.B, rule=safe_c2_left)
70
71 def safe_c2_right(m, b): return m.Indexer1[b] >= C2[b] + CLEARANCE - M * (1 -
       m.Zone_Var[b])
72 model1.SafeC2_R = pyo.Constraint(model1.B, rule=safe_c2_right)
73
74 pyo.SolverFactory('cbc', executable='/usr/bin/cbc',
       validate=False).solve(model1)
75
76 print("--- MODEL 1: MILP BASELINE (VOLUMETRIC) ---")
77 print(f"Total Indexer1 Travel Span: {pyo.value(model1.Indexer1_max) -
       pyo.value(model1.Indexer1_min):.1f} mm")
78 for c in model1.C:
79     print(f"  Config {c}: {pyo.value(model1.Slider[c]):.1f} mm")
80
81 for c in model1.C:
```

```
    print(f"\n--- If using Config {c} ({pyo.value(model1.Slider[c]):.1f} mm)
        ---")
    for b in model1.B:
        if pyo.value(model1.y[b, c]) > 0.5:
            print(f"  Box {b:<6} -> Indexer1:
                {pyo.value(model1.Indexer1[b]):.1f} mm | Indexer2:
                {indexer2_pos[b]:.1f} mm")
```

D.2 Model 2: Name-Based Linear Program (LP)

Listing D.2: Name-Based continuous LP model script.

```
import pyomo.environ as pyo

# ========================================
# MODEL 2: NAME-BASED LP (Volumetric Digital Twin)
# ========================================
boxes_data = {
    "20x15": [163, 184, 161.5, 182.5, 35], "20x12": [164, 184, 162.5, 182.5,
        50],
    "25x12": [174, 195, 173.0, 194.0, 35], "33x15": [180, 228, 178.5, 226.5,
        35],
    "33x12": [180, 229, 178.5, 227.5, 35], "20x24": [216, 184, 214.5, 183.5,
        35],
    "25x20": [229, 192, 228.0, 191.0, 35], "25x24": [230, 193, 228.5, 191.5,
        35],
    "33x24": [239, 229, 237.5, 227.5, 35], "20x35": [269, 184, 268.0, 183.0,
        35],
    "25x30": [286, 192, 284.0, 191.0, 35]
}

box_to_group = {
    "20x15": "Group_12_15", "20x12": "Group_12_15", "25x12": "Group_12_15",
        "33x15": "Group_12_15", "33x12": "Group_12_15",
    "20x24": "Group_20_24", "25x20": "Group_20_24", "25x24": "Group_20_24",
        "33x24": "Group_20_24",
    "20x35": "Group_30_35", "25x30": "Group_30_35"
}

boxes = list(boxes_data.keys())
groups = ["Group_12_15", "Group_20_24", "Group_30_35"]
M = 2000; CLEARANCE = 25; INDEXER1_WIDTH = 90; SLIDER_WIDTH = 45

# Physical Parameters
box_offsets = {b: 27.5 if box_to_group[b] == "Group_20_24" else 0 for b in
    boxes}
C1 = {b: (boxes_data[b][0]/2) - box_offsets[b] for b in boxes}
C2 = {b: (boxes_data[b][0]/2) + boxes_data[b][1] - box_offsets[b] for b in
    boxes}
target_reach = {b: C2[b] + boxes_data[b][2] for b in boxes}
indexer2_pos = {b: (boxes_data[b][0]/2) + boxes_data[b][3] + boxes_data[b][4] +
    box_offsets[b] for b in boxes}

model2 = pyo.ConcreteModel()
model2.B = pyo.Set(initialize=boxes)
model2.G = pyo.Set(initialize=groups)

model2.Indexer1 = pyo.Var(model2.B, bounds=(150, 530),
    domain=pyo.NonNegativeReals)
```

```
model2.Slider = pyo.Var(model2.G, bounds=(0, 210), domain=pyo.NonNegativeReals)
model2.Zone_Var = pyo.Var(model2.B, domain=pyo.Binary)
model2.Indexer1_max = pyo.Var(bounds=(150, 530))
model2.Indexer1_min = pyo.Var(bounds=(150, 530))

def obj2_rule(model): return model.Indexer1_max - model.Indexer1_min
model2.Obj = pyo.Objective(rule=obj2_rule, sense=pyo.minimize)

model2.MaxTrk = pyo.Constraint(model2.B, rule=lambda m, b: m.Indexer1_max >=
    m.Indexer1[b])
model2.MinTrk = pyo.Constraint(model2.B, rule=lambda m, b: m.Indexer1_min <=
    m.Indexer1[b])

# Linkage & Obstruction
def linkage(m, b): return m.Indexer1[b] + m.Slider[box_to_group[b]] +
    INDEXER1_WIDTH + SLIDER_WIDTH == target_reach[b]
model2.Link = pyo.Constraint(model2.B, rule=linkage)

def obstruction(m, b): return m.Indexer1[b] + m.Slider[box_to_group[b]] <= 610
model2.Obstruction = pyo.Constraint(model2.B, rule=obstruction)

# Safety Clearance
def safe_c1(m, b): return m.Indexer1[b] >= C1[b] + CLEARANCE
model2.SafeC1 = pyo.Constraint(model2.B, rule=safe_c1)

def safe_c2_left(m, b): return m.Indexer1[b] + INDEXER1_WIDTH <= C2[b] -
    CLEARANCE + M * m.Zone_Var[b]
model2.SafeC2_L = pyo.Constraint(model2.B, rule=safe_c2_left)

def safe_c2_right(m, b): return m.Indexer1[b] >= C2[b] + CLEARANCE - M * (1 -
    m.Zone_Var[b])
model2.SafeC2_R = pyo.Constraint(model2.B, rule=safe_c2_right)

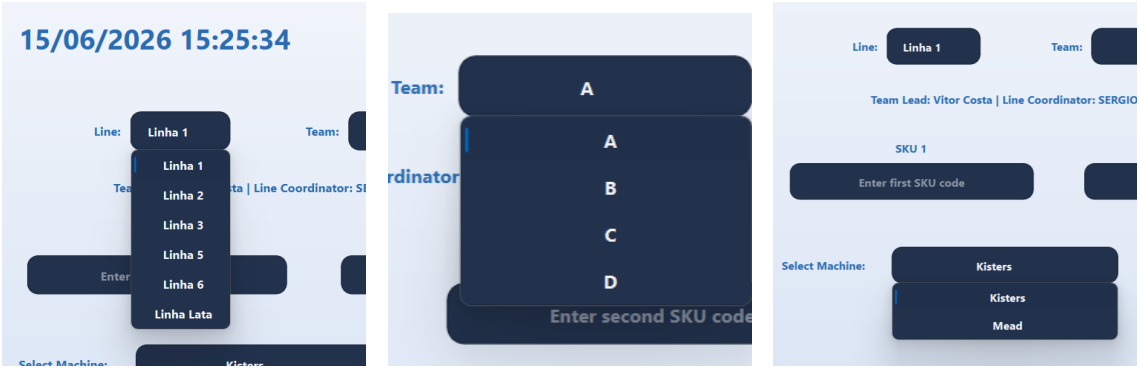
pyo.SolverFactory('cbc', executable='/usr/bin/cbc',
    validate=False).solve(model2)

print("--- MODEL 2: NAME-BASED LP (VOLUMETRIC) ---")
print(f"Total Indexer1 Travel Span: {pyo.value(model2.Indexer1_max) -
    pyo.value(model2.Indexer1_min):.1f} mm")
for g in model2.G:
    print(f"\n--- {g} | Slider = {pyo.value(model2.Slider[g]):.1f} mm ---")
    for b in model2.B:
        if box_to_group[b] == g:
            print(f"  Box {b:<6} -> Indexer1:
                {pyo.value(model2.Indexer1[b]):.1f} mm | Indexer2:
                {indexer2_pos[b]:.1f} mm")
```

Appendix E

Digital Tool Specifications

E.1 Context Initialisation and SKU Validation



(a) Line (b) Team (c) Machine

Figure E.1: Dropdown menus in the initial interface



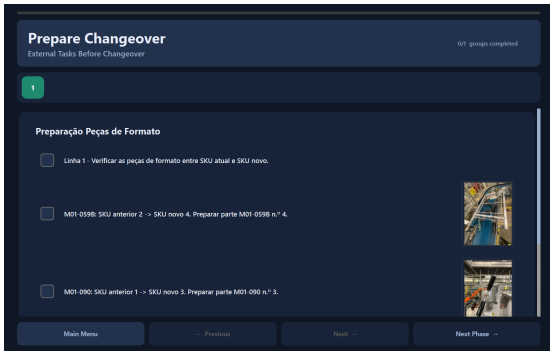
(a) SKU not found output (b) Correct SKU output

Figure E.2: SKU validation states

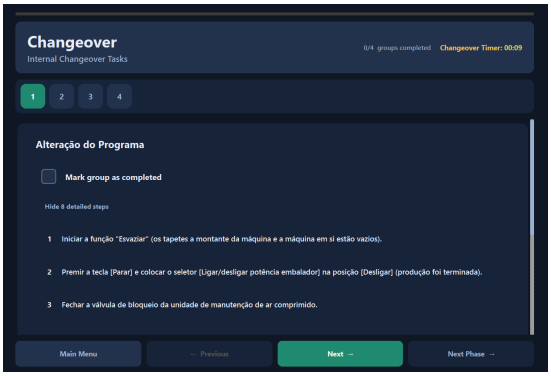


Figure E.3: Complete and correct input data on the first interface

E.2 Guided Execution Workflow

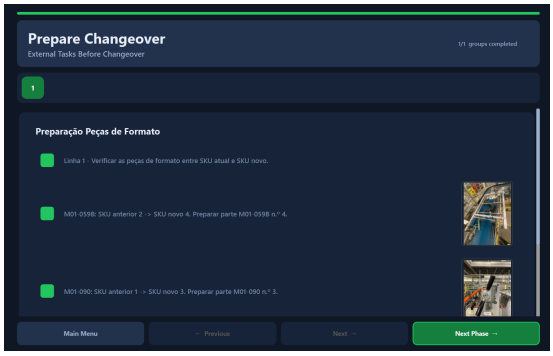


(a) Individual Tasks

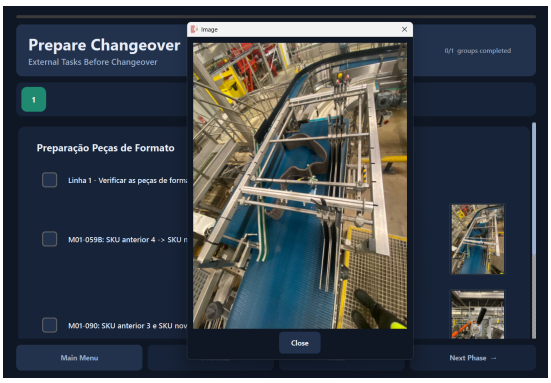


(b) Group Tasks

Figure E.4: Task rendering typologies



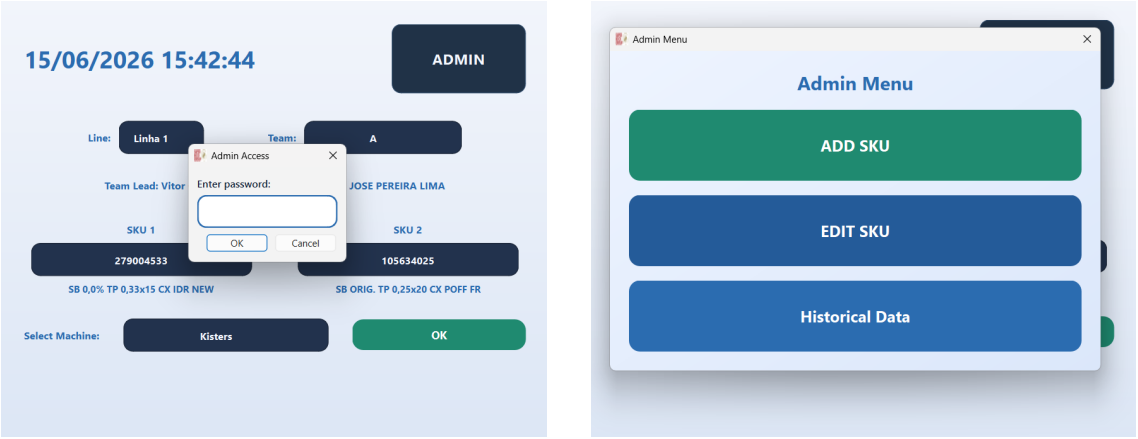
(a) Thumbnails Minimised



(b) Full-Screen View

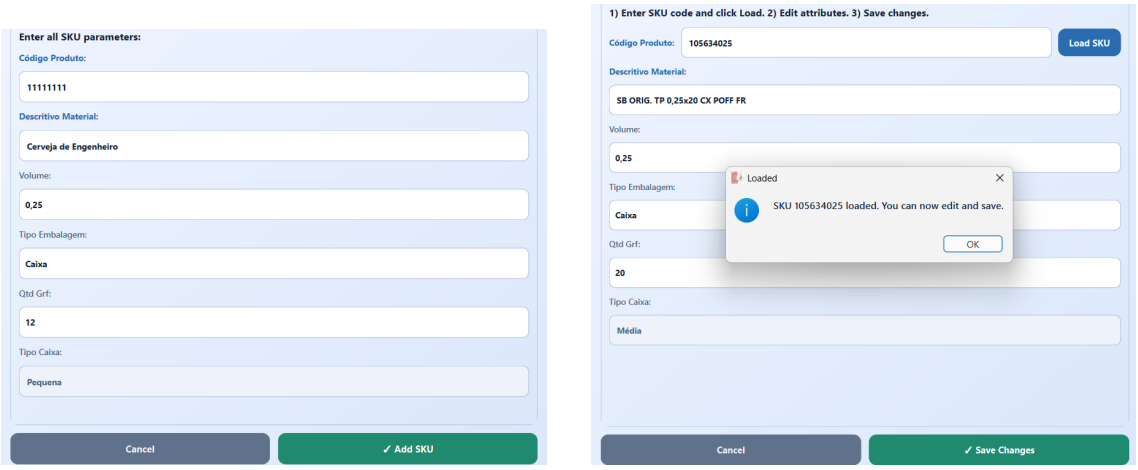
Figure E.5: Line-specific media support

E.3 Administrative Menu



(a) Authentication (b) After Authentication

Figure E.6: Administrative section access



(a) Add SKU Feature (b) Edit SKU Feature

Figure E.7: Add and Edit SKU features in the Admin Menu

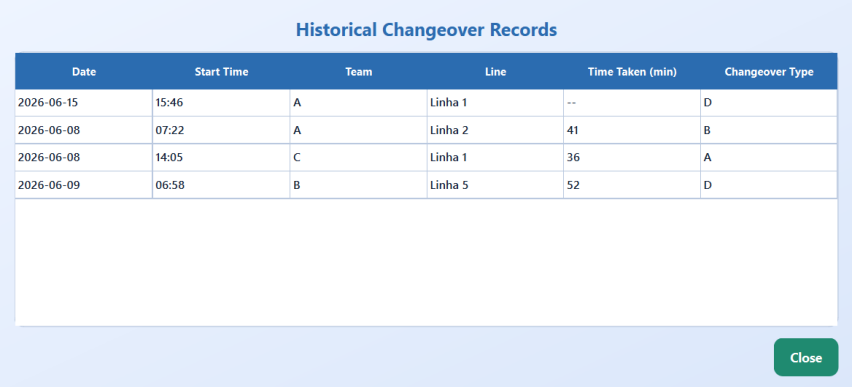


Figure E.8: Historical Data feature inside the Admin Menu

Appendix F

Conceptual Design Trade Studies

This appendix compiles the full working-principle trade-offs for the actuation and transmission candidates evaluated in Section 7.3. The main text retains the selection criteria, the AHP-weighted decision, and the resulting choices; the detailed pros and cons of each candidate are reproduced here for reference.

F.1 Actuation Candidates

- **Open-Loop Stepper Motors:** Move in discrete magnetic steps and generate maximum torque at standstill, making them effective for overcoming initial stiction. *Pros:* cost-effective, simple integration, good holding torque, high precision without a gearbox. *Cons:* no positional feedback — if breakaway friction exceeds motor capacity due to dust accumulation, the motor loses steps without the controller's knowledge, desynchronising the machine.

- **AC Induction Motors (with VFD and Encoder):** Operate on electromagnetic induction; the industry standard for continuous heavy-duty automation. *Pros:* rugged, highly reliable, capable of high continuous torque. *Cons:* bulky, require complex external forced ventilation at low speeds, and precise positional control via a VFD adds significant cost and complexity for a simple intermittent adjustment point.

- **AC/DC Servomotors:** Combine a continuous-rotation motor with a high-resolution encoder and a closed PID loop. *Pros:* high precision, high dynamic speed, flat torque curve, built-in stall detection. *Cons:* expensive, bulky, require complex PID tuning; servos continuously micro-oscillate ("hunt") to hold a static position, risking premature wear on the stationary screw threads.

- **Closed-Loop Stepper Motors:** Pair the high-pole-count stator of a standard stepper with an integrated encoder. *Pros:* retain the high low-speed torque and stable holding of a stepper, while the closed-loop drive detects stalls and corrects lost steps; cost-effective; eliminate

low-speed hunting. *Cons:* torque drops off at higher RPM (pull-out curve) and dynamic acceleration is lower than a servomotor.

F.2 Transmission and Coupling Candidates

- **Metallic Spur Gears:** Direct-meshing carbon-steel or hardened-alloy gears. *Pros:* transmit high torque without elastomer stretch, negligible radial side-loading, long service life if maintained. *Cons:* require wet lubrication to prevent galling; in a cardboard environment exposed grease mixes with dust into an abrasive paste, forcing a sealed, custom-machined enclosure that violates the compact retrofit boundary.

- **Polymer Spur Gears:** Machined from self-lubricating engineering plastics (POM, Nylon). *Pros:* compact, rigid, run dry, solving the contamination issue of metallic gears. *Cons:* fixed centre distances limit spatial flexibility and they suffer inherent backlash; fine particulate can pack into tooth roots over time, causing binding and fracture under the 8.54 Nm breakaway load.

- **Friction Belts (V-Belts / Flat Belts):** Continuous elastomer belt over smooth or grooved pulleys, transmitting torque through static friction. *Pros:* economical, acts as a natural torque limiter (slips before components break during a jam). *Cons:* require high static pre-tension to transmit the breakaway torque, introducing large radial side-loads that damage stepper bearings; inherent kinematic creep (micro-slip) is incompatible with the required multi-turn positional accuracy.

- **Synchronous Timing Belts:** Positive-engagement toothed belt meshing with machined pulleys, using steel or Kevlar tension members. *Pros:* require no lubrication, actively push dust out of the tooth grooves, easily bridge variable centre distances, provide essentially zero-slip positional accuracy. *Cons:* introduce moderate radial side-loading due to tensioning, and require a movable motor bracket to tension the belt during assembly.

- **Rigid Direct Coupling (Muff/Flange):** Solid sleeve rigidly locking the motor shaft collinearly to the spindle. *Pros:* most cost-effective, essentially full torque transfer, zero backlash, no lubrication, unaffected by dust. *Cons:* require near-perfect shaft alignment — any misalignment induces cyclic bending fatigue, shortening bearing life; the collinear architecture forces the motor to protrude axially, often violating aisle-clearance regulations.

- **Flexible Elastomer Jaw Coupling (Spider):** Two interlocking metallic hubs separated by a polyurethane damping insert. *Pros:* safely absorb minor angular and parallel misalignment, protecting the motor bearings; run dry, resist dust; high-durometer spiders offer near-zero backlash. *Cons:* share the rigid coupling's spatial limitation — they extend the overall axial length significantly, which is geometrically restrictive in a confined module.

F.3 Cardboard Storage Unit Torque Derivations

The following per-point derivations support the sizing results summarised in Table 7.12. Each recovers the baseline torque delivered to the legacy entry shaft by extrapolating the measured handle torque across the removed spur-gear stage ($i = 2$, $\eta_{\text{sg}} = 0.95$), then applies $S_f = 1.5$ and $K_a = 1.25$.

M09-025 (direct-to-spindle):

$$T_{\text{shaft}} = T_{\text{measured}} \cdot i \cdot \eta_{\text{sg}} = 1.4 \cdot 2 \cdot 0.95 = 2.66 \text{ Nm} \tag{F.1}$$

$$T_{\text{motor}} = T_{\text{shaft}} \cdot S_f \cdot K_a = 2.66 \cdot 1.5 \cdot 1.25 = 4.99 \text{ Nm} \tag{F.2}$$

M09-021 (retained sequential drivetrain):

$$T_{\text{entry}} = 1.0 \cdot 2 \cdot 0.95 = 1.90 \text{ Nm}, \qquad T_{\text{motor}} = 1.90 \cdot 1.5 \cdot 1.25 = 3.56 \text{ Nm} \tag{F.3}$$

M09-010 / M09-012 (retained chain-driven, parallel):

$$T_{\text{shaft1}} = 1.2 \cdot 2 \cdot 0.95 = 2.28 \text{ Nm}, \qquad T_{\text{motor}} = 2.28 \cdot 1.5 \cdot 1.25 = 4.28 \text{ Nm} \tag{F.4}$$

Appendix G

Transportation System Detailed Calculations

This appendix compiles the intermediate geometric and load derivations supporting the Transportation System embodiment design (Section 7.4.3). The main text retains the governing constraints, decisions, and final results; the rejected baseline configuration and the full belt-length and idler-travel derivations are reproduced here for completeness.

G.1 Rejected Baseline Pulley Configuration

An initial compact baseline pulley set was proposed to minimise spatial volume before the radial-load optimisation described in the main text. Its specifications are given in Table G.1.

Table G.1: Technical Specifications of the Initial Baseline Proposal for the Two-Stage HTD 5M System

Technical Specification	**Pulley 1** (Z_1)	**Pulley 2** (Z_2)	**Pulley 3** (Z_3)	**Pulley 4** (Z_4)
System Role	Motor Driver	Jackshaft Input	Jackshaft Output	Spindle Driven
Number of Teeth (–)	22	32	22	28
Belt Width (mm)	15	15	15	15
Pitch Diameter (mm)	35.01	50.93	35.01	44.56
Maximum Outer Diameter (mm)	33.87	49.79	33.87	43.42

The independent baseline stage reduction ratios (i_1, i_2) and the initial total system mechanical advantage (i_{total}) are defined in Equations G.1 and G.2.

$$i_1 = \frac{Z_2}{Z_1} = \frac{32}{22} = 1.4545, \quad i_2 = \frac{Z_4}{Z_3} = \frac{28}{22} = 1.2727 \tag{G.1}$$

$$i_{\text{total}} = i_1 \cdot i_2 = 1.4545 \cdot 1.2727 = 1.8512 \tag{G.2}$$

Verified assuming the stepper's absolute stall torque capacity ($T_{\text{motor}} = 5.94$ Nm) and a mechanical efficiency of $\eta = 0.95$ per independent stage, the torque progression along the drivetrain is:

$$T_1 = T_{\text{motor}} = 5.94 \text{ Nm} \tag{G.3}$$

$$T_2 = T_3 = T_1 \cdot i_1 \cdot \eta = 5.94 \cdot 1.4545 \cdot 0.95 = 8.208 \text{ Nm} \tag{G.4}$$

$$T_4 = T_{\text{delivered}} = T_3 \cdot i_2 \cdot \eta = 8.208 \cdot 1.2727 \cdot 0.95 = 9.924 \text{ Nm} \tag{G.5}$$

The resulting baseline tangential force at the primary motor driver pulley was:

$$F_{u1} = \frac{2 \cdot T_1}{d_{\text{baselinepitch1}}} = \frac{2 \cdot 5.94 \text{ Nm}}{0.03501 \text{ m}} = 339.33 \text{ N} \tag{G.6}$$

This exceeds the motor's manufacturer-specified radial bearing limit (220 N) by 54.2%, leading to rapid bearing fatigue and premature motor failure. The baseline was therefore rejected in favour of the load-optimised configuration described in the main text.

G.2 Belt Length and Idler Tensioning Travel

This section derives the belt pitch lengths and the idler calibration travel for the finalised two-stage configuration, at the fixed centre distances $C_1 = 120.00$ mm and $C_2 = 90.00$ mm.

Wrap Angle and Teeth in Mesh

The most conservative wrap angle (θ_{wrap}) for each stage is calculated from the pitch diameters and centre distances via Equation G.7.

$$\theta = 180^\circ - 2 \cdot \arcsin\left(\frac{D_{\text{pitch}} - d_{\text{pitch}}}{2 \cdot C}\right) \tag{G.7}$$

$$\theta_1 = 180^\circ - 2 \cdot \arcsin\left(\frac{82.76 - 50.93}{2 \cdot 120}\right) = 164.76^\circ \tag{G.8}$$

$$\theta_2 = 180^\circ - 2 \cdot \arcsin\left(\frac{44.56 - 35.01}{2 \cdot 90}\right) = 173.91^\circ \tag{G.9}$$

The number of actively engaged teeth (TIM) on the smaller pulley of each stage is calculated from Equation G.10.

$$\text{TIM} = Z_{\text{pulley}} \cdot \left(\frac{\theta_{\text{wrap}}}{360^\circ}\right) \tag{G.10}$$

$$\text{TIM}_1 = 32 \cdot \left(\frac{164.76^\circ}{360^\circ}\right) = 14.65 \text{ teeth} \tag{G.11}$$

$$\text{TIM}_2 = 22 \cdot \left(\frac{173.91^\circ}{360^\circ} \right) = 10.63 \text{ teeth} \tag{G.12}$$

Both stages exceed the TIM ≥ 6 threshold required to prevent tooth cam-out, supporting the precision required by the closed-loop encoder system.

Theoretical Belt Length

The theoretical geometric pitch length (L_{belt}) required to wrap each two-pulley open layout is calculated via Equation G.13.

$$L_{\text{belt}} = 2 \cdot C + \frac{\pi}{2}(d_{\text{pitch1}} + d_{\text{pitch2}}) + \frac{(d_{\text{pitch2}} - d_{\text{pitch1}})^2}{4 \cdot C} \tag{G.13}$$

$$L_{\text{belt1}} = 2 \cdot 120 + \frac{\pi}{2}(50.93 + 82.76) + \frac{(82.76 - 50.93)^2}{4 \cdot 120} = 452.11\text{mm} \tag{G.14}$$

$$L_{\text{belt2}} = 2 \cdot 90 + \frac{\pi}{2}(35.01 + 44.56) + \frac{(44.56 - 35.01)^2}{4 \cdot 90} = 305.24\text{mm} \tag{G.15}$$

Fixed-Axis Length Correction

Following the Norelem catalogue assembly instructions [81], the required centre-distance reduction for correct assembly is 21 mm for belt distances below 1525 mm (both pulleys flanged) and 15 mm (single pulley flanged). Because both centre axes are fixed, this reduction translates into a larger belt perimeter rather than an axis displacement, as computed in Equations G.16 and G.17.

$$L_{\text{belt1\_red}} = 2 \cdot (120 - 15) + \frac{\pi}{2}(50.93 + 82.76) + \frac{(82.76 - 50.93)^2}{4 \cdot (120 - 15)} = 422.41\text{mm} \tag{G.16}$$

$$L_{\text{belt2\_red}} = 2 \cdot (90 - 21) + \frac{\pi}{2}(35.01 + 44.56) + \frac{(44.56 - 35.01)^2}{4 \cdot (90 - 21)} = 263.32\text{mm} \tag{G.17}$$

Adding the difference between the theoretical and reduced-centre-distance belt lengths back to the original theoretical length yields the required belt length for the fixed-axis case.

$$L_{\text{belt1real}} = 452.11 + (452.11 - 422.41) = 481.81\text{mm} \tag{G.18}$$

$$L_{\text{belt2real}} = 305.24 + (305.24 - 263.32) = 347.16\text{mm} \tag{G.19}$$

To use standard commercial off-the-shelf components, Stage 1 adopts a standardised belt pitch length of $L_{\text{actual1}} = 475.00$mm and Stage 2 an $L_{\text{actual2}} = 350.00$mm profile. The remaining loop perimeter slack (ΔL) is defined by Equation G.20.

$$\Delta L = L_{\text{actual}} - L_{\text{belt}} \tag{G.20}$$

$$\Delta L_1 = 475.00\text{mm} - 452.11\text{mm} = 22.89\text{mm} \tag{G.21}$$

$$\Delta L_2 = 350.00\text{mm} - 305.24\text{mm} = 44.76\text{mm} \tag{G.22}$$

Idler Plunge Travel

The idler pulley acts against the unconstrained open-air span of the belt. The baseline straight free-span length (L_f) between the pulley tangent planes is evaluated in Equations G.24 and G.25.

$$L_f = \sqrt{C^2 - \left(\frac{D_{\text{pitch}} - d_{\text{pitch}}}{2}\right)^2} \tag{G.23}$$

$$L_{f1} = \sqrt{120.00^2 - \left(\frac{82.76 - 50.93}{2}\right)^2} = 118.94\text{mm} \tag{G.24}$$

$$L_{f2} = \sqrt{90.00^2 - \left(\frac{44.56 - 35.01}{2}\right)^2} = 89.87\text{mm} \tag{G.25}$$

When the idler engages the midpoint of this span, the geometry deforms into an isosceles triangle. The linear plunge stroke (x) required to draw the loop taut is given by Equation G.26.

$$x = \sqrt{\left(\frac{L_f + \Delta L}{2}\right)^2 - \left(\frac{L_f}{2}\right)^2} \tag{G.26}$$

$$x_1 = \sqrt{\left(\frac{118.94 + 22.89}{2}\right)^2 - \left(\frac{118.94}{2}\right)^2} = 38.63\text{mm} \tag{G.27}$$

$$x_2 = \sqrt{\left(\frac{89.87 + 44.76}{2}\right)^2 - \left(\frac{89.87}{2}\right)^2} = 50.12\text{mm} \tag{G.28}$$

Pretensioning and Active Calibration Travel

The strokes above define a touch-tight state with zero slack. To seat the synchronous teeth and stretch the tensile cords, the Norelem catalogue specifies a linear centre-distance extension of $\Delta a_{\text{tension}} = 3.00\text{mm}$. Because the belt spans both parallel tracks, this corresponds to an additional loop perimeter of $\Delta L_{\text{tension}}$ (Equation G.29).

$$\Delta L_{\text{tension}} = 2 \cdot \Delta a_{\text{tension}} = 2 \cdot 3.00\text{mm} = 6.00\text{mm} \tag{G.29}$$

The final physical plunger depth ($x_{\text{tensioned}}$) incorporates both the loop slack and the 6.00 mm pretensioning buffer (Equation G.30).

$$x_{\text{tensioned}} = \sqrt{\left(\frac{L_f + \Delta L + 6.00}{2}\right)^2 - \left(\frac{L_f}{2}\right)^2} \tag{G.30}$$

$$x_{1\_\text{tensioned}} = \sqrt{\left(\frac{118.94 + 22.89 + 6.00}{2}\right)^2 - \left(\frac{118.94}{2}\right)^2} = 43.89\text{mm} \tag{G.31}$$

$$x_{2\_\text{tensioned}} = \sqrt{\left(\frac{89.87 + 44.76 + 6.00}{2}\right)^2 - \left(\frac{89.87}{2}\right)^2} = 54.06\text{mm} \tag{G.32}$$

The active calibration travel (Δx) required at each idler sliding block is the difference between the fully tensioned and zero-slack states:

$$\Delta x_1 = x_{1\_\text{tensioned}} - x_1 = 43.89\text{mm} - 38.63\text{mm} = 5.26\text{mm} \tag{G.33}$$

$$\Delta x_2 = x_{2\_\text{tensioned}} - x_2 = 54.06\text{mm} - 50.12\text{mm} = 3.94\text{mm} \tag{G.34}$$

These travel values ($\Delta x_1 = 5.26$ mm, $\Delta x_2 = 3.94$ mm) assume the worst case, where the idler is centred on the belt span. They define the idler slot geometry specified in the detailed design (Section 7.5.3). Positioning the idler closer to either pulley reduces the required travel.

G.3 Jackshaft Force Resolution, Bearing Reactions, and Fatigue Derivation

Force resolution. The nominal single-side tangential forces at Pulley 2 (Stage 1 driven, $F_{u2max} = 221.61$ N) and Pulley 3 (Stage 2 driver, $F_{u3max} = 523.85$ N) are resolved by orientation, applying the continuous belt-tension factor $b = 2.0$ [83]:

$$F_{2x} = 221.61 \cdot 2 \cdot \sin(70) = 416.491 \text{ N}, \qquad F_{2y} = 221.61 \cdot 2 \cdot \cos(70) = 151.59 \text{ N (downward)} \tag{G.35}$$

$$F_{3x} = 523.85 \cdot 2 \cdot \sin(-55) = -858.226 \text{ N}, \quad F_{3y} = 523.85 \cdot 2 \cdot \cos(55) = 600.936 \text{ N (downward)} \tag{G.36}$$

Bearing reactions. Static equilibrium ($\sum M = 0$, $\sum F = 0$) about Bearing A ($Z = 0$) and

Bearing B ($Z = 109.5$ mm), with F_2 acting at $Z = 89.5$ mm and F_3 at $Z = 22.0$ mm:

$$R_{Ax} = \frac{F_{2x}(20.0) + F_{3x}(87.5)}{109.5} = -609.8 \text{ N}, \qquad R_{Bx} = \frac{F_{2x}(89.5) + F_{3x}(22.0)}{109.5} = 168.0 \text{ N} \tag{G.37}$$

$$R_{Az} = \frac{F_{2z}(20.0) + F_{3z}(87.5)}{109.5} = 507.9 \text{ N}, \qquad R_{Bz} = \frac{F_{2z}(89.5) + F_{3z}(22.0)}{109.5} = 244.6 \text{ N} \tag{G.38}$$

$$R_A = \sqrt{609.8^2 + 507.9^2} = 793.4 \text{ N (governing)}, \quad R_B = \sqrt{168.0^2 + 244.6^2} = 296.8 \text{ N} \tag{G.39}$$

Dynamic life verification (ISO 281):

$$L_{10} = \left(\frac{C_r}{R_A}\right)^3 = \left(\frac{4750}{793.4}\right)^3 \approx 214.6 \times 10^6 \text{ revolutions} \Rightarrow L_{10h} \approx 11{,}920 \text{ h at 300 RPM} \tag{G.40}$$

Stress at the governing section (Pulley 3 journal, $Z = 22.0$ mm, $d = 14.5$ mm):

$$M = R_A \times 22.0 = 17{,}454.8 \text{ N·mm}, \quad \sigma_b = \frac{M}{\pi d^3/32} = 58.32 \text{ MPa}, \quad \tau = \frac{T}{\pi d^3/16} = 15.32 \text{ MPa} \tag{G.41}$$

With DIN 6885 keyway stress-concentration factors ($K_t = 2.14$, $K_{ts} = 3.0$ [84]):

$$\sigma_b' = 124.8 \text{ MPa}, \quad \tau_t' = 46.0 \text{ MPa}, \quad \sigma_{vm}' = \sqrt{(\sigma_b')^2 + 3(\tau_t')^2} = 148.06 \text{ MPa}, \quad S_f = \frac{415}{148.06} \approx 2.80 \tag{G.42}$$

Finite-life fatigue derivation. As a rotating shaft under stationary bending, the jackshaft accumulates one reversed stress cycle per revolution. With a worst-case stroke of 84 mm per actuation, a 4 mm screw lead, and i = 28/22, each actuation produces 27 shaft revolutions; at 250 actuations/year over the 10-year life, N 6.7×10^4 cycles, conservatively evaluated at N = 10^5 — governing the finite-life (Basquin) rather than infinite-life criterion.

$$S_e = k_a k_b k_e \cdot S_e' = (0.809)(0.931)(0.814)(327.5) = 200.8 \text{ MPa} \tag{G.43}$$

with $k_a = 4.51 R_m^{-0.265}$ (machined finish), $k_b = 1.24 d^{-0.107}$ ($d = 14.5$ mm), $k_e = 0.814$ (99% reliability). Local alternating/mean stresses: $\sigma_a' = 124.8$ MPa, $\sigma_m' = \sqrt{3} K_{ts} \tau = 79.6$ MPa. The Basquin finite-life strength at $N = 10^5$ cycles ($f = 0.85$, $S_{ut} = 655$ MPa [84]):

$$a = \frac{(f S_{ut})^2}{S_e} = 1543 \text{ MPa}, \quad b = -\frac{1}{3}\log_{10}\left(\frac{f S_{ut}}{S_e}\right) = -0.148, \quad S_f(10^5) = a N^b \approx 282 \text{ MPa} \tag{G.44}$$

Modified Goodman:

$$SF_{fatigue} = \left(\frac{\sigma_a'}{S_f(2{,}500)} + \frac{\sigma_m'}{S_{ut}}\right)^{-1} \approx 1.77 \tag{G.45}$$

For reference, the infinite-life criterion ($S_e = 200.8$ MPa) gives $SF_{fatigue,\infty} = 1.35$, not governing at this cycle count.

Central locating shoulder (non-governing check). At $Z = 35.0$ mm ($d_3 = 18$ mm), superposition gives $M \approx 14{,}248.5$ N·mm, $\sigma_b = 24.89$ MPa, $\tau = 8.01$ MPa. With sharp-fillet factors ($K_t = 2.7$, $K_{ts} = 2.2$, required by the shoulder's role as a positive pulley-locating face): $\sigma'_{vm} = 73.8$ MPa, $S_f = 415/73.8 \approx 5.62$; fatigue $SF = 3.51$ by the same finite-life basis. Neither governs.

Angular deflection. Treating the shaft conservatively as a uniform $d = 14.5$ mm section across the full span: $\theta_A \approx 0.068$ (governing), $\theta_B \approx 0.043$, both against a 0.5 manufacturer limit.

Appendix H

Housing FEA Result Fields

This appendix presents the boundary-condition, von Mises stress, and displacement fields for the Cardboard Storage Unit and Transportation System housing simulations. The governing results (peak stress, safety factor, peak displacement) are summarised in the corresponding sections of the main text.

H.1 Cardboard Storage Unit Housings

The governing results for these housings are summarised in Table 7.19.

M09-025 Housing

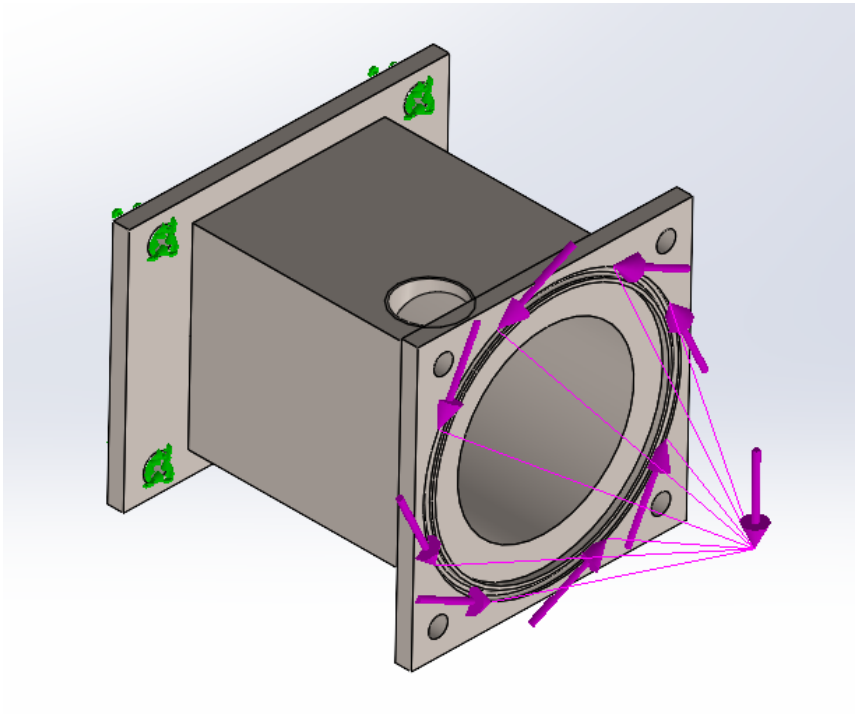
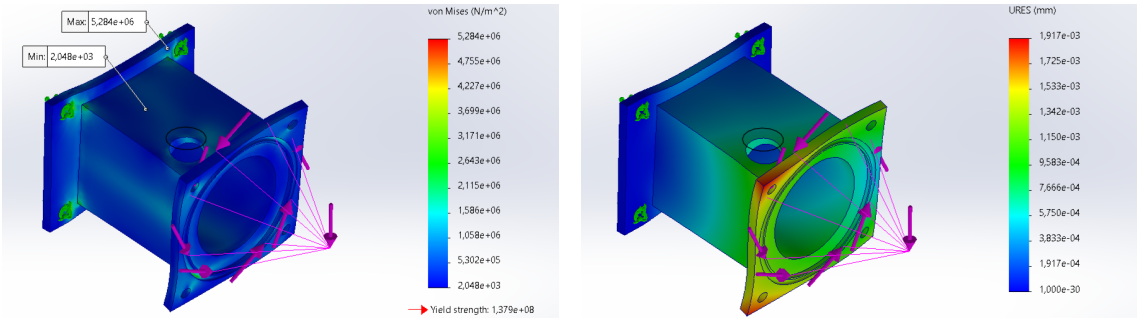


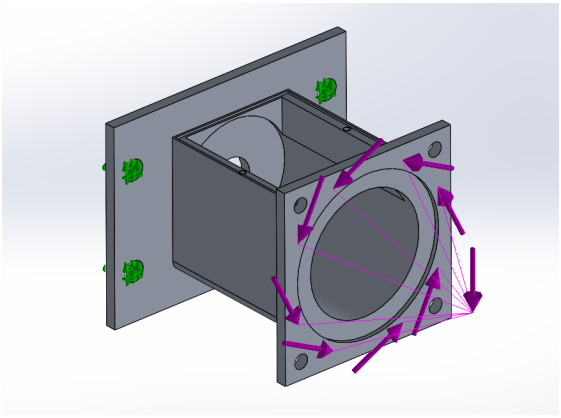
Figure H.1: Boundary Conditions on the M09-025 Housing FEA Simulation



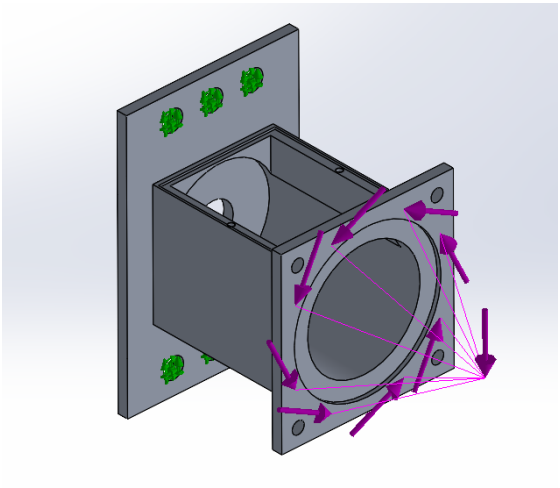
(a) Stress Results (b) Displacement Results

Figure H.2: FEA Simulation Results on the M09-025 Housing

M09-010 / M09-012 and M09-021 Housings

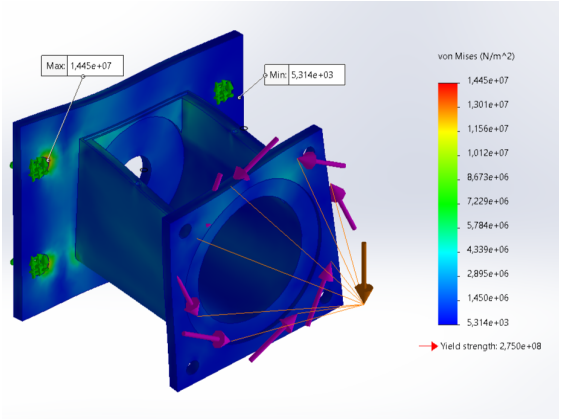


(a) M09-010 and M09-012 Housing Boundary Conditions

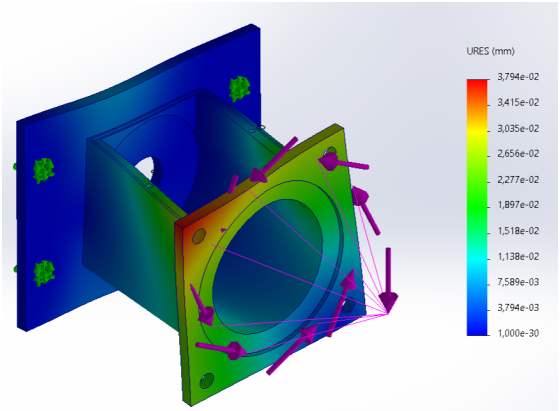


(b) M09-021 Housing Boundary Conditions

Figure H.3: Boundary Conditions Established for Each Cardboard Storage Unit Housing Design

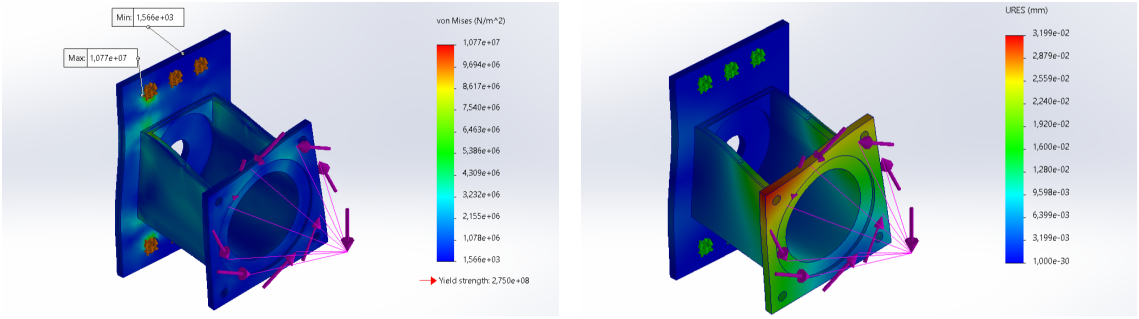


(a) M09-010 and M09-012 Housing FEA Stress Results



(b) M09-010 and M09-012 Housing FEA Displacement Results

Figure H.4: Stress and Displacement Results from the FEA Simulation on the M09-010/012 Housing



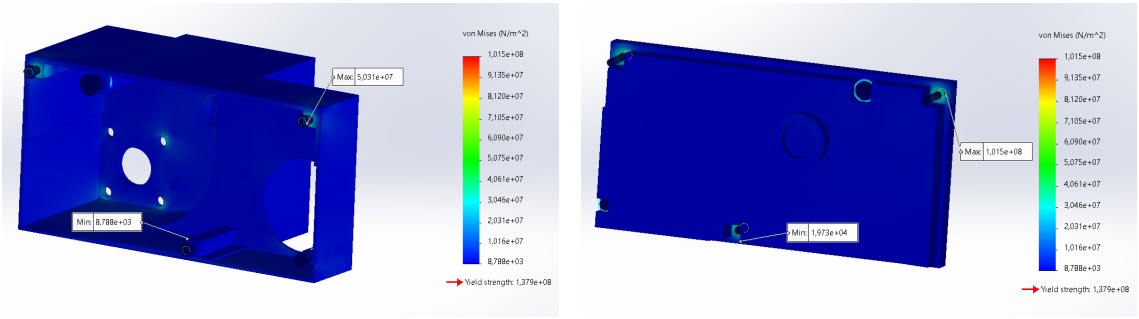
(a) M09-021 Housing FEA Stress Results (b) M09-021 Housing FEA Displacement Results

Figure H.5: Stress and Displacement Results from the FEA Simulation on the M09-021 Housing

H.2 Transportation System Housing

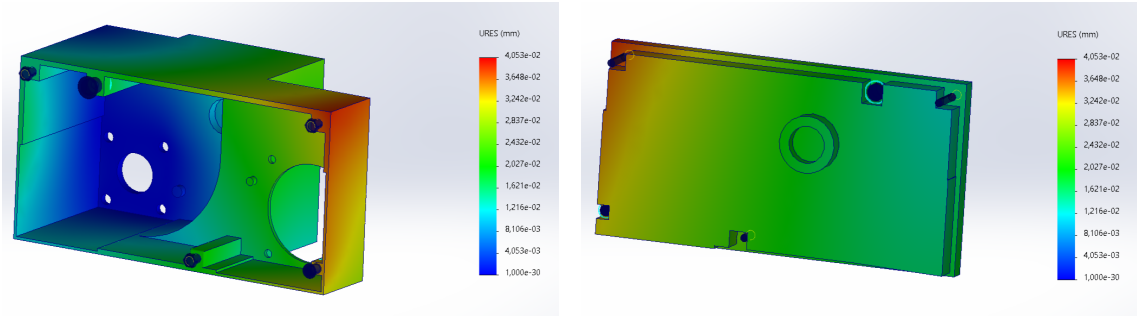
The governing results for the two-part body–lid assembly, in both mounting orientations, are summarised in Section 7.5.3.2. The horizontal orientation governs stress; the vertical orientation governs displacement.

Horizontal Orientation (Linear Units 1 and 3)



(a) Housing-Side Stress Results (b) Lid-Side Stress Results

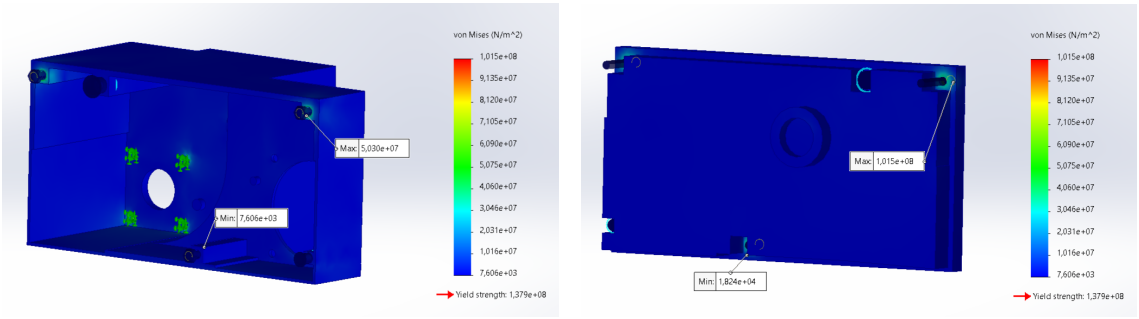
Figure H.6: Stress Results from the FEA Simulation on the Transportation System Housing–Lid Assembly (Horizontal Orientation)



(a) Housing-Side Displacement Results (b) Lid-Side Displacement Results

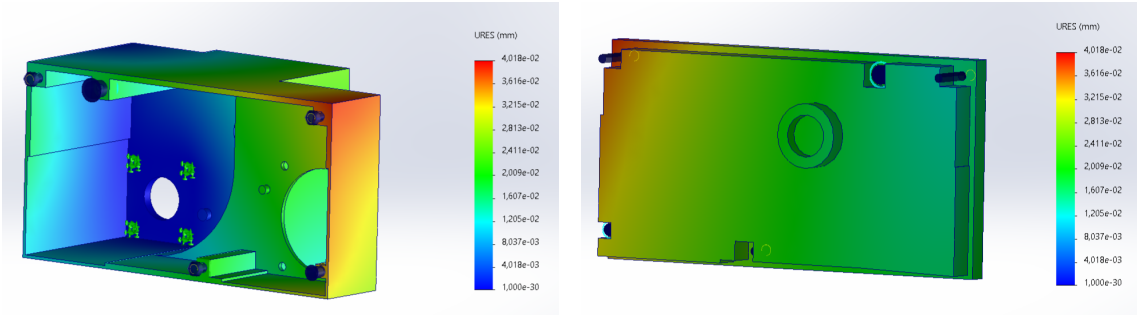
Figure H.7: Displacement Results from the FEA Simulation on the Transportation System Housing–Lid Assembly (Horizontal Orientation)

Vertical Orientation (Linear Unit 2)



(a) Housing-Side Vertical-Orientation Stress Results (b) Lid-Side Vertical-Orientation Stress Results

Figure H.8: Stress Results from the FEA Simulation on the Vertical-Orientation Transportation System Housing–Lid Assembly



(a) Housing-Side Vertical-Orientation Displacement Results (b) Lid-Side Vertical-Orientation Displacement Results

Figure H.9: Displacement Results from the FEA Simulation on the Vertical-Orientation Transportation System Housing–Lid Assembly

Appendix I

Standard Mechanical Components Used

I.1 Linear Units' Reference Sheet

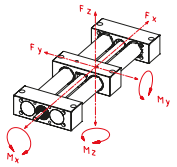
EP(X)-II 30/40 Technical data

General information / operating conditions

	EP-II 30	EPX-II 30	EP-II 40	EPX-II 40
Guide	Slide guide			
Installation position	Any position			
Max. speed	0.015 m/s (stroke independent)		0.02 m/s (stroke independent)	
Max. acceleration	3 m/s²			
Repeatability	± 0,1 mm			
Max. no-load torque	0,6 Nm	0,7 Nm	0,7 Nm	0,8 Nm
Drive	Trapezoidal screw, Ø 14, pitch 3		Trapezoidal screw, Ø 20, pitch 4	
Lead accuracy	(± 0,1 / 300 mm)			
Duty cycle	S3, 30%, base 1h			
Ambient temperature	0 to +60°C			
Protection class	Basic: no / Protect: IP 40			

Static load data*

F Force [N]
M Moment [Nm]
I Geometric moment of inertia [cm⁴]



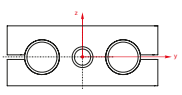
* with reference to carriage (deflection of guide element f = 0.5 mm, static, end elements supported)

Type	Fx	Fy			Fz			Mx	My	Mz
Total length [mm]		500	1000	1500	500	1000	1500			
EP-II 30	800	1000	800	500	550	300	100	60	60	75
EPX-II 30	800	1400	1200	700	650	450	200	80	110	140
EP-II 40	1000	3500	2600	1300	2000	580	120	120	130	150
EPX-II 40	1000	6000	3100	1800	2200	680	220	160	190	240

Geometric moment of inertia

[cm⁴]

Type	Iy	Iz
EP(X)-II 30	3.47	46.57
EP(X)-II 40	14.84	198.06



I.2 Transportation System's Linear Units

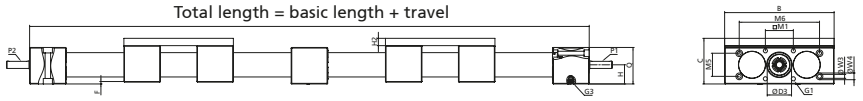
EPX-II 30/40 – Dimensions / ordering data

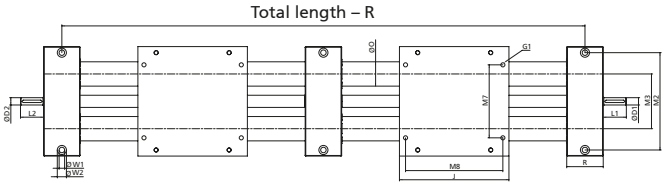
Order instructions:

- Please specify basic length and total travel when placing an order
- Corrosion-protected units available on request
- Second non driven carriage available on request
- Scale upon request
- Protect: version with bellows optional (IP 40)
- Other screw leads available on request

Version ■ Split screw







[mm]

Code No.	Type	Spindel	Basic length	B	C	D1	D2	D3	F	G1	G2	G3	H	H2	J	L1	L2	M1	M2
7983031_1AA_ _ _ _	30	Tr 14x3	410	130	64	8	8	30 H8	2	M6 / 12 deep	M6	M6 / 9 deep	27	10	130	26	26	40x30	114
7984031_1AA_ _ _ _	40	Tr 20x4	540	180	75	12	12	40 H8	3	M8 / 20 deep	M8	M8 / 8 deep	31.5	12	180	38	38	46	160

_ _ _ _ Total length = basic length + travel [mm]

A = standard
B = c/w integrated spindle clamping

M3	M5	M6	M7	M8	O	P 1	P 2	Q	R	W1	W2	W3	W4	Max. travel	Mass [kg]	
															Basic length	per 100 mm travel
70	–	–	80	114	30	2x2x20	2x2x20	52	50	7	11 / 7 deep	–	–	1295	7.2	0.4
90	38	132	120	160	40	4x4x32	4x4x32	60	60	9	15 / 9 deep	6.5	11 / 8.5 deep	2460	16.16	0.96

I.3 Roller Conveyor's linear Units

EP-II 30/40 – Dimensions / ordering data

RK ROSE+KRIEGER

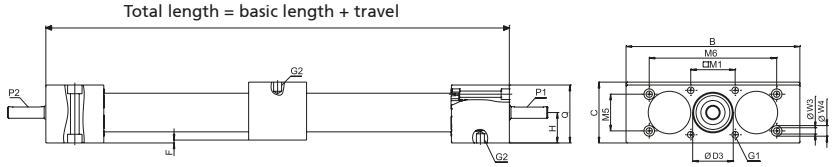
Order informations:

- Corrosion-protected units available on request
- Second non driven carriage available on request
- Scale upon request
- Other screw leads available on request

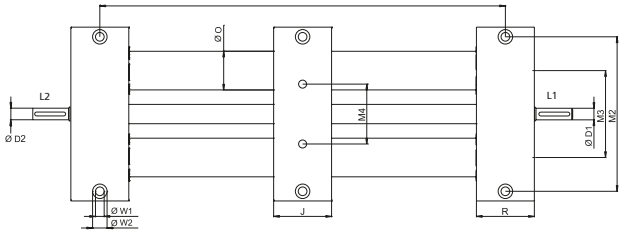
Version ■ Right *or* lefthand thread



Total length = basic length + travel



Total length – R



[mm]

Code No.	Type	Spindle	Basic length	B	C	D1	D2	D3	F	G1	G2	H	J	L1	L2	M1	M2	M3
79_301_ _ _AA_ _ _ _	30	Tr 14x3	150	130	54	8	–	30 H8	2	M6 / 12 deep	M6 / 9 deep	27	50	26	–	40x30	114	70
79_303_ _ _AA_ _ _ _							8								26			
79_401_ _ _AA_ _ _ _	40	Tr 20x4	180	180	63	12	–	40 H8	3	M8 / 20 deep	M8 / 8 deep	31.5	60	38	–	46	160	90
79_403_ _ _AA_ _ _ _							12								38			

_ _ _ _ Total length = basic length + travel [mm] **(Minimum travel: Basic 25 mm, Protect 120 mm)**

Version:
1 = Basic
2 = Protect **(For the Protect version, the stroke must be ordered longer than required by a factor of 1.5 due to the space required for installation of the bellows.)**

A = standard
B = c/w integrated spindle clamping (Only with spindle bearing ball bearing)

Spindle bearing:
1 = ball bearing
0 = slide bearing

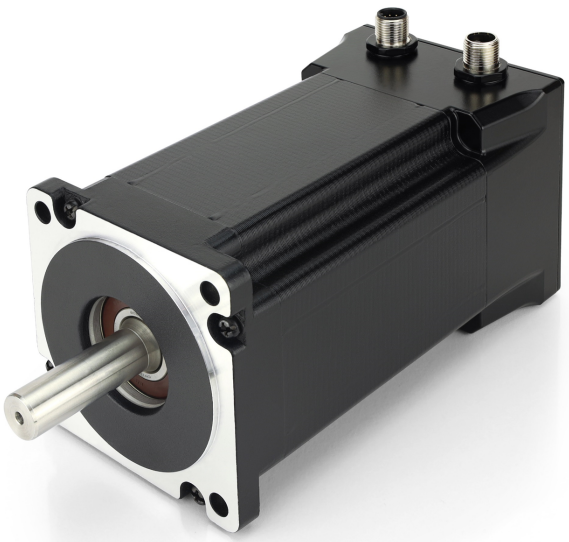
Spindle version:
1 = righthand thread
2 = lefthand thread

M4	M5	M6	O	P1	P2	Q	R	W1	W2	W3	W4	Max. travel	Mass [kg]	
													Basic length	per 100 mm travel
42	–	–	30	2x2x20	–	52	50	7	11 / 7 deep	–	–	1424	2.6	0.4
					2x2x20							1398		
62	38	132	40	4x4x32	–	60	60	9	15 / 9 deep	6.5	11 / 8.5 deep	2820	5.53	0.96
					4x4x32									

I.4 Roller Conveyor's Stepper Motor's Reference Sheet

Nanotec®
PLUG & DRIVE

Reference Sheet ASA86



Version: 1.0.3

Contents

1 Document, audience, intended use....3

2 Your product....3
2.1 Highlights....3
2.2 ASA86 variants....3
2.3 Product layout....3

3 Technical data....4
3.1 Ambient conditions....4
3.2 Motor....4
3.3 Encoder....4
3.4 Pin assignment....5

4 Sensor data format....5

5 Imprint, marking, versions....6

1 Document, audience, intended use

Nanotec's *ASA86* and this document address to technically trained experts alone, such as developers, application / plant engineers, fitters, and service staff. Only experts may install, commission and run the product. Always required is the qualification for the product's assembly, commissioning and maintenance as part of an *overall* machine / system, as well as:

- Training and experience in working with motors, their control and electrostatically threatened components
- Reading and understanding of this and all applicable documents
- Observing all valid regulations

Place this PDF in valid version always to hand and accessible. Use *ASA86* as intended only, within licit technical limits and ambients. For product combinations, please contact Nanotec Sales.

Disclaimer

Product modification / alteration is illicit. Nanotec is not liable for damage / malfunction from installation error, failure to observe this document, or undue repair; nor for product integration in the end system or interaction (= third-party ware). The audience alone is liable for selecting / running / using our products. Our risk analysis for partly completed machinery (if applicable) only rated the hazards of duly installed and networked *single* products. Risks in the *overall* system are exempt and to be rated by the *audience.* The general terms & conditions at *www.nanotec.com* apply (*us.nanotec.com* for clients of Nanotec USA).

2 Your product

ASA86 is a stepper motor in IP65 protection (save shaft outlet) with integrated incremental or multi-turn encoder for drive systems in a wide range of industrial scenarios.

2.1 Highlights

Typical ASA86 features are: size variance, holding force, and precision.

- UL certificate
- 2 motor sizes
- Protection class IP65 (shaft outlet: IP54)
- Optional brake integrated (on request)
- High encoder resolution

2.2 ASA86 variants

Find your product variant by its article number.

ASA8618**x**95-xxX	Motor length **M**edium | **L**arge
ASA8618x95-**xx**X	Encoder **E3:** Incremental | **W1:** SSI

2.3 Product layout

Internalize the *ASA86* product layout and technical data before installation so as to avert added hazards (say, abrupt motor run on defect / inhibition from your **overall** construct).

- ASA86 size sheet
- Flange *NEMA34*
- Torque tool to bolt the motor
- 4 *M6* screws *8.8* (ISO 4762 / 10642)

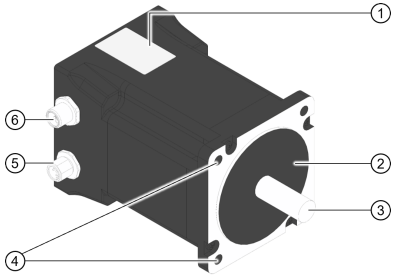


Fig. 1: ASA86 (here: size M).

1. Type label
2. IP54 ball bearing
3. Motor shaft
4. Four fixing bores *M6*
5. Encoder connector
6. Motor connector

3 Technical data

Use the product within its technical limits. The size sheet on our website applies. Select the exact *ASA86* type there and download the needed CAD-/ PDF file.

3.1 Ambient conditions

Except for the shaft / leadscrew outlet and the linear guide itself (= IP54), *ASA86* is IP65-protected. For *overall* IP65, you must seal the outlet installation-ward, say, by O-ring or surface seal.

Protection class	IP65 (shaft outlet: IP54)
Air humidity (non-condensing)	0 to 85 %
Ambient °C (°F)	-10 to +50 °C (+14 to +122 °F)
Axial force *Fa* $N^{max.}$	60
Radial force *Fr* (@ 20 mm) $N^{max.}$	220

The following conditions apply to the motor, but not to encoder and connectors:

Max. Temperature Rise	80 °C (at standstill, 2 phases energized)
Insulation Class	B
Insulation Resistance	100 MΩ
Dielectric Strength	500 V AC (for 1 min, coil to housing)

3.2 Motor

There are two ASA86 lengths, each with a different holding torque.

ASA86 stepper	**M size**	**L size**
$Current^{per\ winding}$ A	9.5	9.5
$Resistance^{per\ phase}$ (@ 25 °C / 77 °F) $\Omega^{\pm 15\%}$	0.23	0.26
$Inductance^{per\ phase}$ (@ 1kHz) $mH^{\pm 20\%}$	2.3	2.4
Rotor inertia kg·m^2 (x10^{-6})	190	300
Holding torque Nm	5.9	9.3
Step angle $^{\circ \pm 5\%}$	1.8	1.8
Axial play (*Fa* = 4.0 N) mm	0.08	0.08
Radial play (*Fr* = 4.0 N) mm	0.02	0.02

3.3 Encoder

ASA86 encoders work incremental or, in the SSI version, *multi-turn*.

	SSI	**Incremental**
Protective circuits	Reverse polarity, short circuit	Overvoltage
Energy harvesting	Wiegand effect	-/-
Operating voltage	4.75 to 15 VDC	5 $VDC^{\pm 10\%}$
Consumption (typical)	≤ 0.3 W	≤ 30 mA (no-load @ 5 V)
Start-up time	100 ms	-/-
Clock input	RS 422	-/-
Sensor type	Magnetic	Magnetic
Incremental cpr / $ppr^{squared}$	-/-	4096 / 16384
SSI (*single-* / *multi-turn*) bit	17 / 16	-/-
Accuracy	±0.0878° (@ room temperature)	±0.2° (@ standstill / constant speed)
Axis rotation $count^{seen\ from\ front}$	Clockwise	Clockwise
Maximum rpm	12,000	14,000

3.4 Pin assignment

NOTICE

Electronic damage: from lack of reverse polarity guard!

►Assign pins correctly.

►Use correct connector types.

Motor and encoder



Fig. 2: Motor. L-coded M12 (m).

1: A\ **2:** A **3:** B **4:** B\ **5:** n/a



Fig. 3: Encoder. A-coded M12 (m).

SSI:	**1:** Clk+	**3:** Data+	**5:** Gnd	**7:** n/c
	2: Clk-	**4:** Data-	**6:** n/c	**8:** +Ub
Incremental:	**1:** A	**3:** B	**5:** Gnd	**7:** I
	2: A\	**4:** B\	**6:** I\	**8:** +Ub

4 Sensor data format

Depending on type, the ASA86's encoder sends the motor position incrementally via two channels **A, B** plus index **I** or via **s**ynchron-**s**eriell-**i**nterface (SSI) as a 33-bit packet (after 16 start bits).

Incremental output

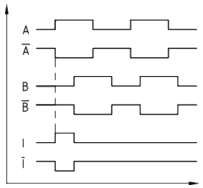


*Fig. 4: The index signal **I** runs in sync with channel **A**'s rising edge.*

If the motor shaft rotates clockwise (seen from front), channel A's signal leads channel B by 90 degrees (electrical).

Ub = 5 V	Load	High level	Low level
A, A\, B, B\, I, I\	35 mA	≥ 4.5 V	≤ 0.3 V

SSI-Output

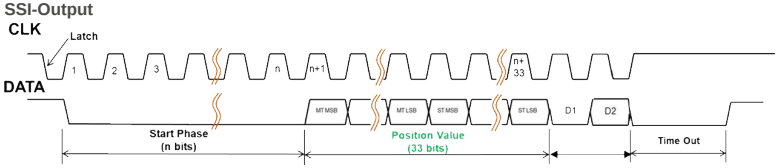


*Fig. 5: By **s**ynchronous **s**erial **i**nterface (SSI), the ASA86's encoder transfers the position values as 33-bit packets.*

- **S303B**
- Cycle: ≥ 50 µs
- Time-out: 7 µs$^{typ.}$
- 16 Start bits (= *0*) + *multi-turn* (16 bits) + *single-turn* (17 bits) + D1 + D2
- D1: Constant value = *0*
- D2: Error-bit for displaying the sensor-internal status (*1* = no error; *0* = error)

Prepare the SSI for *Nanotec CPB* controllers

63	62	61	60	59	58	57	56	55	54	53	52	51	50	49	48
													0	0	0
47	46	45	44	43	42	41	40	39	38	37	36	35	34	33	32
0	0	0	0	0	0	0	0	0	0	0	0	0	POS	POS	POS
31	30	29	28	27	26	25	24	23	22	21	20	19	18	17	16
POS	POS	POS	POS	POS	POS	POS	POS	POS	POS	POS	POS	POS	POS	POS	POS
15	14	13	12	11	10	9	8	7	6	5	4	3	2	1	0
POS	POS	POS	POS	POS	POS	POS	POS	POS	POS	POS	POS	POS	POS	S	E

*Fig. 6: ASA86 uses 51 status, start and position bits: 1 **S** for status (D1), 1 **E** for error (D2), 33 **POS** for position and 16 start bits (= 0).*

- **Bit 0** (= error): value *1* if no error
- **Bit 1**: always value *0*

Edit the 33B0$_h$ **sub-inidices** below so that *Nanotec CPB* controllers in *Autosetup* (see controller manual) duly process the encoder and its data:

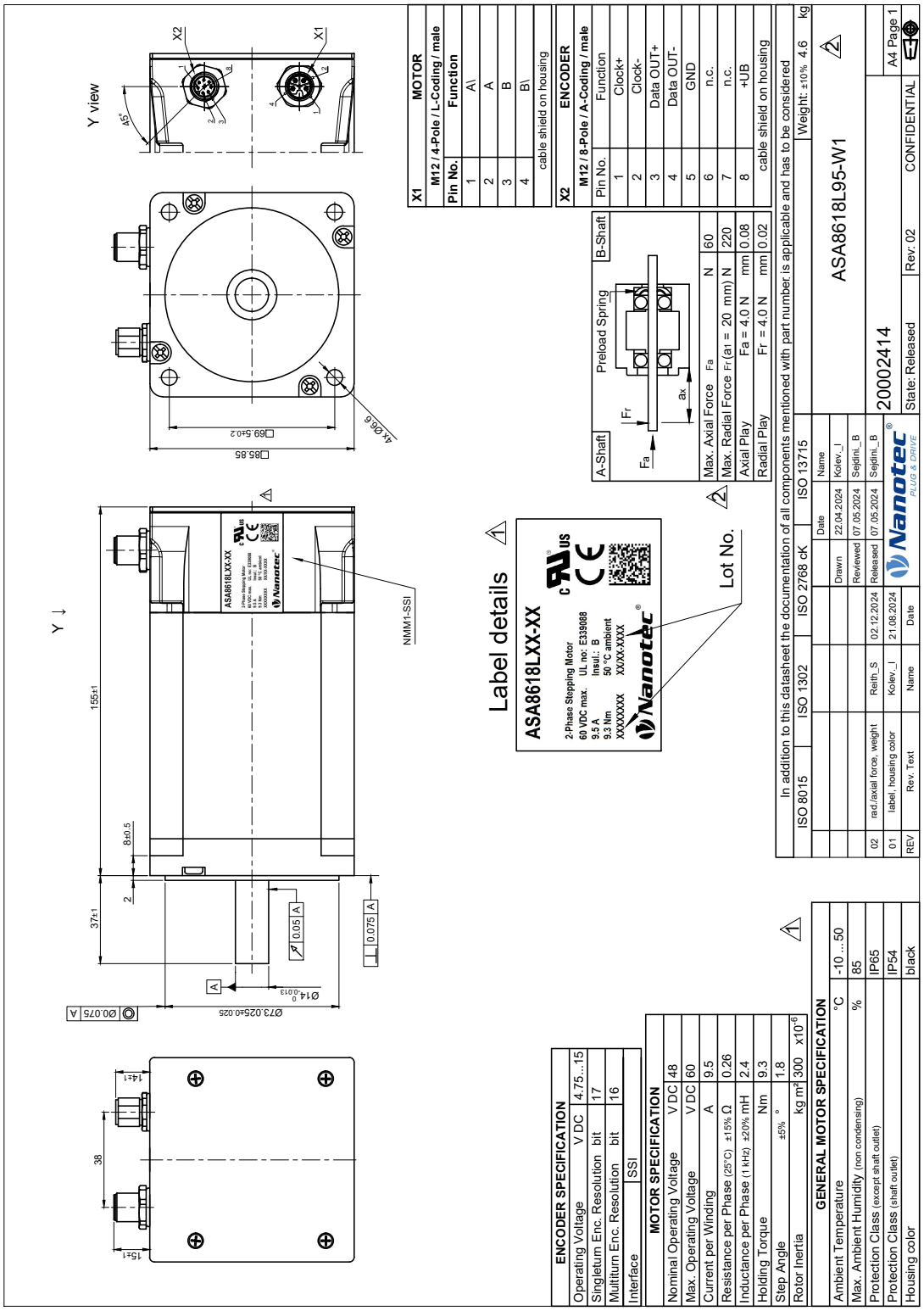
1. Set **33B0$_h$:06$_h$** to *2000000* (baud rate in Hz).
2. Set **33B0$_h$:05$_h$** to *51* (number of bits plus start bits).
3. Set **33B0$_h$:07$_h$** to *FFFFFFFC$_h$* (Position data: *POS* bits 2 to 31).
4. Set **33B0$_h$:08$_h$** to *7* (Position data: *POS* bits 32 to 34).
5. Set **33B0$_h$:09$_h$** to *3* (status and error bits 0 and 1).
6. Set **33B0$_h$:0B$_h$** to *1* (error bit = *1*, status bit = *0*).
7. To store the object: Insert *65766173$_h$* to **1010$_h$:06$_h$**.
8. Restart the controller.

5 Imprint, marking, versions

© 2026 **Nanotec Electronic GmbH & Co. KG** | Kapellenstr. 6 | 85622 Feldkirchen | Germany | Tel. +49 89 900 686-0 | Fax +49 89 900 686-50 | info@nanotec.de | www.nanotec.com | All rights reserved. Error, omission or change possible without notice. Quoted brands / products are trademarks of their owners and to be treated as such. Observed for conformity was: *RoHS Directive 2015/863/EU*, .

Document	+ Added | > Changed | # Fixed
1.0.3 2026.01	> Additional ambient conditions for motor added in Technical data.
1.0.2 2025.07	# Correction of typo in Technical data: incremental encoder typical accuracy is ±0.2°.
1.0.1 2024.12	+ Revision.
1.0.0 2024.09	Release.

I.5 Stepper Motor's Technical Drawing



I.6 Indexing Plungers Technical Sheet

GN 717-5-M8-A-NI

Indexing plungers

Steel / Stainless Steel, with and without rest position
Stainless Steel

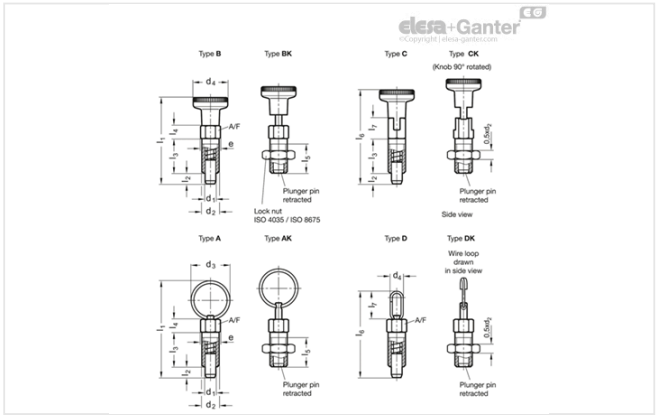


Description
GN 717-5-M8-A-NI

RoHS: Compliant

See GN 717 technical specifications

STAINLESS STEEL



Description	GN 717-5-M8-A-NI
d1 Bore +0.03/+0.08 Pin -0.05	5
d2	M 8
d3	18
d4	-
e	9.2
l1	-
l2	5
l3	16
l4	6
l5 min.	13.5
l6	-
l7	-
A/F	8
Max. tightening torque in Nm	7
Spring load in N ≈ initial	5
Spring load in N ≈ end	24
⚖	8

Standard Machine Elements Worldwide © 2026 Elesa S.p.A. | Otto Ganter GmbH & Co. KG

Standard Machine Elements Worldwide © 2026 Elesa S.p.A. | Otto Ganter GmbH & Co. KG

I.7 M20 Blanking Plug Technical Sheet

Data sheet

VP M20-MS65

Weidmüller Interface GmbH & Co. KG
Klingenbergstraße 26
D-32758 Detmold
Germany

www.weidmueller.com



In addition to cable glands for a wide range of applications, the product portfolio is rounded off by plugs, pressure compensation elements, adaptors and the corresponding accessories such as locknuts, sealing rings, flat washers and earthing rings.

General ordering data

Version	VPMS (blanking plug in brass), Blanking plug, in closed state, M 20, 6 mm, Brass, nickel-plated
Order No.	1777740000
Type	VP M20-MS65
GTIN (EAN)	4032248158010
Qty.	100 items

Data sheet

VP M20-MS65

Weidmüller Interface GmbH & Co. KG
Klingenbergstraße 26
D-32758 Detmold
Germany

www.weidmueller.com

Technical data

Approvals

Approvals	CE
ROHS	Conform

Dimensions and weights

Height	9.5 mm	Height (inches)	0.374 inch
Length	9.5 mm	Length (inches)	0.374 inch
Diameter	22 mm	Wall thickness, min.	0.5 mm
Wall thickness, max.	5 mm	Net weight	7.3 g

Temperatures

Operating temperature	-40 °C...100 °C

Environmental Product Compliance

RoHS Compliance Status	Compliant with exemption
RoHS Exemption (if applicable/known)	6c
REACH SVHC	Lead 7439-92-1
SCIP	0c0edf9f-b35a-4d1f-b8f0-99d4b22ac203

General information

Head diameter	22.00 mm	O-Ring	NBR
Silicone	No	Operating temperature range, max.	100 °C
Operating temperature range, min.	-40 °C	Pitch of thread	1.5 mm
Halogen	No	Protection degree	IP68 - 5 bar (30 min.)
Cable gland	metric	Basic material	Brass, nickel-plated
Diameter of sealing ring	20.00 mm	Sealing	NBR
External thread	M 20	Length of thread	6 mm

Classifications

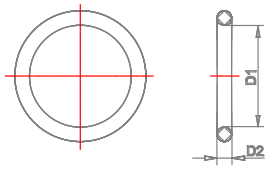
ETIM 8.0	EC000451	ETIM 9.0	EC000451
ETIM 10.0	EC000451	ECLASS 14.0	27-14-08-05
ECLASS 15.0	27-14-08-05		

Creation date 20.02.2026 01:59:53 MEZ
Catalogue status / Drawings

I.8 O-Rings Technical Sheets

Artikelbeschreibung/Produktabbildungen

Zeichnunge



© norelem

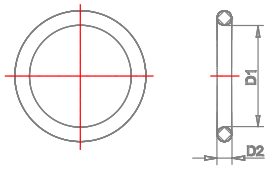
Artikelübersicht

BEST (Bestellnummer)	23900-104300300
D1 (Durchmesser / mm)	43.00
D2 (Durchmesser / mm)	3.00
GEW (Gewicht ca. / kg)	0.0013
BS (Beschreibung)	Infotext
ROHS (RoHS)	Yes
ZTN (Zolltarifnummer)	40169350
EAN (EAN-Nr. norelem)	4059495390291
EOL (End of life)	31.12.2099
STDLZ (Standardlieferzeit)	98% Warenverfügbarkeit. Nahezu alle Artikel aus dem Sortiment sind lagerhaltig verfügbar und werden nach Auftragseingang umgehend aus dem Zentrallager versendet. Nicht lagernde Artikel werden in der Regel zeitnah beschafft. Alle Verfügbarkeiten werden im Shop live angezeigt.
WARTUNG (Betriebs- und Wartungshinweise)	Wartungsintervall siehe Bedienungsanleitung

© norelem

Artikelbeschreibung/Produktabbildungen

Zeichnunge



© norelem

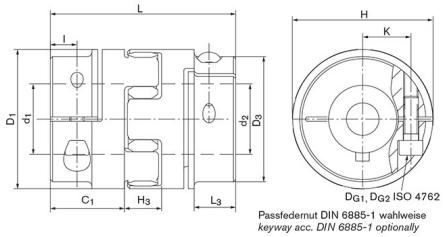
Artikelübersicht

BEST (Bestellnummer)	23900-107500200
D1 (Durchmesser / mm)	75.00
D2 (Durchmesser / mm)	2.00
GEW (Gewicht ca. / kg)	0.0009
BS (Beschreibung)	Infotext
ROHS (RoHS)	Yes
ZTN (Zolltarifnummer)	40169350
EAN (EAN-Nr. norelem)	4059495392752
EOL (End of life)	31.12.2099
STDLZ (Standardlieferzeit)	98% Warenverfügbarkeit. Nahezu alle Artikel aus dem Sortiment sind lagerhaltig verfügbar und werden nach Auftragseingang umgehend aus dem Zentrallager versendet. Nicht lagernde Artikel werden in der Regel zeitnah beschafft. Alle Verfügbarkeiten werden im Shop live angezeigt.
WARTUNG (Betriebs- und Wartungshinweise)	Wartungsintervall siehe Bedienungsanleitung

© norelem

I.9 Elastomer Jaw Coupling Technical Sheet

RINGFEDER POWER TRANSMISSION



Part number
GWE-5104-19-0012-0014-K1__-_

Description
GWE 5104 Elastomer Coupling

Product Attribute	Ref.	Value	Unit
Transmissible torque at given TA	T	17	Nm
Weight	Gw	0.158	kg
Outer diameter hub	D1	40	mm
Min. bore diameter with keyway acc. to DIN 6885-1	d1kmin	6	mm
Max. bore diameter with keyway acc. to DIN 6885-1	d1kmax	20	mm
Min. bore diameter with keyway acc. to DIN 6885-1	d2kmin	6	mm
Max. bore diameter with keyway acc. to DIN 6885-1	d2kmax	20	mm
Total length	L	66	mm
tightened torque of clamping screw (G1)	TA1	11	Nm
Max. rotation speed	nmax	10000	
Quantity of clamping screws (DG1)	nSc1	1	pcs
Naming of the locking screws		DIN EN ISO 4762	
Thread diameter	DG1	6	mm
Size		19	
Total moment of inertia	J	0.036	
Guided length in hub boring	C1	25	mm
Keyway 1		Yes	
Keyway 2		No	

Created: 2026-06-14 04:19:00

Address: RINGFEDER POWER TRANSMISSION GMBH
Werner-Heisenberg-Str. 18
64823 Groß-Umstadt
Germany

Phone: +49 (0)6078 / 9385-0
Fax: +49 (0)6078 / 9385-100
Web: www.ringfeder.com
Email: sales.international@ringfeder.com

I.10 Wiska M12 Blanking Plug and O-Ring Technical Sheets

Product Data Sheet

WISKA make power smile

ORD-E 12 + PG7

O-ring, EPDM, M12 + Pg7



Products may differ in size, colour and appearance to those shown. If you require further information or customisation, please contact us directly.

SPRINT RoHS

Material	EPDM
Temp. range min	-40 °C
Temp. range max	120 °C
Thread type	M
Ø Connection thread D	12
Diameter	9 mm
Thickness	1,5 mm
Product Color	RAL 9005
Order no. RAL 9005	10064697
Type	ORD-E 12 + PG7
Packing unit	100
EAN number	4007685646970
Tariff number	40169300
ETIM-Classification	EC001181

14.06.2026

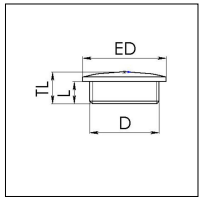
Your Contact:
WISKA Hoppmann GmbH
Kisdorfer Weg 28 · 24568 Kaltenkirchen · Germany
☎ +49-4191-508-0 · 💻 +49-4191-508-209
contact@wiska.de · www.wiska.com

Other technical data on request / subject to change without notice

ESVS 12

Stop end, stainless steel, M12





Products may differ in size, colour and appearance to those shown. If you require further information or customisation, please contact us directly.

RoHS

Material	Stainless steel 1.4305
Protection class	IP54
Thread type	M
Ø Connection thread D	12
Lead	1,5
Length screw-in thread L	5 mm
External diameter ED	14 mm
Total length TL	7,5 mm
Advice	with O-ring IP66/IP68
WISKA-Order no.	10065460
Type	ESVS 12
Packing unit	10
EAN number	4007685654609
Tariff number	73269098
ETIM-Classification	EC000032

Recommended accessories

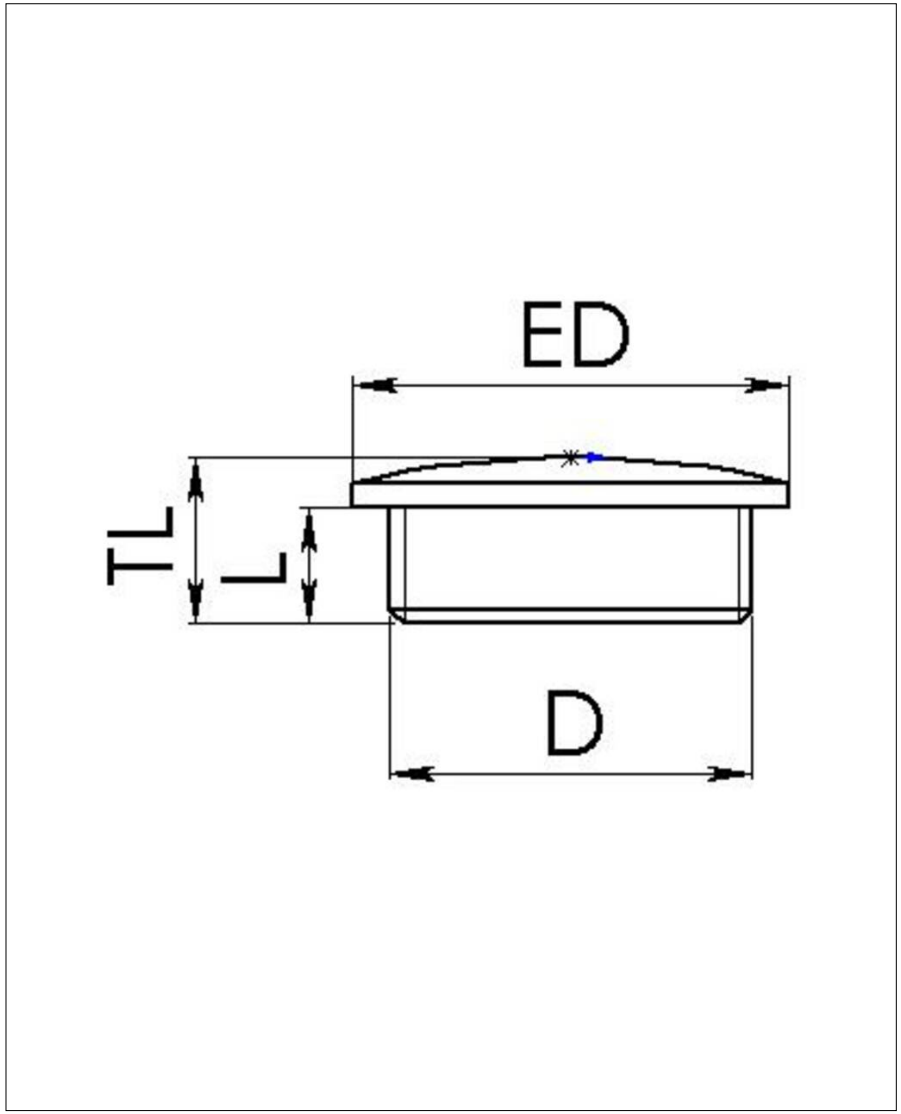
ESMU 12	10064188
ORD-E 12 + PG7	10064697

18.06.2026

Your Contact:
WISKA Hoppmann GmbH
Kisdorfer Weg 28 · 24568 Kaltenkirchen · Germany
☎ +49-4191-508-0 · 🖷 +49-4191-508-209
contact@wiska.de · www.wiska.com

Other technical data on request / subject to change without notice

Product Data Sheet

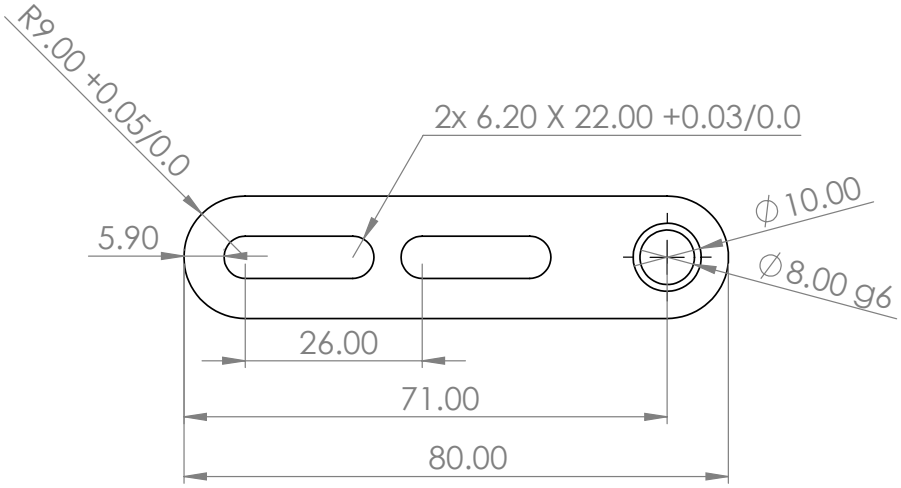


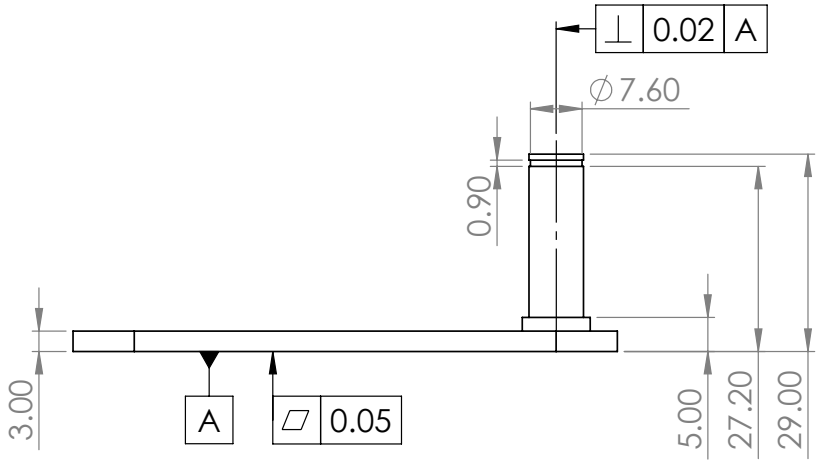
Your Contact:
WISKA Hoppmann GmbH
Kisdorfer Weg 28 · 24568 Kaltenkirchen · Germany
☎ +49-4191-508-0 · 🖷 +49-4191-508-209
contact@wiska.de · www.wiska.com

Other technical data on request / subject to change without notice

Appendix J

Technical Drawings





UNLESS OTHERWISE SPECIFIED: DIMENSIONS ARE IN MILLIMETERS SURFACE FINISH: 3.2 GENERAL TOLERANCES: ISO 2768-fH	FINISH: Passivated (ISO 16048)	DEBURR AND BREAK SHARP EDGES	DO NOT SCALE DRAWING / REVISION

	NAME	SIGNATURE	DATE
DRAWN			
CHK'D			
APPV'D			
MFG			
Q.A			

TITLE: BracketStage2

MATERIAL: AISI 316

DWG NO. IdlerBracket

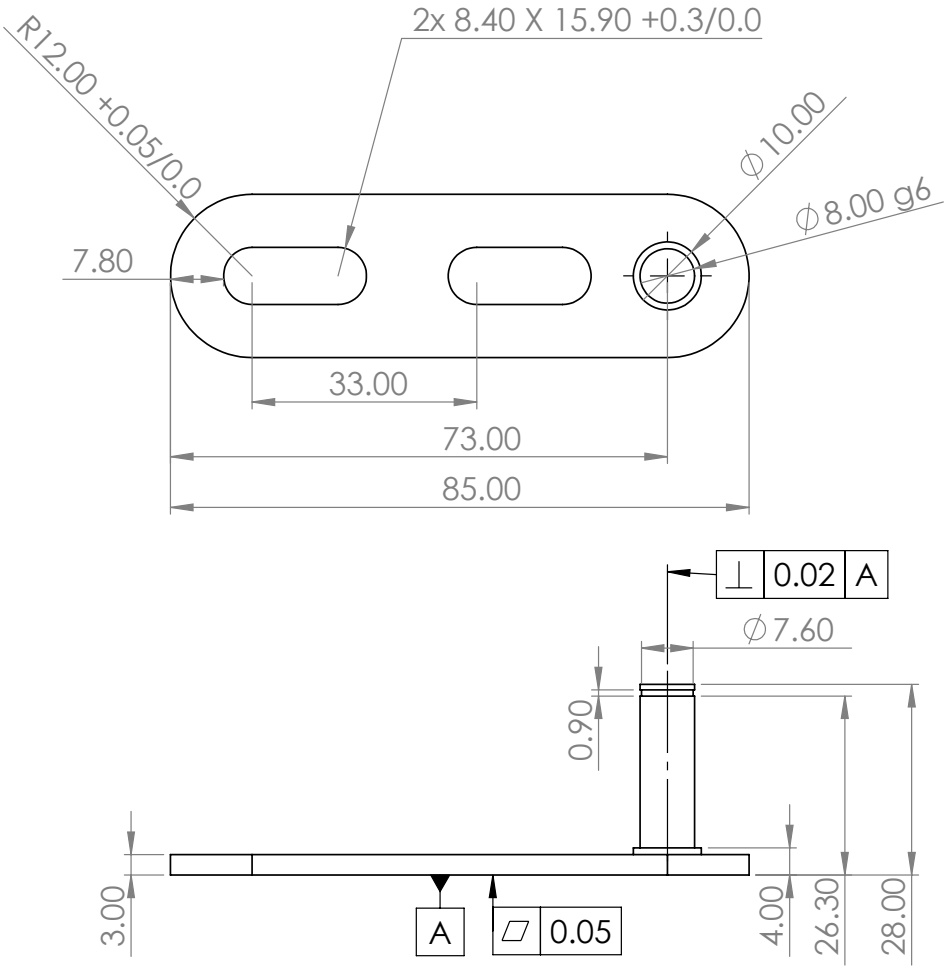
A4

WEIGHT:

SCALE:1:1

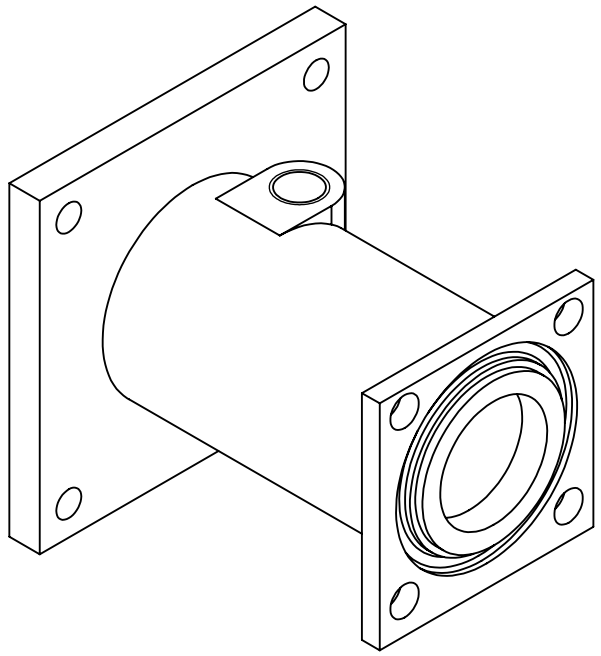
SHEET 1 OF 1

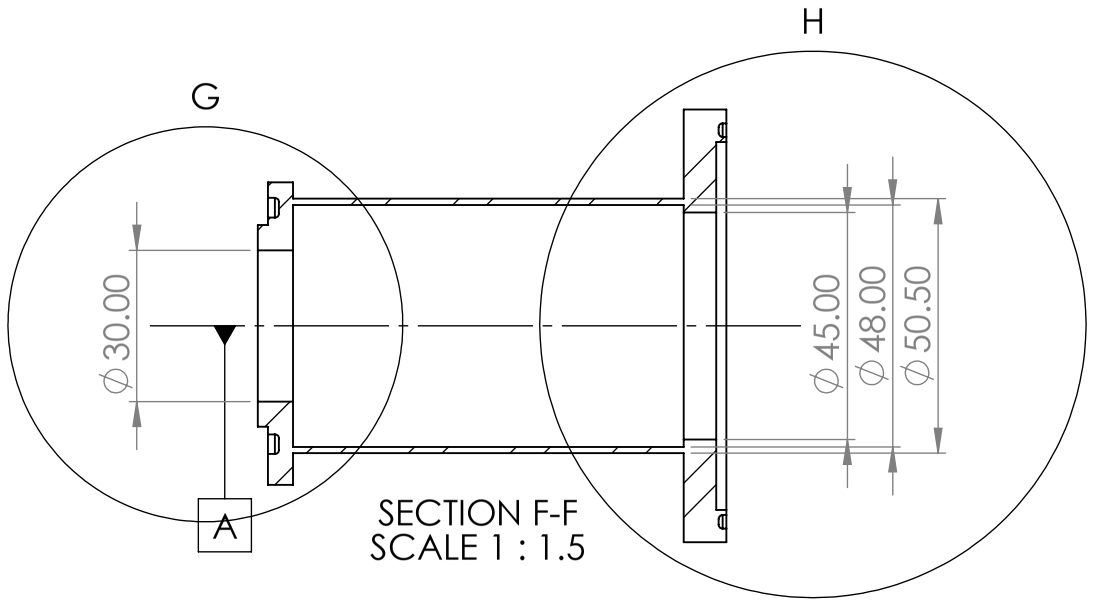
SOLIDWORKS Educational Product. For Instructional Use Only.



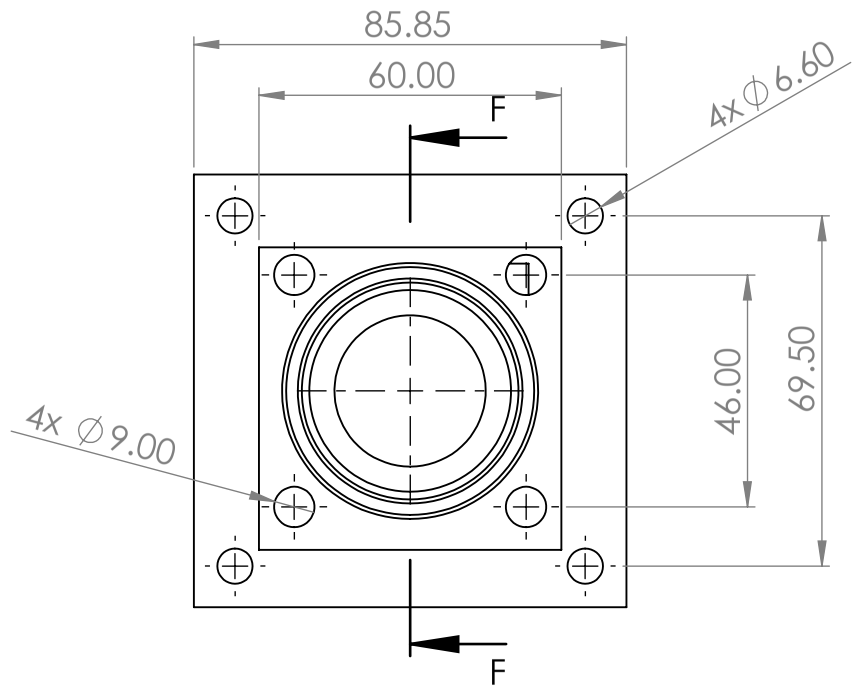
UNLESS OTHERWISE SPECIFIED: DIMENSIONS ARE IN MILLIMETERS SURFACE FINISH: 3.2 GENERAL TOLERANCES: ISO 2768-fH			FINISH: Passivated (ISO 16048)			DEBURR AND BREAK SHARP EDGES	DO NOT SCALE DRAWING / REVISION
	NAME	SIGNATURE	DATE				TITLE: BracketStage2
DRAWN							
CHK'D							
APPV'D							
MFG							
Q.A				MATERIAL: AISI 316			DWG NO. IdlerBracket2 / A4
				WEIGHT:			SCALE:1:1 / SHEET 1 OF 1

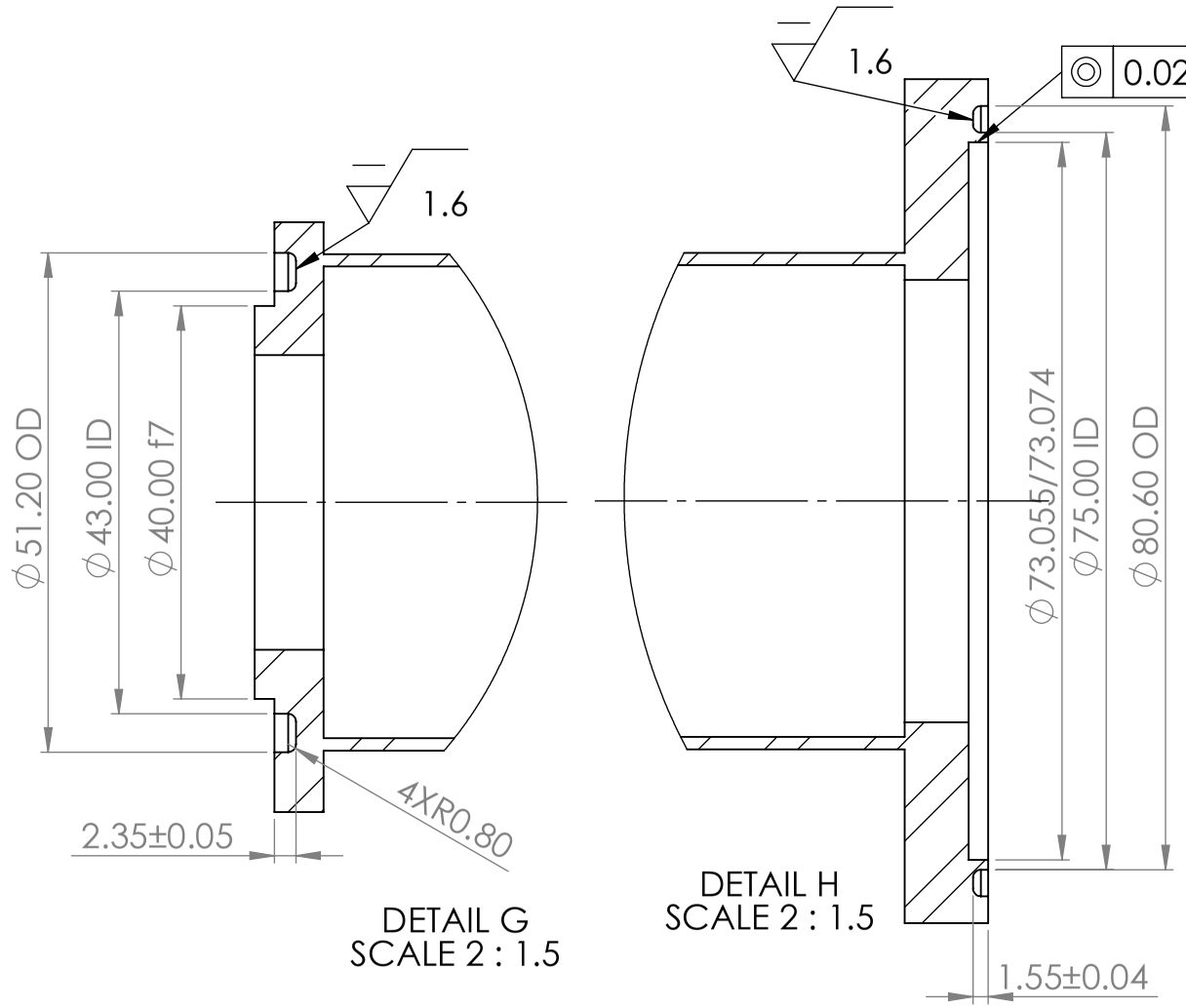
SOLIDWORKS Educational Product. For Instructional Use Only.





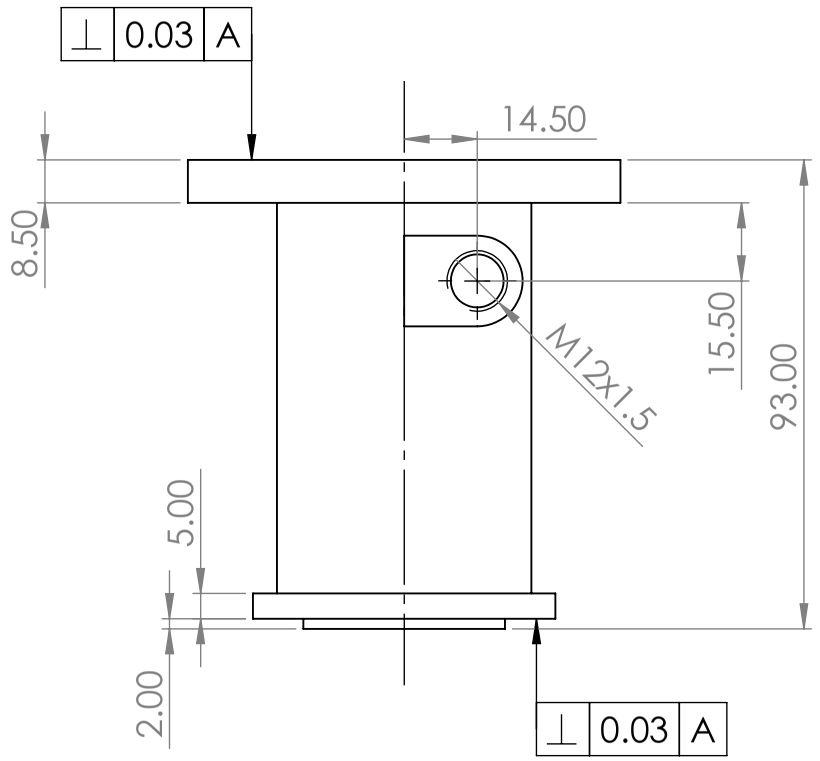
SECTION F-F
SCALE 1 : 1.5





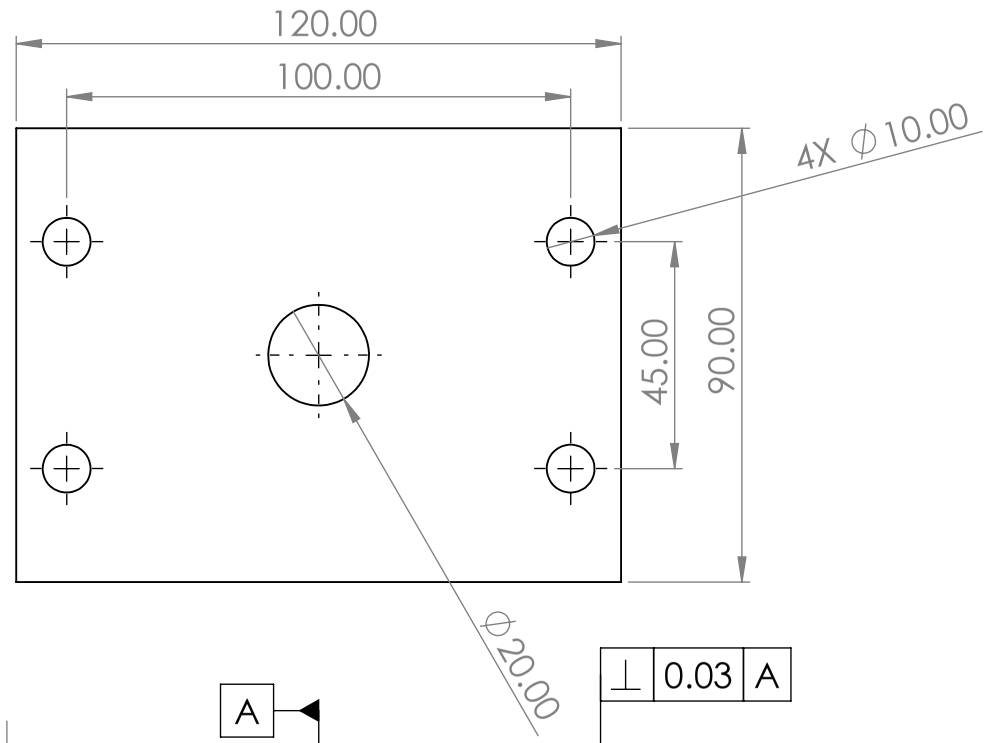
DETAIL G
SCALE 2 : 1.5

DETAIL H
SCALE 2 : 1.5

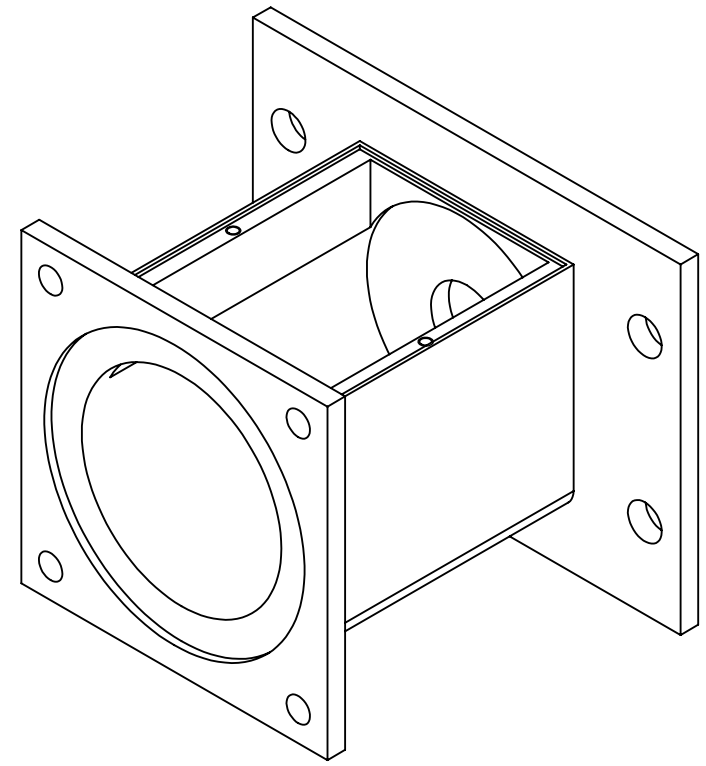


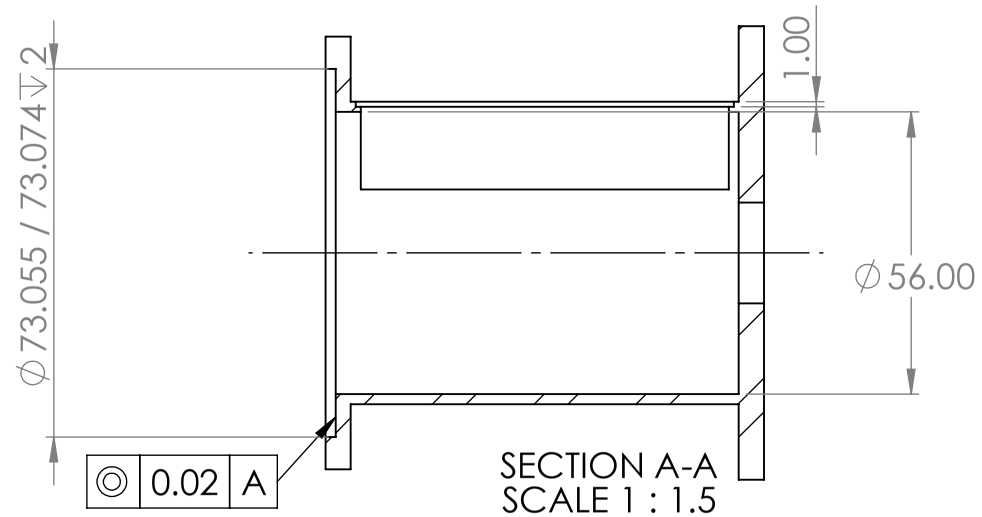
UNLESS OTHERWISE SPECIFIED: DIMENSIONS ARE IN MILLIMETERS SURFACE FINISH: 3.2 GENERAL TOLERANCES: ISO 2768-fH		FINISH: Passivated (ISO 16048)		DEBURR AND BREAK SHARP EDGES ISO 13715		DO NOT SCALE DRAWING	REVISION
	NAME	SIGNATURE	DATE			TITLE: Roller Conveyor's Housing	
DRAWN							
CHK'D							
APPV'D							
MFG							
Q.A				MATERIAL: Stainless Steel AISI 316 (1.4401) Annealed		DWG NO. Housing-RollerConveyor	A3
				WEIGHT:		SCALE:1:2	SHEET 1 OF 1

SOLIDWORKS Educational Product. For Instructional Use Only.

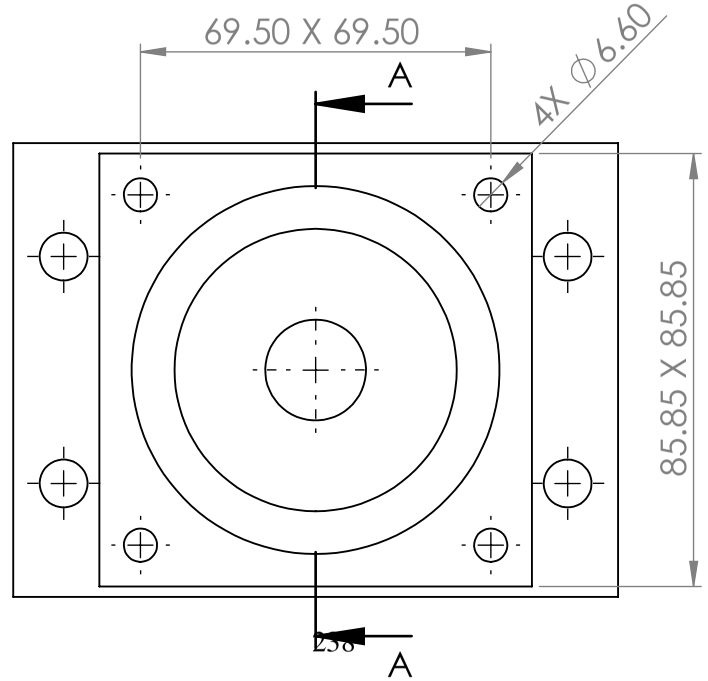


Panel-side holes oversized to permit field alignment to legacy threaded hole pattern prior to fastener torquing.



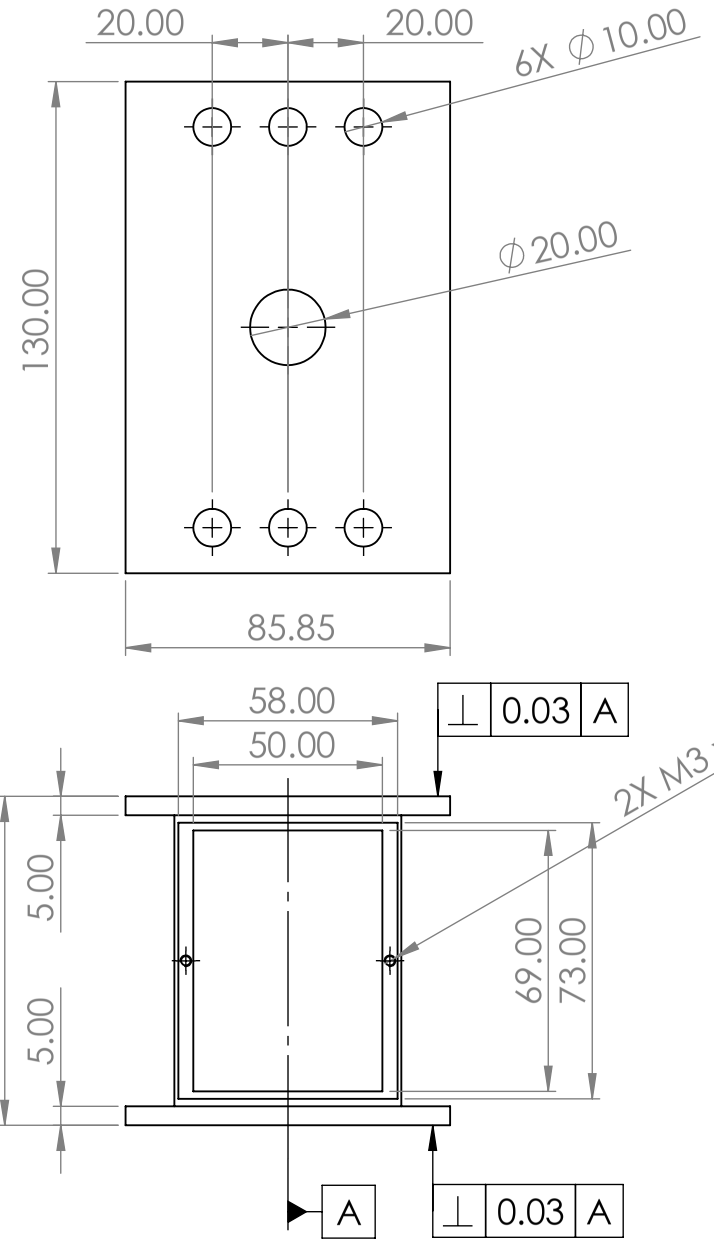


SECTION A-A
SCALE 1 : 1.5

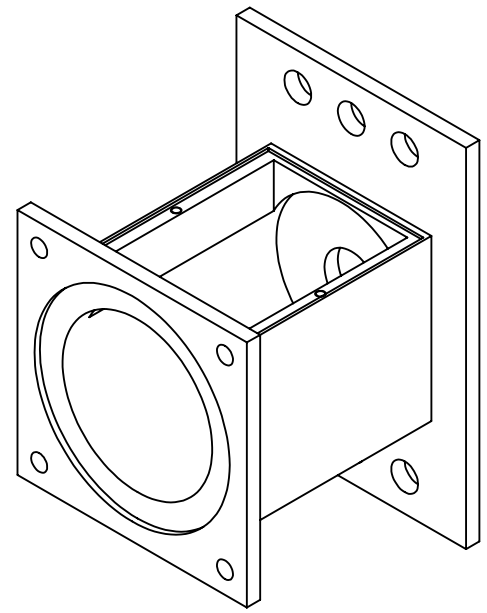


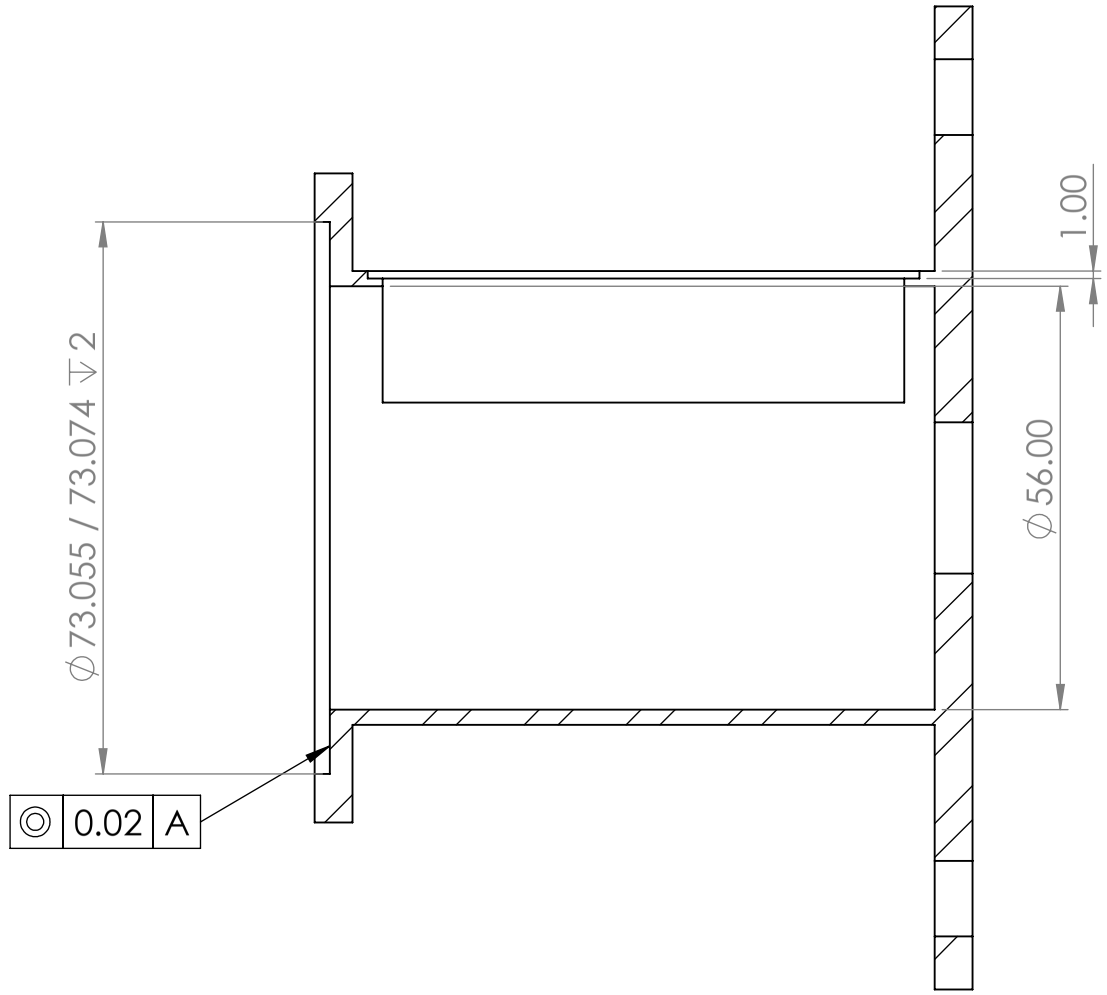
UNLESS OTHERWISE SPECIFIED: DIMENSIONS ARE IN MILLIMETERS SURFACE FINISH: 3.2 GENERAL TOLERANCES: ISO 2768-fH	FINISH: Type III Hardcoat Anodise		DEBURR AND BREAK SHARP EDGES			DO NOT SCALE DRAWING	REVISION
	NAME	SIGNATURE	DATE			TITLE: Housing-M09-010/012	
DRAWN							
CHK'D							
APPV'D							
MFG							
Q.A				MATERIAL: AW-6082-T6		DWG NO. Housing-M09-010/012	A3
				WEIGHT:		SCALE:1:2	SHEET 1 OF 1

SOLIDWORKS Educational Product. For Instructional Use Only.

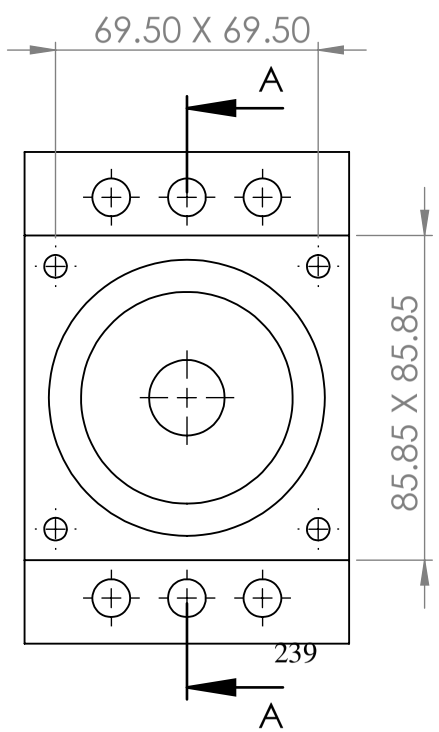


Panel-side holes oversized to permit field alignment to legacy threaded hole pattern prior to fastener torquing.



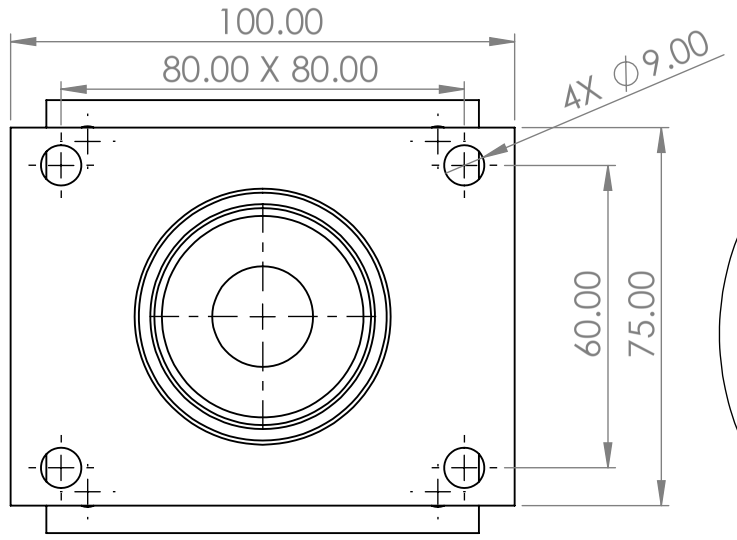


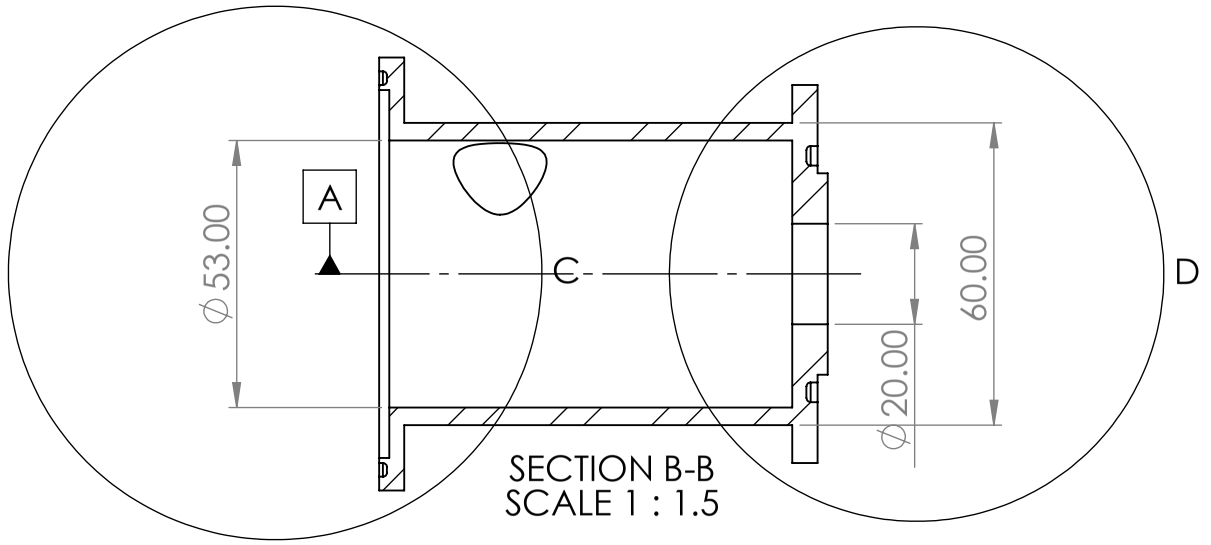
SECTION A-A
SCALE 1 : 1

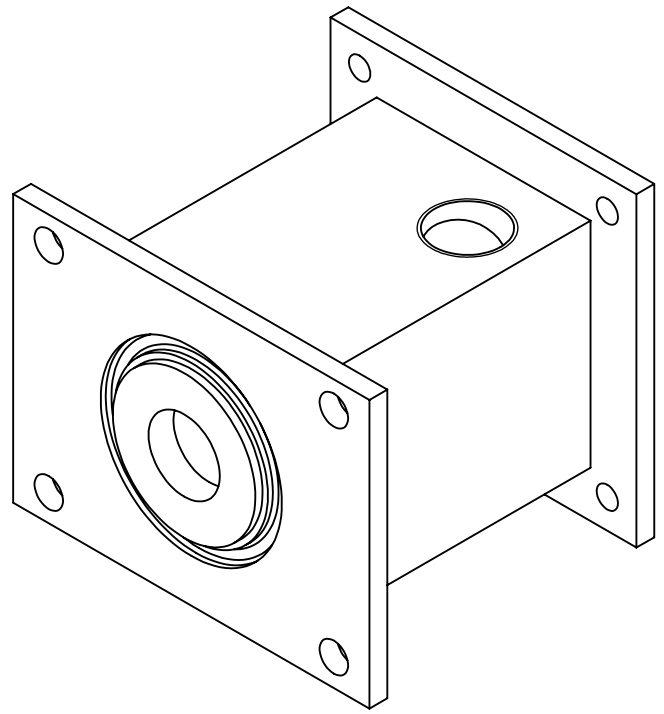


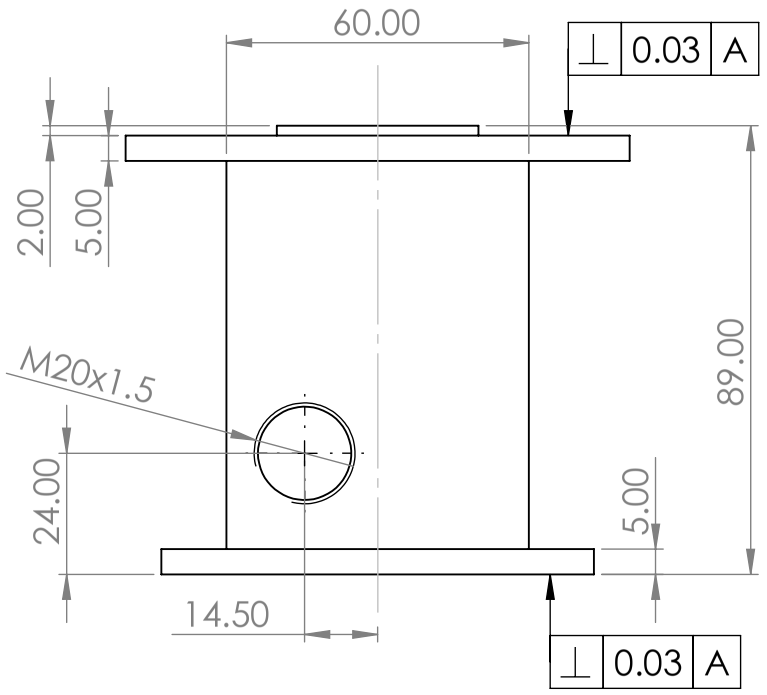
UNLESS OTHERWISE SPECIFIED: DIMENSIONS ARE IN MILLIMETERS SURFACE FINISH: ▽ 3.2 GENERAL TOLERANCES: ISO 2768-fH		FINISH: Type III Hardcoat Anodise		DEBURR AND BREAK SHARP EDGES		DO NOT SCALE DRAWING	REVISION
	NAME	SIGNATURE	DATE			TITLE: Housing-M09-021	
DRAWN							
CHK'D							
APPV'D							
MFG							
Q.A				MATERIAL: AW-6082-T6		DWG NO. Housing-M09-021	A3
				WEIGHT:		SCALE:1:2	SHEET 1 OF 1

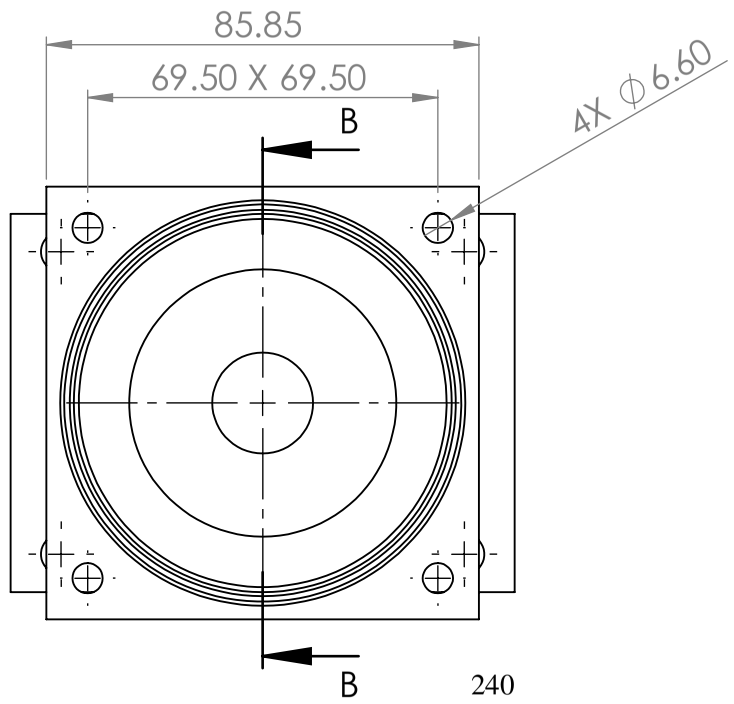
SOLIDWORKS Educational Product. For Instructional Use Only.

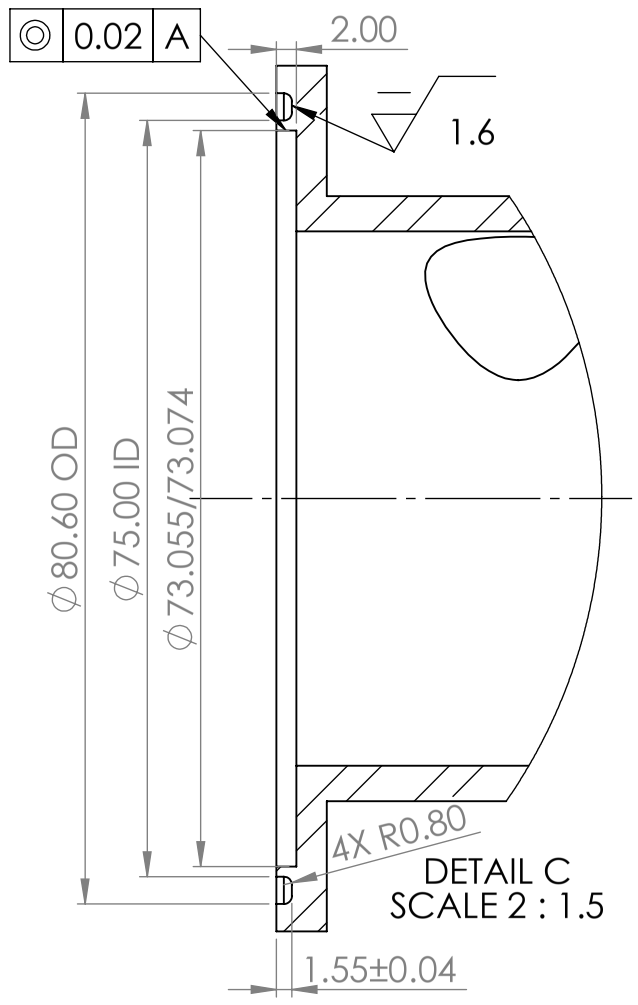


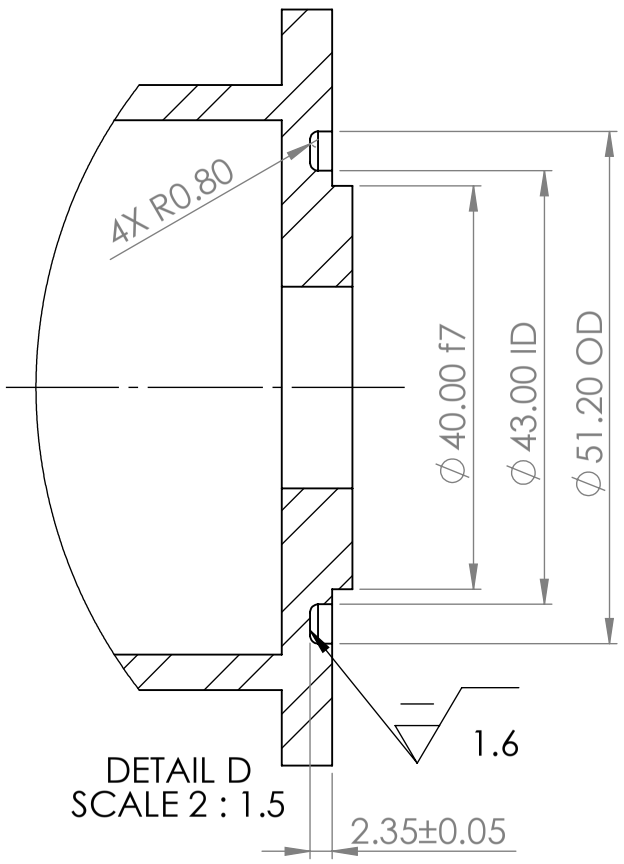






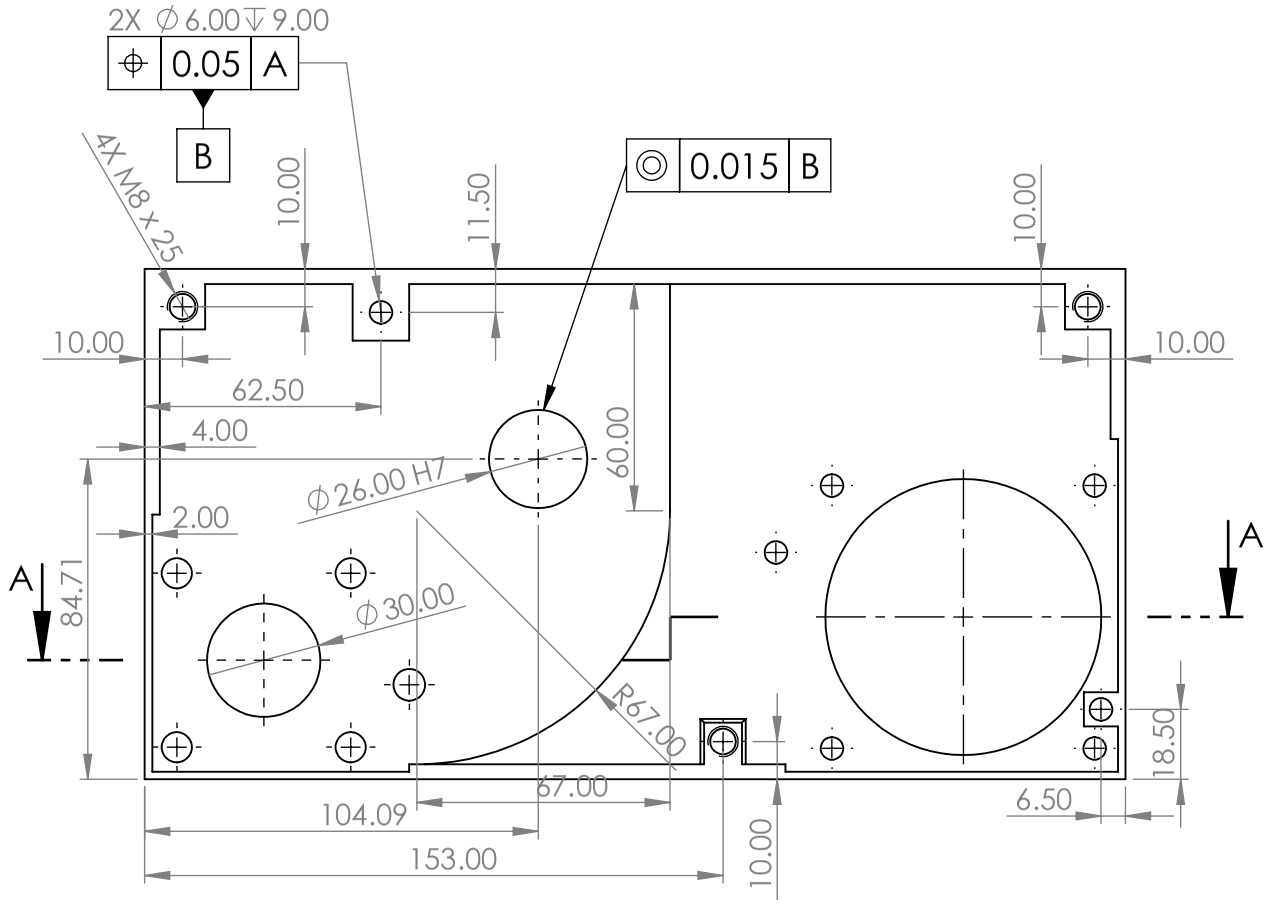


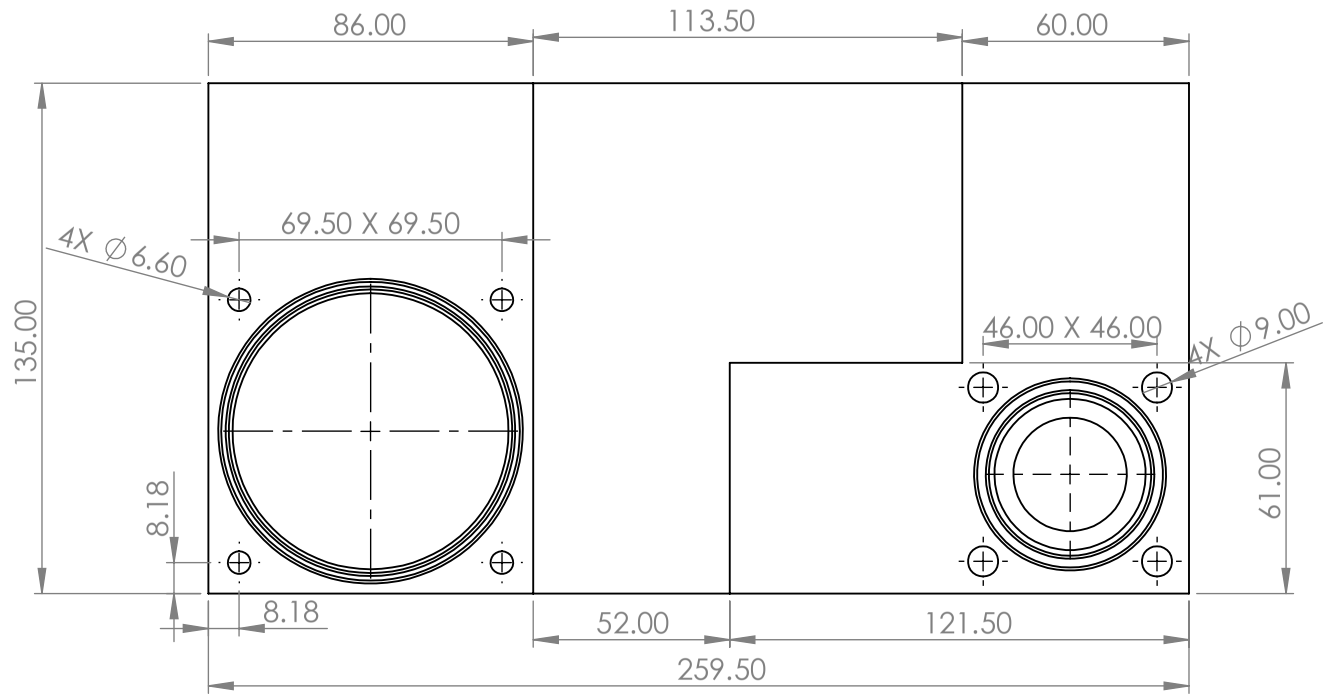


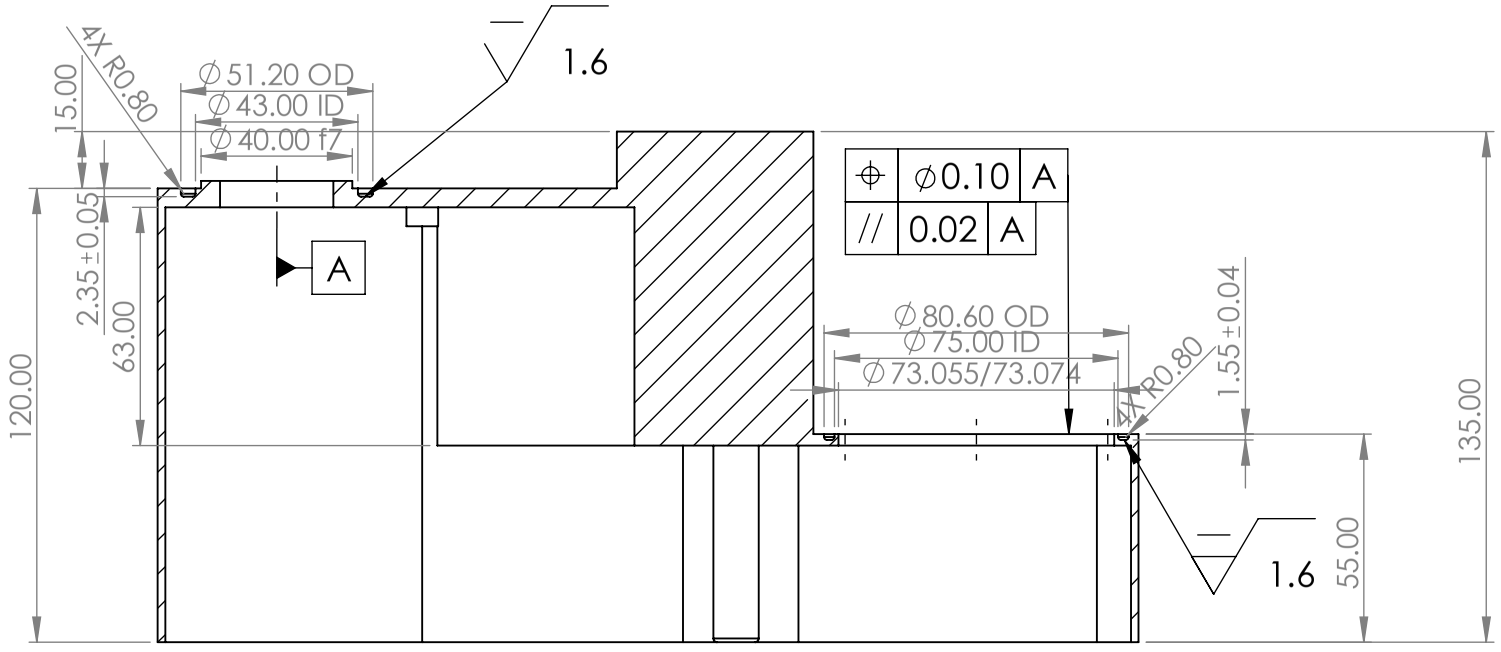


UNLESS OTHERWISE SPECIFIED: DIMENSIONS ARE IN MILLIMETERS SURFACE FINISH: GENERAL TOLERANCES: ISO 2768-fH		FINISH: Passivated (ISO 16048)		DEBURR AND BREAK SHARP EDGES		DO NOT SCALE DRAWING	REVISION
	NAME	SIGNATURE	DATE			TITLE: Housing-M09-025	
DRAWN							
CHK'D							
APPV'D							
MFG							
Q.A				MATERIAL: Stainless Steel AISI 316 (1.4401) Annealed		DWG NO. Housing-M09-025	A3
				WEIGHT:		SCALE:1:2	SHEET 1 OF 1

SOLIDWORKS Educational Product. For Instructional Use Only.



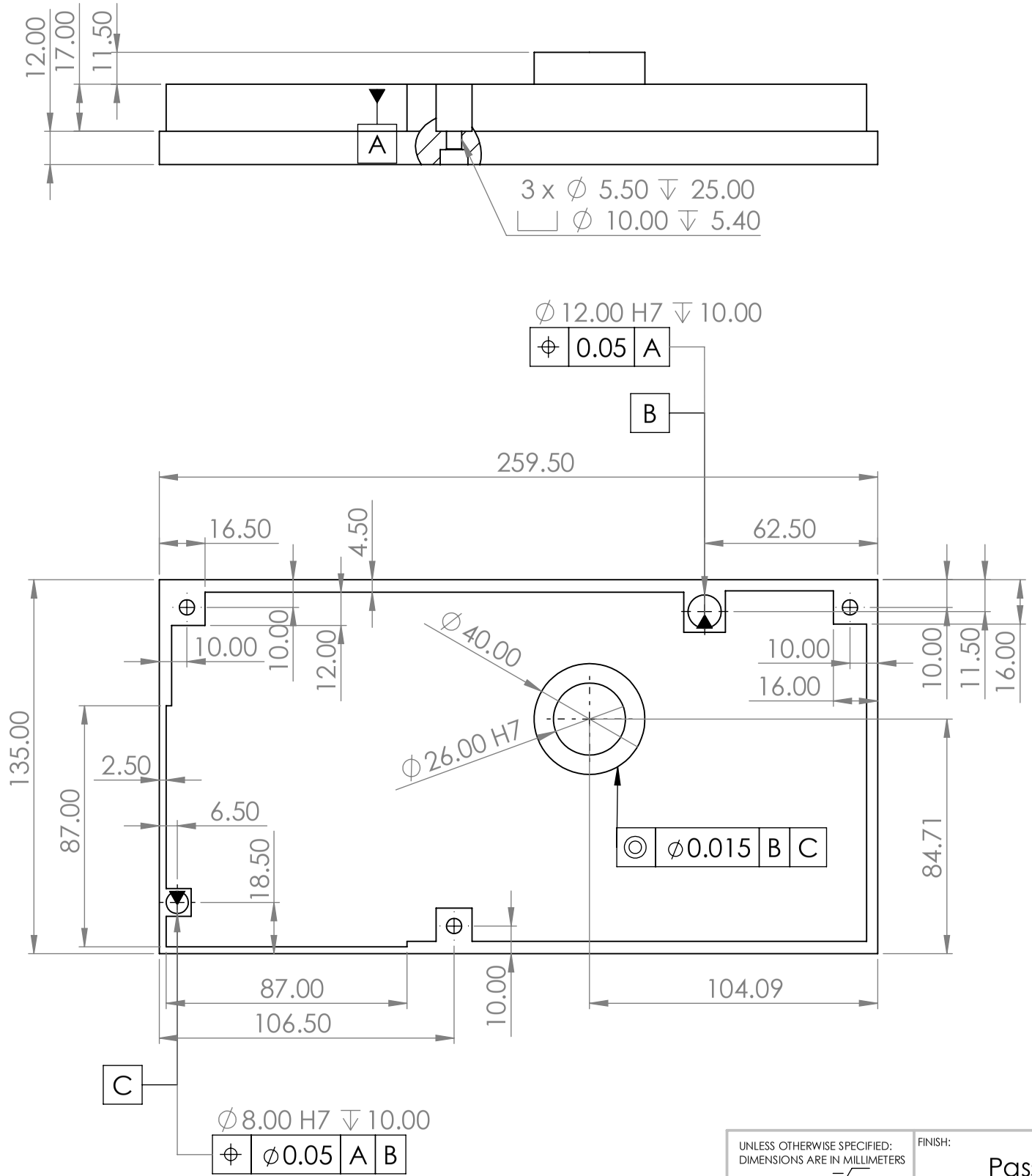




SECTION A-A

UNLESS OTHERWISE SPECIFIED: DIMENSIONS ARE IN MILLIMETERS SURFACE FINISH: GENERAL TOLERANCES: ISO 2768-fH		FINISH: Passivated (ISO 16048)		DEBURR AND BREAK SHARP EDGES		DO NOT SCALE DRAWING	REVISION
	NAME	SIGNATURE	DATE			TITLE: HousingTransportationSystem	
DRAWN							
CHK'D							
APPV'D							
MFG							
Q.A				MATERIAL: AISI 316		DWG NO. HousingTransportationSystem	A3
				WEIGHT:		SCALE:1:2	SHEET 1 OF 1

SOLIDWORKS Educational Product. For Instructional Use Only.



UNLESS OTHERWISE SPECIFIED:
DIMENSIONS ARE IN MILLIMETERS
SURFACE FINISH: 3.2
GENERAL TOLERANCES:
ISO 2768-fH

FINISH: Passivated (ISO 16048)

DEBURR AND BREAK SHARP EDGES

DO NOT SCALE DRAWING | REVISION

	NAME	SIGNATURE	DATE
DRAWN			
CHK'D			
APPV'D			
MFG			
Q.A			

TITLE: LidTransportationSystem

MATERIAL: AISI 316

DWG NO. LidTransportationSystem

A3

WEIGHT:

SCALE:1:2

SHEET 1 OF 1

SOLIDWORKS Educational Product. For Instructional Use Only.

Appendix K

Automatic Adjustment System's SCL Code

Listing K.1: FB_Motion_Sequence

```
FUNCTION_BLOCK "FB_Motion_Sequence"
VAR
    Sequence_State    : Int := 0;
    Power_Independent1 : MC_POWER;
    Power_Master1       : MC_POWER;
    GearIn_Slave1        : MC_GEARIN;
    Move_Master1          : MC_MOVEABSOLUTE;
    Move_Independent1      : MC_MOVEABSOLUTE;
END_VAR
VAR_INPUT
    Start_Adjustment : Bool;
    Selected_Program : Int;
END_VAR
VAR_OUTPUT
    Adjustment_Done : Bool;
    Machine_Busy    : Bool;
    Error_Active    : Bool;
END_VAR

CASE #Sequence_State OF

    0: // IDLE STATE: Wait for start command
        #Adjustment_Done := FALSE;
        #Machine_Busy := FALSE;

        // Forces falling edge on the gear-in block so its rising-edge
        // detection is reset every time the sequence returns here.
        #GearIn_Slave1(Master := "M09-001_Master",
                       Slave := "M09-001-LU1-Slave1",
                       Execute := FALSE);
```

```
31
32          IF #Start_Adjustment AND NOT #Machine_Busy THEN
33              #Machine_Busy := TRUE;
34              #Sequence_State := 10;
35          END_IF;
36
37      10: // POWER UP STATE: Enable all virtual axis drives
38          #Power_Independent1(Axis := "M09-010",
39                              Enable := TRUE,
40                              StartMode := 1);
41          #Power_Master1(Axis := "M09-001_Master",
42                         Enable := TRUE,
43                         StartMode := 1);
44
45          IF #Power_Independent1.Status AND #Power_Master1.Status THEN
46              #Sequence_State := 20;
47          END_IF;
48
49          IF #Power_Independent1.Error OR #Power_Master1.Error THEN
50              #Error_Active := TRUE;
51              #Sequence_State := 0;
52          END_IF;
53
54      20: // GEAR IN STATE: Synchronize the slave to its master
55          #GearIn_Slave1(Master := "M09-001_Master",
56                         Slave := "M09-001-LU1-Slave1",
57                         Execute := TRUE,
58                         RatioNumerator := 1,
59                         RatioDenominator := 1);
60
61          IF #GearIn_Slave1.InGear THEN
62              #Sequence_State := 30;
63          END_IF;
64
65          IF #GearIn_Slave1.Error THEN
66              #Error_Active := TRUE;
67              #Sequence_State := 0;
68          END_IF;
69
70      30: // MOVE STATE: Fetch recipe targets and execute absolute movements
71          #Move_Master1(Axis := "M09-001_Master",
72                        Execute := TRUE,
73                        Position :=
    "Recipe_Memory".Program_Recipes[#Selected_Program]."M09-001_Master",
74                        Velocity := 20.0);
75          #Move_Independent1(Axis := "M09-010",
76                            Execute := TRUE,
77                            Position :=
    "Recipe_Memory".Program_Recipes[#Selected_Program]."M09-010",
```

```
                            Velocity := 20.0);

        IF #Move_Master1.Busy AND #Move_Independent1.Busy THEN
            #Sequence_State := 40;
        END_IF;

    40: // MONITOR STATE: Wait for all axes to report "Done"
        #Move_Master1(Axis := "M09-001_Master", Execute := FALSE);
        #Move_Independent1(Axis := "M09-010", Execute := FALSE);

        IF #Move_Master1.Done AND #Move_Independent1.Done THEN
            #Adjustment_Done := TRUE;
            #Machine_Busy := FALSE;
            #Sequence_State := 0;
        END_IF;

        IF #Move_Master1.Error OR #Move_Independent1.Error THEN
            #Error_Active := TRUE;
            #Sequence_State := 0;
        END_IF;

END_CASE;
```